PART II

DAMAGE CRITERIA ▇

Chapter 9

INTRODUCTION TO DAMAGE CRITERIA ▇

▇ Part I of this manual describes the basic phenomena associated with a nuclear explosion for various burst conditions. These phenomena include: blast and shock, thermal radiation, X-ray radiation, nuclear radiation, transient radiation effects on electronics (TREE), electromagnetic pulse (EMP) phenomena, and phenomena affecting electromagnetic wave propagation. Part II treats the mechanisms of casualty production and damage to military targets, and describes the response of these targets by correlating the basic physical phenomena with various defined degrees of damage.

SECTION I
CONTENT AND LIMITATIONS OF PART II ▇

9-1 Introduction to Chapter 9 ▇

▇ The information in Part I is divided according to the phenomenology, with one chapter being devoted to each of the seven phenomena listed above. This chapter provides a general discussion of the physical damage mechanisms associated with each of the first six phenomena listed above (the last phenomenon does not produce physical damage; the degradation of signals from radio and radar systems is discussed in Chapter 17). Separate sections describe the damage mechanisms associated with each of the six phenomena. In addition, Section IV of this chapter discusses the degradation of equipment by thermal radiation that might affect its response to the blast wave.

9-2 Organization of Part II ▇

▇ Part II of this manual is divided into chapters according to types of targets that exhibit similar response characteristics. Further subdivisions within the chapters separate the types of targets into subtypes, and for each subtype there are frequently further subdivisions according to the phenomena that cause the damage.

▇ The data presented here are interpretations of complex results of the nuclear weapons effects research and test programs of the Department of Defense. A constant effort is made to deduce theoretical models and scaling laws for the various weapons effects that permit a quantitative prediction of the extent of a given effect from a weapon of one yield related to weapons of other yields. Since the initiation of the limited nuclear test ban treaty, a large amount of effort has been devoted to the development of complex computer codes to predict the environments created by the various phenomena resulting from nuclear explosions and the interactions of these environments with personnel and military systems. A large number of scaling laws presented in Part I that are useful in predicting the environment from a given explosion were derived from the calculations performed with these codes. Many additional scaling laws,

derived from field and laboratory experiments, and theoretical studies, as well as the codes, are presented in the chapters of Part II to aid in the predictions of the response of personnel and systems to the environment. Graphical presentation is used in preference to tabular or purely computational presentations wherever possible. The damage curves are drawn for a probability of 50 percent of producing the indicated damage. Curves of 90 and 10 percent probability are included when the quantity and quality of the data permit. In addition, Appendix C provides the methodology for estimating any probability of damage, provided that the median values of the response of a given system are known. Estimates of such median values for the equipment discussed in Sections I through III of Chapter 11 are provided in Appendix C. Effort has been made to provide a comprehensive set of data in a readily usable form; however, certain categories of damage are not amenable to generalization. Some limitations in the content of Part II are discussed in paragraph 9-3.

■ An estimate of the degree of reliability accompanies most of the data presented herein. Statements of the reliability of damage data only pertain to the basic response data, which, for the target analyst represent the "radius of effect." They should not be confused with the terms variability and probability of damage, which pertain to target response; nor do these estimates include operational considerations such as linear, circular, or spherical aiming and fuzing errors, yield variations, and target intelligence.

9-3 Limitations in Part II ■

■ As mentioned in paragraph 9-2, the remaining chapters of Part II each contain descriptions of damage to a category of targets that exhibit similar response characteristics. Unfortunately, the response to certain of the phenomena depends so strongly on a specific system design that it is impossible to present response

data for a "category" of targets (e.g., communications equipment, aircraft, missiles). These phenomena include X-ray radiation and EMP. Therefore, general discussions of the types of systems that are likely to be affected by these phenomena and the general nature of the responses are given in Sections V and VIII of this chapter. No response criteria are provided in subsequent chapters; however, the potential importance of these phenomena are mentioned where appropriate. TREE response is also very dependent on specific system design. The response of electronic components and circuits is described in Section VII of this chapter. Section IV of Chapter 14 contains a brief review of component and circuit response supplemented with discussions of general electrical responses of classes of systems. This latter discussion is intended to include a cross section of systems that should provide some basis for estimating the radiation damage threshold of other similar equipment.

SECTION II
■ **BLAST AND SHOCK DAMAGE** ■

■ When a blast or shock wave strikes a target, the target may be damaged (distorted sufficiently to impair usefulness) by the blast or shock wave itself, by being translated by the blast wave and striking another object or the ground, or by being struck by another object translated by the blast wave. For example, the air blast wave can shatter windows, dish in walls, collapse roofs, deflect structural frames of buildings, and bend or rupture aircraft panels and frames. Vehicles, tanks, artillery pieces, and personnel can strike other objects on the ground while being hurled through the air or tumbled along the ground by the blast wave. Ship hulls may be split or crushed by the water shock wave. Buried structures or structural founda-

tions can be displaced. collapsed, or ruptured by the ground shock wave. Usually, the degree of damage sustained by a particular target cannot be correlated specifically to a single blast or shock parameter. The total damage received by the target may depend on a combination of air blast and ground or water shock parameters. The orientation of the target with respect to the blast wave. and the type of surface (the topography or the type of soil) associated with the target also determine damage.

LOADING

The blast loading on an object is a function not only of the blast characteristics of the incident wave (rise time, peak overpressure, peak dynamic pressure. decay. and duration). but also of the size, shape. orientation. and response of the object. The influence of the target characteristics on the loading is discussed below. with emphasis on air blast loading.

9-4 Air Blast Loading in the Mach Reflection Region

The loading on an object exposed to air blast is a combination of the forces exerted by the overpressure and the dynamic pressure of the incident blast wave. The loading at any point on a surface of an object can be described as the sum of the dynamic pressure, multiplied by a local drag coefficient. and the overpressure after any initial reflections have cleared the structure. Since the loading changes rapidly while the blast wave is reflecting from the front surfaces and diffracting around the object. loading generally comprises two distinct phases: the initial diffraction phase; and the phase following diffraction when the object is completely engulfed by the blast wave. This latter phase approaches a steady state and usually is referred to as the drag phase, because during this phase the drag forces (i.e., the forces resulting from the dynamic pressures) are the predominant factors in the production of

a net translational force on the object. The following discussion of the loading process is based on an ideal blast wave as described in Section I (Figure 2-1), Chapter 2. Where nonideal blast waves. with slow rise time, irregular shapes, and high dynamic pressures (paragraphs 2-21 through 2-31, Chapter 2) introduce complications into the loading process. further explanation is provided. The loading on an object can be described conveniently in three parts: diffraction loading. drag loading. and net loading. These are discussed separately below.

Diffraction Loading. The side of an object facing the shock front of an air blast wave bears overpressures several times that of the incident overpressure because it both receives and reflects the shock. In the Mach reflection region the overpressure incident on the object is actually that of the original free air blast wave which has been reflected from the ground surface to a higher value. The reflection off the object therefore constitutes a second reflection process. In the regular reflection region, the incident overpressure is that of the free air blast wave (see paragraph 9-6). The magnitude of the reflected overpressure depends on the angle between the shock front and the face of the object, the rise time of the incident blast wave. and the initial incident shock strength. The greatest reflected overpressures occur when the direction of propagation of the shock front is normal to the face of the object, when the rise to the peak overpressure is essentially instantaneous. and when the incident shock strength is high. As the blast wave progresses it bends or diffracts around the object, eventually exerting overpressures on all sides. Before the object is entirely engulfed in the pressure region, however, overpressure is exerted on the front side of the object, whereas only ambient air pressure exists on the back side. During the diffraction phase this pressure differential produces a translational force on the object in the direction of blast wave propaga-

tion. When the blast wave has completely surrounded a small object, the translational force that results from diffraction loading is reduced essentially to zero, because the pressures on the front and on the back are almost equal. In the cases of long objects or short duration blast waves, the net force may actually reverse, because the overpressure on the front face may decay to a value lower than that on the rear face. The importance of this translational loading in the production of damage to the target depends on the duration of the loading or on the time required for the shock front to traverse the target and, therefore, on the size of the target. The effects of the translational load decrease as the duration of the load is decreased until, in some instances, translational load effects can be ignored. The overpressures continue on all sides of the object until the positive phase of the blast wave has passed. These pressures may be sufficient to crush an object (a 55-gallon drum may be damaged in this manner in addition to damage that might be incurred by translation). Thus, the diffraction phase translational loading depends primarily on the object size, pressure pulse duration, and on increases in differential overpressures resulting from reflection on the front face.

■ *Drag Loading.* During the time of diffraction and until the blast wave has passed, the wind behind the shock front causes dynamic pressures to be exerted on the object as drag loading. Except in the case where shock strengths are high, these pressures are much lower than the reflected overpressures; however, they produce a translational force that the target component receives for the entire positive phase duration of the blast wave. For a given blast wave, the loading that results from dynamic pressure depends principally on the shape and orientation of the object, ranging from less than four-tenths of the dynamic pressures in the case of a cylinder (when normal to the cylindrical axis), to over twice the dynamic pressures for an irregular, sharp-edged object.

■ *Net Loading.* Net loading is the combined load on the element that tends to translate it in the direction of propagation of the blast wave. Thus, it is the difference between the load on the front face and the load on the back face; the loads on the sides are of no effect in producing translation.

9-5 Qualitative Examples of Net Loading ■

■ The net load on a target can be developed most simply by considering the idealized case shown in Figure 9-1, in which a classical, sharp fronted blast wave moving along the surface of the ground encounters a simple, rigid, fixed cube. When the blast wave arrives at the front face of the target, this face experiences a sudden rise in overpressure to a value p_r that is greater than the peak overpressure Δp of the incident blast wave (also frequently called "side on" overpressure). As the shock wave moves over the cube, subjecting its top and side faces to side on overpressure, the pressure on the front face of the cube begins to drop as the result of rarefaction waves that are generated at the edges of the front face, and which move across that face. When the wave encounters the back face of the cube, that face experiences a gradual pressure increase. The air behind the front of the incident shock wave is in motion, and as the wave envelopes the cube this air motion also affects the pressures experienced by the various faces of the cube.

■ After a time that is related to the cube dimensions and to the velocity of the incident shock wave, the pressure on the front face becomes

$$p_f = \Delta p(t) + C_{df} q(t)$$

where

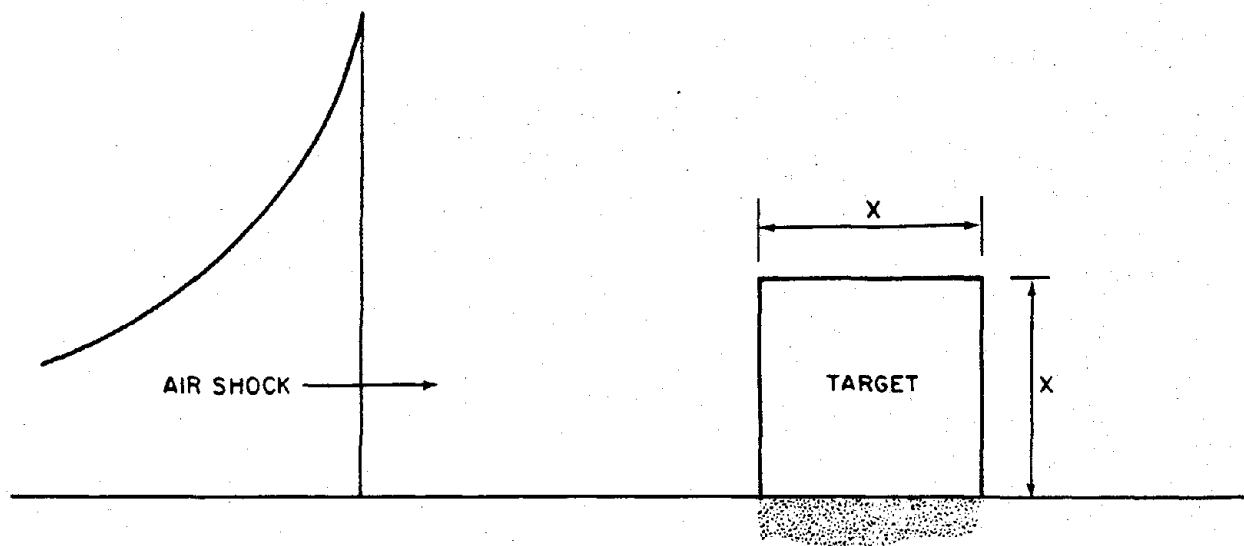$\Delta p(t)$ = the overpressure in the incident shock wave as a function of time, t,

Figure 9-1. ▮ Initial Conditions for Loading
of a Rigid, Fixed Cube ▮

C_{df} = the drag coefficient of the front face of the cube,

$q(t)$ = the dynamic pressure in the incident shock wave as a function of time, t.

After the shock wave has passed over the cube and has reached the back face, the pressure on that face begins to rise and, at a later time also related to the cube dimensions and the velocity of the incident shock wave, the pressure becomes

$$p_b = \Delta p(t) - C_{db} q(t)$$

where

C_{db} = the drag coefficient of the back face of the cube.

Note that both expressions contain overpressure and dynamic pressure components. As far as the *net* horizontal (translational) loading on the cube is concerned (i.e., the pressures tending to move the cube to the right in Figure 9-1), the overpressure contributions must be subtracted from one another (pressure on the back face tends to move the cube to the left) while the dynamic pressure contributions must be added to each other.

▮ It is convenient to consider the two contributions separately. Figure 9-2 illustrates the overpressure loadings only (dynamic pressure contributions are not included) experienced by the front and back faces of the cube both during the early (diffraction) phases — up to time t_1 on the front face and time t_3 on the back face of the cube — and after the times that the equations given above apply.

▮ The incident shock wave is of the classical (peaked) form with peak overpressure and overpressure duration of Δp and t_p^+ respectively; t_1 is the time after which the total front face loading is represented by the equation for p_f
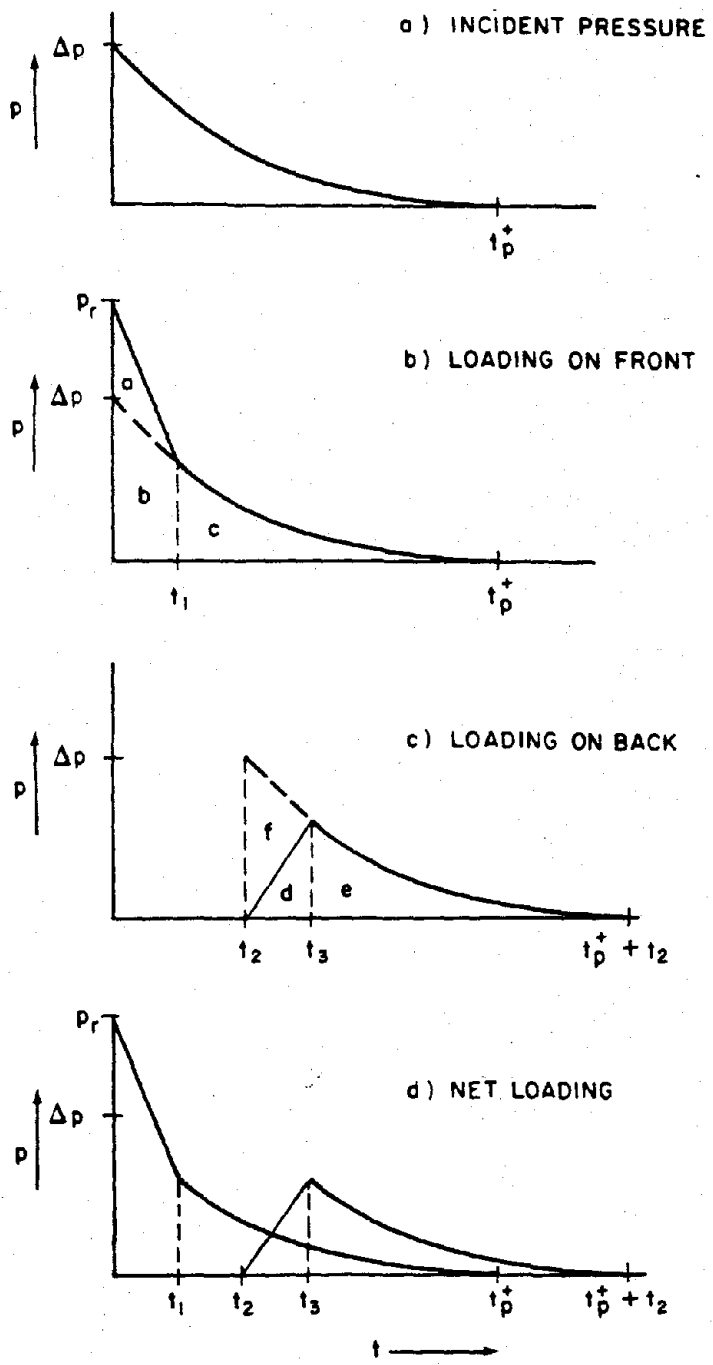
a) INCIDENT PRESSURE

b) LOADING ON FRONT

c) LOADING ON BACK

d) NET LOADING

Figure 9-2. ███ Target Loading by Overpressure ███

above: t_2 is the time for the shock wave to reach the back face, and t_3 is the time after which the total back face loading is represented by the equation for p_b above.

From Figure 9-2b, the total impulse on the front face, I_F (i.e., the area under the curve multiplied by the area of the cube face, A) is equal to the sum of the areas a, b, and c.

$$I_F = (a + b + c)A$$

The total impulse on the back face, I_B, is (Figure 9-2c)

$$I_B = (d + e)A$$

The net overpressure impulse is $I_F - I_B$. If the cube is not too large compared to the duration of the blast wave, the following approximations hold among the areas:

$$b = d + f,$$

$$c = e.$$

Thus, the net overpressure impulse is

$$I_N = (a + f)A.$$

If the initial drop of pressure on the front face and the build up of pressure on the rear face are assumed to be linear, the net impulse is

$$I_N = A\left[1/2\left(p_r - \Delta p\right)t_1 + 1/2\,\Delta p\left(t_3 - t_2\right)\right]$$

in which the term containing t_1 is area "a," and the term containing t_2 and t_3 is area "f" of Figure 9-2. Note in particular that the only times are t_1, t_2, and t_3, i.e., those times related to the initial envelopment of the cube by the blast wave. I_N does not, in this simple analysis, depend on overpressure duration t_p^+.

Substitution of commonly accepted values of t_1, t_2, and t_3 for a curve leads to the following expression for the net impulse from *overpressure* diffraction around the target:

$$I_N = A\left[\frac{X}{2U}\left(3p_r + \Delta p\right)\right].$$

where
  X = one-half the width or the height, which-
     ever is smaller,
  U = velocity of the shock wave.

These values of t_1, t_2 and t_3 originally were derived from early shock tube experiments and full scale nuclear tests on structures at low pressure levels. Consequently, they are used for illustrative purposes only in this simple analysis. More recent work with two and three dimensional models in the shock tube has shown that the exact values for these times depend strongly on model shape and pressure level as well as sound velocity in the reflected pressure region on the face of the model rather than shock front velocity.

The impulse on the cube due to dynamic pressure I_q is

$$I_q = A\int_0^{t^+} q(t)C_d\,dt$$

where
  I_q = drag impulse,
  q = dynamic pressure,
  C_d = drag coefficient of the entire object, a
     combination of C_{df} and C_{db}.

By expressing p_r in terms of Δp and shock strength ξ, and U in terms of the sound velocity, c and the shock strength ξ, the drag impulse equation may be solved in terms of Δp,

ξ, C_d, and shock wave duration* t^+. The combined impulse is

$$I_T = \left\{ \left[\frac{X\Delta p}{2c} \left(\frac{42 + 24\xi}{\xi + 7} + 1 \right) \left(1 + \frac{6\xi}{7} \right)^{-1/2} \right] \right.$$
$$\left. + \left[\frac{0.54\Delta p C_d t^+ \xi}{\xi + 7} \right] \right\}.$$

The first expression in brackets, which is independent of duration, is the overpressure contribution. The second expression is the contribution of dynamic pressure.

If height of burst and ground distance are scaled as the cube root of the yield W for weapons of different yields, Δp remains constant, but the shock wave duration t^+ varies as the cube root of the yield. Thus, the yield dependence is

$$I_T = A \left[B + C \left(W^{1/3} \right) \right]$$

where B, the overpressure contribution (I_N for a 1 kt yield), and C, the dynamic pressure contribution (I_q for a 1 kt yield), are both constants. Thus, the contribution to total impulse from overpressure remains constant, while that from dynamic pressure increases as the cube root of the yield. For very low fractional kiloton yields, the loading is highly impulsive with most of the load coming from the overpressure contribution. As the yield increases, at a constant scaled height of burst and ground distance, the total impulse also increases, with an increasing fraction resulting from dynamic pressure.

Figures 9-3a and b show representative net loadings for two classes of weapon yield and two classes of structures, one small and one large. A small element would be about the size of a telephone pole or a jeep; a large element would be the size of a house or larger. Since the

reflected overpressure is more than twice the incident pressure on the front face of the element, the loading displays an initial peak value. The reflected pressure decays or clears the front face at a time that depends on the size of the element. The rapid decay for the small element may make the reflected pressure spike of no significance, whereas the slow decay for the large element creates a load that may govern the response of the target entirely. For the representative cases shown, the diffraction phase terminates at time t_{diff}, the time at which the reflected pressure has decayed to the incident pressure. At this time the drag phase begins. It continues until the end of the positive phase of the incident blast wave. The load during the drag phase is shown to be equal to the dynamic pressure, i.e., the drag coefficients of the elements are equal to 1.0. The characteristics of the target element determine whether the response of the element is governed primarily by the diffraction phase or the drag phase. Figures 9-3a and b show that for medium and high yield weapons and small elements, a much greater impulse (the area under the loading curve) occurs during the drag phase than during the diffraction phase. As the yield increases the drag phase impulse increases in importance. For large elements and large yield weapons, the diffraction phase and drag phase impulses are about equal. In this latter case the drag phase impulse may still be of no importance, because the significant target response may occur during the diffraction phase. The diffraction phase impulses are not changed by the yield of the weapon (this is true for all but very large structures exposed to low yield weapons), whereas the drag phase impulses are directly related to the weapon yield (for the same peak dynamic pressures).

In this solution it is assumed that the difference between t_p^+ and t_q^+ may be neglected, and $t_p^+ = t_q^+ = t^+$.
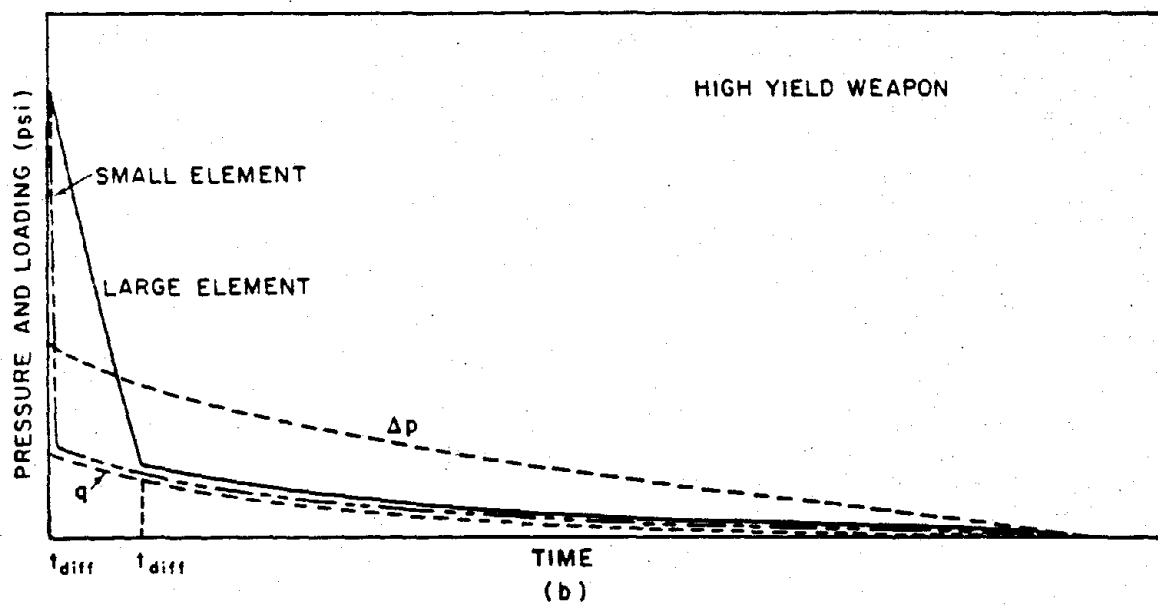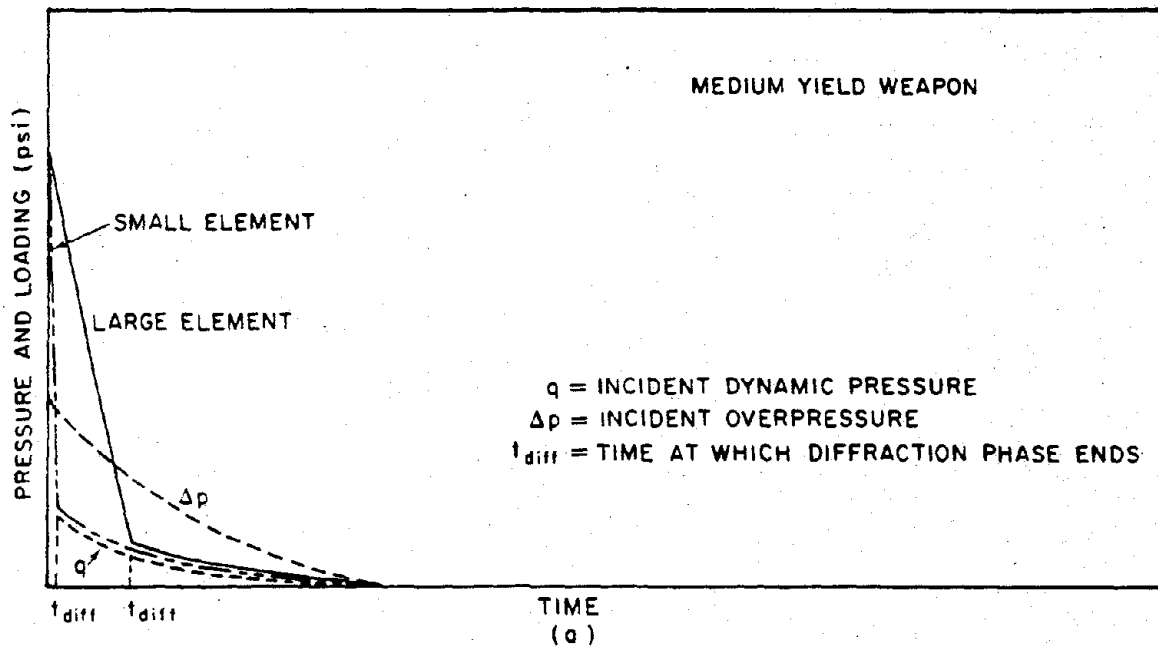
MEDIUM YIELD WEAPON

PRESSURE AND LOADING (psi)

SMALL ELEMENT

LARGE ELEMENT

q = INCIDENT DYNAMIC PRESSURE
Δp = INCIDENT OVERPRESSURE
t_{diff} = TIME AT WHICH DIFFRACTION PHASE ENDS

Δp

q

t_{diff} t_{diff}

TIME

(a)

HIGH YIELD WEAPON

PRESSURE AND LOADING (psi)

SMALL ELEMENT

LARGE ELEMENT

Δp

q

t_{diff} t_{diff}

TIME

(b)

Figure 9-3. ████ Net Blast Loading on Representative Structures ████

9-9

9-6 Regular and Mach Reflection ▮

▮ Specific aspects of the blast wave propagation must be considered when computing the load on a target. The loading of a surface target in the regular reflection region (pargraph 2-18, Chapter 2) is complicated by the vertical component of the incident blast wave, which causes multiple reflections between the ground and the target and additional reflected pressures on horizontal surfaces. In the Mach reflection region (paragraph 2-18), the loading is simplified because the blast wave propagation is horizontal. Near the surface of the ground, the vertical component of the drag forces in the regular reflection region is cancelled by the reflected wave rapidly; therefore, the brief vertical drag loading is ignored, except when the target is near the ground zero of an air burst. For aircraft in flight, the loading may be a single horizontal shock from a Mach stem or two separate shocks; the first from the free air wave and the second from the ground reflected wave. In establishing the damage curves for surface targets, the loadings on targets in the regular reflection region during the diffraction phase are considered separately from the loadings on similar targets in the Mach reflection region. The surface conditions are assumed to be average unless otherwise indicated in the figures that provide the damage curves. Objects that are primarily susceptible to horizontal drag loading in the Mach reflection region may become primarily susceptible to crushing action if they are in the early regular reflection region.

9-7 Target Motion ▮

▮ When air blast loading is considered, the movement of the target component during loading is assumed to have negligible effect on the loading itself. Aircraft and missiles in flight are exceptions. Their speed, orientation, and movement during loading assume increased importance (see Chapters 13 and 16).

9-8 Nonideal Waveforms ▮

▮ As discussed in paragraphs 2-31 and 2-32, ideal waveforms are seldom found along the surface for overpressure levels above 6 psi. The description of the diffraction and drag phases given in preceding paragraphs is not true in regions of nonideal waveforms. If the overpressure wave has a long rise time (30 to 40 msec) to a peak value, full reflection of the wave from the surface of a structure will not occur. At the same time, the relationship between dynamic pressure and overpressure is different from that described for the ideal blast wave. During the diffraction phase, the drag forces caused by high dynamic pressures may be the predominant damage-producing criteria. Since many conventional surface structures sustain severe damage at low peak overpressure levels, and nonideal waveforms occur only in the higher overpressure regions, such waveforms were not considered in determining damage criteria for such structures. Careful consideration must be given to nonideal waveforms when assessing the vulnerability of protective structures that were designed to withstand high overpressures. The dynamic pressures for such waveforms generally will be higher than would be expected if the blast wave were ideal. There are few data on blast loading in the high pressure regions.

9-9 Underwater Shock Wave Loading ▮

▮ The air blast wave operates in a compressible fluid, while the water shock wave operates in a noncompressible fluid. This difference in medium accounts for the differences in detail betweeen air blast and water shock loading. The peak values in water are higher than they would be at the same distance from an explosion of the same yield in air. However, the duration of the shock wave in water is shorter than in air. When the shock wave strikes a rigid, submerged surface, such as the sea bottom, it is reflected.

When the shock wave reaches the air-water surface (a less rigid medium), however, a refraction (or negative pressure) wave occurs. The combination of the surface reflected shock wave and the direct shock wave produces a sharp decrease or "cutoff" in the water shock overpressure, as shown in Figure 9-4. Incidence of a shock wave on a ship or structure produces damage through the direct mechanism of overpressure (or excess impulse) and by imparting a transitional velocity to the target structure.

9-10 Ground Shock Loading

The loading of buried structures by ground shock is connected intimately to the response of the structures. For certain underground structures, serious damage will only occur if the ground shock is so intense that the damage area for those structures is confined closely to the crater area of a surface or underground explosion. For structures near the surface, air blast induced ground shock may cause significant damage. The damage to these structures is more closely related to air blast pressures than it is to crater dimensions. Loading pressures are numerically equal to the ground stress normal to the structure. Such pressures do not produce detectable reflected pressures. Internal equipment of a structure may be subjected to ground shock accelerations that will severely damage the equipment without damaging the structure. For a discussion of accelerations resulting from ground shock see Section III. Chapter 2, and Sections II and III, Chapter 11.

RESPONSE AND DAMAGE

Damage to a target is closely related to, and is a direct derivative of, its response. For targets anchored to the ground, damage is usually the result of displacement of one part of the target with respect to another part, resulting in permanent distortion, collapse, or toppling. For movable targets, however, the target may be moved by the loading with or without a resulting damage. In the latter case, the damage to the target is governed primarily by the manner in which the moving target comes to rest. Whether drag phase loading or diffraction phase loading causes the greater damage will depend upon the weapon yield, target characteristics, and the damage level considered.

9-11 Surface Structures

The predominant cause of failure to large targets, such as buildings that have small window areas compared to wall areas that either support the structure or are as strong as the structural frames, is the pressure differential between the front and rear faces that exists for a relatively long period of time. If the window area is large, the pressure on each wall is equalized quickly by the entry of the blast wave through the windows. The pressures exerted on the inside of the wall reduce the translational force on the wall. This translational force also is reduced because of a smaller wall area on which the pressures can act; however, the force exerted on interior partitions and rear walls tends to offset the reduction in front face loading in the production of total damage. When the overpressures causing translational force on the structural component are equalized quickly as a result of the geometry or construction of the building, the primary damaging forces are those that are significant in damaging structural components that have fairly small cross sections, such as columns and beams. Structures that are normally damaged by drag forces include smoke stacks, telephone poles, truss bridges, and steel or reinforced concrete frame buildings with light walls. These buildings are drag sensitive, because the light walls of corrugated steel, asbestos, or cinder block fail at low reflected pressures, and they do not transmit a significant load to the structure frame. Only the frame is exposed to the blast, and, being composed of small cross
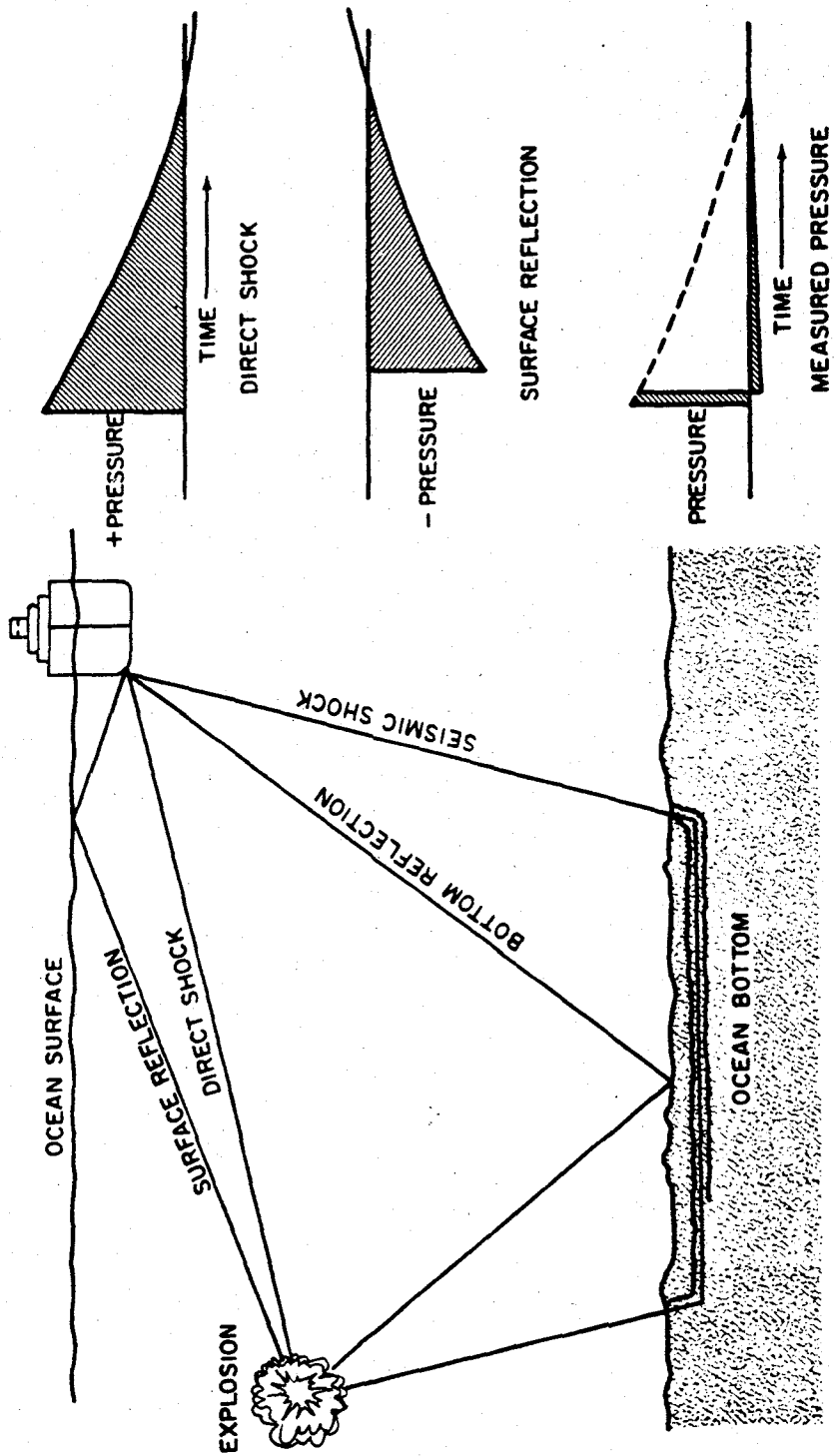
Figure 9-4. Direct and Reflected Shock Waves from an Underwater Burst

section structural elements, it is distorted primarily by drag forces. These buildings are not considered severely damaged unless the structural frame has collapsed or is near the point of collapse. A tree is a good example of a drag sensitive target, because the duration of the diffraction phase is extremely short and there is considerable force applied by the high wind velocity drag loading. Most military field equipment is drag sensitive, because damage generally results from the tumbling or overturning caused by the drag forces.

9-12 Shielded Structures █

█ If the target is shielded from the drag forces, or if it lies within the early regular reflection region, high overpressures may become the damage producing criteria. For blast resistant aboveground structures designed to resist more than 5 to 10 psi overpressure, the distinction between diffraction and drag sensitivity cannot be defined well, because full reflection from the surface of the structure does not occur, and dynamic pressures exceed those expected in the case of the incident waveform. As a result, drag forces may be predominant in producing damage, even during the diffraction phase.

9-13 Aircraft █

█ Aircraft may be damaged by the forces developed in the diffraction phase, in the drag loading phase, or in both. Parked aircraft can receive light, crushing forces corresponding to low overpressures. For example, light skins and frames are easily dished and buckled at relatively low overpressures. At higher overpressure levels, drag loading (referred to as "gust loading" with respect to aircraft) adds to the damage. At these levels, much of the damage may result from translation and overturning of the aircraft. For aircraft in flight, the diffraction and drag forces combine with the existing aerodynamic forces to develop destructive loads on airfoils at low over-

pressure levels. The diffraction or crushing overpressure effects on the fuselage and other thin skinned components, however, are usually of secondary importance for most in-flight aircraft. Responses of aircraft are discussed in more detail in Chapter 13.

SECTION III
█ THERMAL RADIATION DAMAGE █

█ INTRODUCTION █

█ Two important effects of thermal radiation are injuries to personnel (burns) and fires that might be ignited in the target area. Burns to personnel are treated in Section II of Chapter 10. Section VII of Chapter 11 discusses fires in urban areas. Section III of Chapter 15 discusses fires in forest stands. The effects of thermal radiation on various classes of equipment are described in other chapters of Part II. This section contains a description of the properties of materials that might result in ignition or degradation of their physical properties. A brief discussion of survival in fire areas is also provided. Section IV describes the degradation of structural resistance to air blast of materials, primarily metals, as a result of thermal radiation.

█ Chapter 3 provides the data necessary to estimate the thermal environment. In general, thermal damage is likely to be more important than blast damage for surface targets for high yield weapons that are air bursts rather than surface bursts. As discussed in Chapter 3, the influence of weather makes thermal effects much less predictable than blast effects. Clouds or haze can provide a protective screen, and moisture from an earlier rain can reduce the number of fires in outdoor targets. In some cases, cloud cover can enhance thermal effects on the ground. The criteria for thermal damage given in succeeding paragraphs are representative values

for dry materials directly exposed to the thermal source. These values should be applied with the understanding that they can be modified by a variety of factors discussed briefly in the following paragraphs.

9-14 Radiant Exposure

The thermal damage inflicted on a target depends upon the incident energy per unit area. This quantity is called radiant exposure and, as described in Chapter 3, it usually is expressed in calories per square centimeter (cal/cm^2). Radiant exposures below 2 cal/cm^2 will produce little damage other than possible eye injury (Section II, Chapter 10). Radiant exposures above 10 cal/cm^2 usually produce significant damage in unprotected target areas.

9-15 Thermal Pulse Duration

The radiant exposure required to damage a particular target varies with the duration of the thermal pulse. The reason is readily seen from the following example: about 3 to 5 cal/cm^2 from a short thermal pulse, e.g., from a 1 kt detonation, will produce a second degree burn on bare skin, but direct sunlight delivers the same radiant exposure in a little over 2 minutes with no serious effects.

The time scale of the thermal pulse from low altitude nuclear weapon bursts may be characterized by the parameter t_{max}, the time during the final pulse at which the fireball is radiating maximum power. This time increases with increasing yield and decreases with increasing altitude. The relation of t_{max} to pulse duration and the method for calculating t_{max} are given in Chapter 3. As described in Chapter 3, the time scale of the thermal pulse may be specified indirectly in terms of yield for low altitude bursts. The thermal pulse for high altitude bursts (up to about 100,000 feet) may be described in terms of an equivalent sea level burst. Specifying the thermal pulse duration in terms of yield is convenient since it eliminates the necessity to calculate t_{max}; therefore, many damage criteria are given in terms of radiant exposure and yield rather than radiant exposure and time to final maximum.

9-16 Target Response

For most materials, the heat absorbed from the thermal pulse initially is confined to a thin surface layer. Damage usually results from high surface temperatures. The nature and the degree of the damage depend not only on the intensity and duration of the thermal pulse, but also on several properties of the material that are described below.

Thickness. Thick organic materials such as wood, plastics, and heavy fabrics char and may burst into flame while exposed to the thermal pulse; however, this flaming is only a transient effect. As the radiant pulse decays, the absorbed thermal energy continues to penetrate the material. This flow of heat allows the surface to cool to a temperature too low to support combustion.

Thin materials, such as light fabrics, newspaper, dry leaves, and dry grass tend to become hotter than the surfaces of thicker materials since the absorbed thermal energy is confined to a relatively small volume of material. Also, since these materials are heated throughout, they usually continue to burn once they are ignited. Moreover, subsequent arrival of the blast wave frequently will fail to extinguish the fire.

Thermal Conductivity. Most metals allow rapid penetration of thermal energy to depths below the surface as a result of their high values of thermal conductivity. Consequently, the peak surface temperatures induced in thick pieces of metal are considerably less than the peak surface temperatures induced in most nonmetallic materials. Thin pieces of metal may fail as a result of the combined effects of the thermal pulse, which reduces the strength of the metal by heating it, and the blast wave, which causes it to bend or collapse. This effect is dis-

cussed in more detail in Section IV. Dry rotted wood (or punk) has a lower thermal conductivity than sound wood as a result of its porous structure. When the surface of punk is ignited by a thermal pulse, conduction of heat to the interior is too slow to allow significant cooling of the surface, and burning continues.

■ *Color*. Light colored objects of a given thickness are more resistant to thermal radiation than dark colored objects, because they reflect more of the incident energy. Color has little effect on the response of materials that blacken (char) early in the thermal pulse, because the energy delivered during the remainder of the pulse is absorbed efficiently by the charred surface.

■ *Transparency*. Transparent materials are relatively resistant to thermal damage (even though transparency in the visible region does not assure that the material is transparent to infrared) because the radiant energy that passes through them usually does not contribute to heating. Partially transparent materials are thermally resistant because the incident thermal energy is deposited over a range of depths rather than being confined to a thin surface layer. Peak temperatures induced in partially transparent materials therefore are likely to be lower than the peak temperatures produced at the surfaces of opaque materials.

■ *Moisture Content*. Thermal damage to materials that absorb moisture depends on the percentage of water in such materials. Usually, the moisture content varies with the prevailing relative humidity. Exposure to recent rain, however, may alter the moisture content significantly. Scorching or charring of an organic surface by radiant energy is preceded by vaporization of the water. Consequently, more energy is required to produce a given damage effect on wet surfaces or on targets in highly humid atmospheres. Materials located indoors and exposed to thermal radiation through windows are damaged more readily during the latter part of the heating season (late winter and early spring), largely because of decreased interior humidities.

9-17 Target Orientation ■

■ In clear atmospheres and in the absence of reflecting surfaces, the amount of energy incident on a unit area of a target surface is greatest when the surface is directly facing the burst. If the target surface is not facing the burst, the energy per unit area depends on the angle between the perpendicular to the surface and the direction of the incoming radiation.

■ When the atmosphere is hazy, much of the energy received at the target is scattered by atmospheric particles, arrives from all directions, and reaches portions of the target that are not exposed to direct radiation. Scattered energy is likely to be a large fraction of the total energy received when the slant range from the burst to the target exceeds about half the visual range. Reflection from clouds and from the ground can produce similar effects.

9-18 Shielding ■

■ Any object that casts a shadow is capable of shielding objects behind it from the direct component of thermal radiation. Trees, buildings, foxholes, hills, etc. offer effective protection except when the scattered component of thermal radiation is large. After leaves have been stripped by the dynamic pressure (wind) of a nuclear burst, the trees offer little shielding from the thermal radiation produced by a second burst. Reflection of thermal radiation from exposed walls of foxholes is about 5 percent.

■ THERMAL RESPONSE OF MATERIALS ■

■ The amount of thermal radiation that a material will absorb depends on the properties of the material discussed in paragraph 9-16. The amount of energy absorbed usually is determined by multiplying the incident energy by an

absorption coefficient. The absorption coefficient cannot be measured directly, but a good estimate can be made by performing spectral measurements of reflectance (the fraction of incident energy reflected from the surface) over the range of wave lengths of the nuclear spectral distribution and by finding an average value of reflectance. The coefficient of absorptance is equal to one minus the average value of the reflectance. The absorptance determined in this manner is valid only as long as the surface does not change as a result of the absorbed thermal energy. Another approach is to divide the quantity of energy absorbed by the incident energy. The absorbed energy is determined from experimentally determined temperature vs time relationships and appropriate theoretical energy balance relationships. Absorptance is a function of time and temperature although an average value is usually employed. This function when known may be found as an input specification for certain computer programs. In the absence of more definitive data for a specific systems, an absorption coefficient of 0.5 is a reasonable value to assume for many materials, particularly metals. For a conservative defensive assumption, the absorption coefficient may be taken to be 1.0 (i.e., total absorption), particularly for dark porous materials.

In many cases, it is appropriate to consider only one or two fuel types, assuming that these fuels are the critical items that will determine whether fires are started in a particular area. In other cases, more detail is required. For example, an estimate of the thermal energy that will ignite a particular type of material used in military uniforms may be desired. The data contained in the succeeding paragraphs is intended as a guide in the solution of more specific problems.

9-19 Thickness Effects

The time required for thermal energy to penetrate very thin materials is short compared to the duration of the thermal pulse. At the end of the pulse, the absorbed thermal energy is distributed more or less uniformly throughout the material. In very thick materials, the end of the pulse finds most of the absorbed thermal energy in a surface layer, with the bulk of the material almost unaffected.

If the terms thermally "thin" and thermally "thick" are used to distinguish between materials that are heated throughout from those that are initially heated only at the surface, it is apparent that physical thickness is not the only parameter involved. For example, as a result of the rapid penetration of heat into metals, a sheet of metal is more likely to be thermally thin than is a sheet of insulating material of the same physical thickness.

The ability of a short pulse of energy to penetrate a target material is most readily measured in the laboratory and most readily treated analytically if the thermal pulse is given a rectangular waveform rather than the more complex waveform produced by a nuclear weapon. A parameter that is useful for calculating thermal response of materials is the characteristic thermal response time τ_o, given by the equation

$$\tau_o = \rho C_p L^2 / k \text{ sec,}$$

where k is thermal conductivity (cal-sec^{-1} cm^{-1} $^\circ C^{-1}$), ρC_p is heat capacity per unit volume (ρ = density in g-cm^{-3} and C_p = specific heat at constant pressure in cal-g^{-1} $^\circ C^{-1}$), and L is the thickness, in centimeters, of the layer of material.

The quantity

$$\alpha = \frac{k}{\rho C_p}$$

is called thermal diffusivity (cm^2/sec). Use of this quantity simplies the previous equation to

$$\tau_o = \frac{L^2}{\alpha} \text{ sec.*}$$

Thermal diffusivity and other properties of a number of materials are shown in Table 9-1.

■ Characteristic time may be related in several ways to the thermal response of a target. Most important is that the ignition of thin fuels by a rectangular thermal pulse requires the least radiant exposure when pulse duration is about equal to τ_o.

■ Two other relations apply to a thick slab of material. For any particular material exposed to a rectangular pulse of length τ, the previous equation can be transformed to give a characteristic thickness

$$\delta = \sqrt{\alpha\tau} \text{ cm,}$$

for which the characteristic time is equal to the pulse duration. If a thick slab of this material is exposed to a pulse of length τ, the temperature rise at the surface is the same as would be produced by uniformly distributing the absorbed thermal energy in a slab of thickness δ, and the peak temperature rise at depth δ in the thick slab is about half as great as the peak temperature rise at the surface.

■ For example, consider a block of red pine that is exposed to 15 cal/cm² from a rectangular pulse of 3 seconds duration. From Table 9-1, the properties of red pine are

$$\rho = 0.51 \text{ g/cm}^3,$$

$$C_p = 0.4 \text{ cal/g} \cdot {}^\circ C,$$

$$\alpha = 24 \times 10^{-4} \text{ cm}^2/\text{sec.}$$

The characteristic depth is

$$\delta = \sqrt{\alpha\tau} = \sqrt{(24 \times 10^{-3})(3)} = 0.085 \text{ cm.}$$

The mass of wood per unit area in a slab of this thickness is

$$\rho\delta = (0.51)(0.085) = 0.043 \text{ g/cm}^2.$$

The heat absorbed by the wood before it begins to scorch is equal to the product of the incident radiant energy, Q, and the absorption coefficient, A. If the absorption coefficient is assumed to be 0.5,

$$QA = (15)(0.5) = 7.5 \text{ cal/cm}^2.$$

Absorption of this amount of energy in a layer of thickness δ would result in an energy density of

$$\frac{QA}{\rho\delta} = \frac{7.5}{0.043} = 174 \text{ cal/g.}$$

If the energy were evenly distributed through this layer, the resulting temperature rise would be

$$\frac{QA}{\rho\delta C_p} = \frac{174}{0.4} = 435^\circ C.$$

and the peak temperature rise at the surface of the wood would be about the same.

■ The result obtained above may be generalized as follows:

$$\Delta T_s = \frac{QA}{\rho\delta C_p} = \frac{QA}{\rho C_p \sqrt{\alpha\tau}} = \frac{QA}{\rho C_p \sqrt{\tau k/\rho C_p}}.$$

---

* ■ This equation is useful, but it is by no means exact. The simplified heat-flow analysis from which this equation is derived neglects the effects of radiation and convection heat losses from the surfaces of the exposed sample. It also assumes an isotropic medium, i.e., a medium whose structure and properties in the neighborhood of any point are the same relative to all directions through the point. It also neglects the changes in thermal properties that occur as the exposed material heats, volatilizes, chars, and bursts into flame.

Table 9-1. ███ Thermal Properties of Materials ██

Materials	Density, ρ (gm/cm^3)	Specific Heat, C_p (cal/gm $\cdot$ °C)	Conductivity, k (cal/sec $\cdot$ cm $\cdot$ °C)	Diffusivity, α (cm^2/sec)
Insulating Materials				
Air	9.46×10^{-4}	0.24	0.55×10^{-4}	0.22
Asbestos	0.58	0.20	4.6×10^{-4}	$40. \times 10^{-4}$
Balsa	0.12	0.4	1.2×10^{-4}	$25. \times 10^{-4}$
Brick (common red)	1.8	0.2	$16. \times 10^{-4}$	$18. \times 10^{-4}$
Celluloid	1.4	0.35	5.0×10^{-4}	$10. \times 10^{-4}$
Cotton, sateen, green	0.70	0.35	1.5×10^{-4}	2.5×10^{-4}
Fir, Douglas-				
spring growth	0.29	0.4	$2. \times 10^{-4}$	$17. \times 10^{-4}$
summer growth	1.00	0.4	$5. \times 10^{-4}$	$12. \times 10^{-4}$
Fir, white	0.45	0.4	2.6×10^{-4}	$14. \times 10^{-4}$
Glass, window	2.2	0.2	$19. \times 10^{-4}$	$43. \times 10^{-4}$
Granite	2.5	0.19	$66. \times 10^{-4}$	$140. \times 10^{-4}$
Leather sole	1.0	0.36	3.8×10^{-4}	$11. \times 10^{-4}$
Mahogany	0.53	0.36	3.1×10^{-4}	$16. \times 10^{-4}$
Maple	0.72	0.4	4.5×10^{-4}	$16. \times 10^{-4}$
Oak	0.82	0.4	5.0×10^{-4}	$15. \times 10^{-4}$
Pine, white	0.54	0.33	3.6×10^{-4}	$18. \times 10^{-4}$
Pine, red	0.51	0.4	$5. \times 10^{-4}$	$24. \times 10^{-4}$
Rubber, hard	1.2	0.5	3.6×10^{-4}	$60. \times 10^{-4}$
Teak	0.64	0.4	4.1×10^{-4}	$16. \times 10^{-4}$
Metals (100°C)				
Aluminum	2.7	0.22	0.49	1.0
Cadmium	8.65	0.057	0.20	0.45
Copper	8.92	0.094	0.92	1.1
Gold	19.3	0.031	0.75	1.2
Lead	11.34	0.031	0.081	0.23
Magnesium	1.74	0.25	0.38	0.87
Platinum	21.45	0.027	0.17	0.29
Silver	10.5	0.056	0.96	1.6
Steel, mild	7.8	0.11	0.107	1.2
Tin	6.55	0.056	0.14	0.38
Miscellaneous Materials				
Ice (0°C)	0.92	0.492	$54. \times 10^{-4}$	$120. \times 10^{-4}$
Water	1.00	1.00	$14. \times 10^{-4}$	$14. \times 10^{-4}$
Skin (porcine, dermis, dead)	1.06	0.77	$9. \times 10^{-4}$	$11. \times 10^{-4}$
Skin (human, living, averaged for upper 0.1 cm)	1.06	0.75	$8. \times 10^{-4}$	$30. \times 10^{-4}$
Polyethylene (black)	0.92	0.55	$8. \times 10^{-4}$	$17. \times 10^{-4}$

where ΔT_s is the peak temperature rise at the surface. The parameters that define the thermal pulse may be separated from those that define the material properties. and

$$\Delta T_s = \left(\frac{Q}{\sqrt{\tau}} \right) \left(\frac{A}{\sqrt{k\rho C_p}} \right).$$

For a fixed rectangular pulse. $Q/\sqrt{\tau}$ is a constant. and the equation may be written

$$\Delta T_s = (K) \left(\frac{A}{\sqrt{k\rho C_p}} \right).$$

In practice. the surface temperature rise produced in a thick material is approximately proportional to $A/\sqrt{k\rho C_p}$ over a wide range of pulse shapes and pulse times. Thus. this parameter may be used as a measure of the relative susceptibility of various materials to surface heating.

Direct measurements of the ignition properties of a representative cellulosic fuel have been reported. The material is α-cellulose. blackened by the addition of carbon. and made into sheets of various thicknesses. This material has the uniformity required to obtain repeatable test results. and its thermal properties are similar to those of common cellulosic fuels. such as paper and dry leaves.

Figure 9-5 shows the results of exposing this material to the idealized rectangular thermal pulse. Figure 9-6 shows the results obtained in the more practical case of a simulated weapon pulse. These curves show data for black α-cellulose sheets of a variety of thicknesses by using normalized coordinates. The ordinate is normalized radiant exposure. One unit on this scale corresponds to the energy per unit area that will raise the temperature of the entire sheet 1°C. Thus. a given value of the ordinate represents a higher radiant exposure for a thicker sheet of cellulose. The abscissa of Figure 9-5

is normalized pulse duration, the duration of the rectangular pulse divided by τ_o, the characteristic thermal response time of the sheet of material. The abscissa of Figure 9-6 is a similar normalized time. t_{max}/τ_o. Normalization fails in the case of long pulses, and the curves break into families of curves for different thicknesses of material.

If the pulse has such a short duration that the exposed surface reaches the ignition temperature while the back surface remains cool. two distinct ignition thresholds appear. Low values of radiant exposure produce high surface temperatures and flames, but the flames do not persist after the end of the thermal pulse. This region is labeled transient ignition in Figures 9-5 and 9-6. Sustained ignition only occurs when higher radiant exposures raise the temperature throughout the thickness of the cellulose to a level that is sufficiently high to sustain the flow of combustible gases from breakdown of the fuel. It is difficult to supply sufficient energy with short pulses, since a large amount of the energy that is deposited is carried away by the rapid ablation of the thin surface layer. This transient flaming phenomenon is typical of the response of sound wooden boards to a thermal pulse.

If the pulse is of long duration. the ignition threshold rises because the exposed material can dissipate an appreciable fraction of the energy while it is being received. For very long rectangular pulses an irradiance of about 0.5 cal · $cm^{-2} sec^{-1}$ is required to ignite the cellulose. Heat supplied to the material at a slow rate is just sufficient to offset radiative and convective heat losses, while maintaining the cellulose at the ignition temperature of about 300°C.

Materials respond to the thermal pulse from a nuclear weapon in much the same way that they respond to a rectangular thermal pulse; however. a number of practical effects make a thorough analysis of ordinary fuels ignited by
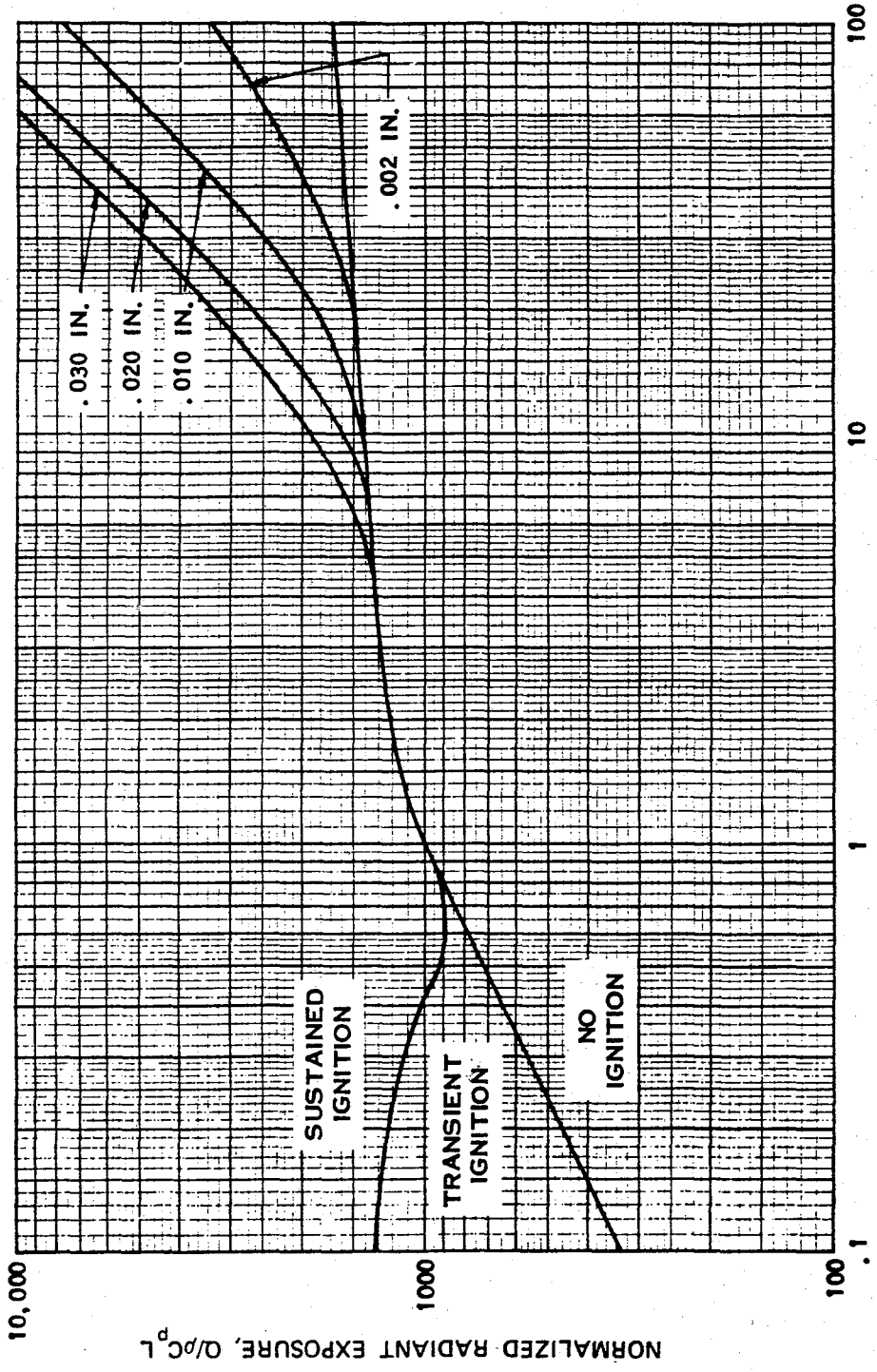
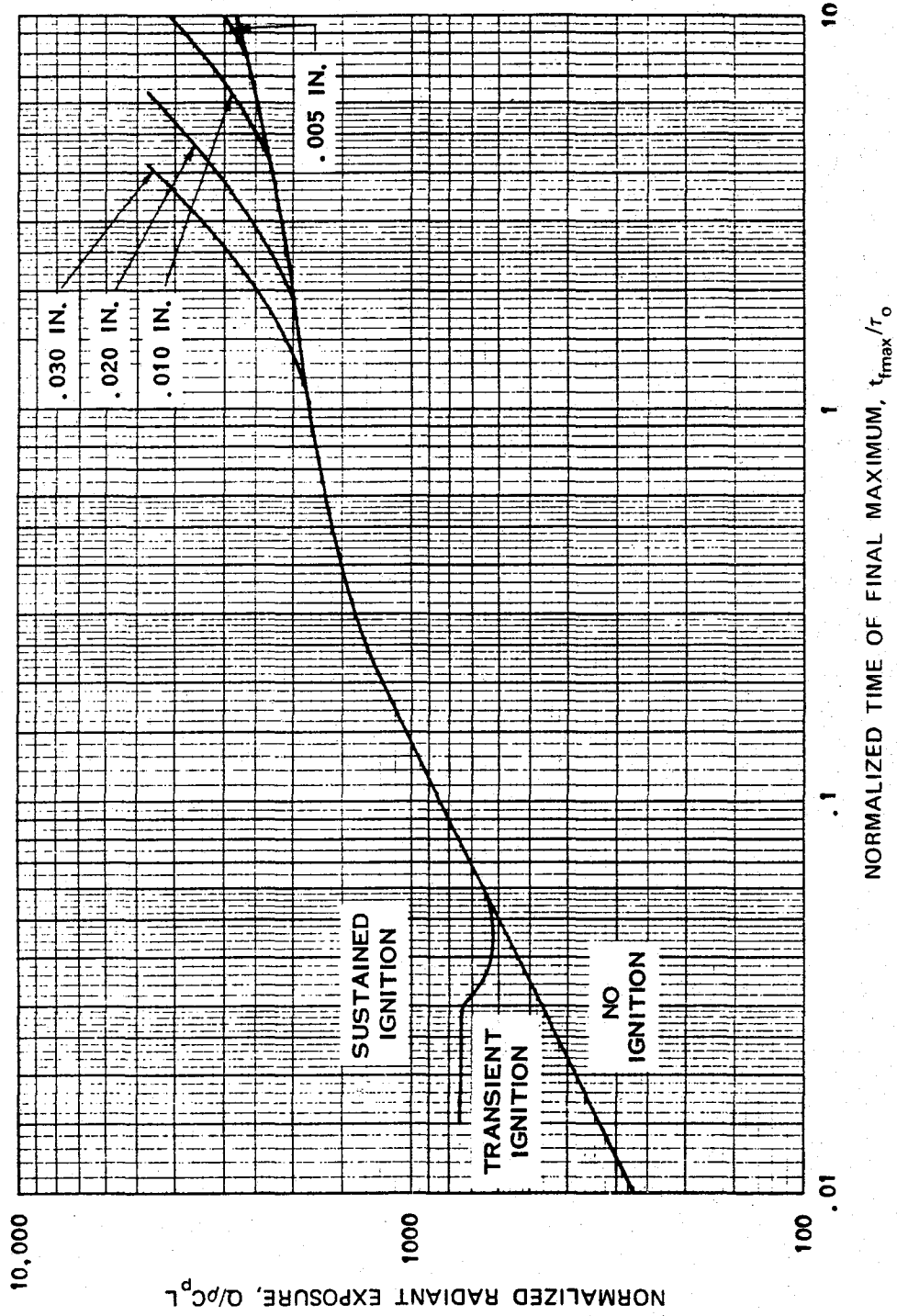Figure 9-5. Ignition Thresholds for Black α-Cellulose Exposed to a Rectangular Thermal Pulse

Figure 9-6. Ignition Thresholds for Black α-Cellulose Exposed to a Simulated Weapon Pulse

weapon pulses difficult. While the fuel absorbs heat and its surface chars, its absorption coefficient changes. As a result, the shape of the energy pulse actually absorbed by the material differs from that of the incident energy pulse (this effect is avoided in the α-cellulose by making the material black initially). A weapon pulse has no single rectangular wave equivalent, since the nature of material response to a thermal pulse varies with pulse shape as well as pulse length. However, for many calculations a rough equivalence may be obtained by assigning between 2.5 and 3 times the irradiance of the rectangular pulse to the weapon pulse.

█ Both rectangular and weapon pulse data show an optimum pulse length for igniting materials. For the rectangular pulse, this optimum occurs with a pulse length slightly shorter than the characteristic thermal response time of the material. A pulse of this optimum duration lasts long enough to allow an appreciable amount of heat to penetrate to the back face, but it is short enough that only a small heat loss occurs during the pulse.

█ For example, consider newsprint that is 0.008 cm thick, which has a thermal diffusivity, α, of 10^{-3} cm^2/sec. From the equation given previously

$$\tau_o = \frac{L^2}{\alpha}.$$

From Figure 9-6, the threshold for sustained ignition of black α-cellulose is a minimum when

$$\frac{t_{max}}{\tau_o} = \frac{t_{max}\alpha}{L^2} = 0.045.$$

The properties of newspaper are similar to those of α-cellulose, so the same relation may be assumed to hold for the newsprint. Thus,

$$t_{max} = 0.045 \frac{L^2}{\alpha} = \frac{(0.045)(0.008)^2}{0.001}$$

$$t_{max} = 2.9 \times 10^{-3} \text{ sec.}$$

From the equation given in Chapter 3

$$t_{max} = 0.043 \ W^{0.43} \ (\rho/\rho_o)^{0.42} \text{ sec.}$$

At sea level $\rho = \rho_o$, and

$$W = (t_{max}/0.043)^{2.3}$$

$$W = \left(\frac{2.9 \times 10^{-3}}{4.3 \times 10^{-2}}\right)^{2.3} = 0.002 \text{ kt.}$$

This yield is so small that little confidence may be placed in the result; however, this example demonstrates the general rule that short thermal pulses are more likely to ignite newsprint than long pulses over the range of yields that probably will be of practical importance.

9-20 Color █

█ Although thermal damage depends on the radiant exposure to which a target is subjected, it depends in a much more direct manner on the amount of thermal energy absorbed. Thus color, which indicates the amount and spectral distribution of the visible energy reflected, is one indication of the resistance of a material to thermal damage.

█ White materials reflect most of the energy in the visible portion of the spectrum that is incident on them, but all cellulosic fuels (which constitute the commonest potential ignition sites) absorb energy in the near infrared region. Cellulosic materials also char in response to high radiant exposures, and once the surface begins to blacken they absorb strongly. The total amount of energy absorbed depends on the absorption coefficient averaged not only over the spectrum of energies contained in the thermal pulse, but also over the interval of time during which the pulse is received. For a thin cellulosic material exposed to a moderately high level of radiant energy (just enough to ignite the ma-

terial) blackening will not occur immediately, and the following rules give an effective average for the absorption coefficient that is roughly correct.

- If the material is white or nearly white, the effective absorption coefficient for the thermal pulse is about the square root of the absorption coefficient for visible light. *Example:* If the visible absorption coefficient is 0.1, the effective absorption coefficient for the thermal pulse is about 0.3.
- If the material has a color that is as dark as or darker than dove gray (a fairly light shade of gray), the effective absorption coefficient for thermal radiation is about equal to the visible absorption coefficient.
- The response of most of the nonwhite materials that provide potential ignition sites may be approximated by assigning an effective absorption coefficient of 0.5.

9-21 Transparency █

█ The energy that passes through a partially transparent material cannot heat it. Thus, the energy deposited in the material is the incident energy minus the reflected energy minus the transmitted energy.

█ The depth of penetration of thermal energy into a partially transparent material is determined by two mechanisms: heat absorbed at or near the surface penetrates by diffusion; and heat penetrates as radiant energy before it is absorbed. As shown in paragraph 9-19, the diffusion of heat may be associated with a transient thickness δ. Similarly, the penetration of thermal energy due to diathermancy (partial transparency) may be associated with a characteristic depth of $1/\beta$, where β is the extinction coefficient. In a practical situation, both of these mechanisms work simultaneously, and the heat penetrates deeper than it would if only one mechanism were effective.

█ Usually, one or the other of the two mechanisms is dominant. If the product $\beta\delta$ exceeds 3 or 4, penetration will occur principally by diffusion. If the product is less than about 1/4, penetration will be principally by transmission of radiant energy. Temperature profiles in a semi-infinite solid are shown in Figure 9-7 in terms of dimensionless parameters, where ΔT is temperature rise, k is thermal conductivity, ρ is density, C_p is specific heat, H is energy absorbed (not the incident energy) per unit area, τ is rectangular pulse duration, and δ is characteristic depth defined in paragraph 9-19.

9-22 Effect of Humidity █

█ The water content of thin fuels responds rapidly to changes in humidity. The radiant exposure that is required to ignite a thin cellulosic fuel is approximately

$$Q = Q_0 \ (1 + h/2).$$

where h is relative humidity and Q_0 is the radiant exposure that will ignite the fuel when it is completely dry.

█ In general, ignition data give radiant exposure thresholds for average rather than extremely dry conditions. If the tabulated value of radiant exposure Q_1 applies to a relative humidity of h_1, the equation given above becomes

$$Q = Q_1 \ \frac{1 + h/2}{1 + h_1/2}.$$

█ For example, if the radiant exposure from a 1 Mt explosion that is required to ignite new white bond paper is 30 cal/cm^2 when the relative humidity is 65 percent, the ignition threshold for the same explosion when the relative humidity is 15 percent is

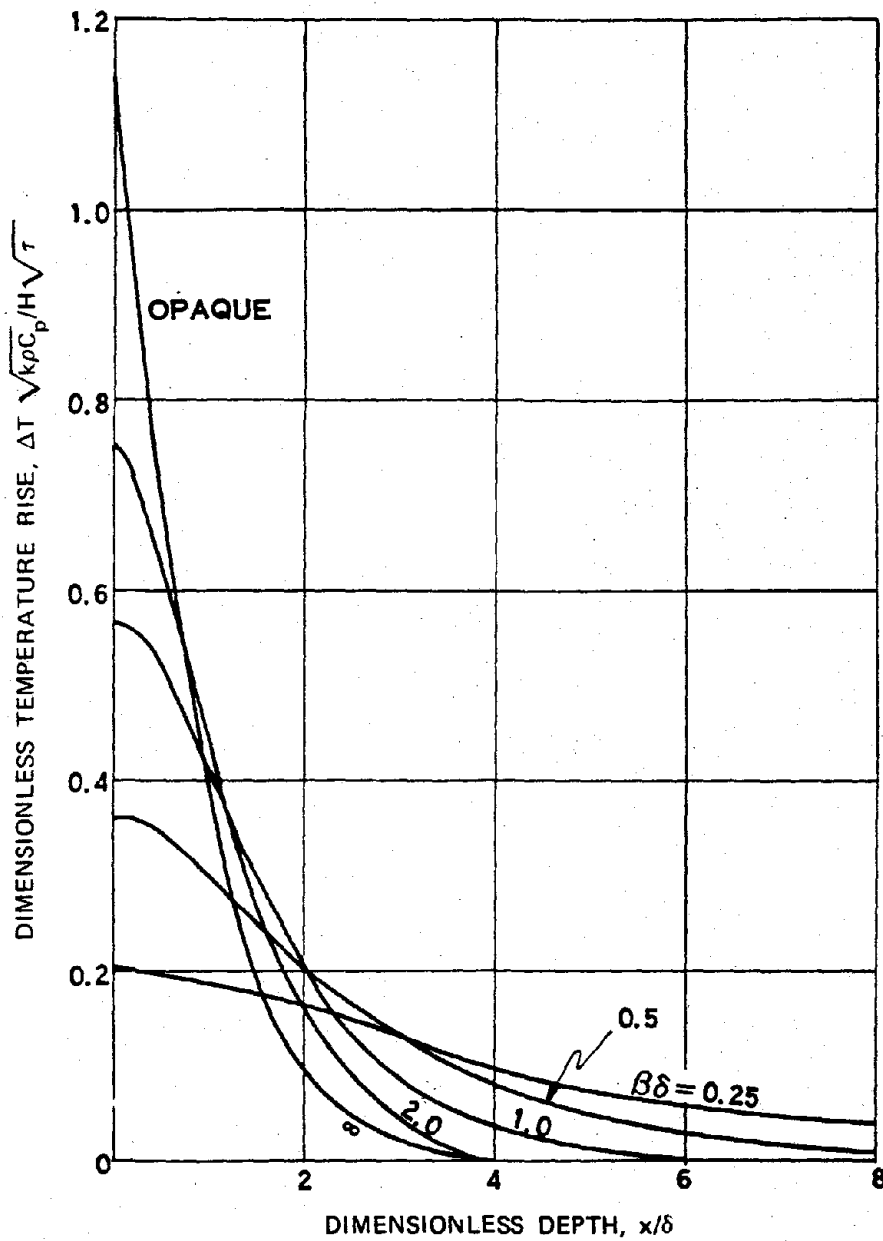$$Q = (30) \left(\frac{1 + 0.15/2}{1 + 0.65/2}\right) = 24 \ \text{cal/cm}^2.$$

Figure 9-7. ▬ Dimensionless Temperature Profiles in Opaque and Diathermanous Semi-Infinite Solids Exposed to a Rectangular Thermal Pulse ▬

9-23 Response of Metal Sheets ▉

▉ Both the tensile strength and the elastic modulus of metals tend to decrease with increasing temperature. Thus, thermal energy has the potential to weaken metallic structural members. If exposed metal parts are essential to the strength of a structure or a piece of equipment, weakening the metal by heating it may make the unit more susceptible to damage by the blast wave.

▉ Most structural metal is relatively immune to this form of damage in the loading levels of interest. If a heavy part such as a steel I-beam is subjected to a thermal pulse that is sufficiently intense to weaken it appreciably, it is probably so close to the burst that the blast wave could demolish the structure without assistance from the thermal pulse. Walls or roofs usually shield heavy structural members from the thermal pulse.

▉ Light weight units are more likely to be vulnerable to this synergistic damage. The outer covering and the materials that give these units mechanical strength are frequently one and the same. The material is likely to be an aluminum alloy, which loses strength at a much lower temperature than steel.

(U) The degradation of the response of metals to the blast wave as a result of thermal exposure is discussed in more detail in Section IV of this chapter.

9-24 Thermal Damage to Various Materials ▉

▉ The general trends discussed in the preceding paragraphs are illustrated by a number of specific examples in Tables 9-2 and 9-3. These tables show the critical radiant exposures for specified damage to fabrics and to various other materials, respectively. The radiant exposures are shown for three weapon pulse durations. The corresponding yields are shown in the footnote for low air bursts (note that altitude scaling is required for a 24 Mt burst to be considered an air burst (see Chapter 3)). Various yield/altitude combinations that will give the same values of t_{max} may be obtained by the methods described in Chapter 3.

▉ The values presented in Table 9-2 for fabrics apply for an ambient relative humidity of 65 percent and an ambient temperature of 20°C. For extremely dry conditions, the values shown for fabrics should be reduced by 25 percent. For extremely high relative humidities, near 100 percent (at 20°C), the values for fabrics should be increased by 25 percent. If the fabrics are water-soaked, the critical radiant exposures should be increased by 300 percent. The values for uniforms in Table 9-2 refer to damage to the material itself. They are not applicable for predicting skin burns under uniforms. However, when the outer garment ignites, the probability of skin burns should be considered.

▉ The effect, "tears on flexing," indicates the radiant exposure level at which the outer garment ceases to serve as a reliable barrier to the environment. Under certain environmental conditions the garment would require immediate replacement.

▉ Cotton or rayon fabrics generally can be ignited by exposure to thermal radiation. Nylons, dacrons, and similar synthetics generally are not ignited but melt at relatively low radiant exposures. Woolens do not ignite, but the fibers scorch and coalesce. When a sufficient thickness of the woolen fabric is scorched it becomes brittle and can be torn or crumbled readily.

▉ Most thick, dense materials that ordinarily are considered inflammable do not ignite to persistent flaming ignition when exposed to transient thermal radiation pulses. Wood, in the form of siding or beams, may flame during the exposure but the flame is extinguished when the exposure ceases.

Table 9-2. ▇ Approximate Radiant Exposures for Ignition of Fabrics ▇

Material	Weight (oz/yd^2)	Color	Effect on Material	Radiant Exposure* (cal/cm^2)		
				t_{max} 0.2 sec	t_{max} 1.0 sec	t_{max} 3.2 sec
Clothing Fabrics						
Cotton	8	White	Ignites	32	48	85
		Khaki	Tears on flexing	17	27	34
		Khaki	Ignites	20	30	39
		Olive	Tears on flexing	9	14	21
		Olive	Ignites	14	19	21
		Dark blue	Tears on flexing	11	14	17
		Dark blue	Ignites	14	19	21
Cotton corduroy	8	Brown	Ignites	11	16	22
Cotton denim, new	10	Blue	Ignites	12	27	44
Cotton shirting	3	Khaki	Ignites	14	21	28
Cotton-nylon mixture	5	Olive	Tears on flexing	8	15	17
	5	Olive	Ignites	12	28	53
Wool	8	White	Tears on flexing	14	25	38
		Khaki	Tears on flexing	14	24	34
		Olive	Tears on flexing	9	13	19
		Dark blue	Tears on flexing	8	12	18
	20	Dark blue	Tears on flexing	14	20	26
Rainwear (double-neoprene-coated nylon twill)	9	Olive	Begins to melt	5	9	13
	9	Olive	Tears on flexing	8	14	22
Drapery Fabrics						
Rayon gabardine	6	Black	Ignites	9	20	26
Rayon-acetate drapery	5	Wine	Ignites	9	22	28
Rayon gabardine	7	Gold	Ignites	**	24†	28†
Rayon twill lining	3	Black	Ignites	7	17	25
Rayon twill lining	3	Biege	Ignites	13	20	28
Acetate-shantung	3	Black	Ignites	10†	22†	35†
Cotton heavy draperies	13	Dark colors	Ignites	15	18	34
Tent Fabrics						
Canvas (cotton)	12	White	Ignites	13	28	51
Canvas	12	Olive drab	Ignites	12	18	28
Other Fabrics						
Cotton chenille bedspread		Light blue	Ignites	**	11†	15†
Cotton venetian blind tape, dirty		White	Ignites	10	18	22
Cotton venetian blind tape		White	Ignites	13†	27†	31†
Cotton muslin window shade	8	Green	Ignites	7	13	19

▇ Radiant exposures for the indicated responses (except where marked †) are estimated to be valid to ±25% under ▇dard laboratory conditions. Under typical field conditions the values are estimated to be valid within ±50% with a greater likelihood of higher rather than lower values. For materials marked †, ignition levels are estimated to be valid within ±50% under laboratory conditions and within ±100% under field conditions. For low air bursts, values of t_{max} of 0.2, 1.0, and 3.2 sec correspond roughly to yields of 40 kt, 2 Mt, and 24 Mt, respectively.

▇ Data are not available or appropriate scaling not known.

Material	Weight (oz/yd²)	Color	Effect of Material	Radiant Exposure* (cal/cm²)		
				t_{max} 0.2 sec	t_{max} 1.0 sec	t_{max} 3.2 sec
Household Tinder Materials						
Newspaper, shredded	2		Ignites	4	6	11
Newspaper, dark picture area	2		Ignites	5	7	12
Newspaper, printed text area	2		Ignites	6	8	15
Crepe paper	1	Green	Ignites	6	9	16
Kraft paper	3	Tan	Ignites	10	13	20
Bristol board, 3 ply	10	Dark	Ignites	16	20	40
Kraft paper carton, used (flat side)	16	Brown	Ignites	16	20	40
New bond typing paper	2	White	Ignites	24‡	30‡	50‡
Cotton rags		Black	Ignites	10	15	20
Rayon rags		Black	Ignites	9	14	21
Cotton string scrubbing mop (used)		Gray	Ignites	10‡	15‡	21‡
Cotton string scrubbing mop (weathered)		Cream	Ignites	10‡	19‡	26‡
Paper book matches, blue head exposed			Ignites	11‡	14‡	20‡
Excelsior, ponderosa pine	2 lb/ft³	Light yellow	Ignites		23‡	23‡
Outdoor Tinder Materials***						
Dry rotted wood punk (fir)			Ignites	4‡	6‡	8‡
Deciduous leaves (beech)			Ignites	4	6	8
Fine grass (cheat)			Ignites	5	8	10
Coarse grass (sedge)			Ignites	6	9	11
Pine needles, brown (ponderosa)			Ignites	10	16	21
Construction Materials						
Roll roofing, mineral surface			Ignites	**	>34	>116
Roll roofing, smooth surface			Ignites	**	30	77
Plywood, douglas fir			Flaming during exposure	9	16	20
Rubber, pale latex			Ignites	50	80	110
Rubber, black			Ignites	10	20	25
Other Materials						
Aluminum aircraft skin (0.020 in. thick) coated with 0.002 in. of standard white aircraft paint			Blisters	15	30	40
Cotton canvas sandbags, dry filled			Failure	10	18	32
Coral sand			Explodes (popcorning)	15	27	47
Siliceous sand			Explodes (popcorning)	11	19	35

* Radiant exposures for the indicated responses (except where marked ‡) are estimated to be valid to ±25% under standard laboratory conditions. Under typical field conditions the values are estimated to be valid within ±50% with a greater likelihood of higher rather than lower values. For materials marked ‡, ignition levels are estimated to be valid within ±50% under laboratory conditions and within ±100% under field conditions. For low air burst, values of t_{max} of 0.2, 1.0, and 3.2 sec correspond roughly to yields of 40 kt, 2 Mt, and 24 Mt, respectively.

*** Data are not available or appropriate scaling not known.

** Radiant exposures for ignition of these substances are highly dependent on the moisture content.

SURVIVAL IN FIRE AREAS ▮

▮ The best documented fire storm in history (but not the one causing the greatest loss of life) occurred in Hamburg, Germany during the night of July 27-28, 1943, as a result of an incendiary raid by Allied forces. Factors that contributed to the fire included the high fuel loading of the area and the large number of buildings ignited within a short period of time.

▮ The main raid lasted about 30 minutes. Since the air raid warning and the first high explosive bombs caused most people to seek shelter, few fires were extinguished during the attack. By the time the raid ended, roughly half the buildings in the 5 square-mile fire storm area were burning, many of them intensely. The fire storm developed rapidly and reached its peak in two or three hours.

▮ Many people were driven from their shelters and then found that nearly everything was burning. Some people escaped through the streets; others died in the attempt; others returned to their shelters and succumbed to carbon monoxide poisoning.

▮ Estimates of the number that were killed range from about 40,000 to 55,000. Most of the deaths resulted from the fire storm. Two equally heavy raids on the same city (one occurred two nights earlier; the other, one night later) did not produce fire storms, and they resulted in death rates that have been estimated to be nearly an order of magnitude lower.

▮ More surprising than the number killed is the number of survivors. The population of the fire storm area was roughly 280,000. Estimates have been made that about 45,000 were rescued, 53,000 survived in non-basement shelters, and 140,000 either survived in basement shelters or escaped by their own initiative.

9-25 Causes of Death ▮

▮ The evidence that can be reconstructed from such catastrophes as the Hamburg fire storm indicates that carbon monoxide and excessive heat are the most frequent causes of death in mass fires. Since the conditions that offer protection from these two hazards generally provide protection from other hazards as well, the following discussion is limited to these two causes of death.

▮ *Carbon Monoxide.* Burning consists of a series of physical and chemical reactions. For most common fuels, one of the last of the reactions is the burning of carbon monoxide to form carbon dioxide near the tips of the flames. If the supply of air is limited, as it is likely to be if the fire is in a closed room or at the bottom of a pile of debris from a collapsed building, the carbon monoxide will not burn completely. Fumes from the fire will contain a large amount of this tasteless, odorless, toxic gas.

▮ During the Hamburg fire, many basement shelters were exposed to fumes. Imperfectly fitting doors and cracks produced by exploding bombs allowed carbon monoxide to penetrate these shelters. The natural positions of many of the bodies recovered after the raid indicated that death had often come without warning, as is frequently the case for carbon monoxide poisoning.

▮ Carbon monoxide kills by forming a more stable compound with hemoglobin than either oxygen or carbon dioxide will form. These latter are the two substances that hemoglobin ordinarily carries through the blood stream. Carbon monoxide that is absorbed by the blood reduces the oxygen carrying capacity of the blood, and the victim dies from oxygen deficiency.

▮ As a result of the manner that carbon monoxide acts, it can contribute to the death of a person who leaves a contaminated shelter to attempt escape through the streets of a burning city. A person recovering from a moderate case of carbon monoxide poisoning may feel well while he is resting, but his blood may be unable

to supply the oxygen his body needs when he exerts himself. After the air raid at Hamburg. victims of carbon monoxide poisoning. apparently in good health. collapsed and died from the strain of walking away from a shelter. It is suspected that many of the people who died in the streets of Hamburg were suffering from incipient carbon monoxide poisoning.

█ *Heat.* The body cools itself by perspiration. When the environment is so hot that this method fails. body temperature rises. Shortly thereafter, the rate of perspiration decreases rapidly. and. unless the victim finds immediate relief from the heat, he dies of heat exhaustion. Death from excessive heat may occur in an inadequately insulated shelter: it also may occur in the streets if a safe area cannot be located in a short time.

9-26 Shelters █

█ The results of the Hamburg fire storm illustrate the value of shelters during an intense mass fire. The public air raid shelters in Hamburg had very heavy walls to resist large bombs. Reinforced concrete three feet thick represented typical walls. Some of these shelters were fitted with gas proof doors to provide protection from poison gas. These two features offered good protection from the heat and toxic gases generated by the fire storm.

█ The public shelters were of three types:

- *Bunkers.* These were large buildings of several shapes and sizes, designed to withstand direct hits by large bombs. The fire storm area included 19 bunkers designed to hold a total of about 15,000 people. Probably twice this number occupied the bunkers during the fire storm, and all of these people survived.

- *Splinterproof Shelters.* These were long single story shelters standing free of other buildings and protected by walls of reinforced concrete at least 2-1/2 feet thick.

No deaths resulting from the fire storm were reported among occupants of these shelters. These structures were not gasproof. Distance from burning structures and low height of the shelters probably provided protection from carbon monoxide.

- *Basement Shelters.* The public shelters that were constructed in large basements had ceilings of reinforced concrete 2 to 5 feet thick. Although reports indicate that some of the occupants of these shelters survived and some did not, statistics to indicate the chance of survival in such structures are not available.

- *Private Basement Shelters.* Private basements were constructed solidly, but most of them lacked the insulating value of very thick walls and the protection of gas-tight construction. Emergency exits (usually leading to another shelter in an adjacent building) could be broken if collapse of the building caused the normal exit to be blocked. As a result of the total destruction in the fire storm area, this precaution was of limited value. Many deaths occurred in these shelters as a result of carbon monoxide poisoning, and the condition of the bodies indicated that intolerable heat followed the carbon monoxide frequently. In some cases, the heat preceded the poisonous gas and was the cause of death. Generally, these shelters offered such a small amount of protection that the occupants were forced out within 10 to 30 minutes. Most of these people were able to move through the streets and escape. Others were forced out later when the fire storm was nearer its peak intensity, and few of these escaped. A few people survived in private basement shelters.

█ Experience in Hamburg and other mass fire areas suggests the following requirements for

shelters for fire protection:

- *Location.* Shelters should be located as far away from combustible structures as possible. The bottom of a mass of burning debris is very hot and can remain so for days. An open area also may be exposed to considerable heat, but not so much as the basement of a burned-out building. Three feet of earth will provide sufficient insulation for a shelter if no heavy fuels are nearby. However, material scattered by the blast wave could fall on a shelter and render it less safe. The choice of a suitable location for a shelter is most difficult in heavily built-up areas, where mass fires are most likely to occur. Shelters in such areas would have to be designed to withstand the severe environment to which they would be subjected in case of a mass fire. When the shelters in Hamburg were built, the problems of mass fires were not anticipated.

- *Ventilation.* Any shelter that is large enough to house its occupants in reasonable comfort contains sufficient air to sustain life for the duration of a mass fire. The shelter should be constructed so that it can be sealed from the entry of gases from the outside during the period of active burning. After the fire subsides, air will be available inside the shelter if burning debris has not fallen on or near the air intake.

- *Provisions.* If escape from a shelter is necessary, wet coats or blankets would improve the chance of survival in the open. Since any shelter built for protection against a mass fire would logically serve also as a fallout shelter, such items as blankets and water normally would be available.

9-27   Escape from the Fire Areas █

█ A large number of people, chiefly the occupants of basement shelters, escaped from the Hamburg fire simply by leaving while the streets were still passable. In areas where damage is sufficiently light that people can attempt escape, the rate at which the fire builds up is expected to be slow enough to allow 30 minutes or more before movement through the streets will become dangerous.

█ Escape from the Hamburg fire storm area was simplified by the limited size of the fire. In the event of a mass fire caused by a nuclear attack, the fire area probably will be much larger. Although escape to the edge of the fire may be impossible, parks, bodies of water, or even areas that are not heavily built up may offer relative safety from the fire.

█ As the fire grows in intensity, selection of a suitable escape route becomes important. Moving through a narrow street, with tall buildings burning intensely on both sides, will subject people to an excessive amount of heat.

█ Preplanned escape routes are desirable. The safest routes are those that minimize exposure to thermal radiation from burning structures. A safe street would be wide compared to the heights of the buildings facing it. Masonry buildings with few windows would be a lesser threat than buildings with many windows. The solid wall blocks radiant exposure from fires burning inside the building, and it also protects the contents of the building from direct ignition by the thermal pulse from the nuclear weapon.

█ Simple rules for distinguishing safe from unsafe streets are not available; however, calculations of the street width for which the thermal radiation would be intense enough to ignite clothing in a short time have been made, assuming that buildings on both sides of the street were burning. The results of these calculations are shown in Table 9-4.

█ Whether or not such streets are safe will depend on many factors, such as fire intensity, percentage of the building fronts occupied by windows, wind speed and direction, protective

clothing. and exposure time. In general, the streets of Hamburg were 45 to 60 feet wide, and the buildings were 3 to 5 stories high. Table 9-4 predicts that such streets would be dangerous. and experience shows that they were. However, even these streets provided escape for some.

Table 9-4. █ Minimum Structure Separation for Escape Route █

Building Height (feet)	Distance Between Buildings (feet)
20	40
30	57
40	67
50	83
60	96

9-28 Safe Areas Within the Fire █

█ Experience indicates that large open areas within a fire storm area probably are safe. A park 1.000 feet in diameter provided adequate protection from the Hamburg fire storm; a similar area of 400 x 400 feet did not.

█ In Tokyo. during the Kanto earthquake and fire of 1923. fire whirlwinds sweeping across some large open areas killed many who would otherwise have survived. Thus. safety in a particular location depends to some extent on unpredictable aspects of the fire.

SECTION IV

█ THERMAL RADIATION DEGRADATION OF STRUCTURAL RESISTANCE TO AIR BLAST █

█ Section III of this chapter contains a description of the properties of materials that might result in ignition or degradation of their physical properties. The emphasis of the discus-

sion in Section III concerns the ignition of combustible materials. This section provides a somewhat expanded treatment of the degradation of structural resistance to air blast that is brought about by exposure to thermal radiation.

█ The problem of integrated thermal/blast effects can be divided into several elements. One element is the free field thermal and air blast environments to which a system element is exposed. Methods of predicting these environments are presented in Chapters 2 and 3. As pointed out in Chapter 3, prediction of the thermal environment is difficult because of the importance of climatic conditions. A statistical or probabilistic description of weather conditions frequently will have to be used to form some estimate of the validity of the results.

█ The first element of the overall problem treated in this section is the coupling of thermal energy into the structure or system element of interest. The condition of the target surface, its orientation to the detonation. and coatings employed all can affect the amount of thermal energy that is absorbed by the target.

█ The second element is the mechanisms for the loss of energy from the structure through convective heat losses or reradiation. The third element is the effect of absorbed energy on the state of the target material. The primary effect of this change of state is the fourth element, which is the change in material properties.

█ The final and fifth element of the problem is the effect of changes in material properties on the structural resistance to air blast loading.

█ Insufficient data are available concerning the thermophysical properties of nonmetallic materials to provide a realistic discussion of the combined blast/thermal effects on such materials. Any current prediction would be highly uncertain, both with regard to the occurrence of any specific physical phenomena and to the quantitative evaluation of the phenomena. Con-

sequently the discussion in this section will be limited to metallic materials.

■ THERMAL ENERGY ABSORBED ■

9-29 Absorption ■

■ The amount of thermal radiation that a metallic element will absorb depends on the properties of the metal, color, surface condition, orientation to the burst, the absence or presence of some type of coating (either accidental such as dirt or grease or intentional such as a paint system).* The amount of thermal energy absorbed by a target usually is determined by multiplying the incident energy by an absorption coefficient. The absorption coefficient cannot be directly measured; however, a good estimate can be made by performing spectral measurements of reflectance over the range of wavelengths representative of the nuclear radiation spectral distribution, and finding an average value of reflectance. The coefficient of absorptance then equals one minus this average value of reflectance. The absorptance determined in this manner is valid only as long as the surface does not change as a result of the absorbed thermal energy. Another approach is to divide the quantity of energy absorbed by the incident energy. The absorbed energy is determined from experimentally determined temperature vs time relationships and appropriate theoretical energy balance relationships.[†] Some typical values for absorption coefficients for bare metals are shown in Table 9-5. A value of 0.5 would be a good value to assume for the absorption coefficient in the absence of more definitive data for a specific system under investigation.

■ A coating or surface treatment on a metal substrate can alter the effective absorption coefficient significantly, and thereby can alter the amount of energy absorbed by the metal structure. The amount of energy absorbed depends on color, thickness, adhesiveness, and heat transfer characteristics of the coating. The

Table 9-5. ■ Absorption Coefficients for Bare Metals ■

Material	Absorption Coefficient
Polished metals	0.25-0.5
Especially clean aluminum	0.2-0.4
Clean aluminum	0.5
Unpolished metals	0.45-0.55
Average over aircraft	0.5

most common type of coating is, of course, paint. The importance of paint in altering the amount of thermal radiation absorbed was noted in early investigations where it was found that the thin aircraft skin under painted insignia had melted, whereas the skin of adjacent areas was not affected. It should not be assumed, however, that paint or other coating is necessarily a detriment. In some instances the smoke that results from the breakdown of the paint can reduce the amount of energy absorbed and thereby reduce the maximum temperature reached by the substrate. Figure 9-8 illustrates this factor. The only true general statement that can be made about coatings is that they can alter the amount of thermal energy absorbed by the substrate. In fact some coatings, even paint systems, can be designed to reduce the amount of energy absorbed. As a general rule, however, most coating systems on present tactical military equipment

*■ Implicit in this statement and throughout this discussion is the fact that energy coupling depends on the wavelength of the incident radiation.

†■ Absorptance is a function of time and temperature, although an average value usually is employed. This function when known may be found as an input specification for certain computer programs.
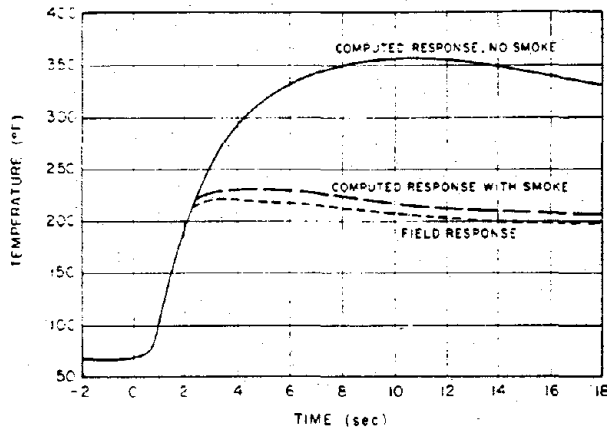
9-32

Figure 9-8. ■ Exposed Facing Temperature-Time Histories of Aluminum Honeycomb. Facing, 0.016-in. Gray Painted Skin; Core 1/8-in., Cell Size 1/2-in. Thick. 21-24.2 cal/cm^2, 3.8 Mt ■

will cause an increase in the amount of energy absorbed. The mechanisms of the response of coatings and the transfer of energy to the substrate are so complex that theoretical descriptions have not been successful. The response of coatings depends upon both the rate at which thermal radiation is received and the total incident energy. A given amount of radiation received at a slow rate may only cause discoloration or slight scorching, whereas if it were received at a very rapid rate it would cause charring or blistering. The latter response is more typical in a nuclear environment. The change in state of the coating reduces the amount of energy available to be transferred to the substrate, because these processes are irreversible. However, the change in state usually increases the absorption coefficient of the coating, and the net result usually is an increase on the amount of energy absorbed by the substrate. An exception occurs if the absorption coefficient was initially high, and energy was absorbed by the smoke layer generated by the decomposing paint. Coatings that respond by

physically separating from the surface, i.e., blister, potentially can reduce the amounts of energy transferred to the substrate. Since the response of the coating-substrate system to nuclear weapon thermal radiation is so complex, effective absorption coefficients usually are determined experimentally.

■ The average value of the absorption coefficient, A, depends on the properties of the substrate as the flow of thermal energy from the coating influences the response of the coating. A series of experiments with laser heating provides data to illustrate this point. Various metallic samples were prepared with a Silicon-carbide-synar binder coating (spectrophotometric measurements gave an average absorption coefficient of 0.85 for the coated aluminum sample for equilibrium temperatures of 70 and 600°F for a 10.6 micron wavelength). The average values of the absorption coefficients for a range of irradiances based on temperature vs time data are shown in Table 9-6. The effect of substrate properties is significant.

■ Values of absorption coefficients are shown in Table 9-7. Generally, values range from 0.3 to 0.6 for light or reflective paints, and from

Table 9-6. ■ Average Absorption Coefficients for Laser Heated Coated Substrates ■

Substrate	Average Absorption Coefficient
2024-T81 clad aluminum alloy	0.7 ± 0.1
6AL-4V annealed titanium	0.35 ± 0.1*
301 full hard stainless steel	0.80 ± 0.05

■ Evaluation of titanium specimens showed considerable scatter. Erratic behavior probably resulted from improper bonding of the coating and cracking or flaking of the coating during straining.

Substrate	Coating or Surface Treatment	Absorption Coefficient
Metallic skins	Aluminum paint	0.5
Painted metals (aircraft skins)	White paint	0.3 - 0.5
	White paint (clean)	0.25
	White paint w/oil film	0.30
	Yellow paint	0.4 - 0.55
	Olive paint	0.6 - 0.7
	Gray paint (clean)	0.6
	Black paint	0.65 - 0.95
	Insignia blue	0.9
5032-H32AL	Black paint	0.7 - 1.0
Aluminums	Reflecting white paint	0.32
	Camouflage paint	1.00
6061 Al-Mg alloy	Haze gray Navy paint	0.78 ± 0.04
	Volcanol	0.99 ± 0.05
2024-T3	Anodized black	0.67

0.6 to 1.0 for dark paints or treated surfaces.

■ It is apparent that the selection of an absorption coefficient based on the information in Table 9-7 for use in analyzing the response of a military system could be in error by as much as ±50 percent. Currently, the best solution is to perform upper and lower bound calculations. The upper and lower bound calculations should be based on the best estimate of the condition of the surface at the time of exposure, i.e., dirty, corroded, prior exposures, etc.

■ One additional factor affects the amount of energy absorbed. This factor is the orientation of the surface to the thermal pulse. Ideally, if incident parallel rays are assumed, with no scattering, reflection or refraction, the target surface receives all of the radiation if it is oriented normal to the rays. If the surface is rotated about an axis normal to the rays, it cuts fewer of the rays, and the amount of thermal energy received is reduced. The energy received by a differential area on a curved surface also can be treated in this manner. With such assumptions, the absorbed energy function takes the following form:

$$Q_a = QA_e \cos \theta$$

where

Q = incident energy, usually expressed in cal/cm^2

Q_a = absorbed energy, usually expressed in cal/cm^2

A_e = effective absorption coefficient

θ = incident angle. angle between a line from the source to the surface and a line normal to the plane of the surface.

Under those ideal conditions. the amount of absorbed energy follows the cosine law; however. there will be conditions where scattering. reflection, and refraction, will invalidate the parallel ray assumption in addition to altering Q. This would principally occur at large angles of incidence such as shown schematically in Figure 9-9. A computer program called TRAP has recently been developed to handle these conditions.

█ Figure 9-9 also illustrates the amount of energy received by the surface of a cylinder with its axis oriented normal to the ray paths. The quantity θ then becomes the distance. in ra-

dians. along the circumference. from the point nearest the source.

█ Both the absorption coefficient and orientation are important in determining the amount of energy absorbed into the target. Errors in orientation are of greater significance at large angles on incidence; however, orientation usually can be inferred, at least for worst cases, whereas the absorption coefficient usually is not well known unless it has been determined experimentally.

9-30 Energy Losses █

█ The absorption of thermal radiation energy into a material has been discussed in the previous paragraph. Before discussing the effect of this absorbed energy on material properties or change in structural resistance. the form and significance of energy losses from the material
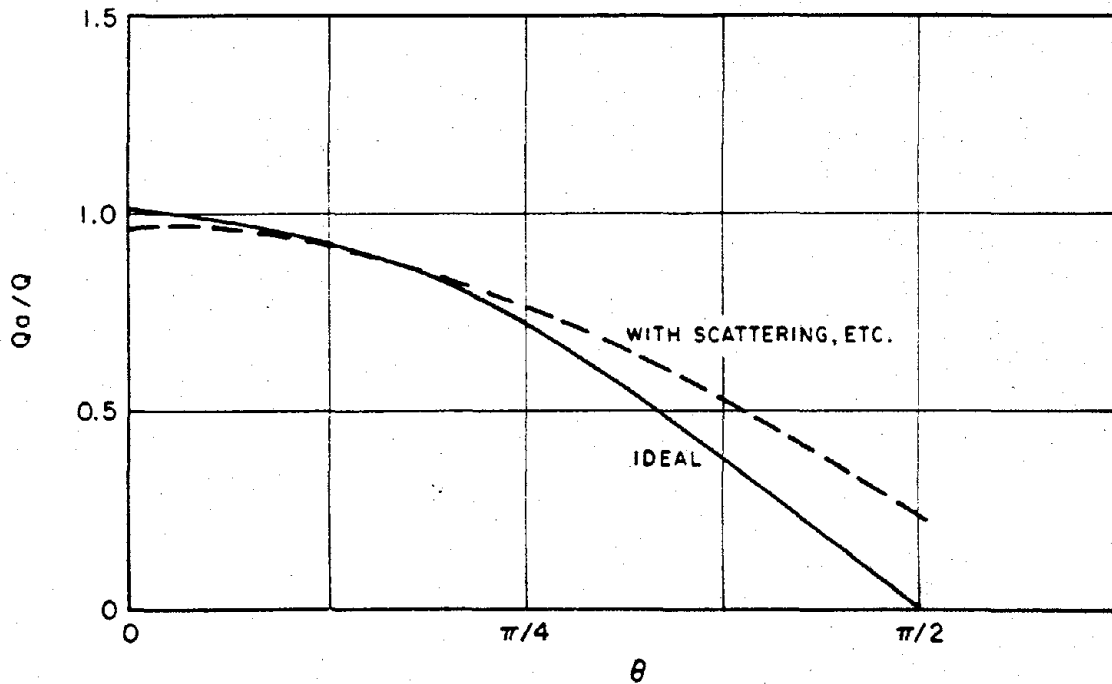
Figure 9-9. █ Schematic Comparison of Ideal Cosine Law with Function Including Scattering, Reflection, and Refraction █

must be discussed. The three ways in which thermal energy can be dissipated are conduction, radiation, and convection. For purposes of this discussion, conductive dissipation is not really a loss, in that energy is redistributed throughout the material system rather than lost from the system. This form of heat dissipation is considered in more detail in the following subsection that discusses the change in material state, and the discussion of temperature profiles.

Radiation losses normally are considered negligible, because the temperature rises in a material are relatively small, even though the radiation heat loss is a function of the fourth power of absolute temperatures. The heat loss through radiation is expressed by:

$$Q_r = \sigma\epsilon(T^4 - T_0^4)$$

where

Q_r = radiative heat loss, cal/cm²-sec,

σ = Stephan Bolzman Coefficient = 1.36×10^{-12} cal/cm² sec °K⁻⁴,

ϵ = emissivity, nondimensional,

T = absolute temperature, °K, of radiator (may be time dependent),

T_0 = absolute temperature, °K, of surrounding air.

If a 200°C temperature difference is assumed, and an emissivity of 0.2 (for oxidized aluminum at temperatures of a few hundred °C), and the ambient air temperature is 300°K, the radiative heat loss becomes:

$$Q_r = (1.36 \times 10^{-12})(0.2)(500^4 - 300^4)$$

$$= 1.48 \times 10^{-2} \text{ cal/cm}^2 \cdot \text{sec}$$

If the temperature rise is 400°C then Q_r becomes equal to 6.3×10^{-2} cal/cm² sec. Thus, it can be seen that even at high elevated temperatures, the heat loss through radiative processes is small.

Convective heat losses occur when there is a flow of air over the heated surface. This type of heat loss is most important for aircraft in flight and is a weak function of position on the airfoil, and the speed and altitude of the aircraft. The rate of convective heat loss also depends on whether the boundary layer flow is laminar or turbulent. These processes are generally understood, and a number of formulas that are available are given below:

$$h_{cv} = 0.67(10)^{-4} T^{0.3} \frac{(V\rho)^{0.8}}{x^{0.2}}$$

where

h_{cv} = convective heat loss coefficient for turbulent flow,

T = air temperature, °R,

V = flight speed, ft/sec,

ρ = density of air, lb/ft³,

x = distance from leading edge of airfoil, ft.

$$h_{cv} = 0.176 \; \rho V C_p (\log_{10} Re)^{-2.45},$$

$$h_{cv} = 0.01445 \; k/x \; (Re)^{0.8} \; (Pr)^{0.33},$$

$$h_{cv} = 0.0282 \; k/x \; (Re)^{0.8} \; (Pr)^{0.33},$$

$$h'_{cv} = 0.318 \; k/x \; (Pr)^{1/3} \; (Re)^{1/2},$$

$$h'_{cv} = 0.332 \; \rho V C_p (Pr)^{-2/3} \; (Re)^{-1/2},$$

where

h_{cv} = convective heat loss coefficient for turbulent flow, cal/cm² · sec · °C

h'_{cv} = convective heat loss coefficient for laminar flow, cal/cm^2 · sec · °C

ρ = density of air, gm/cm^3

V = flight speed, cm/sec

C_p = specific heat of air, cal/gm · °C

Re = Reynolds number, $\rho V x/\mu$, dimensionless

k = thermal conductivity of air, cal/cm · sec · °C

x = distance from leading edge of airfoil, cm

Pr = Prandtl number, $C_p \mu/k$, dimensionless

μ = viscosity of air, gm/sec · cm

These formulas are based on the assumption that a reasonable approximation may be obtained by analysis of airflow over a heated flat plate. Experimental data indicate that the average error in using this approximation may be as much as 30 percent with a mean error of from 10 to 15 percent. The value for h_{cv} ranges from zero to 0.03 cal/cm^2 · sec · °C for a range of reasonable air properties and velocities. Generally, convective heat losses are marginally important for relatively low yield weapons; however, for long duration thermal pulses and under conditions when the temperature difference between the aircraft skin and the air boundary layer is large, the convective heat loss can be significant for high speed aircraft.

███ Values of h_{cv} have been calculated (see Table 9-8) for purposes of comparing the results of the equations given above, under the following assumed conditions.

Aircraft type = fixed wing

Aircraft speed = 100 mph (4.47 x 10^3 cm/sec)

Aircraft altitude = 1,000 ft

Air temperature = 70°F, 20°C

x = 4 ft, 121.92 cm

ρ = 7.5(10)$^{-2}$ lb/ft^3

Table 9-8. ███ Values of h_{cv} Obtained from Various Functions in the Order in Which the Equations are Given Above ███

Flow Condition	h_{cv} $\left(\dfrac{cal}{cm^2 \cdot sec \cdot °C}\right)$
Turbulent	2.27(10)$^{-3}$
	2.27(10)$^{-3}$
	1.14(10)$^{-3}$
	2.23(10)$^{-3}$
Laminar	2.15(10)$^{-4}$
	2.82(10)$^{-4}$

ρ = 1.2(10)$^{-3}$ gm/cm^3

k = 6.0874(10)$^{-5}$ cal/cm · sec · °C

C_p = 0.2404 cal/gm · °C

μ = 1.798(10)$^{-4}$ gm/cm · cm

███ The use of the convective heat loss coefficient, h_{cv}, is shown below:

$$Q_{cv} = h_{cv} (T_s - T)$$

where

Q_{cv} = convective heat loss, cal/cm^2 · sec

T_s = surface temperature, °C (may be time dependent)

T = surrounding air temperature, °C

For high speed aircraft, it may not be appropriate to assume that the temperature of the surrounding air is the temperature of the air boundary layer next to the heated surface. This

is particularly true if aerodynamic heating occurs. For this situation, the recovery temperature T_r should replace T in the equation given above.

■ For tactical systems of interest to this section, radiative and convective heat losses generally can be neglected. However, these are and normally should be included in detailed analyses and computer calculations for completeness, particularly for high speed aircraft and large yield weapons.

■ CHANGES IN MATERIAL STATE AND MATERIALS PROPERTIES ■

9-31 Changes in Material State

■ The change in material state of primary interest is the change in temperature caused by absorbed thermal radiation. The temperature changes are controlled by the energy absorbed in the material as a function of time and position and by the geometry of the member being analyzed. Geometry can have a significant impact on heat flow through the member as well as heat absorption and losses. There are a number of techniques available for determining temperature changes. These techniques vary from simple formulas to large computer programs depending on the simplifying assumptions that are made and the complexity of the system geometry. The greatest amount of effort has been devoted to the study of temperature changes in flat plates, primarily because of the interest in aircraft safety/survivability problems. Therefore, the following discussion is dominated by analysis of flat plates, although most of what can be learned about the processes affecting plate temperature applies to other geometries because the basic equations describing the processes are the same.

■ Plates can be divided into several types according to the temperature profile through the plate. A thermally "thin" plate usually is defined as a plate where the temperature gradient between the front and back of the plate is small. Thermally thin plates simplify the analysis problem, because, if a significant thermal gradient exists, the thermal stresses become more complex. Plates usually are assumed to be one dimensional, with no heat flow to a supporting structure, so heat sink effects can be neglected, unless the plate is part of a fuel tank.

■ Whether a plate is thermally thin depends not only on the thermophysical properties of the material, but also on the thermal pulse characteristics and the time during the pulse that the criterion is applied. Some materials conduct heat more quickly than others, and the temperature on the back face of these materials will not lag behind the temperature on the front as much as for materials with lower conductivities. For example, the thermal conductivity of aluminum is about 0.4 cal/sec · cm · °C, and that of titanium is about 0.04 cal/sec · cm · °C. Therefore, aluminum conducts 10 times as much heat as titanium in a given amount of time. Other material factors that control the ratio of front to back temperature are specific heat, density, and thickness.

■ The temperature difference also depends on pulse characteristics. For a pulse that is delivered slowly, there may be sufficient time for energy to be conducted to the back face, so the thermal gradient at the time of interest is minimized. Conversely, a pulse that is delivered rapidly may cause a steep thermal gradient. For a given pulse, material, and thickness, the time at which the temperature response is of interest determines whether the thermal gradient is small.

■ A number of techniques have been developed to determine whether a plate can be considered to be thermally thin. One technique that gives a good approximation is illustrated in Figure 9-10. The values of $\eta = t/t_{max}$ and $\alpha t_{max}/b^2$ must be evaluated to use the curves in Figure 9-10. From Chapter 3

$$t_{max} = 0.043 \ W^{0.43} \ (\rho/\rho_o)^{0.42} \ sec,^*$$

where t_{max} is the time to the principle thermal maximum, W is the weapon yield in kilotons, and ρ/ρ_o is the ratio of the air density at the burst altitude to the air density at sea level. The parameter α is defined as

$$\alpha = k/\rho_m C_p \ cm^2/sec$$

where

k = thermal conductivity of air, cal/cm · sec · °C.

ρ_m = material density, gm/cm^3.

C_p = specific heat of air, cal/gm · °C

and h is the thickness of the plate in centimeters. The point where the values of η and $\alpha t_{max}/h^2$ meet determines whether the plate is thin, finite, or thick. A thin plate is one in which the difference between back and front temperatures is less than 10 percent. A thick plate is one in which there is no temperature rise on the back face. A finite plate falls between the other two criteria.

A technique for predicting the temperatures of thermally thin plates uses the relationships shown in Figure 9-11. This technique is believed to provide good results over a fairly wide range of problems of interest. The technique assumes that thermophysical properties and the rate of convective heat loss are constant, that radiation losses are negligible, and that there is no heat loss from the back of the plate.

*The examples provided in this section will all be concerned with air bursts that are sufficiently low that the term $(\rho/\rho_o)^{0.42}$ is near enough to 1.0 to be neglected (e.g., at 4,000 feet $(\rho/\rho_o)^{0.42} \approx 0.99$). Therefore, the approximation $t_{max} \approx 0.043 \ W^{0.43}$ will be used throughout the remainder of this section.

Problem 9-1. Calculation of Thermal Thickness of a Metal Plate

Figure 9-10 contains curves that define regions where metal plates may be considered thermally thin, finite, and thick, respectively. The curves are plotted as a function of the parameters η and $\alpha t_{max}/b^2$, which are defined in paragraph 9-31. Their use is demonstrated in the following example.

Example

Given: A 5086 Aluminum alloy plate is an important part of a structure under analysis. The plate is 0.875 cm thick and the range of air blast exposures for the system of which it is a part are expected to be from 8 to 15 psi from a 100 kt explosion at a height of burst of 1,000 feet.

Find: Whether the plate can be considered thermally thin.

Solution: The corresponding height of burst for a 1 kt explosion is

$$h_1 = \frac{h}{(W^{1/3})} = \frac{1,000}{(100)^{1/3}} = 215 \text{ feet.}$$

From Figures 2-18 and 2-19, Chapter 2, the ground distances from a 1 kt explosion at a height of burst of 215 feet that correspond to 15 and 8 psi overpressure are 895 and 1,250 feet respectively. From Figure 2-28, Chapter 2, the times of arrival of the blast wave from a 1 kt explosion to these distances are 0.37 seconds and 0.61 seconds, respectively. The corresponding times for a 100 kt explosion are

$$t = t_1 W^{1/3}$$

$$t = (0.37)(100)^{1/3} = 1.72 \text{ sec for 15 psi,}$$

and

$$t = (0.61)(100)^{1/3} = 2.83 \text{ sec for 8 psi.}$$

The time to final maximum for a 100 kt low air burst is

$$t_{max} \approx 0.043 \ W^{0.43}$$

$$= (0.043)(100)^{0.43} = 0.31 \text{ sec.}$$

Therefore,

$$\eta = t/t_{max}$$

$$\eta = \frac{1.72}{0.31} = 5.5 \text{ for 15 psi,}$$

and

$$\eta = \frac{2.83}{0.31} = 9.1 \text{ for 8 psi.}$$

The properties of the alloy are

$$k = 0.28 \text{ cal/sec} \cdot {}^\circ C,$$

$$C_p = 0.22 \text{ cal/gm} \cdot {}^\circ C,$$

$$\rho = 2.66 \text{ gram/cm}^3.$$

Since

$$\alpha = \frac{k}{\rho C_p},$$

$$\frac{\alpha t_{max}}{b^2} = \frac{k t_{max}}{\rho C_p b^2}$$

$$= \frac{(0.28)(0.31)}{(2.66)(0.22)(0.875)^2}$$

$$= 0.19.$$

Answer: From Figure 9-10, at the 15 psi overpressure level where $\eta = 5.5$, the plate should be considered finite; at the 8 psi overpressure level, where $\eta = 9.1$, the plate can be considered thermally thin.
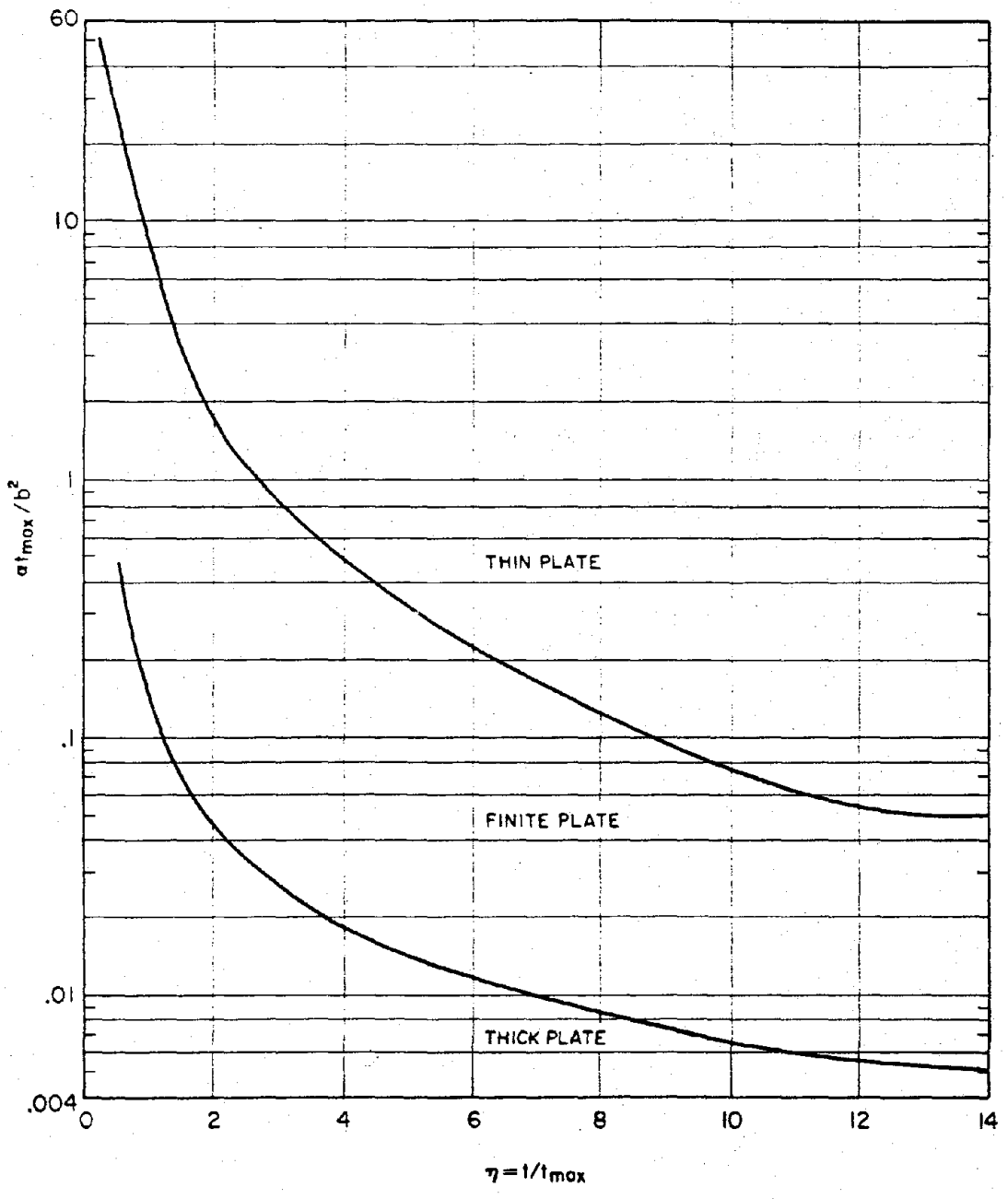
Related Material: See paragraph 9-31.

Figure 9-10. ▓▓▓ Thin Plate, Thick Plate, and Finite Plate Regions for Exposure to Nuclear Weapons Thermal Radiation ▓▓

The variables used in this technique have units in the cgs system and have been defined previously; however, they are listed below for convenience.

T_o = temperature of the plate prior to exposure,

ΔT = temperature rise, °C,

A = absorption coefficient

Q = thermal exposure, cal/cm^2 (effective thermal exposure may be used where $Q = Q \cos \theta$),

ρ_m = specific gravity of material, gm/cm^3,

C_p = specific heat, cal/gm · °C,

b = plate thickness, cm,

h_{cv} = convective heat loss, cal/cm^2 · sec · °C,

$\eta = t/t_{max}$.

Use of the technique is illustrated in Problem 9-2.

Problem 9-2. Calculation of Temperature Rise in a Thermally Thin Plate

■ Figure 9-11 contains a family of curves that relate thermophysical properties of a thin metal plate to thermal pulse parameters in a manner that allows calculation of the temperature rise in the plate. The procedures for the calculation are made clear in the following examples. Symbols for the various parameters are listed in paragraph 9-31.

■ *Example 1* ■
Given: A 6061-T6 Aluminum alloy plate is exposed to the thermal pulse from a 100 kt low air burst at a location where the incident radiant energy is 76 cal/cm² and arrives at an angle of incidence of 30°. Properties of the plate are

$$T_o = 30°C,$$

$$A = 0.8,$$

$$\rho_m = 2.7 \text{ gm/cm}^3,$$

$$C_p = 0.216 \text{ cal/gm} \cdot °C,$$

$$b = 0.15875 \text{ cm},$$

$$h_{cv} = 0.$$

Find: The temperature of the plate when η = 2, 4, and 6.

Solution: The effective radiant exposure is

$$Q_e = Q \cos \theta = 76 \cos 30° = 65.8 \text{ cal/cm}^2.$$

From Figure 9-11, with

$$\frac{h_{cv} t_{max}}{\rho C_p b} = 0,$$

when

$$\eta = 2, \frac{\Delta T}{AQ/\rho C_p b} = 0.47,$$

when

$$\eta = 4, \frac{\Delta T}{AQ/\rho C_p b} = 0.67,$$

and when

$$\eta = 6, \frac{\Delta T}{AQ/\rho C_p b} = 0.74.$$

The value of $AQ/\rho C_p b$ is

$$\frac{AQ_e}{\rho C_p b} = \frac{(0.8)(65.8)}{(2.7)(0.216)(0.15875)} = 569°C.$$

The temperature rises are

$$\Delta T = (0.47)(569) = 267°C \text{ for } \eta = 2,$$

$$\Delta T = (0.67)(569) = 381°C \text{ for } \eta = 4,$$

and

$$\Delta T = (0.74)(569) = 421°C \text{ for } \eta = 6.$$

Answer: The plate temperatures are

$$T = T_o + \Delta T.$$

Therefore,

$$T_{\eta=2} = 30 + 267 = 297°C$$

$$T_{\eta=4} = 30 + 381 = 411°C$$

$$T_{\eta=6} = 30 + 421 = 451°C.$$

■ *Example 2* ■
Given: The same conditions as Example 1,

except that $h_{cv} = 3.0 \times 10^{-2}$ cal/cm$^2 \cdot$ °C.*

    Find: The temperature of the plate when η = 2, 4, and 6.

    Solution:

$$t_{max} = 0.043 \ W^{0.43} = (0.043)(100)^{0.43}$$

$$= 0.31 \ sec.$$

$$\frac{h_{cv} t_{max}}{\rho C_p b} = \frac{(3.0 \times 10^{-2})(0.31)}{(2.7)(0.216)(0.15875)} = 0.1.$$

From Figure 9-11, when

$$\eta = 2, \ \frac{\Delta T}{A Q / \rho C_p b} = 0.44,$$

when

$$\eta = 4, \ \frac{\Delta T}{A Q / \rho C_p b} = 0.53,$$

and when

$$\eta = 6, \ \frac{\Delta T}{A Q / \rho C_p b} = 0.51.$$

From Example 1,

$$\frac{A Q}{\rho C_p b} = 569°C.$$

The temperature rises are

$$\Delta T = (0.44)(569) = 250°C \ for \ \eta = 2,$$

$$\Delta T = (0.53)(569) = 302°C \ for \ \eta = 4,$$

and

$$\Delta T = (0.51)(569) = 290°C \ for \ \eta = 6.$$

    Answer: The plate temperatures are

$$T = T_o + \Delta T.$$

Therefore,

$$T_{\eta = 2} = 30 + 250 = 280°C,$$

$$T_{\eta = 4} = 30 + 302 = 332°C,$$

and

$$T_{\eta = 6} = 30 + 290 = 320°C.$$

    Related Material: See paragraph 9-31.

---

* This value corresponds roughly to an airplane speed of 200 mi/hr.
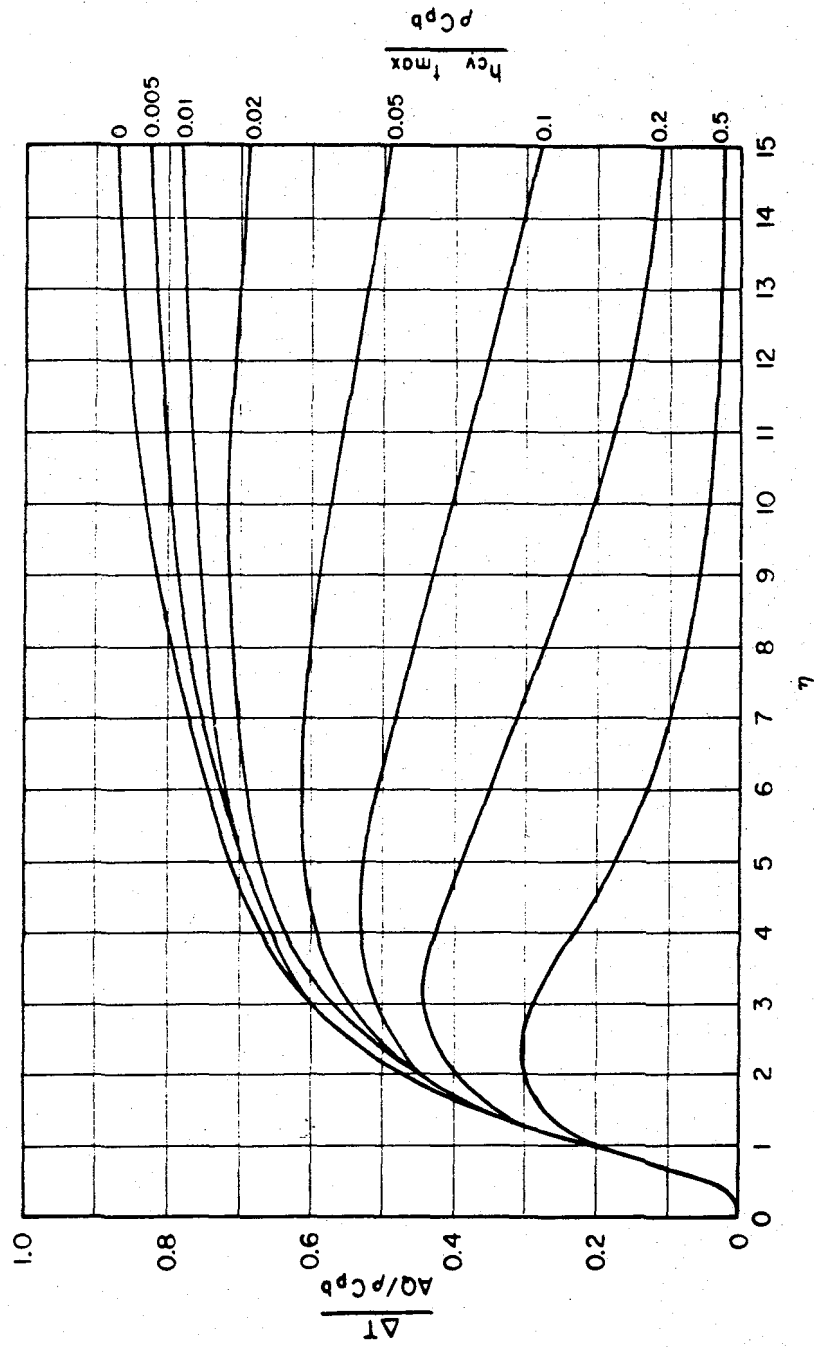
Figure 9.11. Thermal Response of a Thin Plate to Nuclear Weapons Thermal Radiation Pulse

■ Thermally thick plates are those that do not have a temperature rise on the back surface at the time of interest. Finite plates have a temperature gradient between the front and back surfaces and a temperature rise at both surfaces.

■ Computer codes generally are required to calculate the temperature history of thermally thick and thermally finite plates. Simple graphical techniques have been developed to determine the temperature rise on the front face of a thermally thick plate and on the front face, mid place, and back face of thermally finite plates. These are not included herein because the techniques depend upon thermal source characteristics that are very different from the source characteristics described in Chapter 3.* If graphical techniques that are compatible with the thermal source data of Chapter 3 become available, they will be included in revisions to this manual. In the meantime, users who are interested in the techniques should consult "Thermal Degradation of Structural Resistance to Air Blast" (see bibliography).

■ Requirements to analyze geometries that are more complex than single layer plates (even if they are layered thin plates) or to examine plates with temperature dependent thermophysical properties or heat losses require the use of a computer code. Codes for more complex geometries, such as cylinders and tee beams, have been developed specifically for the types of analysis of concern to this section. As noted previously, the TRAP computer program can calculate temperatures and stresses for two dimensional structures.

■ Honeycomb structures or sandwich construction must be considered as a multi-layered system. A five layer system was used to examine thin sandwich construction. The five layers consisted of the core, the two skins, and the two bonding layers between the skins and core. Most sandwich construction has been found to fail at the bonding layer. Consequently, the tempera-

ture of the bond and the thermal stresses in the face sheets (or skins) can be of equal importance. Studies and experiments show that a calculational procedure that includes five layers was required to duplicate experimental results accurately. A code developed for dual layer plates has been used to calculate thick single layer plates by considering both layers to be the same material.

9-32 Change in Materials Properties ■

■ The rise in temperature that occurs when thermal radiation is absorbed can be expected to cause changes in materials prop-

---

*■ The important differences in source characteristics are the time to final maximum, where

$$t_{max} = 0.032 \ W^{1/2} \ \text{sec}$$

was used in developing the graphical techniques, while a more recent value

$$t_{max} = 0.043 \ W^{0.43} \ (\rho/\rho_o)^{0.42} \ \text{sec}$$

is given in Chapter 3, and the power at thermal maximum, where

$$P_{max} \approx 4 \ W^{1/2} \ \text{kt/sec}$$

was used in developing the graphical techniques while a more recent value of

$$P_{max} = \frac{4.3 \ W^{0.6}}{(\rho/\rho_o)^{0.44}} \ \text{kt/sec}$$

is given in Chapter 3. The latter determines the maximum irradiance (thermal energy per unit area per unit time) incident on the target. Actually, the procedures described in Problems 9-1 and 9-2 were developed for use with the older expression for t_{max}; however, since the two expressions agree within a few percent for low air bursts and for yields from a few kt to a few Mt, the use of the techniques with the value of t_{max} from Chapter 3 was illustrated. The values of P_{max} on the other hand, differ widely at all yields. Since the temperature histories presented in the graphical techniques for finite and thick plates depend strongly on irradiance, it is not possible to use the thermal source data with the curves derived for use with the older expression for P_{max}.

erties. Properties of mechanical strength are of greatest concern, since these properties influence structural resistance.

███ Thermal stresses may be present in either unrestrained or restrained structures or elements thereof if thermal gradients, which usually are caused by increased temperatures, are present. The magnitude of the stresses depends upon the amount of expansion the structure experiences, which depends on the value of the coefficient of thermal expansion, α_e, for the material. The dimensions of this coefficient are length per length per temperature unit, often expressed as in./in.°F or cm/cm/°C. The value of α_e depends on the temperature, as shown in Figures 9-12 through 9-15 for a number of materials. Use of an improper value of α_e can cause serious errors in the estimation of the thermal stress level in some materials. For example, the use of the room temperature value of α_e for AISI 301 stainless steel when the value of 1200°F (~650°C) should have been used, would result in a value of thermal stress that is 20 percent too low. For 2024 Aluminum Alloy, the error would be about 18 percent, whereas for Ti-8Mn Titanium Alloy, the error would be 45 percent. Thus, for large temperature rises, the assumption of a constant value for the coefficient of thermal expansion could lead to significant errors. However, for small temperature rises, on the order of 200°F (110°C), the error would not be significant. For most metallic materials, the error in thermal stress is about 2 percent per 100°F or 3 percent per 100°C temperature rise above room temperature values of α_e. Additional data may be obtained from "Metallic Materials and Elements for Aerospace Vehicle Structures" (see bibliography).

███ Changes in mechanical strength are the prime reason for concern about the effects of absorbed thermal radiation. Data from several sources are incorporated into Figures 9-16 through 9-18 to provide some indication of the effects of elevated temperature on the tensile strength properties of 2014-T6 Aluminum Alloy, Titanium Alloy 6AL-4V, and 301 full, hard stainless steel. The various curves in these figures provide some indication of the effect of elevated temperature and also the effects of the speed at which the sample was heated and the time it remained at a given temperature.

███ The data that will be discussed comes from several sources. Since the techniques for testing that were used in these sources differ considerably, it will be of value to discuss the various techniques employed.

███ The four basic types of loading tests that have been used to determine mechanical properties at elevated temperatures are illustrated in Figure 9-19 and 9-20. Figures 9-19a and b illustrate an adaptation of the conventional tensile test for elevated temperature. The sample is heated rapidly to an equilibrium temperature. At some finite time after thermal equilibrium, called the soak time, a conventional tensile loading test is conducted with a constant strain rate loading mechanism. Two loading rates are shown in Figure 9-19a. Figure 9-19b illustrates the type of results that are obtained from the type of test illustrated in Figure 9-19a.

███ Figures 9-19c and d illustrate another type of tensile test where the sample is loaded with a constant load, then heated at some rate until rupture occurs. Figure 9-19d illustrates the type of results that are obtained from the type of test illustrated in Figure 9-19c. Figure 9-20 illustrates two types of short time creep tests and their results.

███ Results from these types of tests are shown for three aluminum alloys in Figures 9-21 through 9-23. Some data shown in Figure 9-21 were obtained by the type of the test illustrated in Figure 9-19a. The soak time of the sample was one-half hour before a standard constant strain rate of 0.00033 in./in./sec tensile test was performed. Other data in Figure 9-21 also were
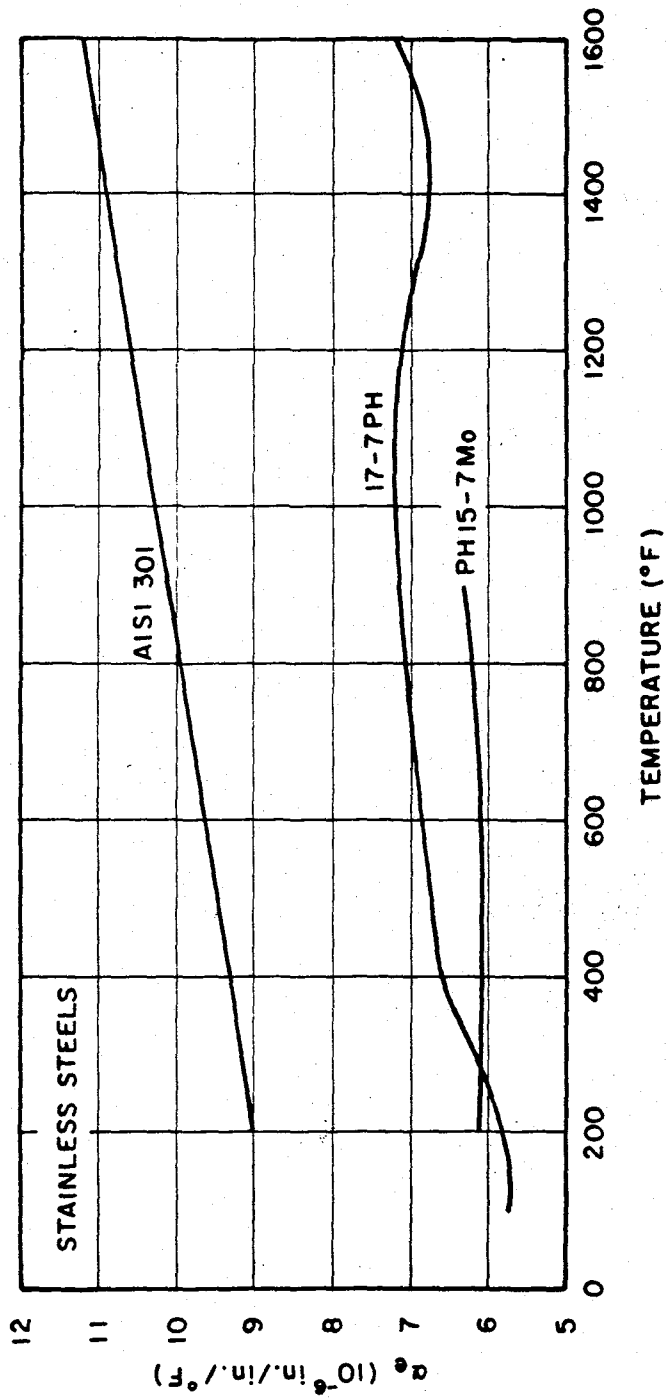
Figure 9-12. Coefficient of Linear Expansion as a Function of Temperature for Stainless Steels
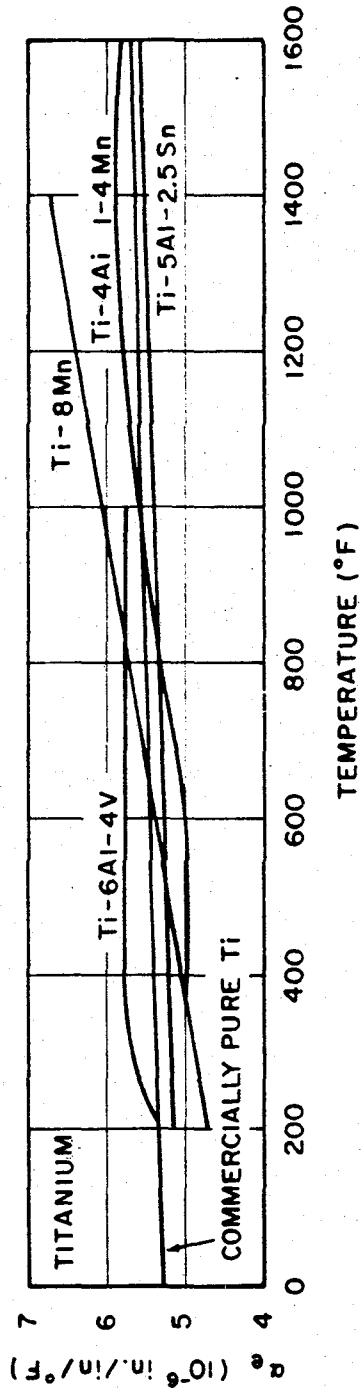
Figure 9-13. Coefficient of Linear Expansion as a Function of Temperature for Titanium Alloys
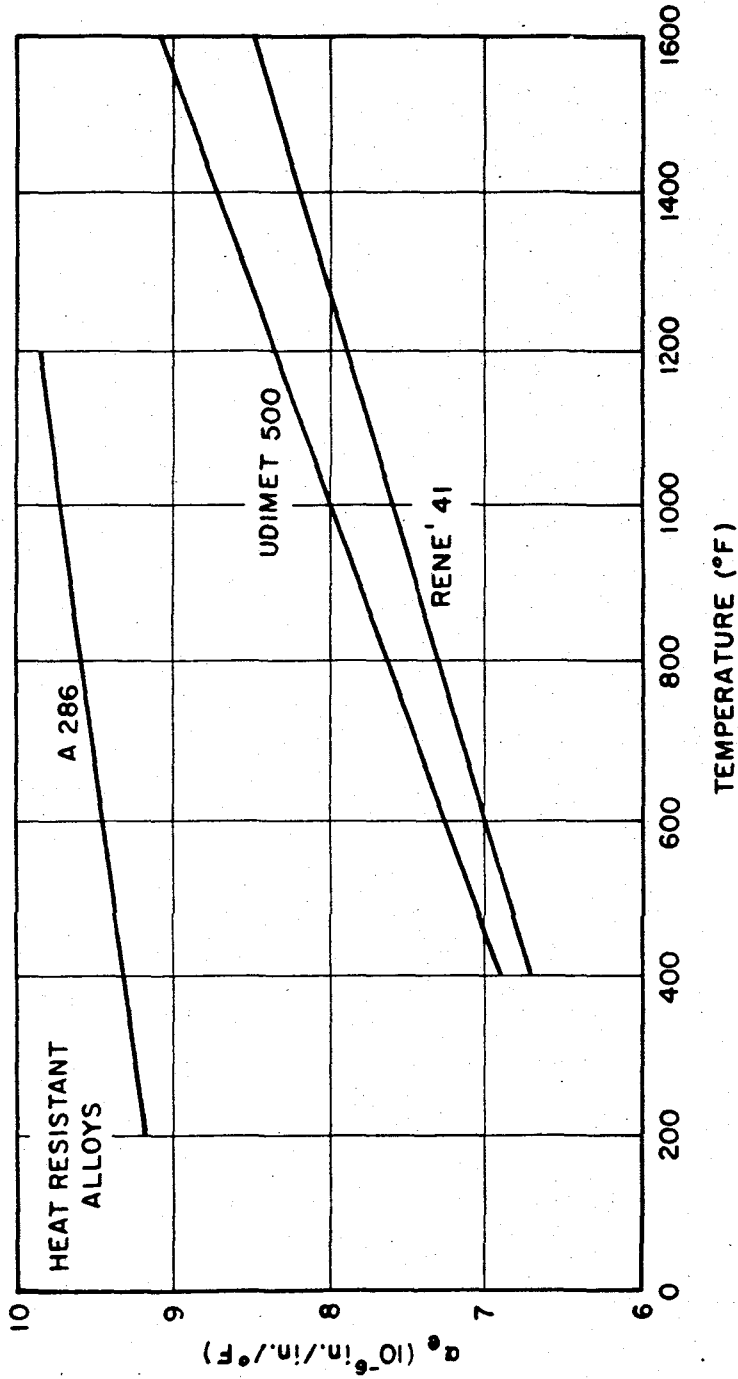
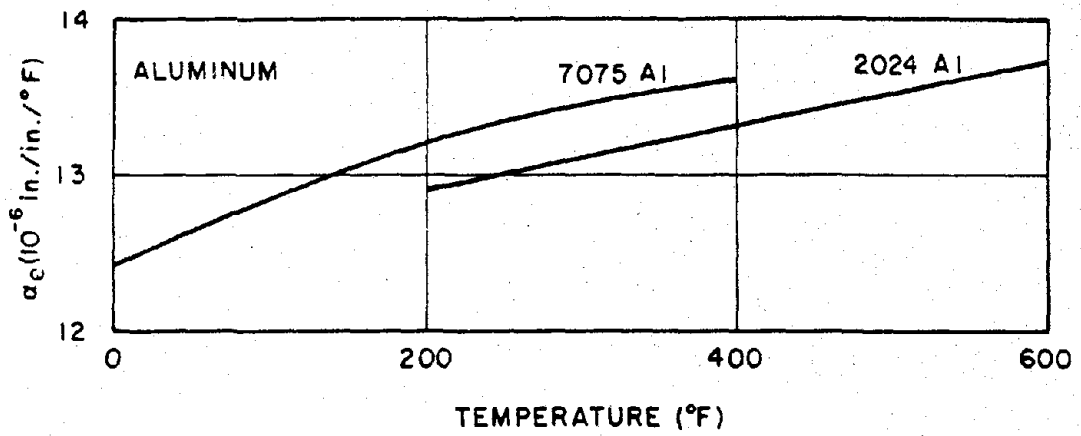Figure 9-14. Coefficient of Linear Expansion as a Function of Temperature for Heat Resistant Alloys

Figure 9-15. ■ Coefficient of Linear Expansion as a Function of Temperature for Aluminum Alloys ■
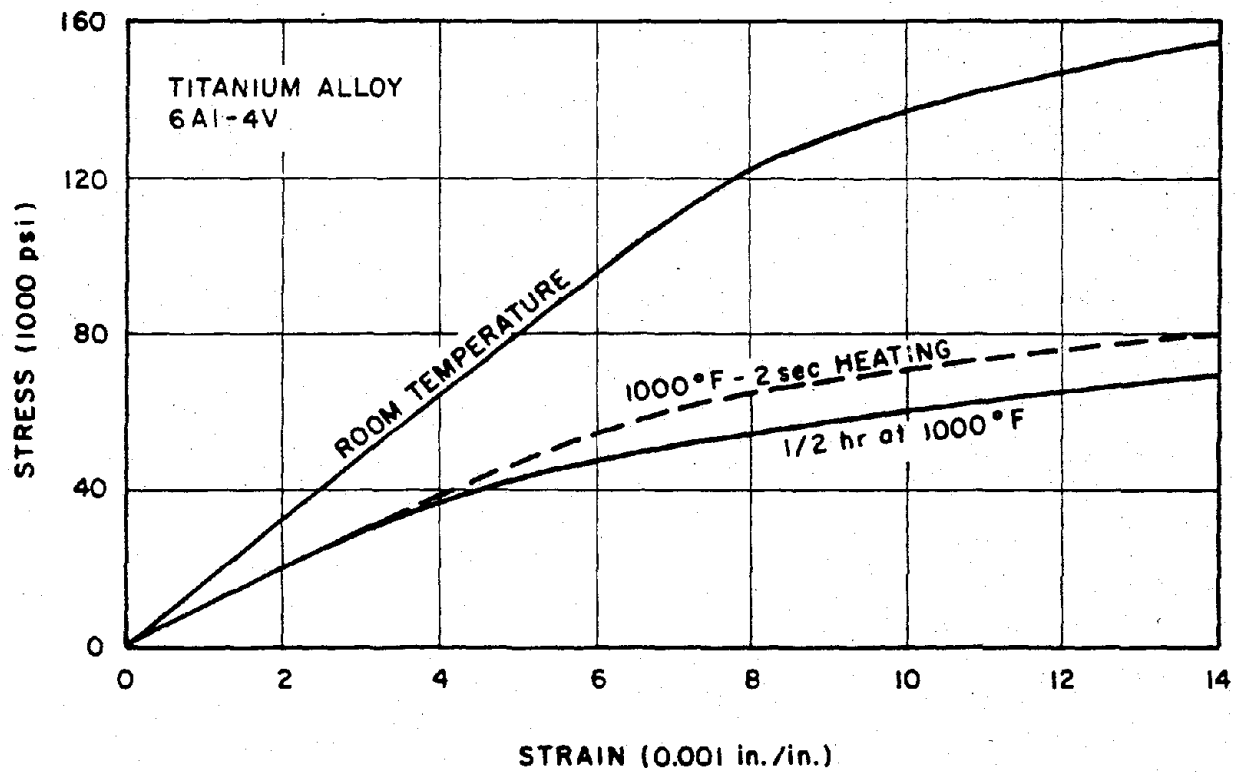
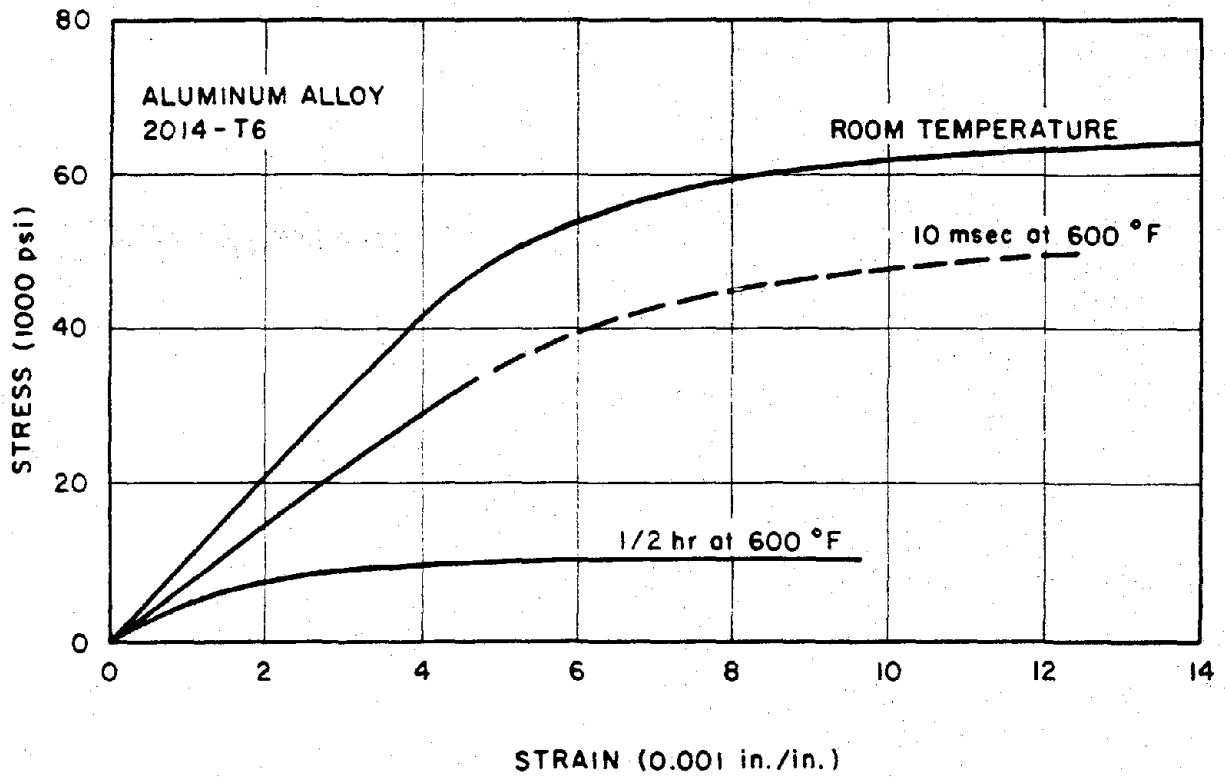Figure 9-16. ███ Typical Stress-Strain Curves for Titanium 6Al-4V Alloy at Room and Elevated Temperatures ███

Figure 9-17. ███ Typical Stress-Strain Curves for 2014-T6 Aluminum Alloy at Room and Elevated Temperatures ███
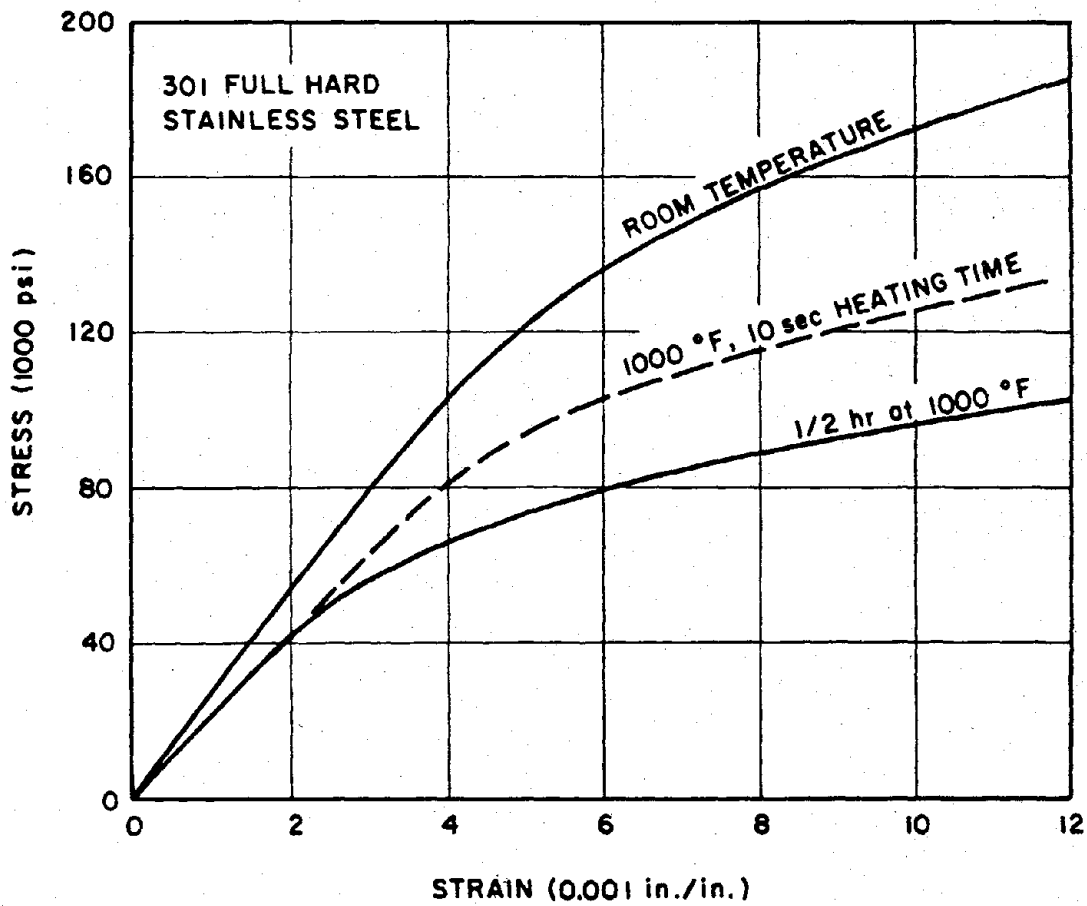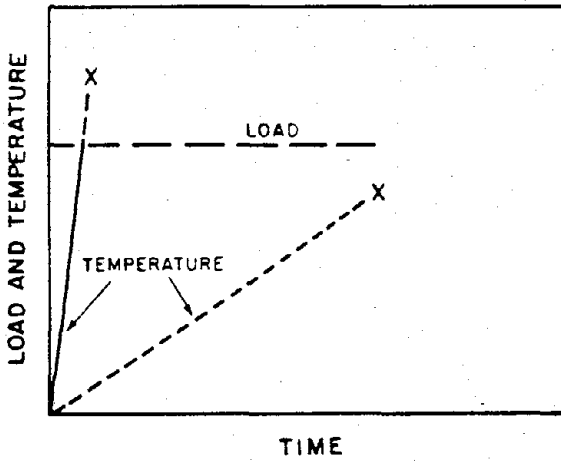
Figure 9-18.　███　Typical Stress-Strain Curves for 301 Stainless
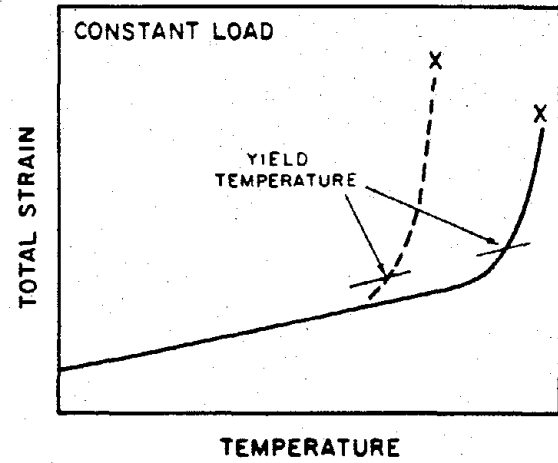Steel at Room and Elevated Temperatures ███
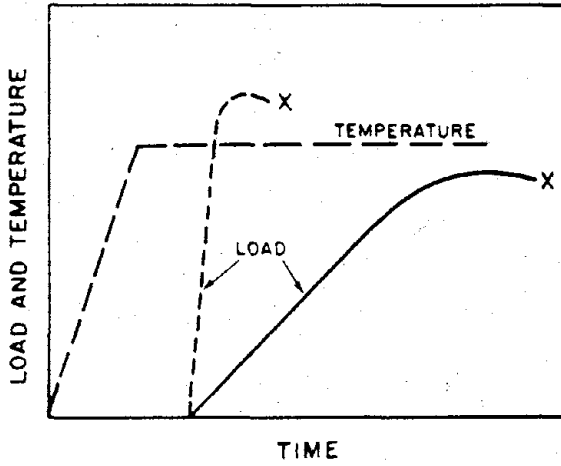
a. Tensile Tests After Rapid Heating
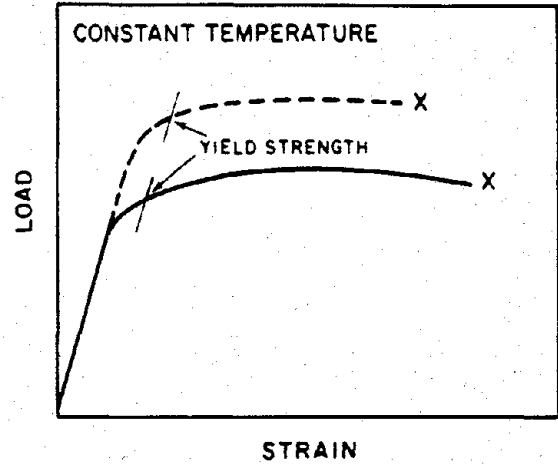
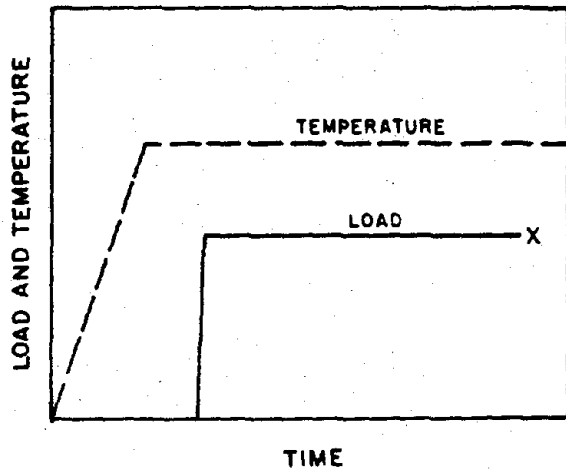b. Load-Strain Curves from Tests
Illustrated in Figure 9-19a.
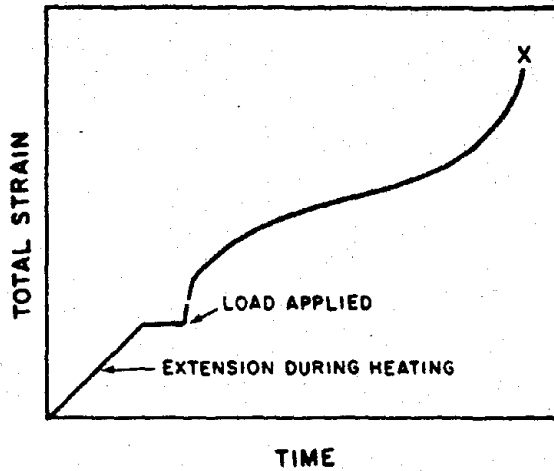
c. Rapid-Heating Constant-Load
Tensile Tests

d. Strain-Temperature Curves from
Tests Illustrated in Figure 9-19c.

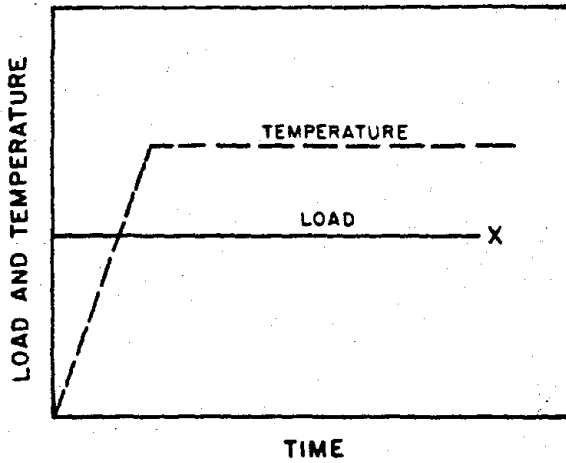Figure 9-19. ███ Types of Rapid Heating Tensile Tests ███

9-55

a. Very Short-Time Creep Tests
   After Rapid Heating

b. Time-Strain Curve

c. Very Short-Time Rapid-Heating
   Creep Tests
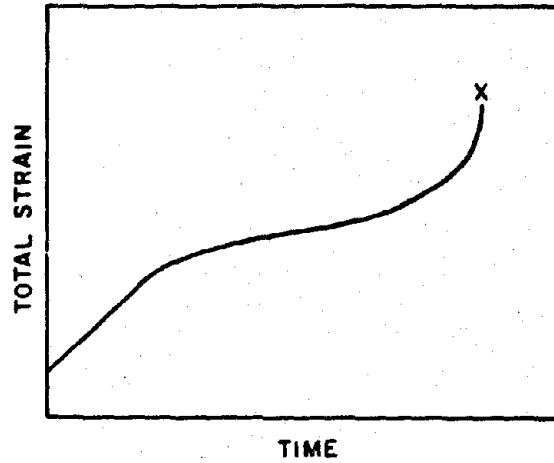
d. Time-Strain Curve

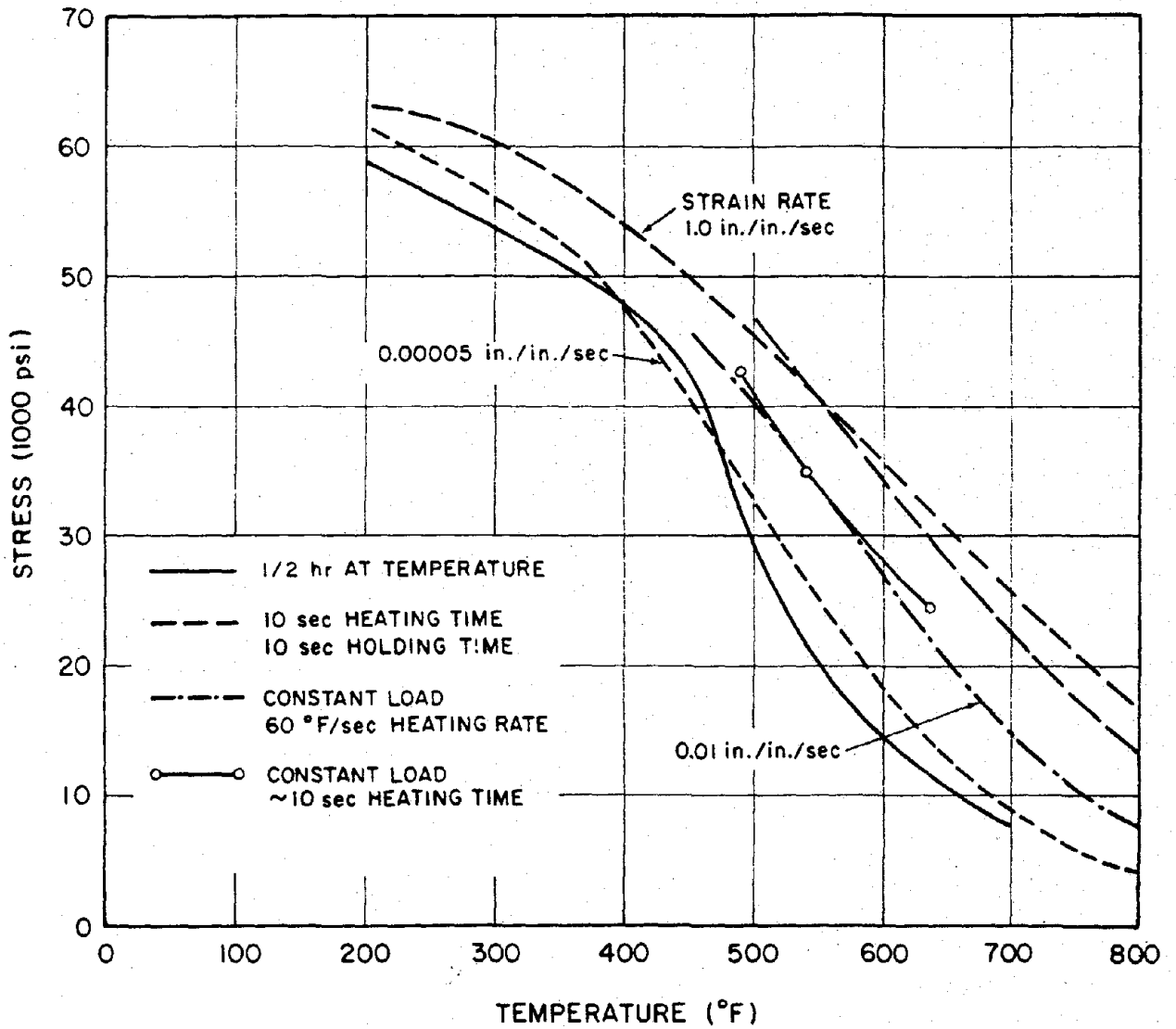Figure 9-20. ▮▮▮ Types of Short Time Creep Tests ▮▮▮

Figure 9-21. ███ 2024-T3 Aluminum Alloy Ultimate Strength
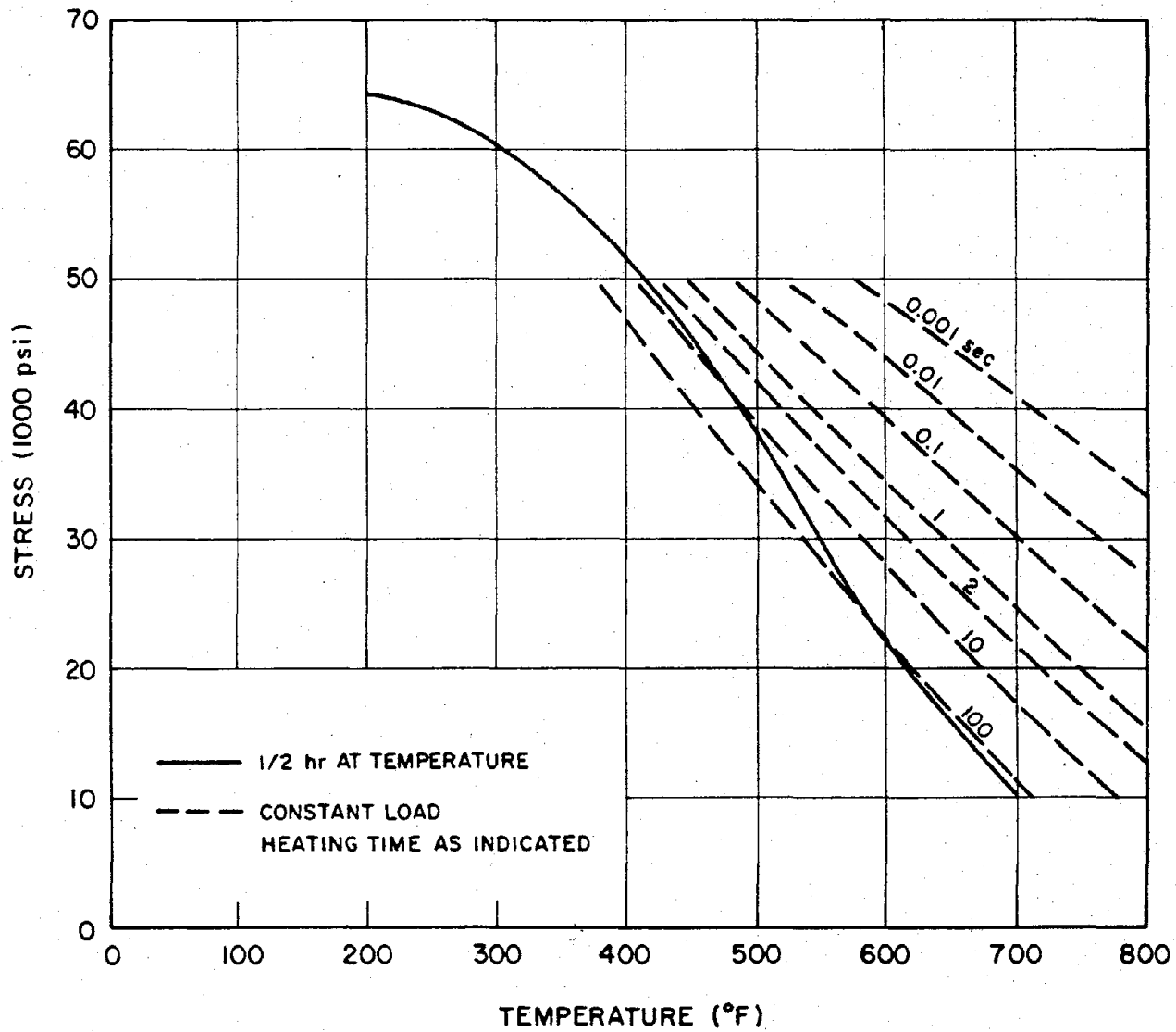at Elevated Temperature ███

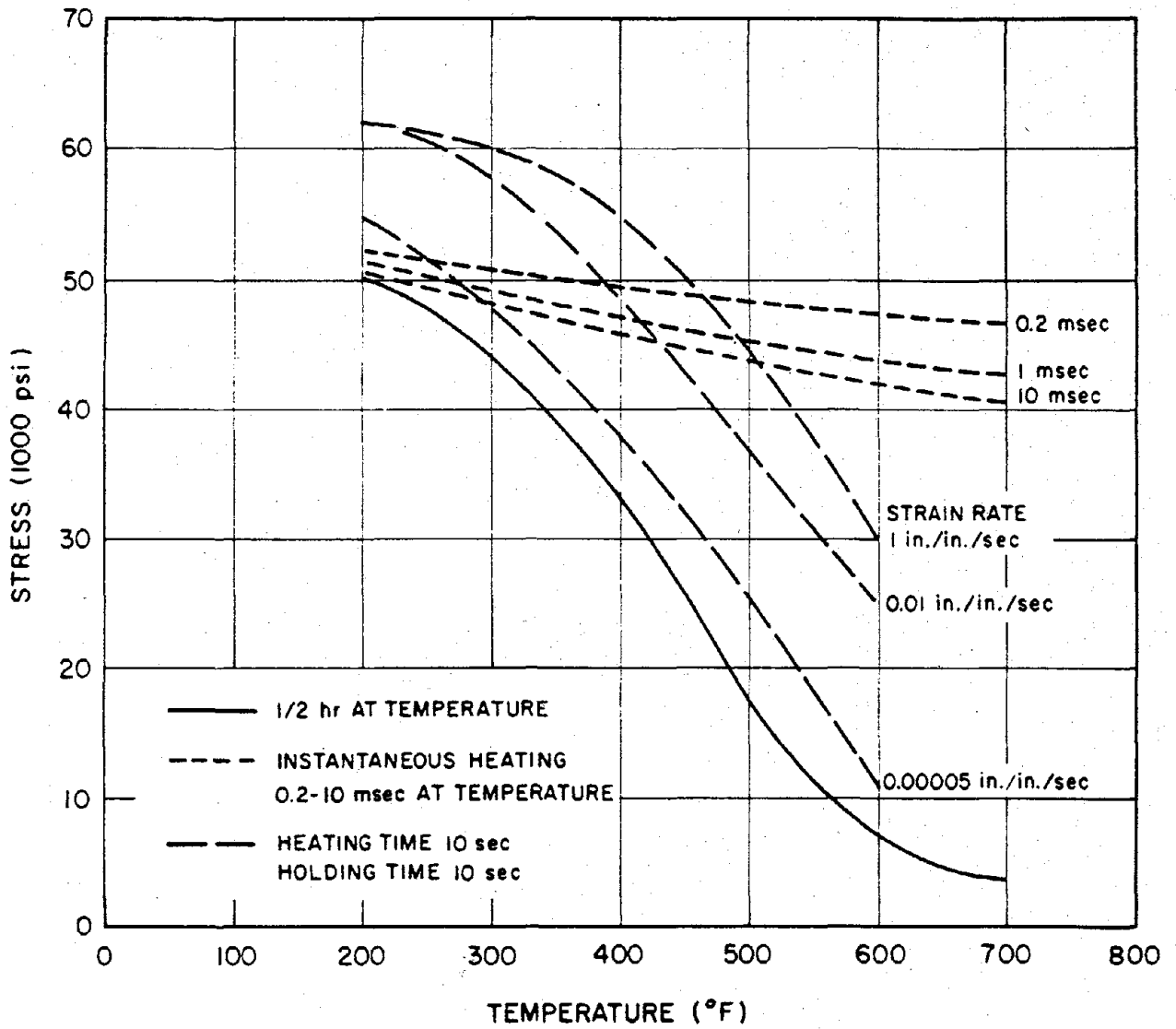Figure 9-22. ▮▮▮▮ 2024-T81 Aluminum Alloy Ultimate Strength
at Elevated Temperature ▮▮▮▮

Figure 9-23. ▮▮▮ 2014-T6 Aluminum Alloy Yield Strength at Elevated Temperature ▮▮

obtained in the manner illustrated in Figure 9-19a, but with the equilibrium temperature being reached in 10 sec and with a 10 sec soak time, and with three different strain rates used in the tensile tests. Other data were obtained in the manner illustrated in Figure 9-19c with a heating rate of 60°F/sec. The final data in Figure 9-21 also were obtained in a manner similar to that illustrated in Figure 9-19c with a heating time and time of rupture each approximately 10 sec.

The ultimate strength data in Figure 9-21 tend to show the importance of temperature and strain rate, but the data from the different sources are not consistent and are, therefore, difficult to evaluate. For example, the 0.00005 in./in./sec strain rate curve for 10 sec soak times from one source lies close to the 0.00033 in./in./sec strain rate curve for one-half hour soak times from a different source. Interpolation between the strain rate data for 10 sec soak times would indicate that a 0.00033 in./in./sec strain rate curve for a 10 sec soak time would lie slightly to the right of the 0.00005 in./in./sec curve and, therefore, slightly to the right of the one-half hour soak time curve. However, there are ample data, as shown in Figures 9-16 through 9-18, to justify the expectation that the 10 second curve should fall significantly to the right of the one-half hour curve; that is, for a given temperature and strain rate, the shorter the soak time, the smaller the decrease in tensile strength. It should also be noted that constant load curves should agree more closely.

The ultimate strength data in Figure 9-22 suggest a similar inconsistency although the data were taken from two different types of loading tests. The one-half hour data is from loading tests similar to that shown in Figure 9-19a, and "constant load, heating time as indicated" data is from loading tests similar to that shown in Figure 9-19c. The latter data clearly shows the influence of heating times or heating

rates on rapid heating, constant load tensile test results.

The yield strength data shown in Figure 9-23 for 2014-T6 Aluminum Alloy is somewhat more consistent. The instantaneous heating data were obtained in a manner similar to that illustrated in Figure 9-19a, although times are very short. Specimens were heated instantaneously by an electron beam, then a stress wave was sent up the specimen. An analysis of the stress wave characteristics on either side of the heated region provided yield and ultimate strength data as well as elastic modulus data. The times indicated for these data are the delay times between time of heating and the arrival of the stress wave. Thus, the data are for instantaneous heating, very short soak times, and extremely high strain rates ($\sim 10^{-9} \text{sec}^{-1}$). The comparable strain rate data for 1/2 hour and 10 sec soak times are in the relative positions that would be expected. The one factor that may explain why the comparable strain rate data of Figures 9-21 and 9-23 are relatively close together despite the different soak times is the heating rate.

Similar data from a single source are shown in Figures 9-24 and 9-25 for 6AL-4V Titanium Alloy and full, hard 301 stainless steel. The data in these figures also illustrates the inconsistencies in data discussed for Figures 9-21 through 9-23.

One other mechanical strength property of interest is the elastic or Young's modulus of the material. One source indicates that for soak times of from 1/2 to 10,000 hours, the elastic modulus depends only on temperature and not on soak time for a number of different materials. A separate source indicates that this is true for 6061-T6 and 2014-T6 Aluminum Alloys with soak times of 0.2, 1, and 10 msec. Although this conclusion has not been validated for other materials at small soak times, it appears reasonable to assume that the elastic
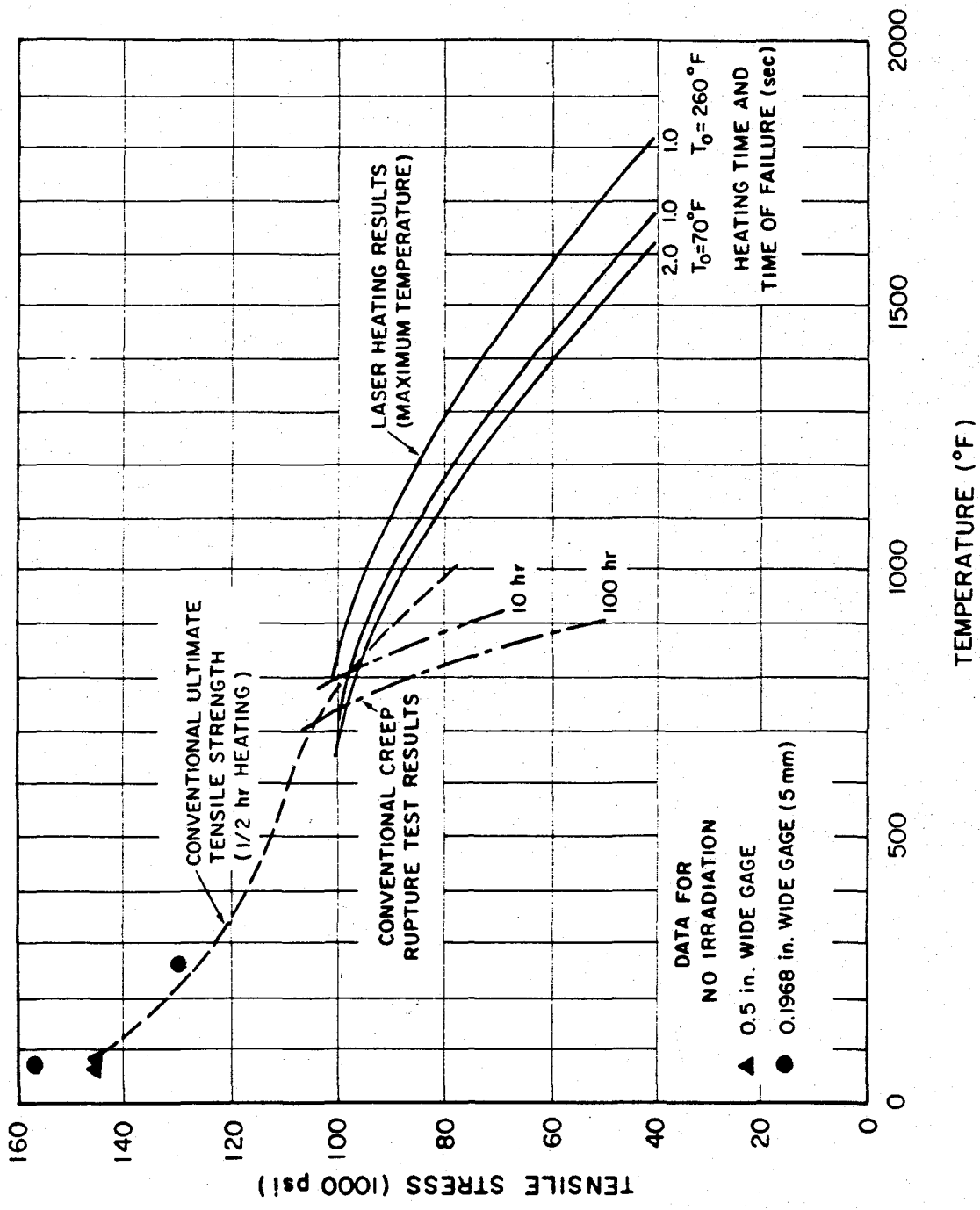
Figure 9-24.   Ultimate Strength Test Results for 6Al-4V Titanium Alloy
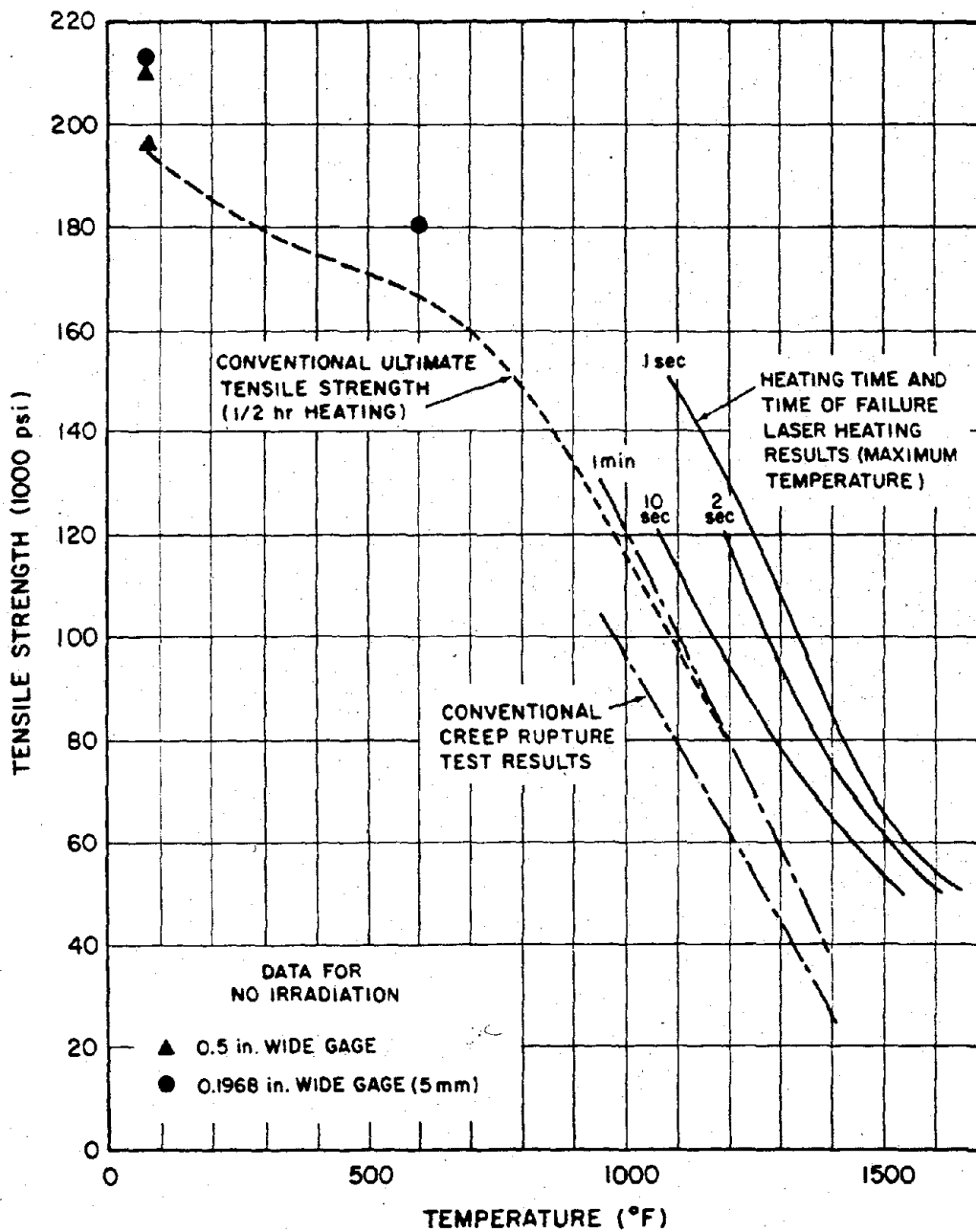at Elevated Temperatures

Figure 9-25. ▓▓▓ Ultimate Strength Test Results for Full Hard
Stainless Steel at Elevated Temperature ▓▓▓

modulus only depends on temperature for metallic materials.

In evaluating the information available on changes in mechanical strength properties of materials. it should be reemphasized that a variety of testing techniques have been used to obtain the data presented in this section. Constant strain rate and constant load techniques have both been used. A variety of heating techniques have been used, including ovens. resistance heating. inductive heating. hot-fluid bath heating. radiant heating. lasers, and electron beams. A considerable amount of data have been obtained on a number of different materials.

The data indicate that there are five basic variables that influence the degradation of mechanical strength properties at elevated temperature for particular materials: initial temperature. heating rate, final temperature, soak time. and strain rate. Not much is known about the effect of initial temperature since most data report "room temperature" as the reference temperature. Increases in heating rate, final temperature. or soak times cause a decrease in ultimate and yield strengths. An increase in strain rate at a particular final temperature apparently increases the strength. Because of the different testing techniques employed, the relative importance of these variables in determining material strengths is difficult to determine; however. it appears that soak time and final temperature are most important. followed closely by strain rate, and finally heating rate as long as final temperature is reached in less than one minute.

Although there are considerable data available on rapid heating effects, it is difficult to extrapolate to other than test conditions with any confidence. In any event, in estimating strength, data available on rapid heating and short times appear to be more appropriate than those for slow heating. long soak times for the general class of problems of interest in this manual.

RESISTANCE TO LOAD

The ultimate concern of combined thermal/blast effects is the change, if any, in the vulnerability/survivability of tactical systems compared to vulnerability/survivability to thermal or blast effects separately.

Figure 9-26 illustrates typical experimental stress-strain curves for 2014-T6 Aluminum Alloy with two approximations to this curve: the more or less classical straight line: and the so-called Bell's stress-strain law for dynamic deformation:

$$\sigma = \beta \left(1 - \frac{T}{T_m}\right) \epsilon^{1/2}$$

where

σ = stress, psi,

ϵ = strain, in./in..

T = temperature of interest, °K.

T_m = melting temperature, °K.

β = parabolic coefficient.

The area under each of these curves is equal to the strain energy absorbed by the material. For the straight line approximation the area under the room temperature curve equals about 433 in. · lb/in.^{3} to a strain (ϵ) of 0.01 in./in. This compares well with the area of 432 in. · lb/in. under the typical curve to the same ϵ. The Bell stress-strain law gives an area of 441 in. · lb/in.^{3}.

The change in allowable uniform equivalent static load that will give the same maximum deflection as a uniform dynamic load has been determined for degraded 2014-T6 Aluminum alloy properties using elastic theory for large deflections of simply supported square plates.* The allowable load was defined as the maximum

---
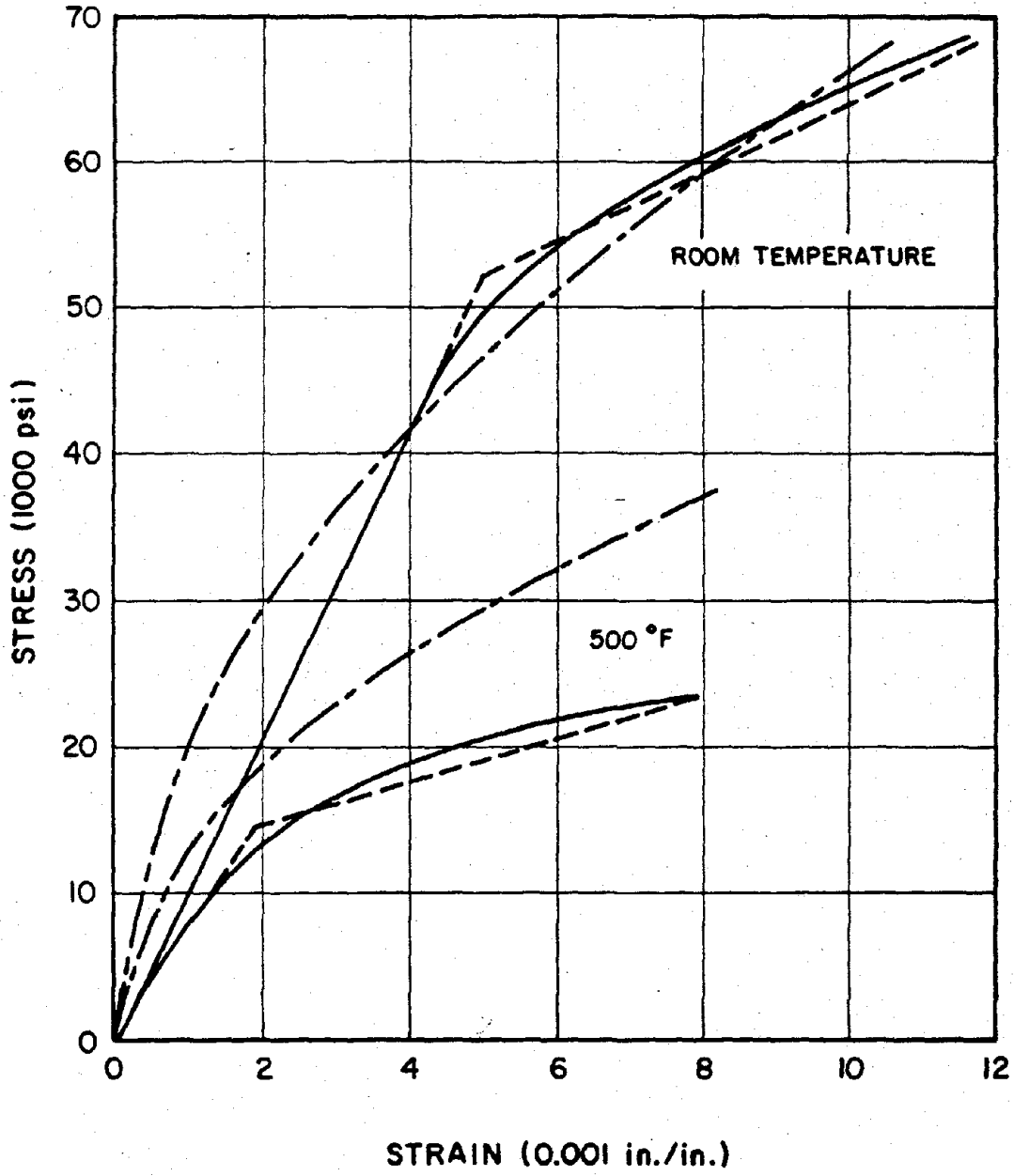*An air blast loading of long duration, or a flat top wave, was assumed.

Figure 9-26. ▢ Stress-Strain Approximation for 2014-T6 Aluminum Alloy ▢

static load the plate could carry without exceeding the yield stress. One-half hour soak time data were used to determine the strength properties, and a 20-in. square plate, 1/4-in. thick was assumed. The results are shown in Table 9-9. As can be seen, the maximum allowable load is almost a linear function of allowable stress. The explanation of this can be seen in the following equation, which is the elastic stress equation for the plate under study.

$$\sigma = 7,356.8p + 4.632E^{1/3}p^{2/3}.$$

The second term of the equation is for membrane stresses and is the only term that contains the temperature dependent Young's modulus. As the temperature increases, the value of E decreases, so the contribution from the second term is further decreased, and a fairly linear dependence on the pressure, p, remains.

The allowable stress in the above example was taken from 1/2 hour soak time data. This provides a lower bound for the allowable load. Examination of Figure 9-21 through 9-25 indicates that the rapid heating, short soak time data generally fall above the 1/2 hour soak time curves. More reliable estimation of allowable loads will depend on the availability and appropriateness of the material data that is required for the type of analysis and calculation techniques being employed by an investigator.

The truly dynamic case may be analyzed similarly. In both cases, however, the basic factor that influences structural degradation is allowable stress as long as the elastic analysis approach is used.

Where deformation or plastic response is responsible for failure, allowable stress no longer can be used to determine allowable load; either total deformation or total energy absorbed must be used.

The energy approach consists of stating that the energy absorbed by a structure as it deforms is proportional to the product of the overpressure and the impulse values, ΔpI, of the blast wave that causes the deformation. Thus, for a constant value of absorbed energy used as a measure of damage, any combination of overpressure and impulse that yields the same product will cause the same amount of "damage."

The effect of elevated temperature on the damage values has been investigated. One source indicates that for face-centered cubic materials, such as aluminum, the value of the parabolic coefficient of Bell's stress-strain law varies linearly with the temperature. For 2014-T6 Aluminum, the equation would be

$$\sigma = 9.65 \times 10^5 \epsilon^{1/2}$$

Table 9-9. ▮ Allowable Uniform Static Load for Aluminum Plate at Three Temperatures ▮

Temperature (°F)	σy (10^3 psi)	Young's Modulus, E (10^6 psi)	Deflection (in.)	Allowable Load (psi)
70	57	10.5	0.323	7.25
350	43	9.77	0.261	5.45
500	17	8.4	0.117	2.10

where the value of β was obtained by fitting the curve to pass through the room temperature yield stress for the material. The Bell's law equation indicates that the energy under the stress-strain curve is a linear function of temperature by varying values of β linearly. This infers that the damage value, ΔpI, should depend on a linear function of temperature, i.e.,

$$(\Delta pI)_{T_2} = (\Delta pI)_{T_1} \left[\frac{1 - \dfrac{T_2}{T_m}}{1 - \dfrac{T_1}{T_m}} \right]$$

where

$(\Delta pI)_{T_1}$ = damage value at temperature T_1

and

$(\Delta pI)_{T_2}$ = damage value at temperature T_2.

If this relation were true, it would be a simple matter to evaluate the vulnerability of a structure. Once the value of ΔpI had been determined for ambient temperatures, the ΔpI value at elevated temperatures could be determined easily.

The Bell's law equation also indicates that yield strength, ultimate strength, and Young's modulus are linear functions of temperature for dynamic deformation. The data that were used to develop the equation were obtained from impact tests of oven heated samples. No information was provided as to what the heating rates or soak times were. The only other comparable data, at least in the dynamic sense, were shown in Figure 9-24, which indicate that data from dynamic tests do seem to approximate a straight line to some degree.

Thus, with further testing and research, it may be that a relatively simple approach to assessing structural vulnerability to combined thermal/blast effects will be possible for dynamic deformation damage criteria.

The previous discussion has been concerned primarily with unstressed, unrestrained structural elements. There are three main structural conditions that are encountered in the analysis of structural response to combined thermal/blast effects. These are: unstressed members with no edge or end restraints; unstressed members with restraints; and prestressed members with restraints. These conditions refer to the status of a structure before either thermal or blast loading. The first condition is the easiest to analyze since there are no restraints to dimensional changes during or after heating so the thermal degradation of mechanical strength properties is the main concern. The second condition is more complex since dimension changes are prevented in varying degrees and appreciable thermal stresses may exist at the time of blast loading. The inclusion of these thermal stresses is not uncommon in structural elastic analysis. Thermal stresses caused by thermal gradients in the structural member also are included under this condition. The inclusion of stresses induced by the thermal gradient in an elastic structural analysis generally will require the use of a finite element structural analysis computer code. Unfortunately, it cannot be assumed that either form of thermal stress will be inconsequential, and they should both be addressed specifically in the solution of a particular problem. The final condition is the most difficult to analyze because a member may be stressed prior to thermal or blast loading.

The final factor to consider in determining structural response is the possibility of changes in failure modes, particularly materials rupture. Visual examination of a 1/4-in. by 0.040-in. 2024-T3 Aluminum specimen that fail-

ed indicated little necking down at the failure point. This may be due to the small area (about 17 mm diameter) exposed to thermal radiation. Failure occurred on a 45° plane, with no cupping. Postshot photos of cylindrical/aluminum shells, exposed to HE air blast after rapid heating, indicated an almost brittle-like fracture mode of failure. Failure of similar shells at normal temperature under the same type of loading was of a ductile deformation type. The possibility of a change in failure mode under dynamic loading at elevated temperatures has not been investigated, but is of concern since residual load carrying capabilities of deformed structures are sometimes used in determining vulnerability.

In summary, if elastic criteria are used to determine survivability/vulnerability, and if the necessary materials strength properties are known, a fairly straight forward but not necessarily simple stress analysis may be performed. If dynamic or deformation criteria are necessary, the problem becomes very difficult, if not impossible, because of the lack of validated analysis techniques. A third criterion, material melting, may be used to bound the problem. A temperature criterion may be chosen that is or nearly equal to the melting point of the material with the inference that, at that temperature, the material has no strength, and therefore, no resistance to load. This latter criterion has been used, for example, to establish kill criteria for Army aircraft.

SECTION V
X-RAY DAMAGE EFFECTS

INTRODUCTION

Nuclear weapons as X-ray sources and the environments they produce are described in Chapter 4. This section discusses the interaction of the X-ray environment with aerospace systems and some typical damage mech-

anisms that result from the interaction. The damage mechanisms depend on the fluence and energy, or temperature, of the X-rays and on the protective and structural materials involved in the interaction. For purposes of discussion the damage mechanisms can be divided conveniently into the effects caused by hot X-rays and those caused by cold X-rays. Some familiarity with the material discussed in Chapter 4 is assumed in the following discussion.

Cold X-rays (typically 1 to 3 keV black body temperatures) are absorbed in a thin surface layer. At sufficiently high fluence, a short pulse of X-rays can heat the surface rapidly and may cause it to vaporize and blow off. This results in: (1) an impulse imparted to the total structure; and (2) generation of a strong shock wave that propagates into the structure, and which may cause spallation of material at free boundaries and internal fracture of materials and bonds. These latter effects are produced by shock wave propagation through the thickness of a surface structure such as the thermal protection shell of a reentry vehicle. The former effects may produce damage by whole vehicle modes of response to the net impulse.

The hot X-rays are more penetrating. They can cause: (1) thermally generated shock waves in the vehicle structural materials and internal components; (2) melting and vaporization of the substructure; (3) internal deposition of energy in electronic components producing transient or permanent damage (see Chapter 6 and Section 7 of this chapter); or (4) produce internal EMP signals (see Chapter 7).

While some nuclear weapons emit only cold X-rays, all hot X-ray weapons have a cold component. Hence, for exoatmospheric events the hot X-ray effects are accompanied by cold X-ray effects. On the other hand, for endoatmospheric explosions, the cold X-rays have short mean free paths, and the X-ray effects beyond distances of a few tens of meters are produced by hot X-rays alone.

■ Damage to a particular system depends on the structural details of the system as well as the X-ray spectrum. Accurate damage prediction even for the simplest geometries, generally require elaborate computer programs to calculate the energy deposition and the response of the system. All vulnerability analyses follow similar computational steps:

1. The X-ray energy deposition is computed using known processes for the materials and structure. This energy is assumed most often to be deposited instantaneously.

2. From the calculated energy deposition and the equation of state for the materials in the structure (if known) for the liquid, solid, and vapor phases of the material, a stress wave, which propagates through the surface structure, is calculated.

3. Damage to the surface structure that results from the stress wave (spallation, internal fracturing, delamination and debonding), is determined. These calculations generally are based on experimentally derived damage response curves. A good deal of progress has been made in the last few years in understanding and predicting fractures in most homogeneous and some composite materials. Even a small amount of fracturing may cause a significant loss in strength of material. One of the most complicating factors involved in making reliable damage predictions is that of in-depth heating prior to stress wave propagation through the material.

4. The response of the whole structure that results from the impulse imparted to it is determined. This response also is generally based on experimentally determined damage or properties degradation measurements. In these computations, the effects of the loss of strength of the structural material as a result of fracturing caused by the immediately preceding stress wave or by in-depth heating must be included. The structure may be broken by the impulse loading, or it may be weakened (buckled) so that it will fail under subsequent stresses, for example, reentry into the atmosphere.

■ X-RAY ENERGY DEPOSITION CALCULATIONS ■

■ The starting point of all X-ray vulnerability analysis is a calculation of the X-ray energy deposition. The determination of the transmitted X-ray fluence, or shine through, into the interior of the aerospace system, is implicit in these calculations. Calculation of X-ray energy deposition involves the use of energy dependent photon absorption cross sections and energy and angle dependent scattering cross sections. Corrections for fluorescence, i.e., reradiation of X-rays, may be significant for high energy photons in certain materials. Sophisticated energy deposition and transport calculations, using detailed energy dependent cross sections and their angular dependence can be made by computers using Monte Carlo techniques. The results serve as an accuracy check and provide "effective" cross section data for simpler techniques. Approximation techniques greatly reduce the amount of effort and time involved in system analysis. Fairly accurate approximate values sometimes can be obtained even by hand calculations, as will be shown with examples.

9-33 X-ray Cross Sections ■

■ The probability of a photon of energy $h\nu$ traversing a distance of absorbing material x is $e^{-\mu x}$, where μ is the linear attenuation coefficient. This probability also can be written as $e^{-(\mu/\rho)\rho x}$, where μ/ρ is the mass attenuation coefficient for the material (see paragraph 4-3). In this representation, μ/ρ is in cm^2/gm and ρx is the thickness in gm/cm^2, i.e., the mass of material in the column of 1 square centimeter cross section and x centimeters long.

■ If the monoenergic X-ray fluence incident normal (perpendicular) to the material sur-

face is φ_0. the direct fluence after traversing a thickness ρx of absorbing material is

$$\varphi_{\mathrm{dir}} = \varphi_0 e^{-(\mu/\rho)\rho x} \ \mathrm{cal/cm^2}.$$

The total mass attenuation coefficient μ/ρ is the sum of several components that represent the various mechanisms that can remove a primary photon from the direct flux, while it traverses a material. These mechanisms are described in paragraph 4-3, Chapter 4, and are: the photoelectric process. Compton inelastic scattering. Compton elastic scattering (incoherent elastic scattering) and Rayleigh elastic scattering (coherent elastic scattering). The first two processes result in photon energy being absorbed and the production of secondary electrons, the photoelectrons and Compton recoil electrons, respectively. The kinetic energy of these electrons is dissipated in the material and heats it. Energy deposition usually is calculated to have occurred at the depth at which the electrons are produced. However, in the case of very thin samples, the range of the freed electrons can exceed the material thickness, and energy deposition cannot be considered to be local. The energy removed from the primary photon beam in the Compton elastic process or the Rayleigh elastic process is not locally absorbed. A clear distinction must be made between attenuation of the primary flux and absorption of energy from the primary flux. For this reason the total linear attenuation coefficient usually is written as $\mu = \mu_a + \mu_s$. Here, μ_a is an absorption coefficient. It represents the first two processes mentioned above, which result in energy absorption. The second term, μ_s, is an elastic scattering coefficient, which contributes to the attenuation of the primary flux but not to local energy absorption. It is sometimes convenient to ignore the Rayleigh coherent scattering coefficient in the total attenuation coefficient. The coherent radiation has the same energy, and nearly the same

direction, as the primary photon and cannot be distinguished from it in the "bad" geometry situations that usually occur in nuclear effects applications.*

Mass attenuation coefficients for the elements beryllium, aluminum, iron, copper, tungsten, and uranium are given in Tables 9-10 through 9-15, and Figures 9-27 through 9-32, respectively. These are representative of metallic materials used in aerospace systems. Mass attenuation coefficients for ablator materials, carbon phenolic and tape-wound silicon phenolic are shown in Figures 9-33 and 9-34, respectively. In these tables and figures, Z is the atomic number, μ_{ce}/ρ is the coherent elastic scattering coefficient, μ_{ie}/ρ is the incoherent Compton elastic coefficient, μ_{is}/ρ is the inelastic Compton coefficient, and μ_p/ρ is the photoelectric coefficient. As designated previously, μ_a/ρ and μ/ρ are the energy absorption coefficient and the total attenuation coefficient.[†]

9-34 X-ray Energy Deposition and Shine Through Fluences

X-ray energy deposition in a thickness δ at a depth x due to direct fluence photons is given by

$$A'_{\mathrm{dir}} = \varphi_0 \left[1 - e^{-\left(\frac{\mu_a}{\rho}\right)\rho\delta} \right] e^{-\left(\frac{\mu}{\rho}\right)\rho x}.$$

If $\mu_a \delta \ll 1$, and if φ_0 is in cal/cm^2, this expression can be written as

$$A'_{\mathrm{dir}} = \varphi_0 \left(\frac{\mu_a}{\rho}\right) \rho\delta \ e^{-\left(\frac{\mu}{\rho}\right)\rho x} \ \mathrm{cal/cm^2}.$$

---

* A "good" geometry is one in which the distinction between primary and scattered photons can be made accurately.

† The symbols K, L_1, L_2, etc., in the tables and figures indicate the binding energies of the various electron shells (see paragraph 4-3, Chapter 4).

Frequently, the absorption is written in terms of cal/gm by dividing out the thickness $\rho\delta$,

$$A_{dir} = \varphi_o \left(\frac{\mu_a}{\rho}\right) e^{-\left(\frac{\mu}{\rho}\right)\rho x} \quad \text{cal/gm.}$$

This expression for the absorption is in terms of a dose; however, this assumes that very little of the flux is absorbed in the deposition region at depth x, i.e., the deposition region considered is very thin. Clearly, more energy than is in the incident flux cannot be absorbed.

The equation for direct fluence (φ_{dir}) given in paragraph 9-32 can be used to represent a small energy band of photons in X-ray energy spectra such as those tabulated in Table 4-3, Chapter 4, for various black body spectra. The total energy in the direct X-ray fluence after traversing thickness x is obtained by summing over the energy bands.

$$\varphi = \sum_i \varphi_{oi} \, e^{-\left(\frac{\mu}{\rho}\right)_i \rho x} \quad \text{cal/cm}^2.$$

In a like manner, the total direct fluence X-ray energy absorption at depth ρx is obtained by summing for each energy band.

$$A = \sum_i \left(\frac{\mu_a}{\rho}\right)_i \varphi_{oi} \, e^{-\left(\frac{\mu}{\rho}\right)_i \rho x} \quad \text{cal/cm}^2.$$
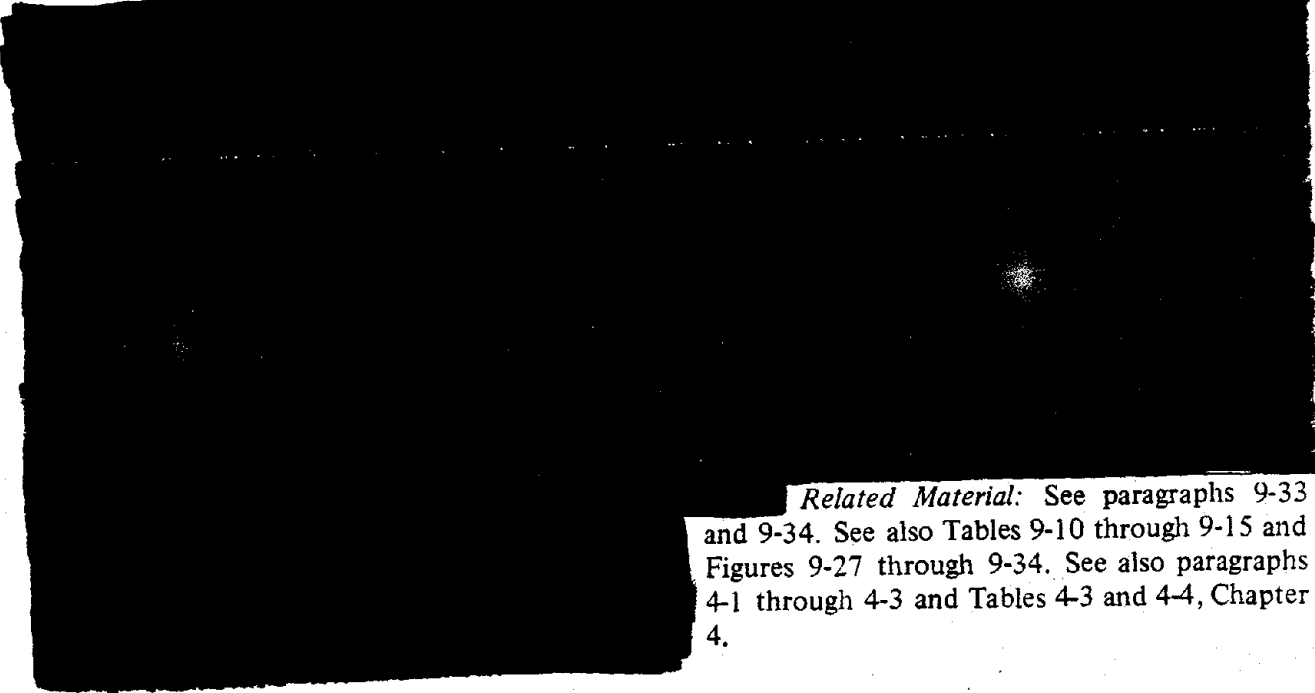
Problems 9-3 and 9-4 illustrate how these equations can be used to calculate approximate values for energy deposition and shine through.

The information contained in Tables 9-10 through 9-15 and Figures 9-27 through 9-34 together with the equation for energy absorption given in paragraph 9-34 provide the means to obtain the approximate X-ray energy absorbed for various spectra and several materials. If the energy deposition at the surface on which the X-rays are incident is desired, the thickness, x, reduces to zero, and the energy deposition equation becomes

$$A = \sum_i (\mu_a/\rho)_i \, \varphi_{oi} \ \text{cal/gm.}$$

9-71

Page 9-72 deleted.

Related Material: See paragraphs 9-33 and 9-34. See also Tables 9-10 through 9-15 and Figures 9-27 through 9-34. See also paragraphs 4-1 through 4-3 and Tables 4-3 and 4-4, Chapter 4.

Problem 9-4. Calculation of X-ray Energy Deposition at a Depth in a Material and the Shine Through Fluence

The information contained in Tables 9-10 through 9-15 and Figures 9-27 through 9-34 together with the equation for energy absorption given in paragraph 9-34 provide the means to obtain the approximate X-ray energy absorbed for various spectra and several materials at a depth x in the materials, as well as the fluence at that depth or the fluence emerging from the back face of the material (shine through).

Problem 4-1, Chapter 4, describes the method to obtain energy distributions for various source temperatures from the normalized Planck distributions given in Table 4-1, Chapter 4.

9-74

Page 9-75 deleted.

Reliability: The reliability of the procedures described above depends on the X-ray spectrum and the absorbing material. The accuracy depends primarily on the relative importance of the scattering cross sections, and, for some materials, fluorescence. No definite reliability estimate can be made.

Related Material: See paragraphs 9-33 and 9-34. See also Tables 9-10 through 9-15 and Figures 9-27 through 9-34. See also paragraphs 4-1 through 4-3 and Tables 4-3 and 4-4, Chapter 4.

Table 9-10. ■ X-ray Cross Sections, Beryllium $Z = 4$ (cm^2/gm) ■

Photon Energy keV	μ_{ce}/ρ	μ_{ie}/ρ	μ_{is}/ρ	μ_{p}/ρ	μ_{a}/ρ	μ/ρ
0.1	7.097-1*	1.154-3	2.770-7	1.507+4	1.507+4†	1.507+4
0.111K	7.094-1	1.331-3	3.560-7	1.109+4	1.109+4	1.109+4
0.111	7.094-1	1.331-3	3.560-7	2.323+5	2.323+5	2.323+5
0.15	7.079-1	2.007-3	7.257-7	1.105+5	1.105+5	1.105+5
0.2	7.054-1	2.972-3	1.421-6	5.302+4	5.302+4	5.302+4
0.3	6.984-1	5.171-3	3.685-6	1.816+4	1.816+4	1.817+4
0.4	6.889-1	7.660-3	7.223-6	8.292+3	8.292+3	8.292+3
0.5	6.770-1	1.039-2	1.218-5	4.456+3	4.456+3	4.456+3
0.6	6.631-1	1.332-2	1.866-5	2.662+3	2.662+3	2.662+3
0.8	6.306-1	1.972-2	3.650-5	1.165+3	1.165+3	1.165+3
1.0	5.939-1	2.674-2	6.137-5	6.072+2	6.072+2	6.078+2
1.5	4.986-1	4.648-2	1.591-4	1.820+2	1.820+2	1.825+2
2.0	4.153-1	6.151-2	2.771-4	7.626+1	7.626+1	7.674+1
3.0	3.019-1	7.946-2	5.309-4	2.199+1	2.199+1	2.237+1
4.0	2.371-1	9.009-2	7.911-4	9.004	9.004	9.332
5.0	1.968-1	9.831-2	1.066-3	4.481	4.482	4.778
6.0	1.685-1	1.053-1	1.356-3	2.527	2.528	2.802
8.0	1.285-1	1.170-1	1.971-3	1.019	1.021	1.267
10.0	1.003-1	1.261-1	2.613-3	5.024-1	5.050-1	7.314-1
15.0	5.780-2	1.386-1	4.173-3	1.384-1	1.426-1	3.390-1
20.0	3.677-2	1.432-1	5.589-3	5.539-2	6.098-2	2.410-1
30.0	1.844-2	1.433-1	8.064-3	1.525-2	2.331-2	1.851-1
40.0	1.098-2	1.395-1	1.017-2	6.126-3	1.630-2	1.668-1
50.0	7.251-2	1.348-1	1.199-2	3.027-3	1.502-2	1.570-1
60.0	5.132-2	1.299-1	1.357-2	1.705-3	1.528-2	1.503-1
80.0	2.947-3	1.207-1	1.617-2	6.930-4	1.686-2	1.406-1
100.0	1.898-3	1.126-1	1.819-2	3.464-4	1.854-2	1.331-1
150.0	8.554-4	9.646-2	2.164-2	9.953-5	2.174-2	1.191-1
200.0	4.811-4	8.476-2	2.364-2	4.159-5	2.368-2	1.089-1
300.0	2.138-4	6.877-2	2.559-2	1.241-5	2.560-2	9.458-2
400.0	1.203-4	5.830-2	2.630-2	5.346-6	2.631-2	8.473-2
500.0	8.019-5	5.080-2	2.645-2	2.811-6	2.645-2	7.733-2
600.0	5.346-5	4.516-2	2.634-2	1.675-6	2.634-2	7.156-2
800.0	2.807-5	3.708-2	2.571-2	7.501-7	2.571-2	6.282-2
1000.0	1.737-5	3.157-2	2.487-2	4.074-7	2.487-2	5.646-2

■ 7.097 − 1 = 7.097 x 10^{-1}.
† 1.507 + 4 = 1.507 x 10^4.

Table 9-11. ■ X-ray Cross Sections, Aluminum $Z = 13$ (cm^2/gm) ■

Photon Energy keV	μ_{ce}/ρ	μ_{ie}/ρ	μ_{is}/ρ	μ_{p}/ρ	μ_{a}/ρ	μ/ρ
0.1	2.504	5.614-4*	1.348-7	4.462+5†	4.462+5	4.462+5
0.118L_1	2.503	7.044-4	1.998-7	2.849+5	2.849+5	2.849+5
0.118	2.503	7.044-4	1.998-7	4.273+5	4.273+5	4.273+5
0.15	2.501	9.872-4	3.568-7	2.192+5	2.192+5	2.192+5
0.2	2.496	1.473-3	7.102-7	9.926+4	9.926+4	9.926+4
0.3	2.482	2.591-3	1.874-6	3.250+4	3.250+4	3.250+4
0.4	2.463	3.867-3	3.706-6	1.472+4	1.472+4	1.472+4
0.5	2.439	5.276-3	6.286-6	7.962+3	7.962+3	7.964+3
0.6	2.411	6.799-3	9.696-6	4.819+3	4.819+3	4.822+3
0.8	2.345	1.015-2	1.917-5	2.183+3	2.183+3	2.185+3
1.0	2.269	1.384-2	3.251-5	1.181+3	1.181+3	1.183+3
1.5	2.063	2.431-2	8.474-5	3.866+2	3.866+2	3.887+2
5.560K	2.036	2.533-2	9.169-5	3.473+2	3.473+2	3.493+2
1.560	2.036	2.533-2	9.169-5	4.403+3	4.403+3	4.405+3
2.0	1.869	3.295-2	1.514-4	2.352+3	2.352+3	2.354+3
3.0	1.557	4.629-2	3.164-4	8.087+2	8.087+2	8.103+2
4.0	1.326	5.732-2	5.166-4	3.674+2	3.674+2	3.688+2
5.0	1.143	6.618-2	7.381-4	1.960+2	1.960+2	1.972+2
6.0	9.910-1	7.543-2	1.004-3	1.162+2	1.162+2	1.172+2
8.0	7.482-1	9.132-2	1.598-3	5.004+1	5.004+1	5.088+1
10.0	5.730-1	1.045-1	2.258-3	2.571+1	2.571+1	2.639+1
15.0	3.272-1	1.228-1	3.861-3	7.471	7.475	7.925
20.0	2.133-1	1.319-1	5.390-3	3.057	3.062	3.407
30.0	1.148-1	1.388-1	8.161-3	8.505-1	8.587-1	1.112
40.0	7.319-2	1.394-1	1.052-2	3.394-1	3.499-1	5.625-1
50.0	5.116-2	1.374-1	1.256-2	1.657-1	1.783-1	3.668-1
60.0	3.792-2	1.343-1	1.432-2	9.199-2	1.063-1	2.785-1
80.0	2.209-2	1.268-1	1.719-2	3.625-2	5.344-2	2.024-1
100.0	1.466-2	1.194-1	1.943-2	1.759-2	3.702-2	1.711-1
150.0	6.855-3	1.035-1	2.324-2	4.728-3	2.797-2	1.383-1
200.0	3.935-2	9.131-2	2.549-2	1.868-3	2.736-2	1.226-1
300.0	1.775-3	7.425-2	2.775-2	5.092-4	2.826-2	1.043-1
400.0	1.000-3	6.297-2	2.861-2	2.044-4	2.881-2	9.279-2
500.0	6.384-4	5.490-2	2.880-2	1.014-4	2.890-2	8.444-2
600.0	4.397-4	4.880-2	2.868-2	5.749-5	2.874-2	7.797-2
800.0	2.455-4	4.012-2	2.798-2	2.374-5	2.800-2	6.837-2
1000.0	1.540-4	3.417-2	2.706-2	1.208-5	2.707-2	6.139-2

* $5.614 - 4 = 5.614 \times 10^{-4}$.
† $4.462 + 5 = 4.462 \times 10^{5}$.

Table 9-12. ▮▮▮ X-ray Cross Sections, Iron Z = 26 (cm^2/gm) ▮

Photon Energy keV	μ_{se}/ρ	μ_{te}/ρ	μ_{is}/ρ	μ_p/ρ	μ_a/ρ	μ/ρ
0.1	4.842	2.910-4*	6.986-8	1.036+6†	1.036+6	1.036+6
0.15	4.838	5.217-4	1.879-7	3.413+5	3.413+5	3.413+5
0.2	4.833	7.893-4	3.798-7	1.552+5	1.552+5	1.553+5
0.3	4.817	1.415-3	1.023-6	5.115+4	5.114+4	5.115+4
0.4	4.796	2.140-3	2.063-6	2.327+4	2.327+4	2.327+4
0.5	4.769	2.950-3	3.557-6	1.263+4	1.263+4	1.263+4
0.6	4.737	3.835-3	5.522-6	7.665+3	7.665+3	7.670+3
0.708L_3	4.696	4.867-3	8.224-6	4.870+3	4.870+3	4.874+3
0.708	4.696	4.867-3	8.224-6	1.741+4	1.741+4	1.742+4
0.721L_2	4.691	4.995-3	8.597-6	1.652+4	1.652+4	1.653+4
0.721	4.691	4.995-3	8.597-6	2.479+4	2.479+4	2.479+4
0.8	4.658	5.800-3	1.105-5	1.838+4	1.838+4	1.838+4
0.840L_1	4.638	6.280-3	1.265-5	1.564+4	1.564+4	1.564+4
0.840	4.638	6.280-3	1.265-5	2.346+4	2.346+4	2.346+4
1.0	4.564	7.993-3	1.897-5	1.449+4	1.449+4	1.450+4
1.5	4.288	1.431-2	5.045-5	4.505+3	4.505+3	4.509+3
2.0	3.989	2.022-2	9.432-5	1.966+3	1.966+3	1.970+3
3.0	3.419	3.115-2	2.148-4	6.112+2	6.112+2	6.146+2
4.0	2.917	4.126-2	3.757-4	2.668+2	2.668+2	2.697+2
5.0	2.487	5.035-2	5.713-4	1.402+2	1.402+2	1.428+2
6.0	2.128	5.855-2	7.910-4	8.293+1	8.293+1	8.511+1
6.404L_3K	1.994	6.147-2	8.830-4	6.873+1	6.873+1	7.079+1
7.112K	1.796	6.649-2	1.055-3	5.081+1	5.081+1	5.267+1
7.112	1.796	6.649-2	1.055-3	4.197+2	4.197+2	4.215+2
8.0	1.594	7.257-2	1.288-3	3.095+2	3.095+2	3.112+2
10.0	1.241	8.321-2	1.832-3	1.714+2	1.714+2	1.727+2
15.0	7.684-1	1.013-1	3.263-3	5.622+1	5.622+1	5.709+1
20.0	5.320-1	1.118-1	4.688-3	2.483+1	2.483+1	2.548+1
30.0	2.931-1	1.211-1	7.311-3	7.632	7.639	8.054
40.0	1.828-1	1.242-1	9.651-3	3.258	3.268	3.575
50.0	1.242-1	1.240-1	1.168-2	1.675	1.687	1.935
60.0	8.974-2	1.223-1	1.341-2	9.709-1	9.843-1	1.196
80.0	5.290-2	1.172-1	1.623-2	4.104-1	4.266-1	5.967-1
100.0	3.479-2	1.114-1	1.843-2	2.108-1	2.292-1	3.754-1
150.0	1.593-2	9.800-2	2.220-2	6.353-2	8.573-2	1.997-1
200.0	9.058-3	8.699-2	2.441-2	2.751-2	5.192-2	1.480-1
300.0	4.053-3	7.124-2	2.665-2	8.699-3	3.535-2	1.106-1
400.0	2.281-3	6.057-2	2.752-2	3.945-3	3.146-2	9.432-2
500.0	1.457-3	5.284-2	2.778-2	2.175-3	2.996-2	8.425-2
600.0	1.008-3	4.698-2	2.770-2	1.354-3	2.905-2	7.704-2
800.0	5.618-4	3.863-2	2.707-2	6.590-4	2.773-2	6.692-2
1000.0	3.548-4	3.291-2	2.619-2	3.863-4	2.658-2	5.984-2

* 2.910 − 4 = 2.910 × 10^{-4}.
† 1.036 + 6 = 1.036 × 10^6.

Table 9-13. ▮ X-ray Cross Sections, Copper $Z = 29$ (cm^2/gm) ▮

Photon Energy keV	μ_{ce}/ρ	μ_{ie}/ρ	μ_{is}/ρ	μ_p/ρ	μ_a/ρ	μ/ρ
0.1	5.295	1.655-4*	3.975-8	3.001+5†	3.001+5	3.001+5
0.120M_1	5.294	2.185-4	6.291-8	1.976+5	1.976+5	1.976+5
0.120	5.294	2.185-4	6.291-8	2.174+5	2.174+5	2.174+5
0.15	5.292	3.090-4	1.112-7	1.293+5	1.293+5	1.293+5
0.2	5.288	4.814-4	2.315-7	6.645+4	6.645+4	6.646+4
0.3	5.276	8.992-4	6.502-7	2.602+4	2.602+4	2.602+4
0.4	5.259	1.401-3	1.350-6	1.338+4	1.338+4	1.338+4
0.5	5.238	1.975-3	2.380-6	7.984+3	7.984+3	7.990+3
0.6	5.213	2.615-3	3.774-6	5.238+3	5.238+3	5.243+3
0.8	5.151	4.072-3	7.768-6	2.693+3	2.693+3	2.698+3
0.931L_3	5.102	5.145-3	1.138-5	1.896+3	1.896+3	1.901+3
0.931	5.102	5.145-3	1.138-5	8.043+3	8.043+3	8.048+3
0.951L_2	5.094	5.314-3	1.201-5	7.593+3	7.593+3	7.598+3
0.951	5.094	5.314-3	1.201-5	1.139+4	1.139+4	1.139+4
1.0	5.074	5.741-3	1.364-5	9.932+3	9.932+3	9.937+3
1.097L_1	5.020	6.617-3	1.722-5	7.725+3	7.725+3	7.730+3
1.097	5.020	6.617-3	1.722-5	1.159+4	1.159+4	1.159+4
1.5	4.840	1.071-2	3.782-5	4.935+3	4.935+3	4.940+3
2.0	4.569	1.578-2	7.372-5	2.254+3	2.254+3	2.258+3
3.0	4.006	2.566-2	1.775-4	7.465+2	7.465+2	7.505+2
4.0	3.470	3.499-2	3.191-4	3.409+2	3.409+2	3.444+2
5.0	2.987	4.352-2	4.938-4	1.856+2	1.856+2	1.886+2
6.0	2.571	5.130-2	6.952-4	1.129+2	1.129+2	1.155+2
8.0	1.934	6.489-2	1.155-3	5.156+1	5.156+1	5.356+1
8.048L_3K	1.921	6.517-2	1.166-3	5.073+1	5.073+1	5.272+1
8.979K	1.697	7.046-2	1.399-3	3.765+1	3.765+1	3.941+1
8.979	1.697	7.046-2	1.399-3	2.978+2	2.978+2	2.995+2
10.0	1.499	7.607-2	1.676-3	2.234+2	2.234+2	2.250+2
15.0	9.085-1	9.494-2	3.065-3	7.373+1	7.373+1	7.473+1
20.0	6.245-1	1.059-1	4.458-3	3.285+1	3.285+1	3.358+1
30.0	3.479-1	1.166-1	7.071-3	1.026+1	1.026+1	1.073+1
40.0	2.195-1	1.201-1	9.378-3	4.434	4.443	4.783
50.0	1.502-1	1.203-1	1.137-2	2.301	2.312	2.583
60.0	1.090-1	1.187-1	1.309-2	1.344	1.357	1.585
80.0	6.473-2	1.140-1	1.587-2	5.736-1	5.895-1	7.678-1
100.0	4.256-2	1.085-1	1.803-2	2.963-1	3.143-1	4.654-1
150.0	1.958-2	9.568-2	2.172-2	8.966-2	1.114-1	2.267-1
200.0	1.117-2	8.510-2	2.390-2	3.869-2	6.259-2	1.589-1
300.0	5.014-3	6.974-2	2.609-2	1.204-2	2.813-2	1.129-1
400.0	2.821-3	5.933-2	2.696-2	5.346-2	3.231-2	9.466-2
500.0	1.804-3	5.177-2	2.721-2	2.882-3	3.009-2	8.367-2
600.0	1.249-3	4.603-2	2.715-2	1.754-3	2.890-2	7.619-2
800.0	6.967-4	3.785-2	2.654-2	8.161-4	2.736-2	6.590-2
1000.0	4.407-4	3.224-2	2.568-2	4.584-4	2.614-2	5.882-2

* $1.655 - 4 = 1.655 \times 10^{-4}$.

† $3.001 + 5 = 3.001 \times 10^5$.

Photon Energy keV	μ_{ce}/ρ	μ_{ie}/ρ	μ_{is}/ρ	μ_p/ρ	μ_a/ρ	μ/ρ
0.1	1.191+1*	1.678-4*	4.091-8	3.230+6	3.230+6	3.230+6
0.15	1.191+1	2.957-4	1.070-7	1.089+6	1.089+6	1.089+6
0.2	1.190+1	4.421-4	2.123-7	5.037+5	5.037+5	5.037+5
0.3	1.188+1	7.791-4	5.609-7	1.699+5	1.699+5	1.699+5
0.4	1.184+1	1.165-3	1.120-6	7.857+4	7.857+4	7.858+4
0.492N_3	1.181+1	1.553-3	1.841-6	4.520+4	4.520+4	4.522+4
0.492	1.181+1	1.553-3	1.841-6	4.972+4	4.972+4	4.974+4
0.5	1.180+1	1.590-3	1.915-6	4.752+4	4.752+4	4.753+4
0.595N_2	1.176+1	2.028-3	2.906-6	2.981+4	2.981+4	2.982+4
0.595	1.176+1	2.028-3	2.906-6	3.279+4	3.279+4	3.280+4
0.6	1.175+1	2.052-3	2.965-6	3.206+4	3.206+4	3.207+4
0.8	1.163+1	3.066-3	5.907-6	1.483+4	1.483+4	1.484+4
1.0	1.149+1	4.186-3	1.008-5	8.152+3	8.152+3	8.164+3
1.5	1.104+1	7.370-3	2.633-5	2.749+3	2.749+3	2.760+3
1.809M_5	1.070+1	9.219-3	3.957-5	1.664+3	1.664+3	1.674+3
1.809	1.070+1	9.219-3	3.957-5	4.159+3	4.159+3	4.170+3
1.872M_4	1.063+1	9.599-3	4.262-5	3.798+3	3.798+3	3.808+3
1.872	1.063+1	9.599-3	4.262-5	5.696+3	5.696+3	5.707+3
2.0	1.052+1	1.039-2	4.926-5	4.768+3	4.768+3	4.779+3
2.281M_3	1.016+1	1.198-2	6.459-5	3.352+3	3.352+3	3.362+3
2.281	1.016+1	1.198-2	6.459-5	4.022+3	4.022+3	4.033+3
2.575M_2	9.844	1.368-2	8.289-5	2.907+3	2.907+3	2.916+3
2.575	9.844	1.368-2	8.289-5	3.197+3	3.197+3	3.207+3
2.820M_1	9.613	1.510-2	9.999-5	2.507+3	2.507+3	2.516+3
2.820	9.613	1.510-2	9.999-5	2.757+3	2.757+3	2.767+3
3.0	9.457	1.616-2	1.136-4	2.335+3	2.335+3	2.344+3
4.0	8.471	2.164-2	2.013-4	1.080+3	1.080+3	1.088+3
5.0	7.580	2.681-2	3.092-4	5.937+2	5.937+2	6.013+2
6.0	6.791	3.164-2	4.342-4	3.642+2	3.642+2	3.710+2
8.0	5.500	4.012-2	7.259-4	1.684+2	1.684+2	1.740+2
10.0	4.521	4.786-2	1.078-3	9.260+1	1.260+1	9.717+1
10.207L_3	4.424	4.849-2	1.114-3	8.766+1	8.766+1	9.213+1
10.207	4.424	4.849-2	1.114-3	1.824+2	1.824+2	1.869+2
11.544L_2	3.884	5.238-2	1.351-3	1.300+2	1.300+2	1.339+2
11.544	3.884	5.238-2	1.351-3	1.950+2	1.950+2	1.989+2
12.100L_1	3.694	5.392-2	1.453-3	1.713+2	1.713+2	1.751+2
12.100	3.694	5.392-2	1.453-3	2.570+2	2.570+2	2.608+2
15.0	2.936	1.162-2	2.030-3	1.423+2	1.423+2	1.453+2
20.0	2.071	7.112-2	3.079-3	6.448+1	6.448+1	6.663+1
30.0	1.227	8.246-2	5.173-3	2.113+1	2.113+1	2.245+1
40.0	8.196-1	8.822-2	7.145-3	9.575	9.582	1.049+1
50.0	5.854-1	9.076-2	8.918-3	5.182	5.191	5.867

Table 9-14.   (Concluded)

Photon Energy keV	μ_{ce}/ρ	μ_{ie}/ρ	μ_{is}/ρ	μ_p/ρ	μ_a/ρ	μ/ρ
59.318L_3K	4.454-1	9.151-2	1.039-2	3.238	3.248	3.785
60.0	4.373-1	9.150-2	1.050-2	3.138	3.148	3.677
69.525K	3.377-1	9.100-2	1.180-2	2.092	2.104	2.533
69.525	3.377-1	9.100-2	1.180-2	1.020+1	1.021+1	1.064+1
80.0	2.597-1	9.037-2	1.313-2	7.367	7.380	7.730
100.0	1.741-1	8.768-2	1.522-2	4.265	4.280	4.542
150.0	8.216-2	8.022-2	1.884-2	1.471	1.490	1.652
200.0	4.733-2	7.237-2	2.086-2	6.666-1	6.875-1	8.071-1
300.0	2.141-2	6.024-2	2.287-2	2.144-1	2.373-1	3.189-1
400.0	1.209-2	5.160-2	2.365-2	9.661-2	1.203-1	1.839-1
500.0	7.750-3	4.522-2	2.387-2	5.287-2	7.674-2	1.297-1
600.0	5.366-3	4.031-2	2.383-2	3.281-2	5.664-2	1.023-1
800.0	3.014-3	3.323-2	2.334-2	1.606-2	3.940-2	7.565-2
1000.0	1.916-3	2.831-2	2.263-2	9.610-3	3.224-2	6.246-2

1.191 + 1 = 11.91.
1.684 - 4 = 1.684 x 10⁻⁴.

Table 9-15. ▉ X-ray Cross Sections, Uranium Z = 92 (cm²/gm) ▉

Ph. Energy keV	μ_{ce}/ρ	μ_{ic}/ρ	μ_p/ρ	μ_τ/ρ	μ_a/ρ	μ/ρ
0.1	1.423+1*	3.177-5	7.748-9	1.180+6	1.180+6	1.180+6
0.15	1.422+1	6.810-5	2.473-8	4.701+5	4.701+5	4.701+5
0.2	1.421+1	1.169-4	5.624-8	2.446+5	2.446+5	2.446+5
0.3	1.417+1	2.507-4	1.804-7	9.744+4	9.744+4	9.745+4
0.4	1.413+1	4.307-4	4.138-7	5.071+4	5.071+4	5.072+4
0.5	1.407+1	6.551-4	7.884-7	3.055+4	3.055+4	3.057+4
0.6	1.400+1	9.230-4	1.334-6	2.020+4	2.020+4	2.021+4
0.8	1.383+1	1.585-3	3.054-6	1.051+4	1.051+4	1.052+4
1.0	1.362+1	2.410-3	5.803-6	6.333+3	6.333+3	6.347+3
1.273M_5	1.327+1	3.791-3	1.160-5	3.664+3	3.664+3	3.677+3
1.273	1.327+1	3.791-3	1.160-5	4.030+3	4.030+3	4.043+3
1.441M_4	1.306+1	4.785-3	1.650-5	3.040+3	3.040+3	3.053+3
1.441	1.306+1	4.785-3	1.650-5	3.344+3	3.344+3	3.358+3
1.5	1.305+1	5.160-3	1.850-5	3.052+3	3.052+3	3.065+3
2.0	1.230+1	8.109-3	3.849-5	1.588+3	1.588+3	1.601+3
3.0	1.113+1	1.464-2	1.033-4	6.327+2	6.327+2	6.438+2
3.552M_3	1.043+1	1.819-2	1.513-4	4.313+2	4.313+2	4.417+2
3.552	1.043+1	1.819-2	1.513-4	9.717+2	9.717+2	9.822+2
3.728M_2	1.024+1	1.935-2	1.687-4	8.640+2	8.640+2	8.742+2
3.728	1.024+1	1.935-2	1.687-4	1.296+3	1.296+3	1.306+3
4.0	9.966	2.118-2	1.977-4	1.092+3	1.092+3	1.102+3
4.303M_1	9.619	2.277-2	2.281-4	9.140+2	9.140+2	9.236+2
4.303	9.619	2.277-2	2.281-4	1.097+3	1.097+3	1.106+3
5.0	8.944	2.642-2	3.059-4	7.616+2	7.616+2	7.705+2
5.182N_2	8.763	2.721-2	3.262-4	6.981+2	6.981+2	7.069+2
5.182	8.763	2.721-2	3.262-4	7.679+2	7.679+2	7.767+2
5.548N_1	8.430	2.883-2	3.691-4	6.506+2	6.506+2	6.590+2
5.548	8.430	2.883-2	3.691-4	7.156+2	7.156+2	7.241+2
6.0	8.064	3.078-2	4.249-4	5.916+2	5.916+2	5.997+2
8.0	6.649	3.780-2	6.857-4	2.939+2	2.939+2	3.006+2
10.0	5.564	4.232-2	9.528-4	1.709+2	1.709+2	1.765+2
15.0	3.753	5.184-2	1.718-3	6.377+1	6.377+1	6.760+1
17.166L_3	3.246	5.562-2	2.090-3	4.594+1	4.594+1	4.924+1
17.166	3.246	5.562-2	2.090-3	9.787+1	9.787+1	1.012+2
20.0	2.725	6.021-2	2.611-3	6.586+1	6.586+1	6.865+1
20.948L_2	2.568	6.145-2	2.785-3	5.841+1	5.841+1	6.104+1
20.948	2.568	6.145-2	2.785-3	6.663+1	6.663+1	6.926+1
21.757L_1	2.443	6.247-2	2.935-3	6.030+1	6.030+1	6.281+1
21.757	2.443	6.247-2	2.935-3	9.045+1	9.045+1	9.296+1
30.0	1.601	7.173-2	4.528-3	3.883+1	3.883+1	4.050+1
40.0	1.043	7.894-2	6.444-3	1.821+1	1.821+1	1.933+1
50.0	7.277-1	8.241-2	8.168-3	1.012+1	1.012+1	1.094+1

Table 9-15. (Concluded)

Photon Energy keV	μ_{ce}/ρ	μ_{ie}/ρ	μ_{is}/ρ	μ_p/ρ	μ_a/ρ	μ/ρ
60.0	5.339-1	8.375-2	9.690-3	6.261	6.271	6.888
80.0	3.178-1	8.353-2	1.226-2	2.936	2.948	3.349
98.440L_3K	2.176-1	8.189-2	1.416-2	1.700	1.714	2.014
100.0	2.114-1	8.166-2	1.431-2	1.632	1.646	1.939
115.606K	1.646-1	7.956-2	1.560-2	1.114	1.130	1.374
115.606	1.646-1	7.956-2	1.560-2	5.035	5.046	5.295
150.0	9.832-2	7.573-2	1.799-2	2.166	2.184	2.358
200.0	5.627-2	6.872-2	1.999-2	9.940-1	1.013	1.139
300.0	2.533-2	5.625-2	2.150-2	3.873-1	4.088-1	4.904-1
400.0	1.429-2	4.935-2	2.273-2	2.034-1	2.261	2.898-1
500.0	9.149-3	4.340-2	2.299-2	1.196-1	1.426	1.952-1
600.0	6.343-3	3.869-2	2.292-2	7.428-2	9.720-2	1.422-1
800.0	3.557-3	3.128-2	2.200-2	3.107-2	5.307-2	8.792-2
1000.0	2.264-2	2.725-2	2.178-2	1.381-2	3.559-2	6.511-2

$1.423 + 1 = 14.23$.

† $3.177 - 5 = 3.177 \times 10^{-5}$.
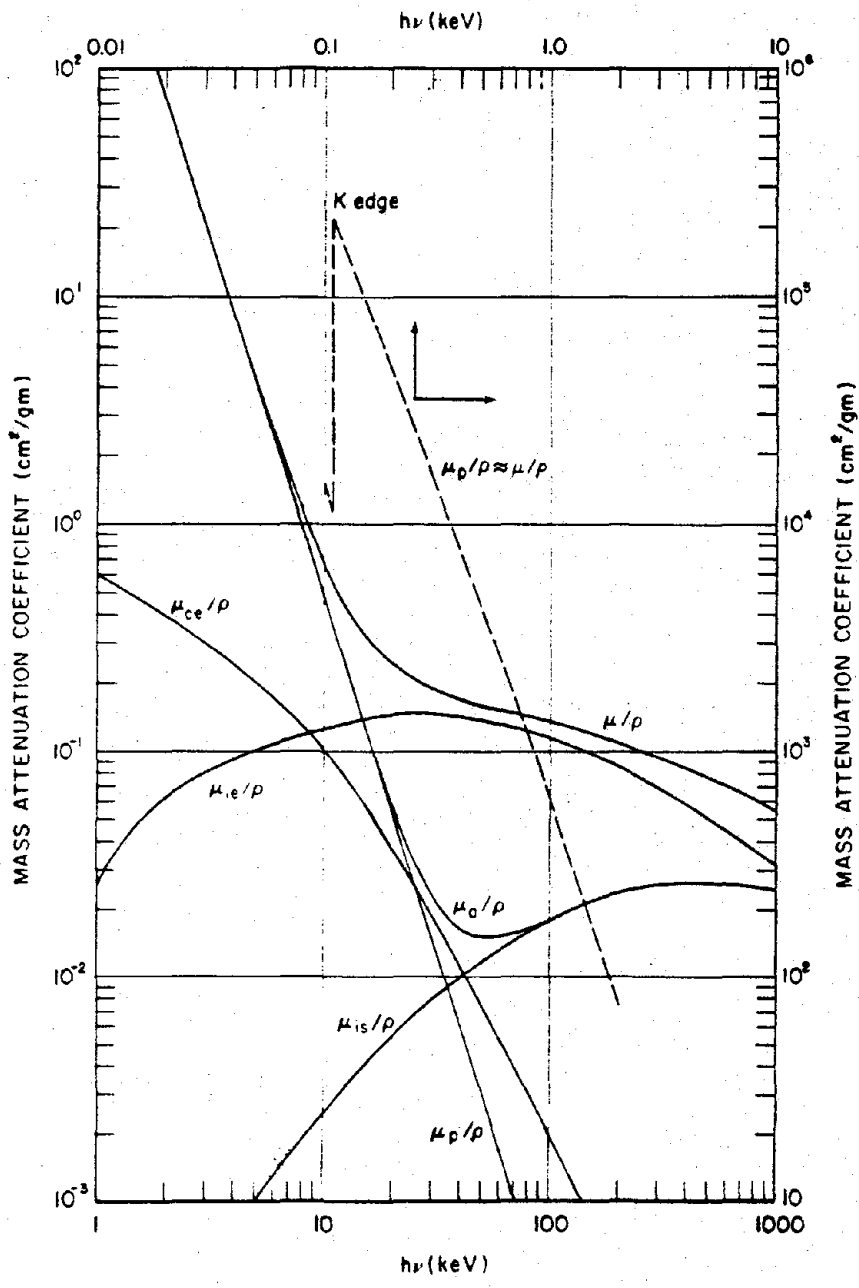
Figure 9-27. ▮ Photon Cross Sections in Beryllium ▮
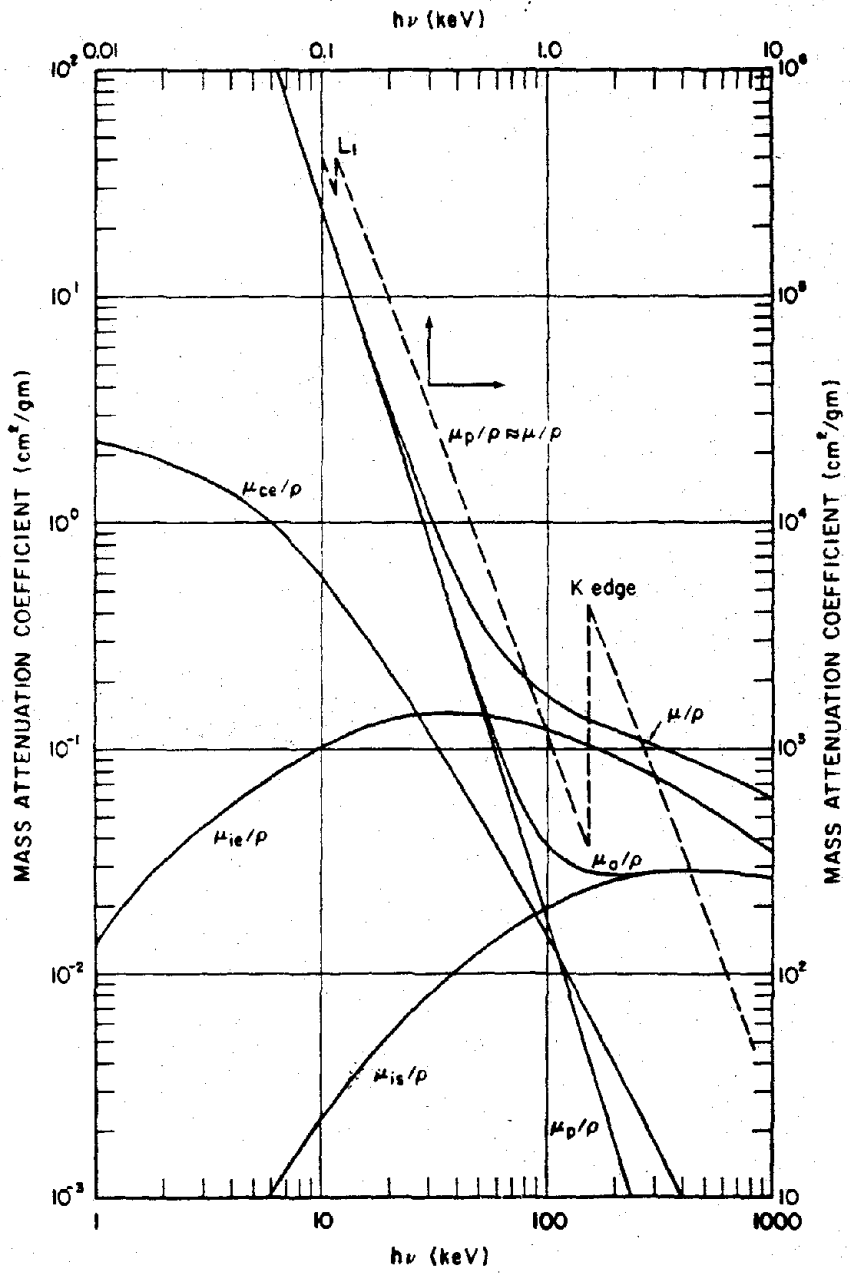
Figure 9-28. ▆▆ Photon Cross Sections in Aluminum ▆▆
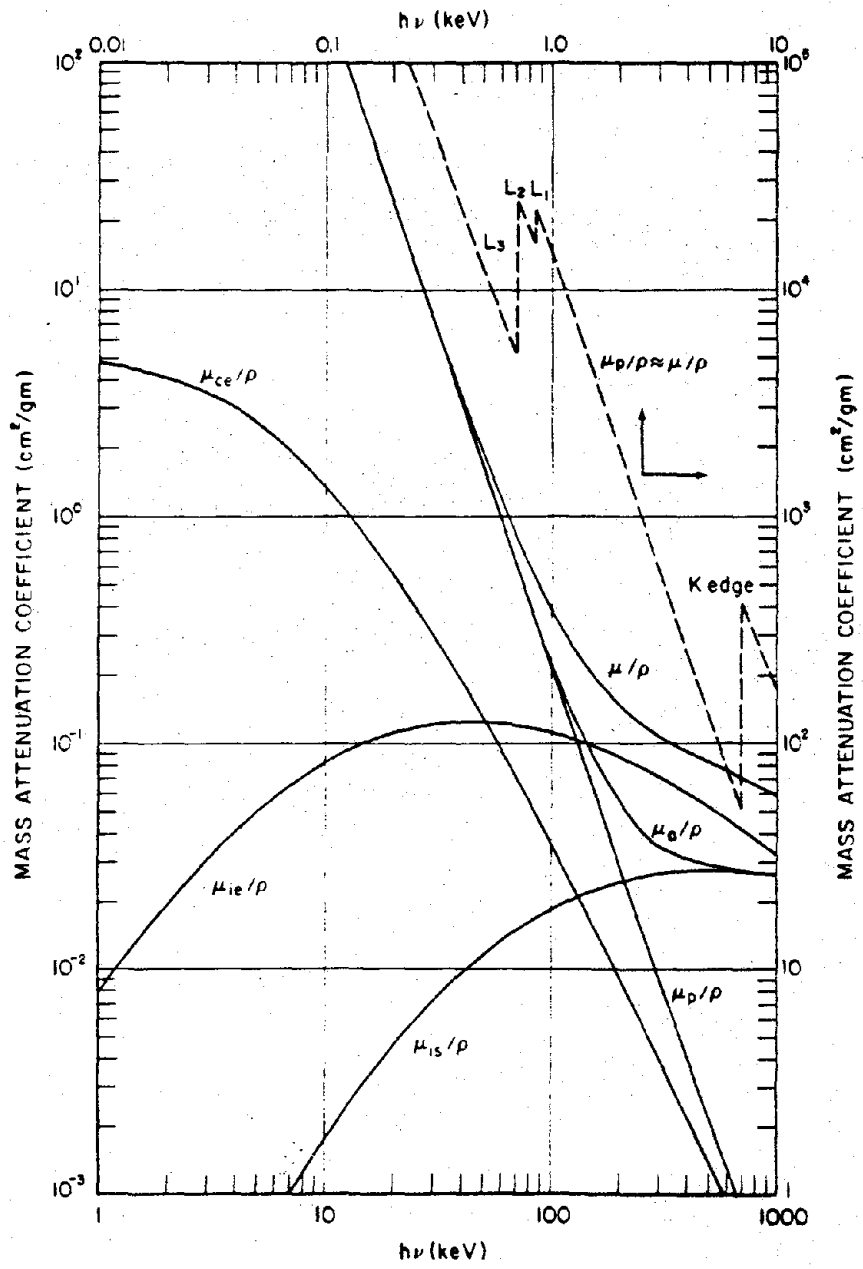
Figure 9-29. ▮▮▮▮ Photon Cross Sections in Iron ▮▮▮
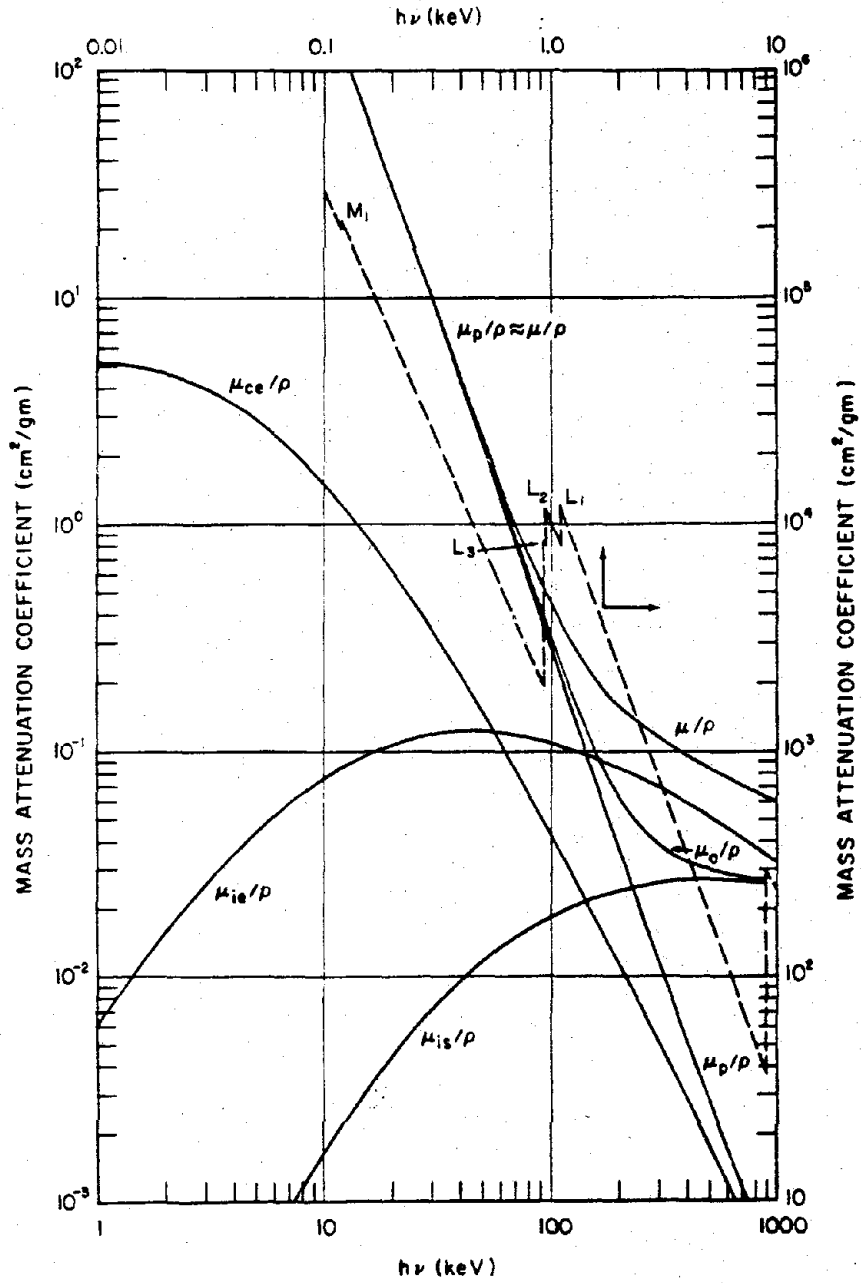
Figure 9-30. ███ Photon Cross Sections in Copper ███
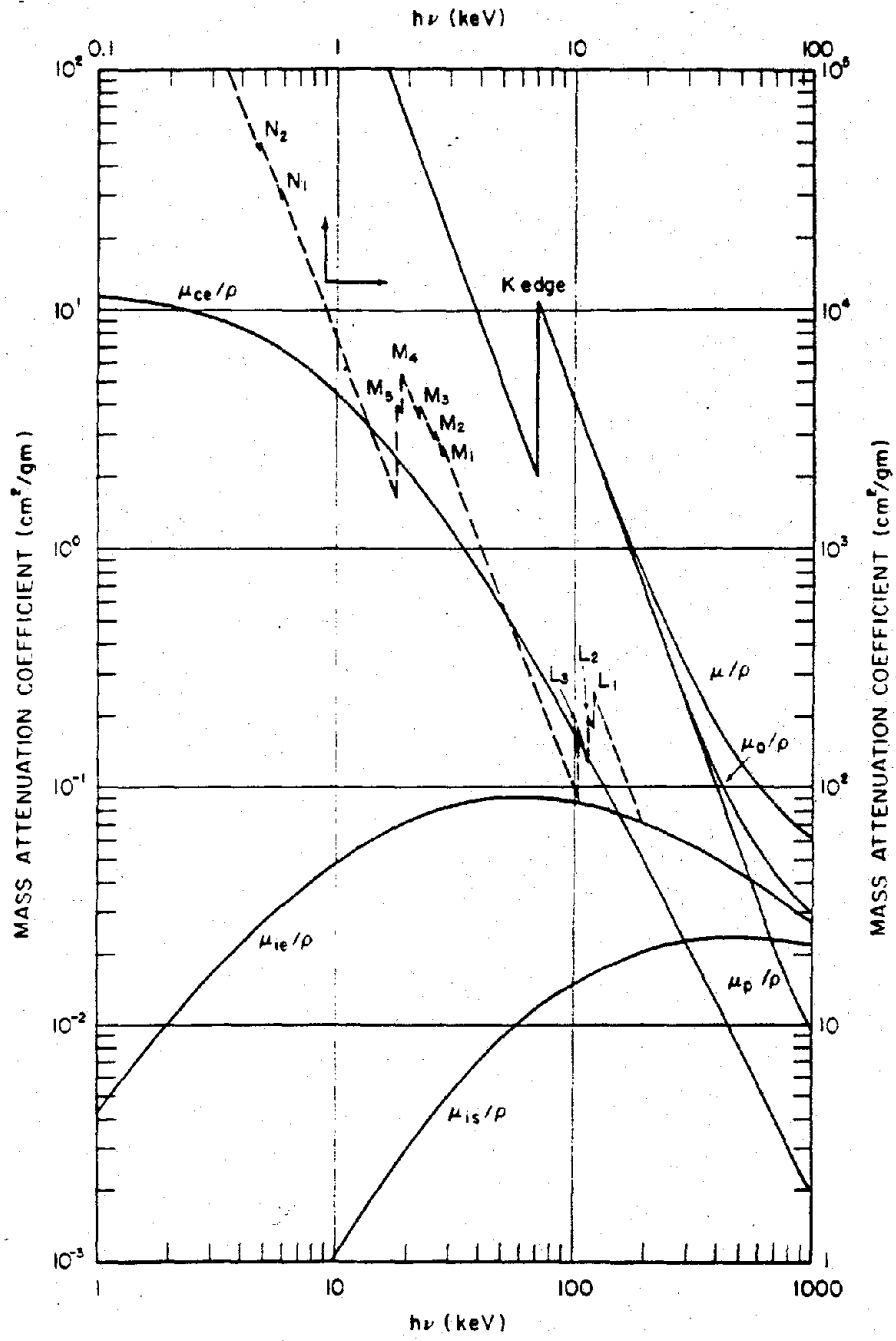
Figure 9-31. ▮ Photon Cross Sections in Tungsten ▮
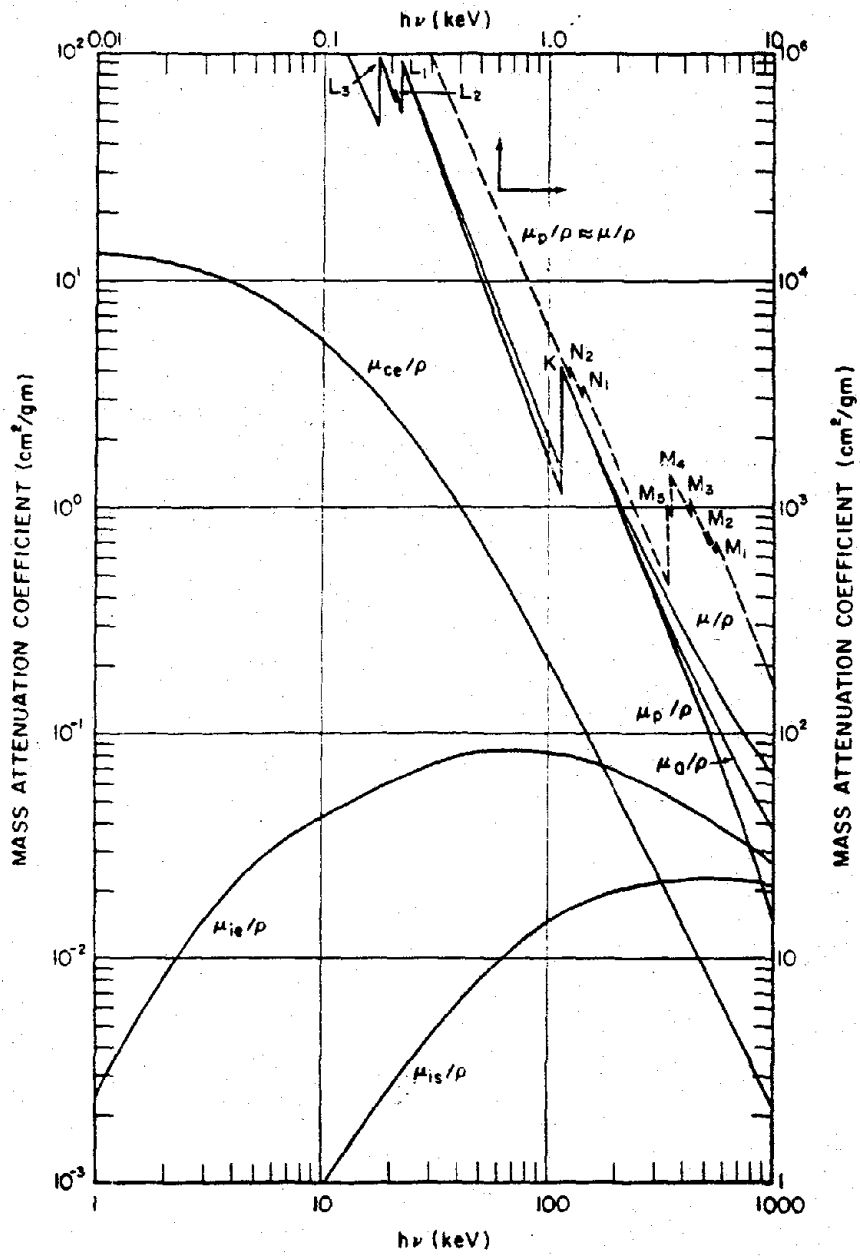
Figure 9-32. ▮▮▮ Photon Cross Sections in Uranium ▮▮▮
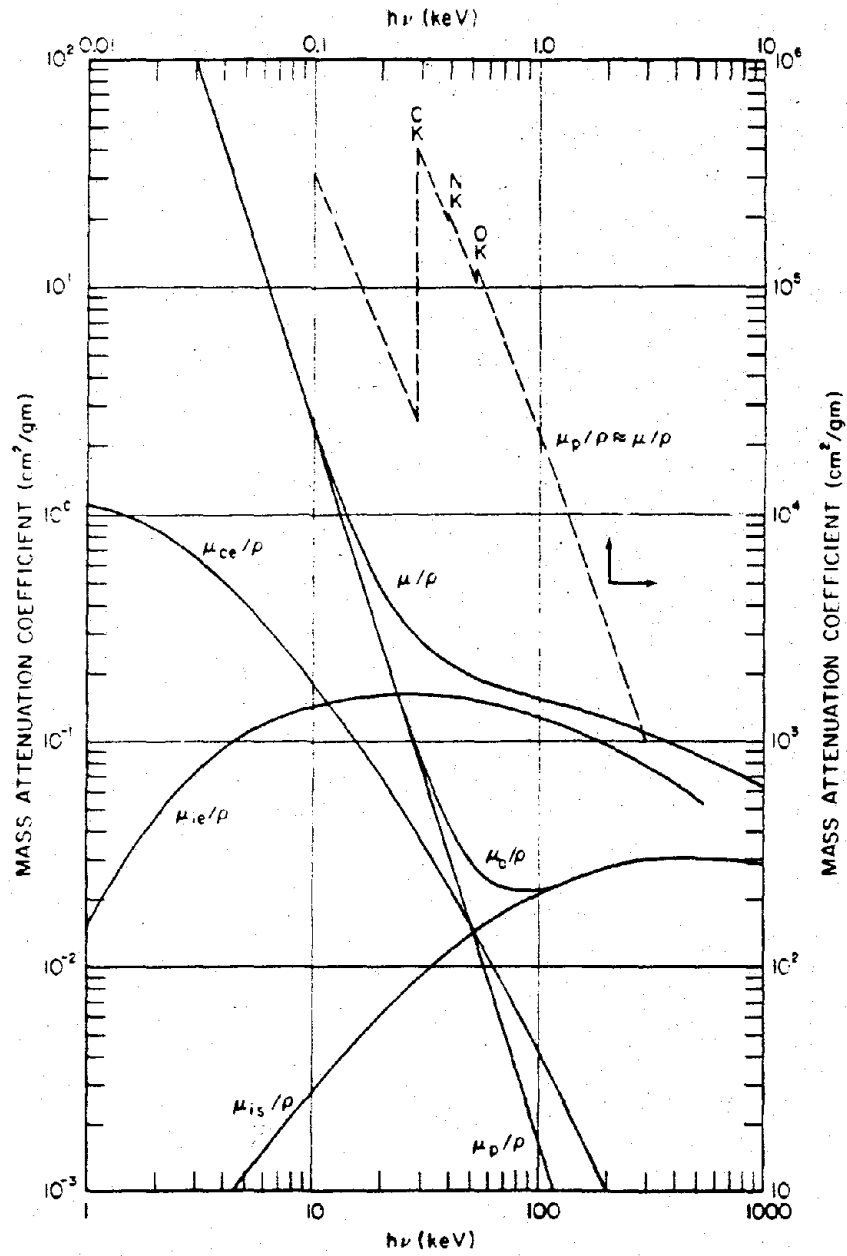
Figure 9-33. ■ Photon Cross Sections in Carbon
Phenolic (CP), $\bar{Z} = 6.08$ ■

7
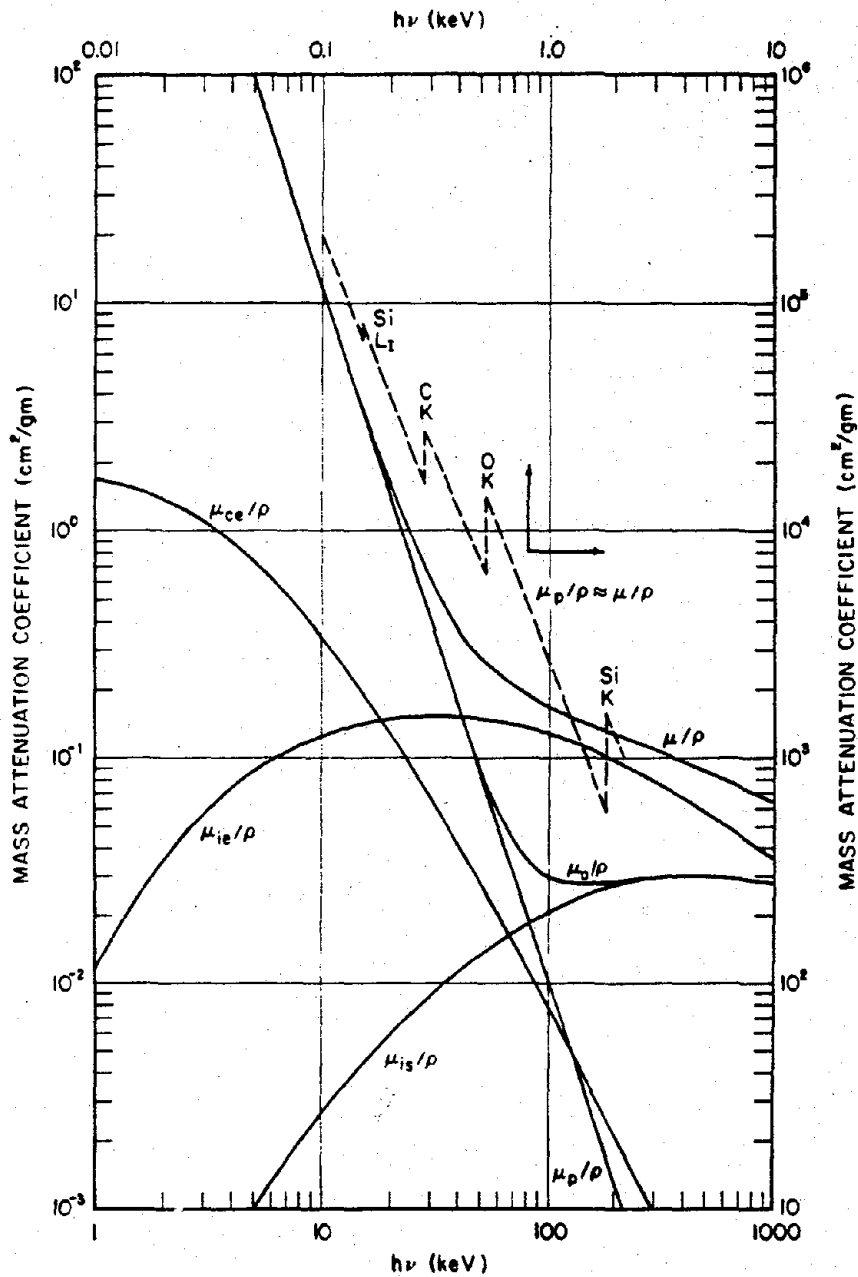
Figure 9-34. ▇▇▇ Photon Cross Sections in Tape Wound Silicon Phenolic (TWSP), $\bar{Z} = 9.01$ ▇

9-35 X-ray Energy Deposition Summary

The methods described in paragraphs 9-33 and 9-34 and illustrated in Problems 9-3 and 9-4 allow the calculation of curves that show approximations of energy deposition as a function of depth for black body spectra incident on any material, if the cross sections are known for the material

INITIAL PRESSURIZATION OF MATERIALS DUE TO X-RAY DEPOSITION

An immediate consequence of the deposition of X-ray energy is the rapid heating of the material. This heating causes an initial pressure distribution as a function of depth in the structure. The initial pressurization generates shock waves that propagate through the thickness of the shell of the structure. The heating can result in a solid material changing phase, that is, melting or vaporizing. The melting and vaporization cause blowoff, which imparts an impulse to the structure and excites whole structure modes of response.

9-36 Phase Changes Induced by X-ray Heating

In most nuclear weapon X-ray environments, the X-ray energy is deposited in a very short time, a few nanoseconds to a few hundred nanoseconds. The material cannot expand appreciably during this time, so the energy deposition process can be considered to occur at a constant volume or at normal material density, ρ_0. Rapid melting and vaporization are accompanied by enormous pressure increases. Values

DNA
(b)(3)

Deleted

Figure 9-35. ▮▮▮▮ Energy Deposited in Aluminum
by Black Body Spectra ▮▮

Deleted

Figure 9-36. ███████ Energy Deposited in Copper by
Black Body Spectra ███

DNA
(b)(3)

Deleted

Figure 9-37. ██████ Energy Deposited by Black Body
X-ray Spectra in Carbon Phenolic (CP) ██

Deleted

Figure 9-38. ▮▮▮▮ Energy Deposited by Black Body X-ray Spectra in
Tape Wound Silica Phenolic (TWSP) ▮

for enthalpy changes for melting and vaporization for the metals discussed in the previous subsection are given in Table 9-17. These values are for one atmosphere pressure. In most X-ray problems of interest the material is initially at very high pressure. so these values can be considered to be only approximate. This approach is not correct for ablators as a class although it might apply to carbon phenolic in a cold environment. Confining the discussion to metals will not restrict the transfer of principles.*

■ The rising pressure that results from heating at constant density is illustrated in Figures 9-39 and 9-40 where isoenergy lines of aluminum are shown in pressure-density plots. If the internal energy is above tne critical energy, 3,016 cal/gm for aluminum, the material can be considered as a vapor. Figure 9-40 shows the high pressure, high energy intercepts with the normal density abscissa (ρ_o = 2.7 gm/cm^3). The release adiabats for expansion from density ρ_o to low density and pressure also are shown in this figure. Expansion along the adiabat results in decreasing internal or potential energy as the material develops kinetic energy during "blowoff." For example. a 6,000 cal/gm energy depo-

sition in aluminum at ρ_o = 2.7 gm/cm^3 results in a pressure of about 1.5 megabars (Mb). The aluminum would expand from that state to low pressure and density, with final internal energy of about 3,000 cal/gm and about 3,000 cal/gm of kinetic energy. The 3,000 cal/gm of internal or potential energy is used to overcome the physical and chemical forces that bind the atoms together in the solid. This leads to the concept of heat of sublimation. The heat of sublimation at absolute zero, E_{so}, is the energy required to form the saturated vapor from the solid at a temperature of absolute zero. Thus, E_{so} does not include any energy of kinetic motion. The energy of sublimation generally is a function of temperature becoming larger for larger deposition energies (temperatures).

*■ The problem of phase changes in a composite heat shield ablator is more complicated since different deposition profiles, material enthalpy, and thermal conductivities are involved in the calculations. While some materials, e.g., tape-wrapped carbon phenolic, may behave like metals in a cold environment, the techniques described here generally are not applicable to the description of the blowoff process in the broad category of composite materials that use three dimension (3-D) weaves for heat shields or for X-ray shields that use dispersed high Z materials for loading.

Table 9-17. ■ Enthalpy Change for Selected Metals ■
(cal/gm)

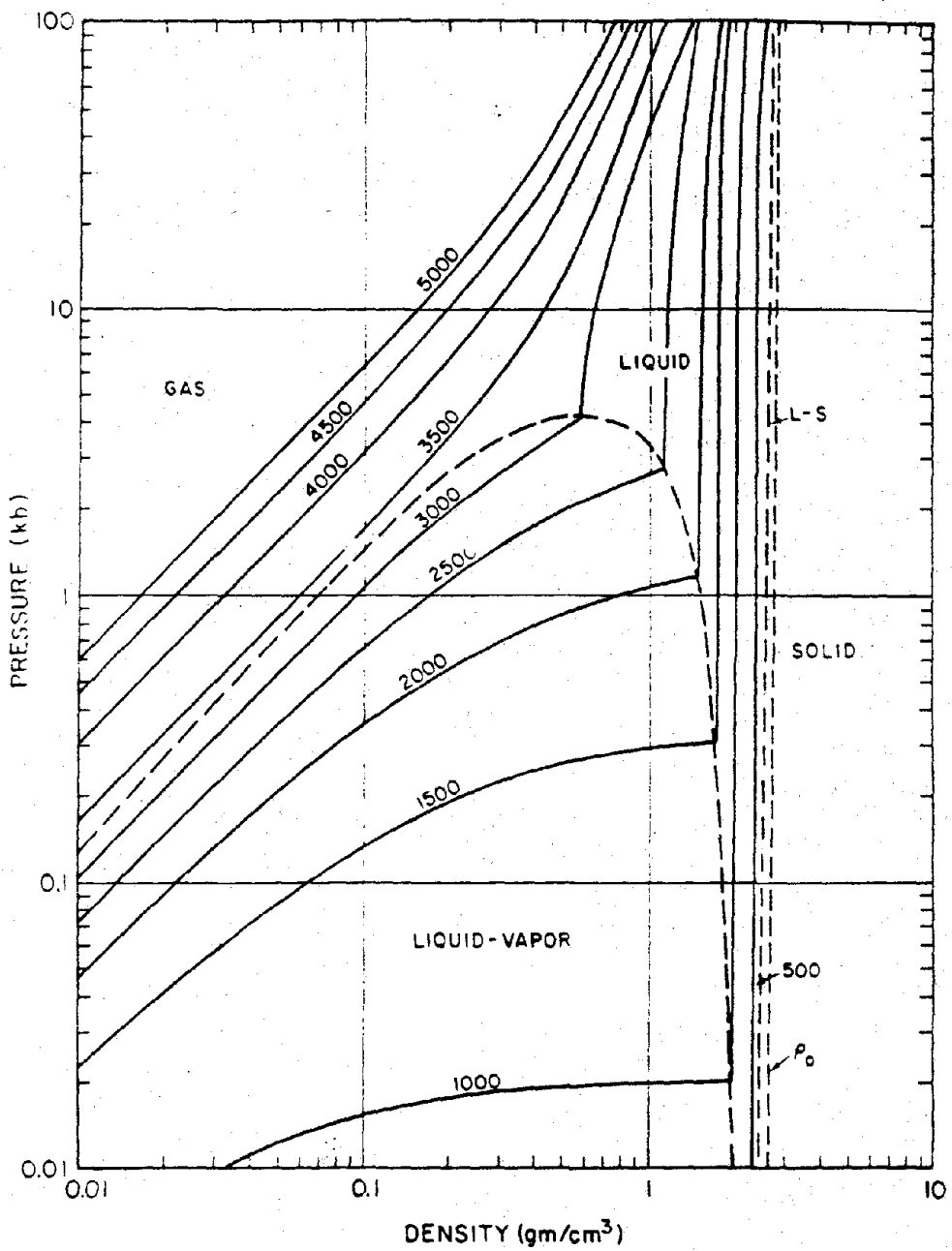| Metal-Atomic Weight	To Melt	Through Melt	To Vapor	Through Vapor	Sublimation Energy
Be 9.013	876.0	1,187.0	2,147.0	10,040.0	8,682.0
Al 26.98	160.4	255.3	771.1	3,347.0	2,891.0
Fe 55.85	250.8	315.8	573.0	2,071.0	1,782.0
Cu 63.54	110.0	160.0	336.0	1,481.0	1,275.0
W 183.85	153.9	200.0	304.0	1,353.0	1,110.0
U 238.00	49.0	64.5	171.9	596.1	492.1

Figure 9-39. ▮▮▮ Aluminum Isoenergy Lines.
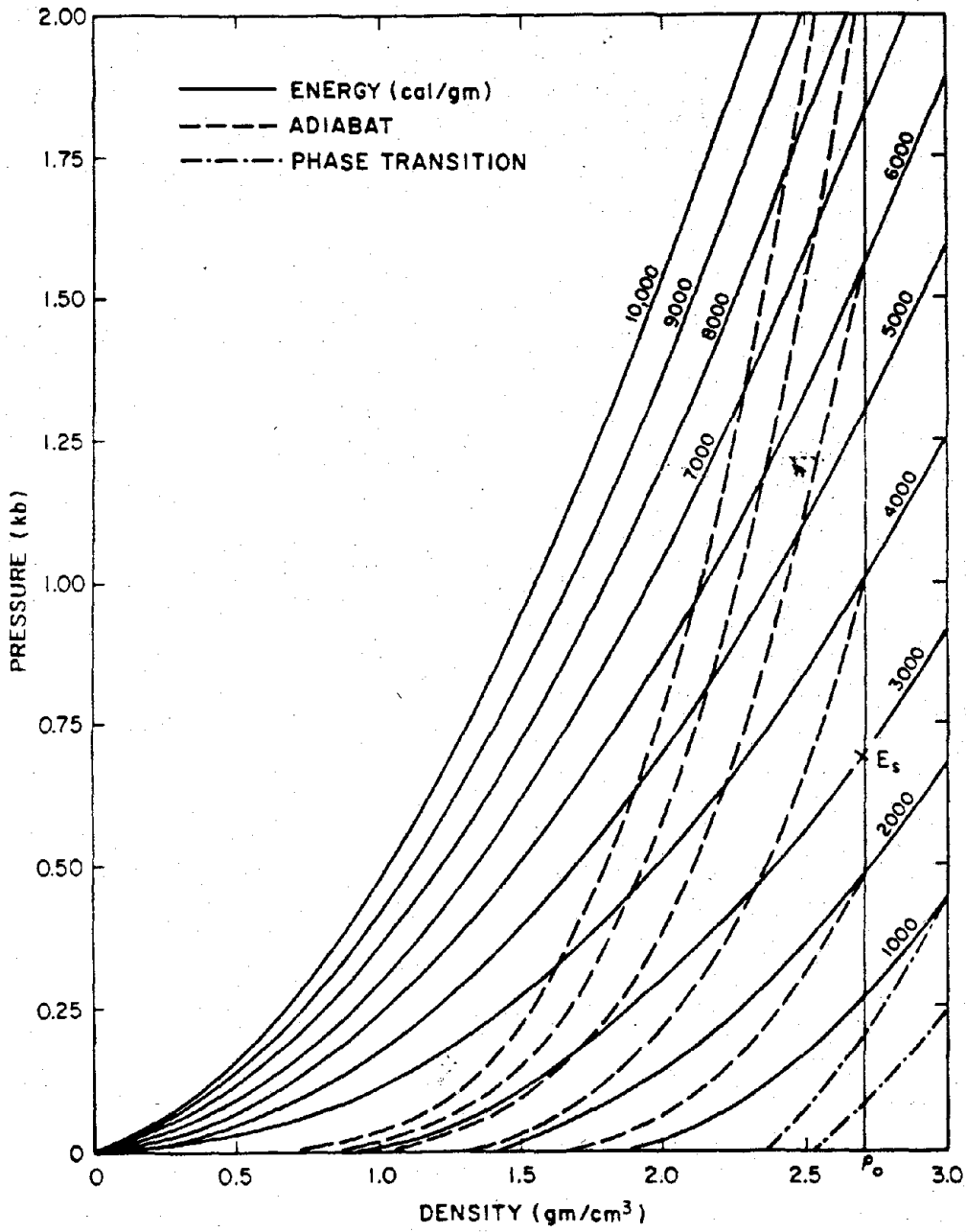Parameter is Energy in cal/gm ▮▮▮

Figure 9-40. ████ Aluminum Isoenergy Lines and Adiabats ████

9-37 The Grüneisen Parameter and the Equation of State ▮

▮ As a first approximation to the equation of state of material, it is assumed that the pressure in the material increases linearly with the deposited internal energy per unit volume,

$$P = G\eta\epsilon,$$

where G is the Grüneisen ratio for the material, ϵ is the internal energy per unit volume, and $\eta =$

9-101

ρ/ρ_0, the ratio of the density to a normalized density of the material, usually the ambient density. In codes used to calculate shock wave propagation, for example the PUFF type codes, more elaborate equations of state are used to fit the experimentally determined behavior of the solid and vapor phases. The equations used in the PUFF codes reduce to the equation given above when $\eta = 1$, and generally only one value of G is used to specify a material.

■■■ Although there may be small errors in calculating the X-ray energy deposition as a function of depth, the significant sources of errors in pressure predictions are the accuracy and validity of the Grüneisen parameter for solid and vapor equations of state. Experimental values of G obtained by different methods result in factors of about two uncertainty even for some of the common materials such as aluminum, beryllium, and tungsten. Even though indications are that G is not well known as a function of deposited energy, some very good correlations have been obtained for computed and measured values of pressure waves in X-ray tests, when careful calculations are made employing elastic plastic properties of the materials.

■■■ Initial pressurization in distended materials such as porous metals and foams present a particularly difficult and uncertain condition for current analytical techniques.

The units for ϵ in the equation given above are energy per unit volume, which have the same dimensions as pressure. Therefore, the energy required in cal/gm for a phase change can be expressed in units of pressure, if the density of the material is specified. If the internal energy, E, is given per unit mass, the relation to ϵ is

$$\epsilon \text{ (cal/cm}^3) = E \text{ (cal/gm) } \rho_0 \text{ (gm/cm}^3).$$

The value of ϵ in megabars may then be obtained by the relation

$$\epsilon \text{ (Mb)} = \epsilon \text{ (cal/cm}^3) \times 4.18 \times 10^7 \left(\frac{\text{erg}}{\text{cal}}\right)$$

$$\times 1 \left(\frac{\text{dyne} \cdot \text{cm}}{\text{erg}}\right) \times 1 \left(\frac{\text{Mb}}{10^{12} \text{ dyne/cm}^2}\right)$$

$$\epsilon \text{ (Mb)} = 4.8 \times 10^{-5} \epsilon \left(\frac{\text{cal}}{\text{cm}^3}\right)$$

$$= 4.18 \times 10^{-5} \rho_0 E \left(\frac{\text{cal}}{\text{gm}}\right).$$

Thus, the previous equation for pressure may be written

$$P \text{ (Mb)} = G \frac{\rho}{\rho_0} \epsilon \text{ (Mb)},$$

or

$$P \text{ (Mb)} = 4.18 \times 10^{-5} G\rho E \text{ (cal/gm)}.$$

The enthalpy changes of the metals shown in Table 9-17 in cal/gm are given in Table 9-19.

Table 9-19. ■ Enthalpy Changes ϵ (Mb) ■

Metal	ρ_0 (gm/cm^3)	To Melt	Through Melt	To Vapor	Through Vapor	Sublimation Energy, E_s
Be	1.85	0.068	0.0918	0.166	0.776	0.671
Al	2.70	0.0181	0.0288	0.087	0.378	0.326
Fe	7.86	0.0824	0.1036	0.188	0.680	0.585
Cu	8.92	0.0410	0.0596	0.125	0.552	0.475
W	19.3	0.124	0.161	0.245	1.092	0.895
U	18.7	0.0383	0.0504	0.134	0.466	0.385

Metal	G	To Melt	Through Melt	To Vapor	Through Vapor	Sublimation Energy, E
Be	1.45	0.099	0.133	0.241	0.12	0.973
Al	2.13	0.0386	0.0613	0.185	0.805	0.694
Fe	1.69	0.139	0.175	0.318	1.15	0.989
Cu	2.00	0.082	0.119	0.250	1.10	0.950
W	1.43	0.177	0.230	0.350	1.56	1.28
U	2.03	0.078	0.102	0.273	0.946	0.782

The pressures associated with these changes at ambient density, i.e., when $\rho = \rho_o$, and P (Mb) = Ge (Mb), are shown in Table 9-20.

From Table 9-20, aluminum has a sub██████ limation pressure of about 0.7 Mb at ambient density, corresponding to sublimation energy of about 2,900 cal gm (Table 9-17). This point is shown in Figure 9-40, labeled E at about 3,000 cal gm. Table 9-20 indicates that the pressures associated with vaporization of metals at ambient density are with some exceptions about 1 Mb. A survey of more than 30 common metal elements indicates that an average of 1 Mb for vaporization is a good approximation, especially if the Grüneisen value for the material is uncertain. Since a bar corresponds to 14.7 psi a Mb is the enormous pressure of about 1.45×10^7 psi. Thus, tremendous forces are involved in the pressure gradients associated with metal vaporization at ambient density. Table 9-17 shows that vaporization usually involves several thousand calories per gram of energy. High explosive materials (TNT, etc.) release about 1,000 cal/gm. Therefore, on a mass basis there is more energy associated with metal vaporization than with high explosives. Generally, the thicknesses of material evaporated by X-ray absorption is small, and, the total mass of material that is vaporized generally is small.

SHOCK WAVE PROPAGATION AND DAMAGE PREDICTIONS ██

The sequence of events for the generation and propagation of a stress wave through the thickness of an aerospace shell and the damage produced is illustrated in Figure 9-41. Cold X-rays are deposited primarily in a relatively thin sheet of material at the front surface (Figure 9-41a). After the energy is deposited a compression wave propagates inward from the front surface, followed by a rarefaction that causes the vapor and liquid to blow off (Figure 9-41b). This rarefaction also may cause a spall of solid material from the front surface (Figure 9-41c). Later the compression wave reflects from the back surface and returns as a rarefaction wave. This rarefaction wave, or the coincidence of this wave with the rearward moving rarefaction may cause the rear surface to spall (Figure 9-41d), or may cause fracturing or debonding. This process occurs within the order of a microsecond and generally is complete before the overall structural motion occurs. The shock effects are
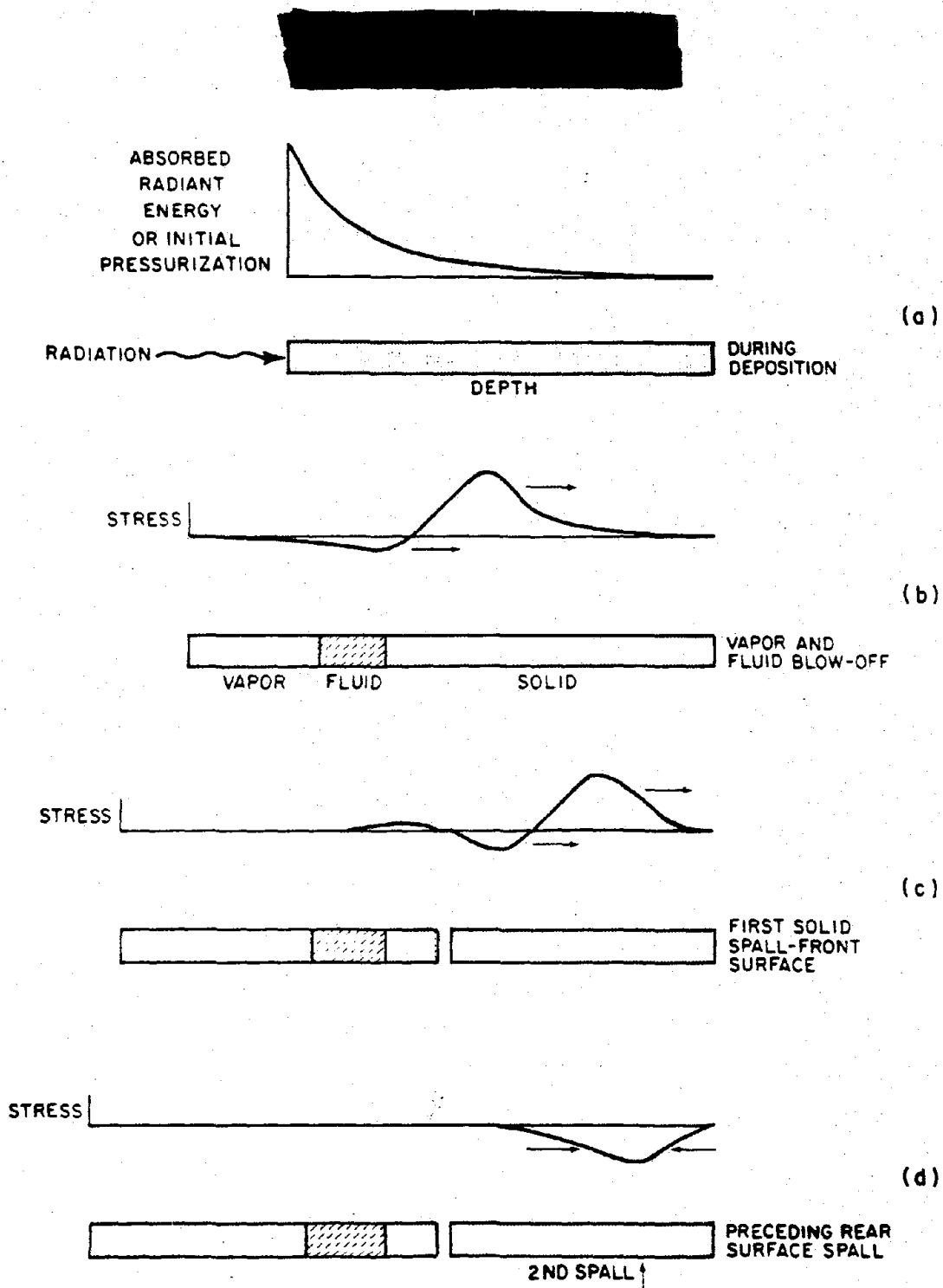
ABSORBED
RADIANT
ENERGY
OR INITIAL
PRESSURIZATION

(a)

RADIATION $\longrightarrow$ | DURING DEPOSITION

DEPTH

STRESS

(b)

| VAPOR | FLUID | SOLID | VAPOR AND FLUID BLOW-OFF

STRESS

(c)

FIRST SOLID SPALL-FRONT SURFACE

STRESS

(d)

PRECEDING REAR SURFACE SPALL

2ND SPALL

Figure 9-41. ▆ Sequence of Spallation Following
Radiation Deposition ▆

9-104

extremely local. depending on the sheet thickness and not on the overall geometry of the structure. so spall damage. including fracturing and debonding. usually cannot be scaled according to the laws that govern structural behavior. Since the spall damage occurs early, possibly weakening the structure. it can have a strong effect on the subsequent response to the structure to the impulse that has been imparted.

Propagation of stress waves and the damage predictions are not amenable to hand calculations. Most stress wave propagation calculations are performed on computers using one dimensional (1-D) models to represent a cross section of an aerospace vehicle shell. These stress wave propagation calculations are used routinely in design analysis and are the direct outputs of PUFF-like codes or their variations. The stress wave propagation predictions are used to:

1. Obtain a calculated pressure time history at the rear surface of a 1-D sample for direct comparison to experimental values that are obtained by laboratory simulation or by underground nuclear tests. The agreement or lack of correlation serve as an important criteria for judging the adequacy of analytical techniques. The conclusions are almost universal that the largest sources of error in stress wave propagation codes are associated with the mechanical aspects of the material behavior. such as failure criteria. and the elastic-plastic models. which should include strain rate and temperature dependence.

2. Obtain maximum tension as a function of depth in the materials to indicate regions of potential material failure. debonding. and spalling. Definitions that are required for the materials failure level under these dynamic tensile loads are obtained experimentally.

3. Obtain input data for structural response analysis.

There also are some 2-D shock propagation codes being used for specific calculations involving cylinders, nose tips. etc. Peak pressure predictions using pure hydrodynamic representations of the material in code calculations are generally high by a factor of 2 to 4. If a dynamic elastic-plastic constitutive relationship is included. the predictions are improved significantly.

9-38 Through-the-Thickness Elastic-Plastic Shock Propagation

Considerable progress has been made in correlating measured and calculated through-the-thickness shock propagation in one dimension by using the elastic-plastic materials description in PUFF-type codes. The stress strain diagram shown in Figure 9-42 illustrates a two-wave nature of the elastic-plastic shock wave propagation. The total stress. σ, is the sum of the hydrostatic pressure, P, and an elastic stress offset of $2/3\ Y_o$. where Y_o is the yield strength of the material (its compressive yield strength if that is different from its yield strength in simple tension). The effect of the yield stress path OAB is to propagate two stress waves having different velocities into the undisturbed material. The slope of the elastic portion. OA. is larger than the plastic portion. AB. The propagation speed is larger if the slope of the stress strain curve is larger. Hence, an elastic precursor shock traveling with the elastic velocity, c_E, runs in front of the slower total stress wave which propagates with a bulk sound speed, c_o

$$c_E = \sqrt{\frac{K}{\rho_o} + \frac{4/3 S^*}{\rho_o}}$$

$$c_o = \sqrt{\frac{K}{\rho_o}}$$

where K is the bulk modulus and S^* is the shear modulus.

An elastic rarefaction stress (4/3 Y_o or twice the stress offset) propagates from the rear of the shock wave at velocity c_E and overtakes
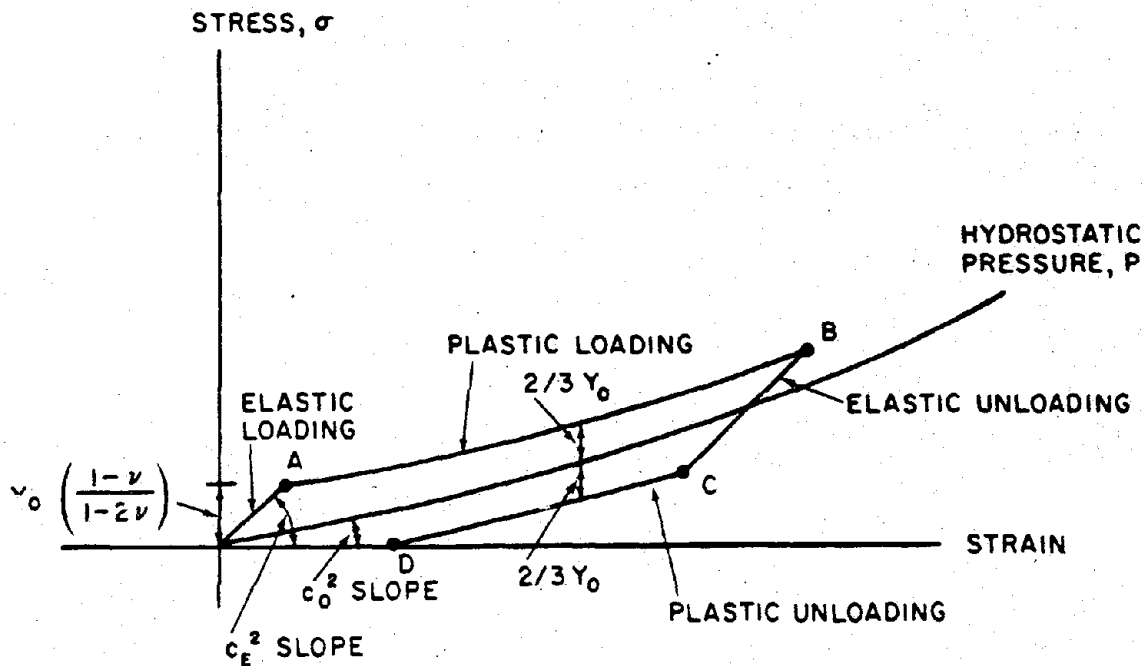
Figure 9-42. ▓ Equation of State for Elastic-Plastic Material Description ▓

the slower plastic wave (path BC). This rarefaction wave causes a greater attenuation of the main stress pressure wave than is obtained in pure hydrodynamic calculations (up and down the Hugoniot). This greater attenuation of the elastic plastic wave propagation compared to purely hydrodynamic calculations results in better correlation with measured values of stress. The plastic unloading to a stress-free condition, path CD in Figure 9-42, also propagates with velocity c_0 and completes the cycle.

▓ Although the elastic-plastic code calculations improved the correlation of measured and computed through-the-thickness stresses for some materials, if a material has strong strain rate or temperature dependence these features also must be incorporated into the calculations. Stress wave propagation through materials such as foams require an entirely different constitu-

tive expression, and anisotropic materials such as three-dimensional quartz phenolic, can have quite different material properties in different directions. Similarly, propagation characteristics of inhomogeneous materials or materials that contain small radiation absorbers lead to complicated propagation analysis. Propagation in these materials has not been treated in an analytically satisfactory manner. Most of the current analytical techniques used in the solution of stress wave propagation in the materials are deficient in varying degrees in the following ways.

1. There is incomplete understanding of the material behavior under the types of conditions that result from X-ray energy deposition, so the material representations are inadequate in most cases.

2. Experimental data for verification and modification of the equations of state and con-

stitutive relations in the analytical techniques have been limited and of poor quality.

9-39 Through-the-Thickness Material Response

Simulation tests and underground nuclear weapons tests can identify failure and damage modes that result from shock wave propagation and through-the-thickness material response on samples that are meaningful in terms of the expected response of reentry vehicles or aerospace shells. The experimental results are most meaningful when appropriate analytical techniques are used to correlate the experimental results with the stress wave characteristics producing the response modes. Hundreds of complex aerospace structure composites as well as samples of metals and plastics have been exposed during underground nuclear weapons tests at various X-ray fluence levels with different X-ray spectra and deposition times.

IMPULSE AND STRUCTURAL RESPONSE ANALYSIS

The vapor and/or liquid blowoff following X-ray deposition imparts a reactive impulse to the aerospace structure. The structural response takes place for the most part after the shock wave discussed in the last section has dissipated. This shock wave may have damaged or weakened the structure by spallation, debonding, or fracture. The damage to the structure should be considered in the structural response analysis if an accurate prediction is to be made. Obviously, this is a complicated problem and is not amenable to hand calculation. However, some rough estimates of impulse can be made and serve to illuminate the processes that take place.

9-40 Impulse Calculations

Page 9-108 deleted.

Deleted

Figure 9-43. Normalized Vapor Impulses Produced in Aluminum by Various Black Body X-ray Spectra

Deleted

Figure 9-44.   Normalized Vapor Impulses Produced in Copper by Various Black Body X-ray Spectra

Pages 9-111 and 9-112 are deleted.

Problem 9-5.   Calculation of Vapor Blowoff Impulse

The information presented in the preceding paragraphs provides a means to obtain an approximation of blowoff impulse for certain materials. The following example is presented to illustrate the procedures. In practice, these calculations are performed with computer codes.

DNA
(1)(3)
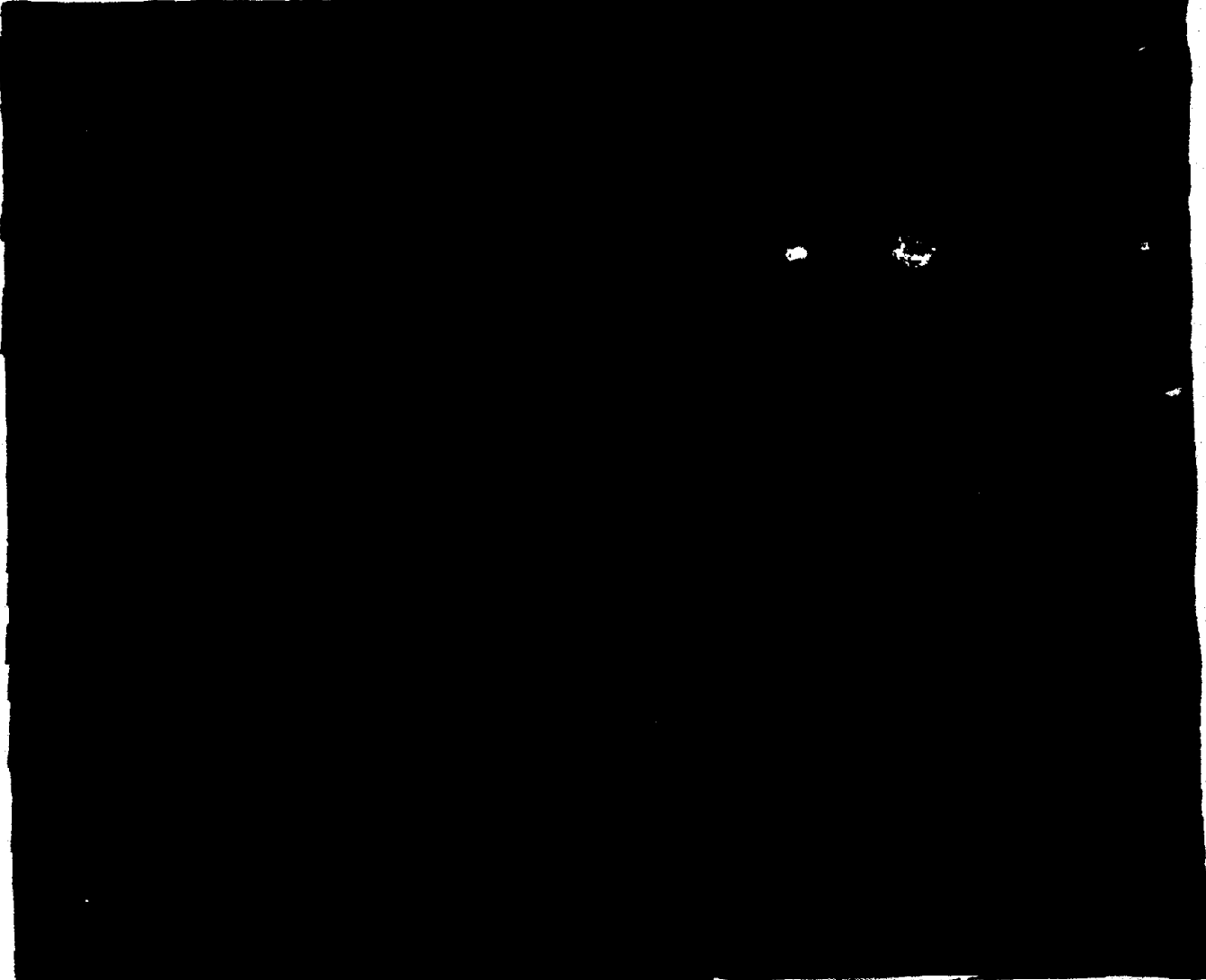
Related Material: See paragraphs 9-34 through 9-37, and 9-40. See also Figures 9-35 through 9-38, 9-43 and 9-44, and Table 9-17.

Problem 9-6.   Calculation of the Location of Phase Change Boundaries

The preceding paragraphs provide the information necessary to calculate the location of the various phase change boundary layers. The procedure is illustrated in the following example.

DNA
(b)(3)

DNA
(U)(3)

Most of the structure response analyses of reentry vehicles have been developed for survivability. Since low level failure criteria responses have been selected, only elastic deformation has been considered. Such survivability analyses are probably inadequate for the determination of inelastic deformation failure modes and the levels required to define lethality. Essentially all structural response calculations require data on: (1) structural material properties such as stress and strain relations as a function of strain rate and temperature, for yield, stress and strain, fracture points, elastic moduli; and so forth; (2) structural response forcing functions, including asymmetric impulse loads, and in-depth heating and thermal loads applied as distributed and point loads; and (3) structural variation in shell wall thickness and material densities in various layers.

DNA
(U)(3)

REENTRY VEHICLE HARDENING

X-ray hardening refers to techniques

that reduce the susceptibility of reentry vehicles to damage from X-rays.

It is beyond the scope of this manual to provide a complete discussion of reentry vehicle hardening techniques. Therefore, a brief general discussion of the techniques, with a few specific examples, is presented in the following paragraphs.

9-42 Balanced Hardening with Respect to Neutrons and X-rays

Page 9-117 deleted.

SECTION VI
NUCLEAR RADIATION SHIELDING

Any mass of material between a nuclear radiation source and personnel or sensitive equipment will reduce the dose to the personnel or equipment compared to the free field dose at the same location relative to the source. The dose received by a person behind a building, in a building, in a field fortification, in a tank, or in a

ship will be less than that which would be received in an exposed free field position.

In principle, it would be possible to calculate the dose behind a shield by using simplified neutron and gamma ray transport equations similar to those given in Chapter 5; however, several considerations make hand calculations impractical.

- The neutrons and gamma rays will arrive at the shield from many directions after having been scattered during their transport through the atmosphere.

- Calculation of radiation transport from a point source through single geometries can be done with reasonable accuracy by using an exponential factor and a buildup factor similar to those described in Section I, Chapter 5 for transport through homogeneous air, but the geometries of shielding enclosures are seldom simple, and, as mentioned above, the radiation incident on the shield is not unidirectional. This has the effect of making the problem similar to a multi-source problem.

- The attenuation of neutrons by inelastic scatter or radiative capture results in the emission of one or more gamma rays, which can contribute to the dose within the shielded area even though the neutrons are removed from the penetrating radiation beam.

- The specific location of the burst and the receiver can affect the degree of attenuation, e.g., different members of a tank crew will have different degrees of protection from the same explosion, and any particular member of the crew will have a different degree of protection from initial radiation from bursts at different locations relative to the tank. In other words, each location within each shielded structure must be evaluated separately, or at least a sufficient number of locations must be evalu-

ated to determine the overall shielding efficiency of the structure or piece of equipment.

These complexities, and others, make it necessary to use computer codes to determine the shielding efficiency of any structure or piece of equipment. Even when using the codes, some simplification in the description of the shield geometry usually is necessary. However, satisfactory methods for treating fairly complex geometries have been developed. These are described in DASA 1892, "Weapons Radiation Shielding Handbook" (see bibliography). Results of some sample calculations are also provided. Unfortunately, sufficient calculations have not been performed to permit the development of a generalized simple method for shielding calculations that would be suitable for inclusion in this manual.

Table 9-22 provides some estimates of the shielding afforded by various structures and types of military material. These estimates are given in terms of a "dose transmission factor," which is defined as the ratio of the dose measured behind the shield to the dose that would be measured in the absence of the shield. Some of the transmission factors shown in Table 9-22 were obtained by measurements at weapon tests or are extrapolations from such measurements. Other transmission factors were obtained by relatively detailed calculations, while still others are mere estimates. Ranges of values are given for the dose transmission factors for most structures. These ranges result from two causes: uncertainty in the estimates themselves, and variations in the degree of shielding that may be obtained at different locations within a structure. Separate transmission factors are given for initial gamma rays and residual (fallout) gamma rays for two reasons: the average energy of the initial gamma rays is higher than the average energy of the residual gamma rays, and there are different source geometries.

Table 9-22. ███ Estimated Dose Transmission Factors (Interior Dose/Exterior Dose) ███

DNA
(A)(1)

Deleted

9-120

No specific reliability can be attached to the dose transmission factors shown in Table 9-22. They are felt to be reasonable values for generalized applications: however. specific shielding problems should be addressed by methods such as those described in DASA 1892.

SECTION VII

TREE – COMPONENT PART AND CIRCUIT RESPONSE

This section contains a discussion of the effects of nuclear radiation on electronic component parts and circuits. The intent is to provide an introduction to the failure modes and responses that result from ionization. displacement. and thermomechanical shock. A more detailed description of the effects is contained in the TREE Handbook (see bibliography).

Since semiconductor devices generally are considered to be the most sensitive devices in an electronic circuit. emphasis is placed on them. However, the discussion does include other electronic component parts.

Within the scope of this manual, this section can only aid in establishing levels where electronic equipment might experience failures as a result of the radiation environment and indicate the extent of the problems. The numbers presented are only estimates for a generic grouping or subgrouping. It must be understood that it is very difficult to give accurate radiation effects data for generic types of electronics. For example. transistors can show sufficient amplification loss to be useless after receiving 10^{10} to 10^{15} n/cm^2 ($E > 10$ keV, fission). That is 5 orders of magnitude difference and is relatively useless information. Fortunately, transistors can be subgrouped to improve their characterization. The problem of accurate prediction, however, is not completely solved. Even if one particular type of transistor is considered, the neutron fluence required to reduce the amplification to a

particular value can vary more than an order of magnitude. Additionally, the failure threshold for a transistor in one circuit may be greatly different from the failure threshold for that same transistor in a different circuit. i.e., the response of each component part and the circuit configuration must be known to make a reasonable estimate of circuit response.

The transient radiation effects are classified into three groups: transient. permanent. and thermomechanical. The transient effects result from nonequilibrium free-charge conditions introduced through the ionization phenomena (see Chapter 6). The permanent effects are attributed to physical property changes of the irradiated materials caused by energetic particles (neutrons and secondary electrons). The thermomechanical effects result primarily from the absorption of low energy photons.

The class of effect is defined by the primary effect induced by the radiation. For example. the short term currents that result from ionization may trigger a digital state change or may permanently damage a device in some other manner. This phenomenon is treated as a transient effect, because the permanent consequences result from circuit action and/or device construction rather than from direct radiation induced material property change.

The terms "radiation hardened" or "radiation resistance" frequently are connotated incorrectly. These terms mean that someone or some group has examined the component part, circuit. or system, made some modification and/or used part selection criteria and has determined that the electronics will withstand certain levels of certain types of radiation. The experience of the person making the examination as well as the resulting modifications can both vary widely. Consequently, when these terms are used they should be accompanied by the answers to the following questions.

● Hardened to what type of radiation?

- Hardened to what levels of radiation?
- What procedure was used for hardening?
- How has the hardening been verified?

Based on the answers to these questions, the applicability of that "hardened" component part, circuit, or system for his intended use can be judged.

SEMICONDUCTOR COMPONENT PARTS

9-44 Transient Effects

The transient effects observed in semiconductor devices exposed to nuclear radiation result from the creation of excess charge carriers (ionization) that cause current and voltage changes. These changes do not cause permanent damage directly to the semiconductor material. However, their presence may produce permanent changes as a result of current overloads to some components, loss of information stored in memory units, or by the creation of premature signals. Furthermore, such transients can cause saturation of some circuits for times that are long compared to the duration of the ionizing radiation pulse, and may thus cause system failure during a significant and possibly critical period.

Most of the ionization produced in a nuclear weapon environment is due to the photons and 14-MeV-neutrons, although all nuclear radiation can contribute. Because of this predominance of photon excitation of carriers, the observed currents and voltages are often referred to as photocurrents and photovoltages, even though the prefix may not always be proper. The mechanisms whereby this ionization occurs are described in Chapter 6.

Before discussing the transient effects in particular semiconductor devices, it is desirable to review briefly the important basic physical processes responsible for device behavior. These processes are common to all semiconductor devices and must be reasonably well understood before the description of the device response can be followed intelligently.

Current is the manifestation of charge carrier movement within a material. As described in paragraph 6-4, the movement may be random, random with a diffusion from regions of high concentration to regions of low concentration, or, if an electric field is present, the movement may be a drift in the field superimposed on the normal random scattering. Carriers may be trapped by impurities, which are always present in solid state devices. Eventually, the trapped carriers may be annihilated by their mates (oppositely charged carriers) in a process called recombination. The net result of these processes is that the free carriers diffuse and/or drift until they are trapped and are then promptly recombined. Therefore, any electrical currents in the materials are considered to have two components — the drift component and the diffusion component. The time during which a charge carrier is free to move by drift and/or diffusion is called the lifetime of the charge carrier.

The simplest semiconductor device is the diode. The diode is made up of pure semiconductor material doped with impurities so as to be considered to have two regions. Using pure silicon as the example, its atomic structure is considered to have four electrons in the outer orbit. In its crystal form, these outer orbiting electrons are considered to be shared with neighboring silicon atoms (see Figure 9-45). When the pure silicon is doped with an impurity, the impurity atom replaces one of the silicon atoms in the crystal lattice. The impurities are selected to have either three or five outer orbiting electrons. Silicon doped with an impurity having five outer orbiting electrons will have extra electrons that are more or less free to move around, and hence are available for conduction. Silicon doped with impurities with only
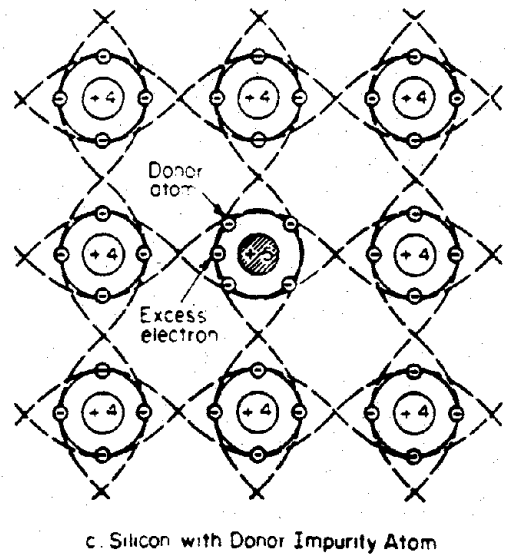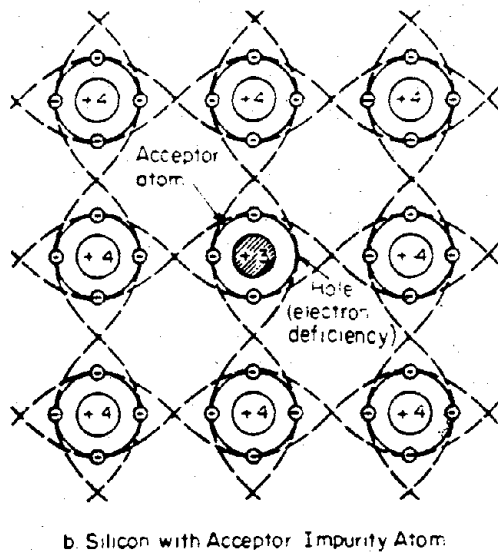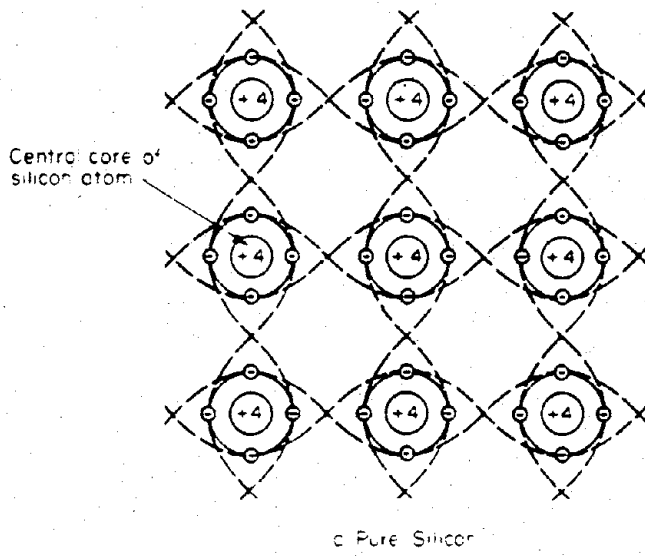
Central core of silicon atom

c. Pure Silicon

Acceptor atom

Hole (electron deficiency)

b. Silicon with Acceptor Impurity Atom

Donor atom

Excess electron

c. Silicon with Donor Impurity Atom

Figure 9-45. █ Two-Dimensional Lattice Structure of Silicon █

three orbiting electrons does not have sufficient electrons to share with its neighboring silicon atoms. This lack of an electron is called a hole. For conceptual purposes, the hole can be treated like an electron with a positive charge. Consequently, in semiconductor discussion the term charge carriers refers to the electrons and holes made available for the conduction process by the impurity doping.

Figure 9-46 illustrates a semiconductor junction (diode), with the two impurity regions shown separated by a solid line. This represents what conceptually would be the junction of the two materials. However, in reality the silicon is all one crystal. and there is really no physical junction. There are. as illustrated. regions at both ends of the crystal which are predominantly either P type (excess of free holes) or N type (excess of free electrons). A transition region, called the depletion region. exists in the center. Within this region. holes from the P region combine with equal numbers of electrons from the N region. As a result. only a few free charge carriers remain in the region when equilibrium has been reached. Depending on the number of charges removed from each region. a voltage (electric field) will be developed across the depletion region. The voltage across the depletion region under equilibrium is such that any

holes (positive charge carriers) introduced into the region would migrate by the drift process to the P region, and a negative charge carrier (electron) introduced into the depletion region would migrate by the drift process to the N region. Under normal conditions conventional current flow* would allow current to flow for ideal diodes only from the P side to the N side. If, however, free carriers were generated in the depletion region, conventional current flow would dictate that a current, proportional to the number of free charge carriers generated, would flow from the N region to the P region. This is in the reverse direction from the normal conventional current flow through an ideal diode. This reverse current, if generated in the depletion region by ionizing radiation, is called the drift component of the photocurrent in a PN junction. The diffusion component of the photocurrent is the result of free carrier generation by the ionizing radiation in the P and N regions near the depletion region. Those hole-electron pairs generated far from the depletion region will be trapped and recombined before they can become effective. The effect of the radiation is to

*In this chapter, normal current flow is considered to be conventional current flow. This is opposite to actual electron flow.

Where junction would be if it were a line

Excess of free holes — P   N — Excess of free electrons

Actually this region constitutes the junction and is called the depletion region.
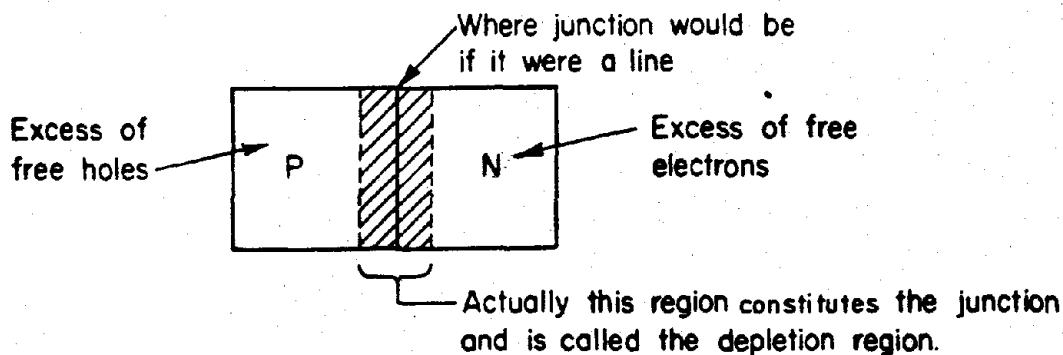
Figure 9-46.   Illustration of a Semiconductor Junction

generate a current in the reverse direction through the diode junction, which tends to forward bias the diode. An expression that generally will predict the photocurrent for many cases of interest is:

$$I_{pp\ max} = qK_g \dot{D}A\ (w + L).$$

where

$I_{pp\ max}$ = the maximum* primary photocurrent for a PN junction

q = electronic charge 1.60 x 10^{-19} coulombs

K_g = the energy-dependent free-charge-carrier-generation constant (electron-hole pairs/ cm^3 · roentgen)

K_g (for silicon) = 4.2 x 10^{13} electron-hole pairs/cm^3 · R

K_g (for germanium) = 1 x 10^{14} electron-hole pairs/cm^3 · R

$\dot{D}$ = the gamma exposure rate, R/sec (The gamma ray photons have energies which would give best results with the K_g constants given above.)

A = junction area in cm^2 (A can typically vary from 0.3 x 10^{-4} to 0.2 x 10^{-1} cm^2)

w = depletion layer width in cm (w varies with applied voltage and is best expressed as w = $w_1\ (V_o - V_j)^{-b}$ where V_o is the built-in junc-

tion potential (~0.35 volts for germanium and ~0.72 volts for silicon) w_1 typically varies from 0.5 x 10^{-4} cm to 1 x 10^{-3} cm, V_j is the junction voltage. and b typically varies from 0.05 to 0.5.

L = diffusion length for minority carriers on the side of the junction with the longer diffusion length in cm (L can vary typically from 0.15 x 10^{-1} cm to 0.2 x 10^{-4} cm).

The duration of the photocurrent depends on the time required for free holes and free electrons to be trapped and to recombine. Since these times are short, the photocurrent is a pulse of current of relatively short duration. Typical pulse shapes are shown in Figure 9-47.

Tunnel diodes are at least an order of magnitude more radiation resistant than diodes in general, since they are characterized by small geometry, heavily doped PN regions, and narrow junctions. The short-circuit photocurrent can be estimated from the equations applicable to general diodes. Since the lifetime of minority carriers in tunnel diodes is very short, the response of a tunnel diode to a pulse of radiation is expected to follow the radiation pulse. Normally, the width of the depletion region for tunnel diodes is so narrow that the photocurrent will consist primarily of the diffusion component. The maximum photocurrent under short

---

* For those more theoretically inclined this equation applies in the case where $\tau < t_p/4$ and is the steady-state value. A more detailed equation and development is the *TREE Handbook*.
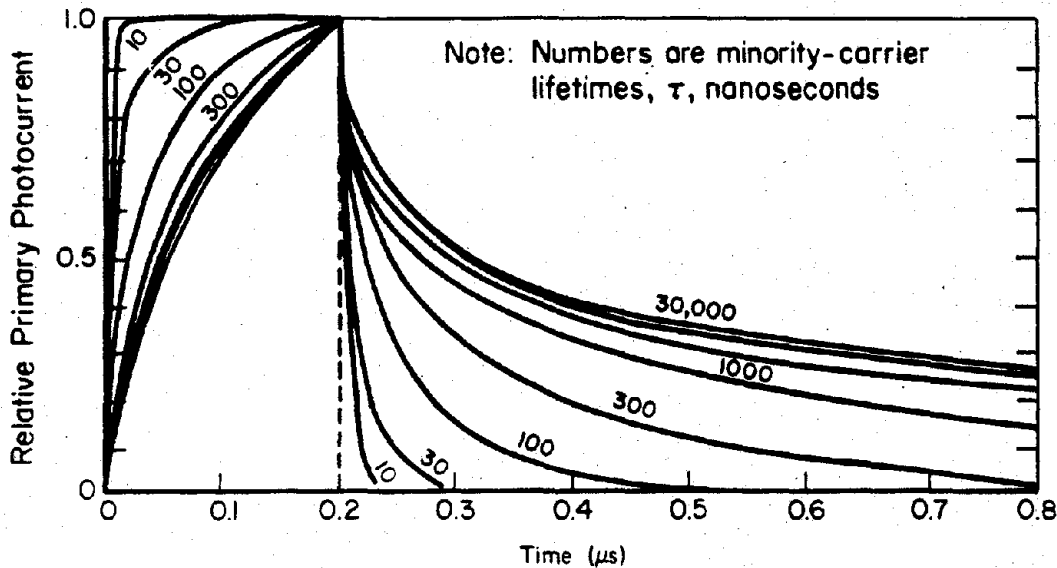
Figure 9-47. ▇ Relative Shapes of Diffusion Component
of Primary Photocurrent ▇

circuit conditions can thus be estimated as follows:

$$I_{pp\ max} = qK_g\dot{D}A\ (L_n + L_p)$$

where

q, K_g, $\dot{D}$ and A are defined as in the diode expression, and L_n and L_p are the diffusion lengths in the N and P regions, respectively. Diffusion lengths are comparable on each side of the junction.

▇ The radiation induced offset voltage in an open circuited tunnel diode is influenced by the tunneling current at low dose rates, but at higher dose rates a tunnel diode behaves like a conventional diode. This behavior occurs because very little induced voltage is required to set up a tunneling current equal to the diffusion current of excess carriers. When the tunneling current reaches a maximum, the induced voltage

rises sharply to the value for a conventional diode.

▇ A transistor is a more complicated device than a diode, both structurally and functionally. The main functional advantage of the transistor is the fact the transistor has the ability to amplify its input signal. The transistor has three impurity regions that alternate, i.e., NPN or PNP. When an operating transistor* is exposed to transient ionizing radiation, a current pulse is observed in the external circuit. This current pulse, which may be orders of magnitude larger than that of a diode with comparable dimensions, can reach a peak value at a time later than the radiation peak, and can, in some cases, continue for milliseconds.

*▇ The following paragraphs are concerned with bipolar transistors; not to MOS, junction field-effect transistors, or thin-film transistors.

9-126

This characteristic behavior of transistors is the result of the amplifying properties acting on the primary radiation induced photocurrents. The electrical action of the transistor creates a secondary photocurrent that is typically greater than the primary photocurrent by a factor equal to the gain (a measure of ability of the transistor to amplify) of the transistor. Analysis of the radiation response of a transistor involves the determination of the primary photocurrent, followed by a calculation of the magnitude and duration of secondary photocurrents under the given circuit conditions.

In transistors, the primary photocurrent is generated in five regions: in the collector- and emitter-junction depletion regions, in the base, and in the emitter and collector bodies lying within a diffusion length of the junctions. In most cases, the generation of primary photocurrent in the emitter body and within the junctions can be neglected since the emitter body and the junction volumes are a relatively small part of the total generating volume (see Figure 9-48).

The secondary photocurrent is produced by the accumulation of excess majority carriers in the base region as a result of the flow of primary photocurrents across the PN junctions of the device. This excess charge, which is confined in the base by the built-in junction fields, is the correct polarity to forward bias the emitter base junction and to cause normal current to flow. The collector current that is produced is called secondary photocurrent. This collector
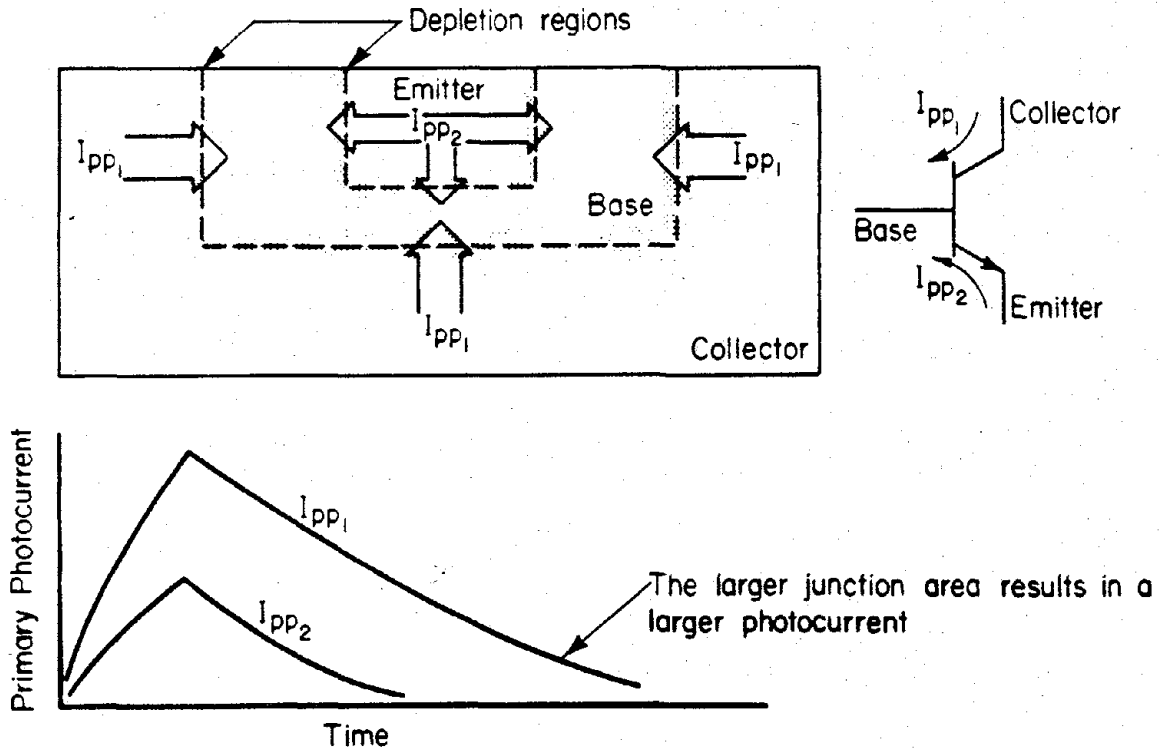

Figure 9-48.   NPN Transistor Illustrating the Primary Photocurrent

current continues to flow until the excess charge stored in the base can either recombine with minority carriers or flow out through the external base lead.

The magnitude of the collector current pulse will depend on the dose rate if the radiation pulse is long compared to the lifetimes of the transistor base and collector, but it will depend on the total dose if the pulse is shorter than those lifetimes. This results from the charge transferred from the collector by the primary photocurrent being stored in the base region. Since many transistors have lifetimes that are as long as or longer than typical nuclear weapon radiation pulses. the prompt dose is quite often the most important factor.

A simplified linear approximation of the primary photocurrent in a transistor can be estimated with the following equation:

$$I_{PP} = \frac{\dot{D}}{CONST.} \; [t_s + 0.03],$$

where

D = the gamma ray exposure rate, R/s

$CONST.$ = 0.83 x 10^8 for NPN devices and 0.42 x 10^8 for PNP devices*

t_s = charge storage time (in μs) for the device of interest (t_s typically can vary from a few nanoseconds to hundreds of microseconds).

The duration of the photocurrent response depends on the radiation pulse width, the radiation storage time (which is different than the charge storage time (t_s)), and the time for holes and electrons to recombine. The radiation pulse width is determined by the weapon. The time for holes and electrons to recombine is illustrated for a diode in Figure 9-47, which applies generally for transistors. The radiation storage time, t_{sr}, is defined by Figure 9-49a. The radiation storage times for several dose rates are shown in Figure 9-49b. These latter curves are
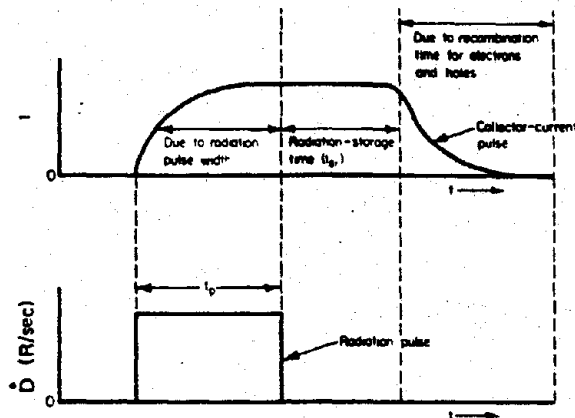
a. Definition of the Device Radiation-Response Times
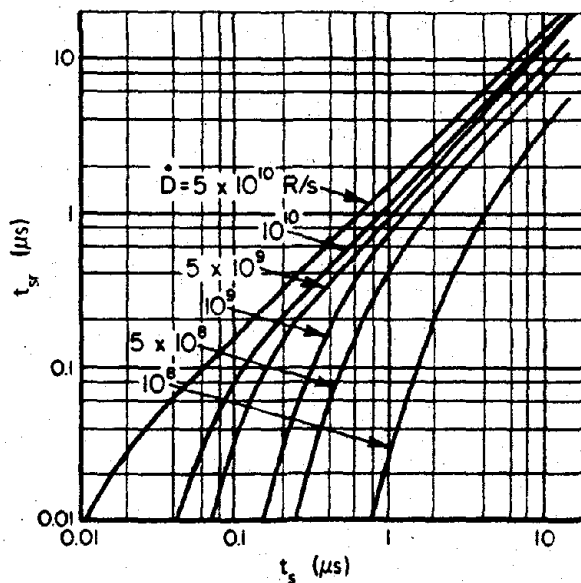
b. t_{sr} vs t_s Curves

Figure 9-49. ⬛ Radiation Storage Time ⬛

■

for a particular bias and radiation condition during storage. They are presented as being illustrative. and no attempt should be made to generalize from the curves. It is necessary to analyze a transistor or diode in the particular circuit configuration in which it is used to determine the threshold for circuit malfunction. As a result of the many different circuit configurations and bias conditions that can occur for transistors and diodes. failure thresholds that would be of value can not be specified generally for the TREE environment.

■ A silicon controlled rectifier (SCR) is a solid state semiconductor device composed of four layers of alternate-impurity semiconductor material containing three PN junctions. The SCR is an active switching element that will remain in a nonconducting or "off" state until turned on or "fired" by a low-level control signal on the gate. It will then remain "on" without need for a sustaining control signal. The SCR is turned "off" by reducing its output (anode) current below the "dropout" level. Radiation induced currents. like those discussed for diodes and transistors. are a direct function of the junction areas. diffusion lengths. etc.. and thus are difficult to predict since values for the parameters usually are not available. Since these currents. above a threshold. can induce changes in the state of an SCR. some method is required to predict the magnitude of the radiation induced currents. or, more specifically. the radiation threshold above which switching occurs.

■ It has been found that the transient radiation switching thresholds (critical radiation exposure rate) for SCR's are functions of the radiation pulse width. The exposure rate required to trigger an SCR becomes constant for pulse widths longer than a critical value. This critical value is a function of the device minority carrier lifetime and the device delay "turn on" time. For pulse widths less than the critical value. the exposure rate required to trigger an

SCR increases rapidly as the pulse width approaches zero. The dependence of the switching threshold of a 3A60A SCR on pulse widths and gamma ray exposure rate is shown in Figure 9-50. The critical pulse width for this device is approximately 2 microseconds.

■ Typically the SCR type of device would not be expected to fire below 10^6 rads (Si)/sec. For most cases. however. the pulse width is sufficiently short that the devices are dose dependent. Failures occur typically at prompt doses between 0.1 and 1 rad (Si).

■ Field-effect transistors (FET) are a family of unipolar devices that have pentode-like characteristics. The three major categories within this family are the junction FET, the metal-oxide insulated-gate FET (MOSFET), and the thin-film insulated-gate FET (TFT). The geometry and construction features of typical field-effect transistors are shown in Figure 9-51. The basic structure of the FET devices involves a source. a gate. and a drain in rough functional correspondence to the familiar cathode, grid, and plate of vacuum tube technology.

■ The mechanisms by which radiation generates photocurrents in an FET are not substantially different from those for bipolar transistors and diodes. The important radiation parameters in an FET are the transient gate and drain-to-source currents. Possible sources of transient currents in FET's can be grouped into the following categories:

- Leakage currents across PN junctions that behave like PN junction photocurrents discussed previously.

- Direct modulation of the channel conductivity and mobility (usually applicable at high ($>10^8$ rads (Si)/s) dose rates).

- Leakage currents through the gate oxide layer (applicable to the metal oxide and thin-film FET's).

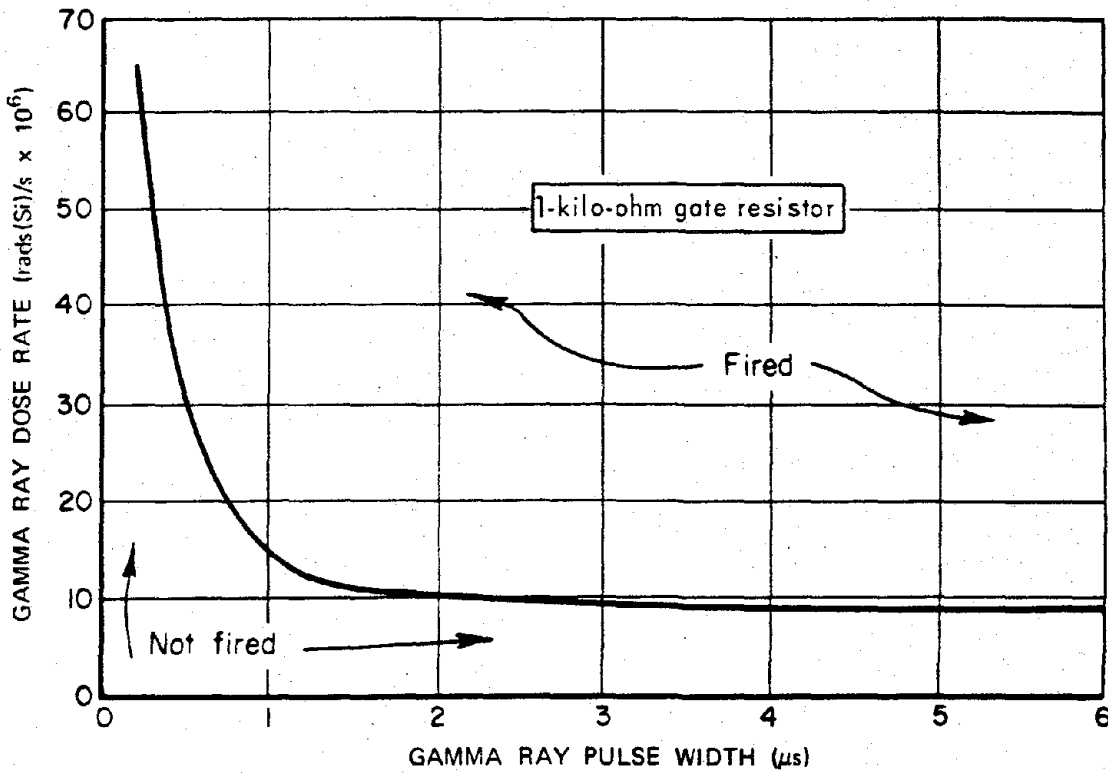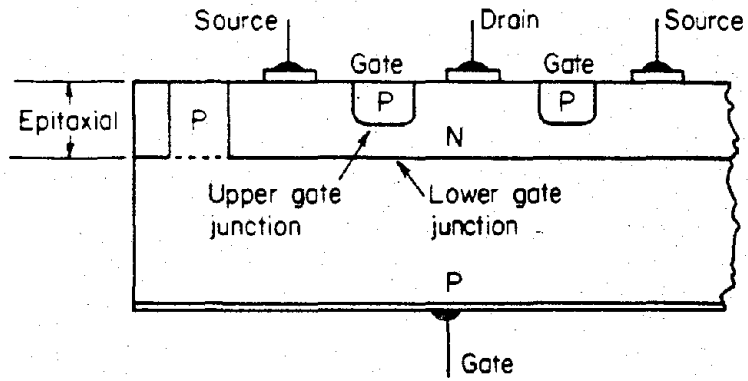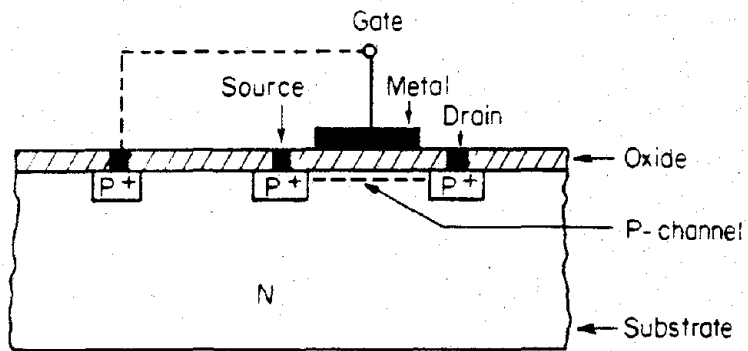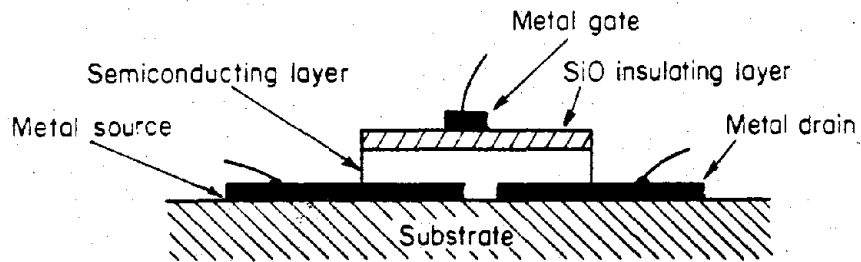- Secondary emission (see Chapter 6) and atmosphere ionization currents.

Figure 9-50. ▦ Gamma Ray Exposure Rate as a Function of Pulse Width Switching Thresholds for a 3A60A SCR ▦

a. Junction Field-Effect Transistor

b. MOS Field-Effect Transistor

c. Thin-Film Field-Effect Transistor

Figure 9-51. ███ Construction of Typical Junction, MOS, and Thin-Film Field-Effect Transistors ███

Significant problems generally are not caused in field-effect transistors at dose rates below 10^6 rads (Si)/sec.

9-45 Permanent Effects

Permanent effects in semiconductor devices are those that can be attributed to physical property changes that result from the direct interaction of the radiation with the material of interest. These property changes typically last for periods that are long with respect to the recovery times of the components. These property changes occur in a very short time period and result in a rapid change in the operating characteristics of the device. A closely related effect is called rapid annealing, which is the process by which an initially large change in device parameters recovers very rapidly, approaching the smaller change observed several minutes after the radiation exposure.

Most permanent effects in semiconductor devices subjected to a nuclear radiation pulse result from damage to the semiconductor material by energetic neutrons ($E > 10$ keV); however, the effects of gamma rays and secondary electrons must not be underestimated. In certain devices such as MOS field-effect transistors the effects of ionizing radiation can be the principal causes of permanent failure.

Permanent effects can be grouped into two categories — bulk, and surface effects. Bulk effects are changes in the device characteristics that can result from damage to the bulk material. Surface effects are changes that are generally caused by radiation induced ionization near the surface of the device. Bulk damage effects from neutron radiation usually can be predicted within a factor of 2, while surface effects are generally unpredictable.

Bulk effects result from electron, gamma ray, and neutron induced lattice displacements in the bulk of the material (see Chapter 6). Fast neutrons lose energy primarily by elastic colli-

sions with the semiconductor atoms and cause large disordered clusters to be formed within the material. Gamma radiation loses energy by creating Compton electrons (see Section I, Chapter 5), which may cause lattice displacements. Since electrons have such a small mass, they primarily cause vacancy-interstitial pairs rather than clusters of defects that are typical of neutron damage. Lattice damage that results from gamma radiation usually is of secondary importance, unless a large gamma dose ($>10^5$ rads) is absorbed by the material.

Lattice damage degrades the electrical characteristics of semiconductor devices by increasing the number of trapping, scattering, and recombination centers.

- The trapping centers remove carriers from the conduction process.
- The additional scattering centers reduce the mean free path of the free carriers. Since the mobility is directly proportional to the mean free path, radiation exposure reduces the mobility of charge carriers.
- The recombination centers decrease the minority carrier lifetime according to the relationship (see Chapter 6).

$$\frac{1}{\tau_\varphi} = \frac{1}{\tau_0} + K\varphi,$$

where

τ_φ = minority-carrier lifetime at fluence φ in seconds,

τ_0 = initial minority-carrier lifetime (bulk lifetime), in seconds,

K = lifetime damage constant, $cm^2/$ (neutron-seconds),

φ = fast neutron fluence, neutrons/cm^2.

Permanent effects also can be caused by radiation induced changes in the semiconductor surface. The changes in the surface conditions

attributed to radiation that can cause permanent effects are surface charging mechanisms and changes in the surface recombination velocity. The most likely charging mechanisms are the collection of ions from a gas in the atmosphere surrounding the semiconductor device and the ejection of electrons from dielectric materials which are either deposited on the semiconductor surface or in which the device is encapsulated. These ions migrate under the influence of electric fields. As a result of the collection of these charges, inversion layers can form near the surface, causing large increases in leakage currents. In silicon devices these leakage currents result from recombination-generation in the enlarged depletion region.

█████ Ionizing radiation can cause changes in recombination velocity, which has deleterious effects on the effective lifetime according to the relation

$$\frac{1}{\tau_{eff}} = \frac{1}{\tau_\varphi} + \frac{1}{\tau_{surf}},$$

where

τ_{eff} = effective lifetime,

τ_φ = bulk lifetime,

τ_{surf} = surface lifetime (an inverse function of recombination velocity).

Surface effects usually are negligible compared to bulk lifetime damage for most conventional devices in a transient radiation environment. Field-effect devices, where radiation induced surface changes are the primary damage mechanisms, represent an important exception. ████ The general effects of nuclear radiation on semiconductor diodes are summarized below and are illustrated in Figure 9-52 and 9-53.

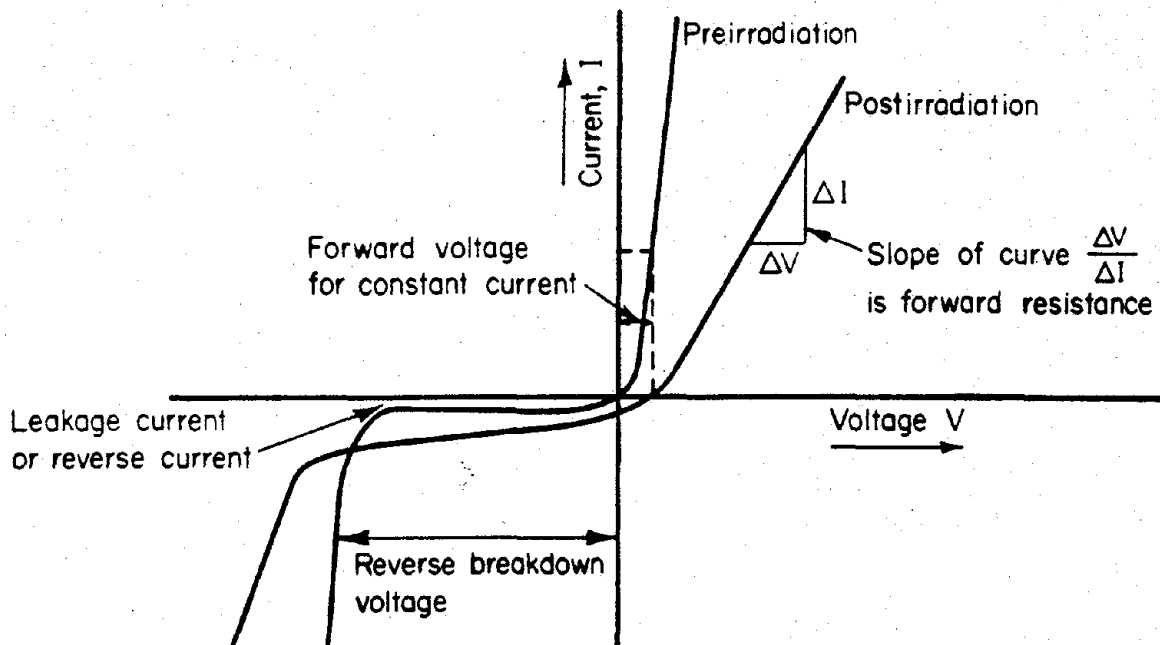● The forward voltage of the diode at constant current normally will increase as a

Figure 9-52. █████ An Illustrative Diode Characteristic for Pre- and Post-irradiation by Neutrons ███
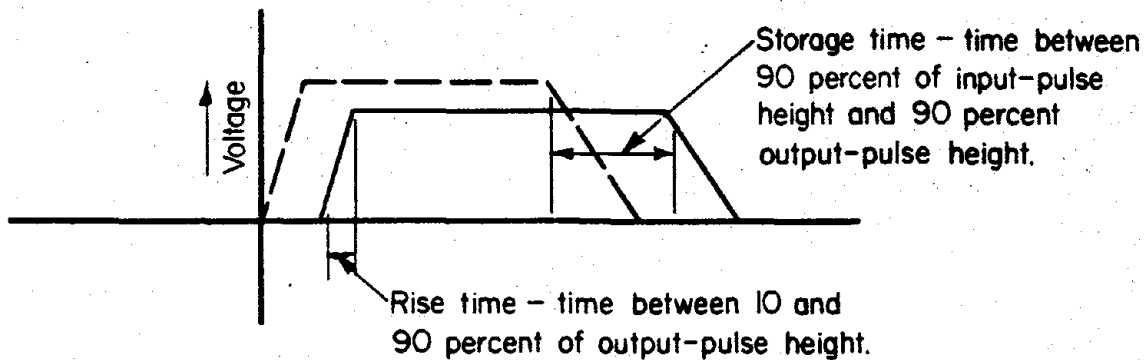
Figure 9-53. ⬛ An Illustration of Rise Time and Storage Time ⬛

result of changes in resistivity and mobility in the bulk material.

- The dynamic forward resistance will increase as a result of changes in resistivity and conductivity modulation.

- The surface effects and increases in carrier generation in the space-charge region will cause the reverse current to increase.

- The reverse breakdown voltage normally will increase because of an increase in resistivity.

- The switching characteristic of the diode generally will be changed. The rise time will increase, and the storage time will decrease as a result of lifetime damage.

Diodes generally are an order of magnitude more resistant to radiation than transistors of similar type. For this reason, theoretical and experimental studies have concentrated on transistors rather than diodes. Prediction techniques for diodes are complicated by the fact that the various bulk and surface damage mechanisms interact in an intricate manner. The wide variety of diode types, i.e., material, doping level and profile, geometry, etc., all tend to make comprehensive prediction schemes difficult and inaccurate. However, some quantitative trends in the changes in diode parameters can be given. The

more important changes in diode characteristics. from a circuits point of view, are the increase in forward voltage at constant current and the increase of reverse leakage current. Changes in the dynamic forward resistance, breakdown voltage, and switching characteristics usually are of secondary importance.

The forward voltage at constant current generally starts to increase at a fluence of 10^{13} to 10^{14} n/cm^2 ($E > 10$ keV, fission), though some diodes exhibit changes at fluences as low as 10^{12} n/cm^2 ($E > 10$ keV, fission) while others show no change up to fluences as large as 10^{15} n/cm^2 ($E > 10$ keV, fission). Usually, fluences of about an order of magnitude greater than the fluences required to cause the initial change will double the forward voltage.

The reverse leakage current usually increases with exposure, but decreases also have been observed. Nominally, changes begin at fluences from 10^{13} to 10^{14} n/cm^2 ($E > 10$ keV, fission). Gamma ray doses as low as 5×10^4 rads (Si) have caused significant leakage currents. Germanium devices generally have larger changes in leakage current than silicon devices.

The changes in breakdown voltage are typically the largest for diodes with high breakdown voltage. Reference voltage diodes (zener

diodes) are relatively resistant to radiation with reference voltage changes less than 5 percent at 10^{15} n cm^2 ($E > 10$ keV, fission).

The storage time is directly proportional to lifetime. Hence, the fluence at which the storage time will be reduced to one-half the preirradiation value will be

$$\varphi = \frac{1}{\tau_o K} \; .$$

where

τ_o is the minority carrier lifetime.

K is the damage constant (see Chapter 6).

Other diode types are specifically designed for rectifier application where high breakdown voltage and a low voltage drop are required even at high current. These diodes usually are designed with a PIN junction, which results in a device that is less sensitive to radiation than the standard type diodes.

Selenium rectifiers and hot carrier diodes (metal semiconductor junction) appear to be more radiation resistant than either germanium or silicon diodes because of their material and structural differences. Reactor tests conducted on the HPA-2300 series hot carrier diodes confirm the relative radiation hardness of these devices. Most units tested remained within manufacturer's specifications at fluences of 3 x 10^{15} n/cm^2 ($E > 0.1$ MeV, fission) and 9 x 10^5 rads (Si).

Diodes classified as "tunnel diodes" are easily recognized by their forward current characteristic, which shows a region of negative resistance. The effect of radiation on tunnel diodes is observable on the current-voltage (I-V) characteristic at fluences between 10^{15} and 10^{16} n/cm^2 ($E > 10$ keV, fission), and can be summarized as follows:

● The slope of the primary tunneling current is not changed; however, the peak current

is slightly reduced as a result of the redistribution of the electrons in the defect states.

● The valley current at a given voltage increases due to the additional tunneling via defect states.

● For voltages larger than valley voltage, there is an increased current for a given voltage due to the excess current, which predominates over the diminishing normal diode current.

Figures 9-54 and 9-55 show representative germanium and silicon tunnel diodes under neutron irradiation. The figures show that tunnel diodes are still operational at 5 x 10^{15} n/cm^2 ($E > 10$ keV, fission), which indicates the relative radiation hardness of these devices.

The general effects of nuclear radiation on bipolar transistors can be summarized as follows:

● The current gain (amplification) of the transistor will be degraded as a result of lifetime damage to the bulk material. Degradation of gain will be greatest immed-
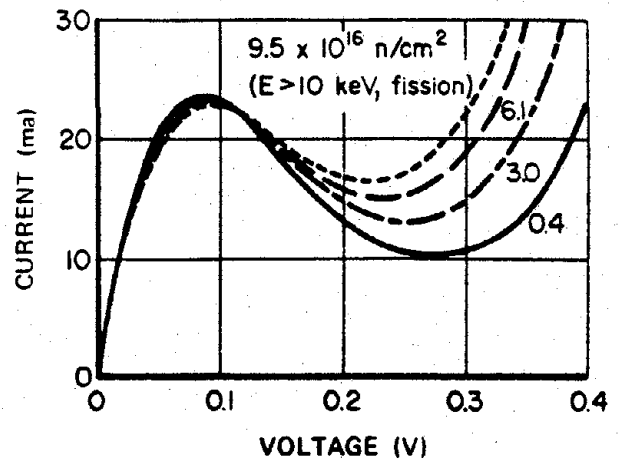

Figure 9-54. ██ Fast Neutron Bombardment Effect on Voltage-Current Characteristic of a Germanium Tunnel Diode ██
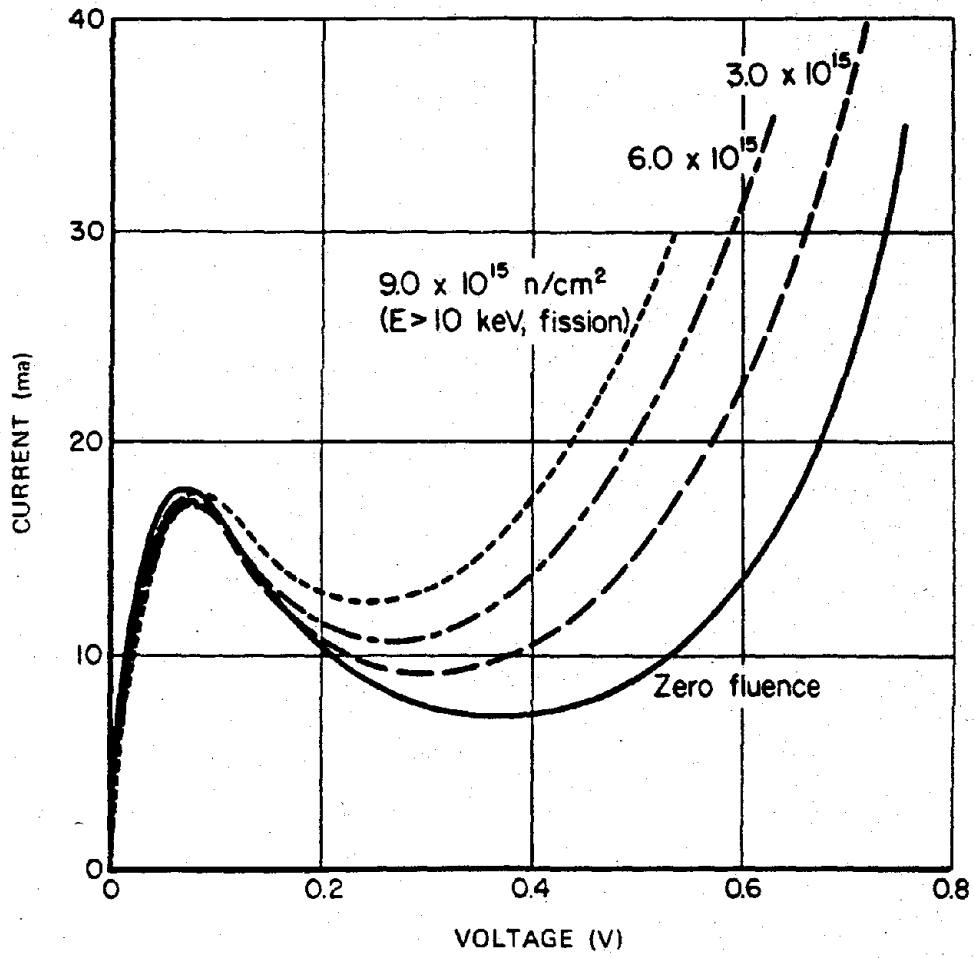
Figure 9-55. ▮▮▮ Fast Neutron Bombardment Effect on
Voltage-Current Characteristic of a
Silicon Tunnel Diode ▮▮▮

iately following a burst of nuclear radiation. and the gain will recover rapidly to a quasi steady-state value. The annealing can go on for weeks. but usually the current gain recovery is small or negligible after the initial recovery.

- The reverse leakage current will increase as a result of surface effects and carrier generation in the space-charge region.

- Changes occur in the punch-through voltage. and the base-to-emitter and collector-to-base breakdown voltage as a result of changes in resistivity.

- Increases in base-spreading resistance. collector body resistance, and saturation voltage result from changes in resistivity and conductivity modulation.

- The switching characteristics also are changed slightly — exemplified by decreased storage time and increased turn-on time as a result of changes in lifetime and resistivity.

Since transistors usually are the most vulnerable devices used in conventional circuits. predictions of circuit response under radiation conditions will be limited by the accuracy with which transistor behavior can be predicted. The reduction of current gain generally will limit the usefulness of the component before the other factors listed above become a serious problem. Therefore, emphasis is placed on the prediction of current gain degradation. However, in some applications saturation voltages and/or leakage currents across reverse biased junctions may be the limiting factors.

The structure of a device is an important factor in determining its radiation resistance. A general rule is that the thinner base, higher frequency, and smaller junction area devices usually have better radiation resistance. For example. the diffused-junction devices usually offer a resistance to radiation about one order of magnitude better than that offered by the alloy-junction devices.

Experimental data for conventional transistors in the form of generalized gain degradation curves are shown in Figure 9-56 for some common transistor types. The ratio β_φ/β_o represents the ratio of gain at some fast neutron fluence to the gain prior to irradiation. Figure 9-56 is representative of preliminary data from steady-state reactor experiments. The transistor types have been placed in their respective regions on the basis of where a majority of samples of a given type fell on the graph. Caution should be exercised in using and interpreting the information in the figure, since irradiation temperature, irradiation source. measurement conditions. etc. are not specified.

A further word of caution should be injected concerning the interpretation of gain degradation data. A sharp decrease in β occurs during exposure and then rapidly anneals to a final value that is commonly measured. The time dependence of gain degradation can best be interpreted with the use of the annealing factor, F, defined as follows:

$$F(t) = \frac{\dfrac{1}{\beta_\varphi(t)} - \dfrac{1}{\beta_o}}{\dfrac{1}{\beta_\varphi(\infty)} - \dfrac{1}{\beta_o}} = \frac{K(t)}{K(\infty)} \ ,$$

where

$\beta_\varphi(t)$, $K(t)$ are gain and damage constants as a function of time after a fast burst of nuclear radiation.

$\beta_\varphi(\infty)$, $K(\infty)$ are the steady-state values of gain and damage constants.

The magnitude and form of F varies with temperature, injection level, doping level, and impurity content. Typical values for the annealing factor at 1 msec range from approximately two to three for NPN transistors and

β_φ/β_o vs FAST NEUTRON FLUENCE (n/cm^2)

Legend: I, II, III, IV, V
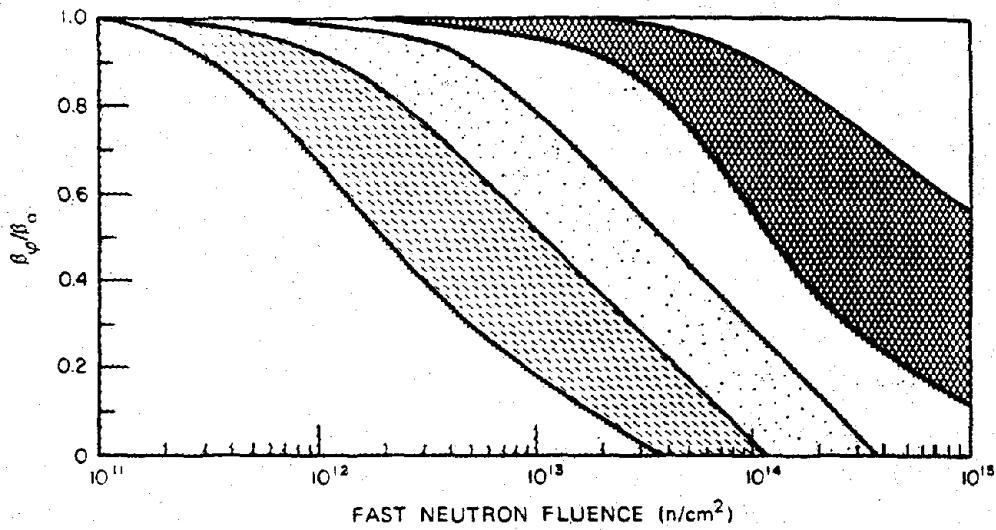
I	II	III		IV			V
2N329A	2N336	2N697	2N3244	2N404	2N2708	S-7241	2N700
2N1016E	2N699	2N708	2N3251	2N585	2N2784	S-7242	2N706B
2N1486	2N861	2N718	2N3252	2N705	2N2808	PT 2600	2N709
2N1653	2N917	2N720A	2N3300	2N706	2N2845	XF 805	2N797
2N1722	2N1016	2N722	2N3444	2N707A	2N2857	4907974	2N918
2N2187	2N1132	2N869	2N3486	2N708	2N2894		2N955A
2N2484	2N1184	2N910	2N3497	2N743	2N3013		2N964
	2N1613	2N1306	2N3499	2N744	2N3017		2N1195
	2N1711	2N1342	2N3509	2N834	2N3119		2N1709
	2N1900	2N1506	3TE240	2N835	2N3209		2N2537
	2N1936	2N1717	BR100A	2N914	2N3227		2N2616
	2N2187	2N1893	7900302	2N915	2N3252		2N2808
	2N2219	2N2192A	7900329	2N916	2N3287		2N3014
	2N2223	2N2193A		2N917	2N3303		2N3283
	2N2243A	2N2217		2N1306	2N3309		2N3287
	2N2297	2N2222		2N1307	2N3327		2N3309
	2N2411	2N2223		2N1506	2N3375		S-6781
	2N2878	2N2368		2N1709	2N3546		
	2N3072	2N2461		2N2218	2N3570		
	2N3439	2N2699		2N2369	2N3633		
	2N3499	2N2801		2N2538	2N3723		
	2N3501	2N2887		2N2540	FT 0040		
	2N3502	2N2907		2N2656			
	2N3637						

Figure 9-56. ███ Current Gain Degradation Characteristics for Some Common Transistor Types ███

slightly smaller for PNP transistors. The annealing factor can be as high as 7 for low injection situations and immediately after turning on a device that was off during the neutron pulse.

Other transistor parameters also can be degraded. Permanent increases occur in leakage currents across reverse-biased junctions. In general. the discussion of diode leakage is applicable to transistor leakage.

Changes in breakdown voltages. punch-through voltage. and collector and emitter body resistances are negligible at fluences where the gain is still usable. The effects of nuclear radiation on these parameters can be analyzed from comments made about diodes.

The changes in saturation voltage and in the switching time as a result of nuclear radiation are of interest for switching applications. In many cases the saturation voltage may appear to increase at relatively low levels of radiation. but actually the transistor is losing base drive and is coming out of saturation. The only significant increases in saturation voltage are seen at high collector currents. These increases. however. occur at high neutron fluences.

The switching time of a transistor is referred to as the turn-on time and the turn-off time. which consist of the delay time. t_d. the rise time. t_r. the storage time. t_s. and the fall time. t_f. First-order theory indicates that. with the exception of the rise time. these parameters either remain relatively constant or decrease with radiation. Normally. the decreases are larger than the increases in these parameters: thus a net reduction of transistor switching time occurs with radiation. which usually is desirable. The largest changes occur in the storage time. which is proportional to the lifetime. Thus,

$$\varphi = \frac{1}{K\tau_o}$$

is the fluence at which the storage time is reduced by one half.

The general effects of nuclear radiation on field-effect transistors can be summarized as follows:

- Changes occur in the threshold voltage. V_T. These changes in threshold voltage affect most of the field-effect transistor parameters.
- Increases in leakage current occur.
- Changes in channel resistivity and carrier mobility occur.

Damage in MOS field-effect transistors is due primarily to ionizing radiation. For this reason damage is reported in terms of dose (in rads) or exposure (in Roentgens) rather than fluence (in n/cm^2). The most sensitive parameter to radiation in field-effect transistors is the threshold voltage. V_T. In general. degradation in V_T proceeds rapidly in the range of 10^3 and 10^4 rads (Si). but becomes more gradual above this dose. Complete failures. i.e.. complete degradation in transconductance. have been observed at doses of 10^6 to 10^7 rads (Si).

Considerable interest has been shown in the use of junction field-effect transistors (JFETS) in a radiation environment. since these are unipolar devices and do not depend on minority-carrier lifetime for operation. The primary effect of radiation on JFET's is the removal of carriers in the channel region. Radiation induced carrier removal is a strong function of resistivity. Thus. increased radiation tolerances is expected from JFET's with a high initial carrier concentration. The planar process has allowed heavily doped JFET's to be manufactured with the necessary control to make them commercially available. These heavily doped JFET's have demonstrated a very significant improvement in radiation hardness. e.g.. approximately 15 percent degradation in transconductance after a neutron fluence of 7×10^{14} n/cm^2 ($E > 10$ keV. fission).

Thin-film field-effect transistor (TFT) devices have been found to be more radiation

resistant than conventional field-effect transistors. Tests indicate that both the cadmium selenide and the silicon on sapphire type TFT's are operational at 10^6 rads (Si) or 10^{15} n/cm² $(E > 10\ keV,\ fission)$.

█ The negative resistance characteristic of the unijunction transistor depends upon the conductivity modulation of a moderately high resistivity silicon bar by means of injected minority carriers from the rectifying emitter contact. This transistor is highly sensitive to radiation induced changes in minority-carrier lifetime and resistivity. Typical failure thresholds for unijunction transistors are of the order of 5×10^{11} to 5×10^{12} n/cm² $(E > 10\ keV,\ fission)$. The degradation is manifested by an increase in valley voltage, a decrease in valley current, and increases in the interbase and emitter-base resistances.

█ The three basic types of silicon PNPN devices are: the silicon-controlled rectifier, SCR; the silicon-controlled switch, SCS, and the Shockley diode. All of these devices may be considered to consist of overlapping NPN and PNP transistors, the primary difference being the external accessibility of the various layers; that is, the Shockley diode provides external access to only the outer P- and N-layers, the SCR has leads to all but the central N-region, and the SCS has leads to all four regions. The "two transistors" of the PNPN structure operate in a positive-feedback configuration, and the current-transfer ratios of the two sections add together for the composite device.

█ As previously discussed for transistors, radiation induced defects reduce the current gain for both "transistors" so that the required gate current, holding current, and breakover voltage should increase with radiation at fluences comparable to the bulk damage fluence levels in silicon transistors. Theoretical considerations of the mechanisms of PNPN device operation also indicate that excessive leakage currents will cause premature triggering of the devices.

Hence, increases in surface and bulk leakage currents induced by radiation may cause the device to conduct continuously. This effect will depend upon the bias level applied in the application.

█ Since PNPN devices are used in medium- to high-power applications, they cannot be compared to high-frequency transistors in radiation resistance. Typical failure thresholds for PNPN devices range between 10^{12} and 5×10^{14} n/cm² $(E > 10\ keV,\ fission)$. Some narrow base PNPN devices have performed well at 10^{15} n/cm² $(E > 10\ keV,\ fission)$.

9-46 Heating and Thermomechanical Damage █

█ Any electronic component parts in which sufficient energy has been deposited by the electronic system environment will experience a transient rise in its temperature. The performance characteristics of most component parts are sensitive to temperature. Therefore, a temporary perturbation in the response of electronic component parts can be expected. The severity of the perturbation is a function of the deposited energy and the manner in which components are interconnected and mounted. Semiconductor devices are particularly vulnerable to temperature transients.

█ Fortunately, most of the common circuit design techniques for compensation for temperature rises are directly applicable to the circumvention of heating effects caused by the TREE environment. Consequently, heating effects seldom are emphasized, and other effects predominate. However, in some particularly sensitive components such as inertial-guidance devices, heating effects remain a serious problem.

█ The thermomechanical-shock effects arise from the deposition of short pulses of high intensity X-ray energy. The component part response differs from the effects discussed so far in that the primary manifestation is the loss of

mechanical integrity. The processes of spallation, blowoff, and delamination combine to produce mechanical damage. In most cases, this mechanical damage results in a permanent, catastrophic electrical failure of the component parts. All electronic components are potentially vulnerable to thermomechanical shock, but semiconductor devices are among the most vulnerable components. The failure modes for transistors exposed to X-rays depend on the materials and geometries employed in their construction. It is, therefore, worthwhile to consider device fabrication in some detail.

Transistors are composed of a combination of materials, and the relationship of these materials to each is best illustrated in terms of the processes by which these devices are fabricated. Transistors are produced from single crystal semiconducting material, which is processed into regions of desired type and resistivity to form the junctions necessary for transistor action. The many techniques employed to achieve the required junction configurations include growing the desired material from suitably doped melts and alloying-in the dopant impurities from appropriately metallized surfaces. However, the most prevalent technology being used to fabricate silicon transistors is the so-called "planar" process in which the required dopants are allowed to diffuse through area-defining masks formed on the surface of the silicon. These masks are made of silicon dioxide, which (1) is thermally grown on the surface of the silicon, (2) may be etched to form windows for diffusion, and (3) is a natural barrier to the diffusion of phosphorous and boron (the most commonly employed dopants for producing N- and P-type silicon, respectively). The windows in the silicon dioxide are defined by photoetching techniques initially developed and employed in the fabrication of etched wiring boards and subsequently refined in resolution to permit application in the fabrication of semiconductor devices.

Figure 9-57 shows the steps employed in the fabrication of a typical transistor by the planar process. The oxide layer grown in Step (a) is removed in a selected area by photoetching (Step b), and a P-type dopant is allowed to diffuse into the starting N-type silicon to form what will be the base region of the transistor (Step c). A new oxide is grown next (Step d) and is photoetched to form a window over a smaller area, and an N-type dopant in high concentration is allowed to diffuse into this portion of the P-type region (Step e), converting it to (N^+)-type silicon. This forms the emitter region of the transistor. Depth of penetration of the dopant materials is controlled by the times and temperatures at which the diffusion operations are conducted. A final oxide growth (Step f) and selective photoetching (Step g) expose the emitter and base contact points. The whole surface is subsequently coated with aluminum (Step h) and selectively etched to produce the desired current paths and land areas (tabs) for connection (Step i).

Since transistors fabricated in the above manner usually are prepared in multiple arrays containing hundreds of identical devices, the next steps are the separation of the individual devices by some technique such as diamond scribing and the mounting of each of the resultant chips (or dice) into a separate package. Typical chips for high-frequency transistors are less than 0.025 x 0.025 in. in area.

The transistor package can take many forms (see Figure 9-58a), but in each form there is usually a section of the package that contains the lead wires to which the emitter, base, and collector portions of the device must be connected. This section is called the header. In a typical package this is the bottom section of the can, which contains the three lead wires. A cap is attached to complete the package. The header usually is made of Kovar, a nickel-iron alloy frequently used for glass-to-metal seals because of their comparable thermal-expansion coefficients.
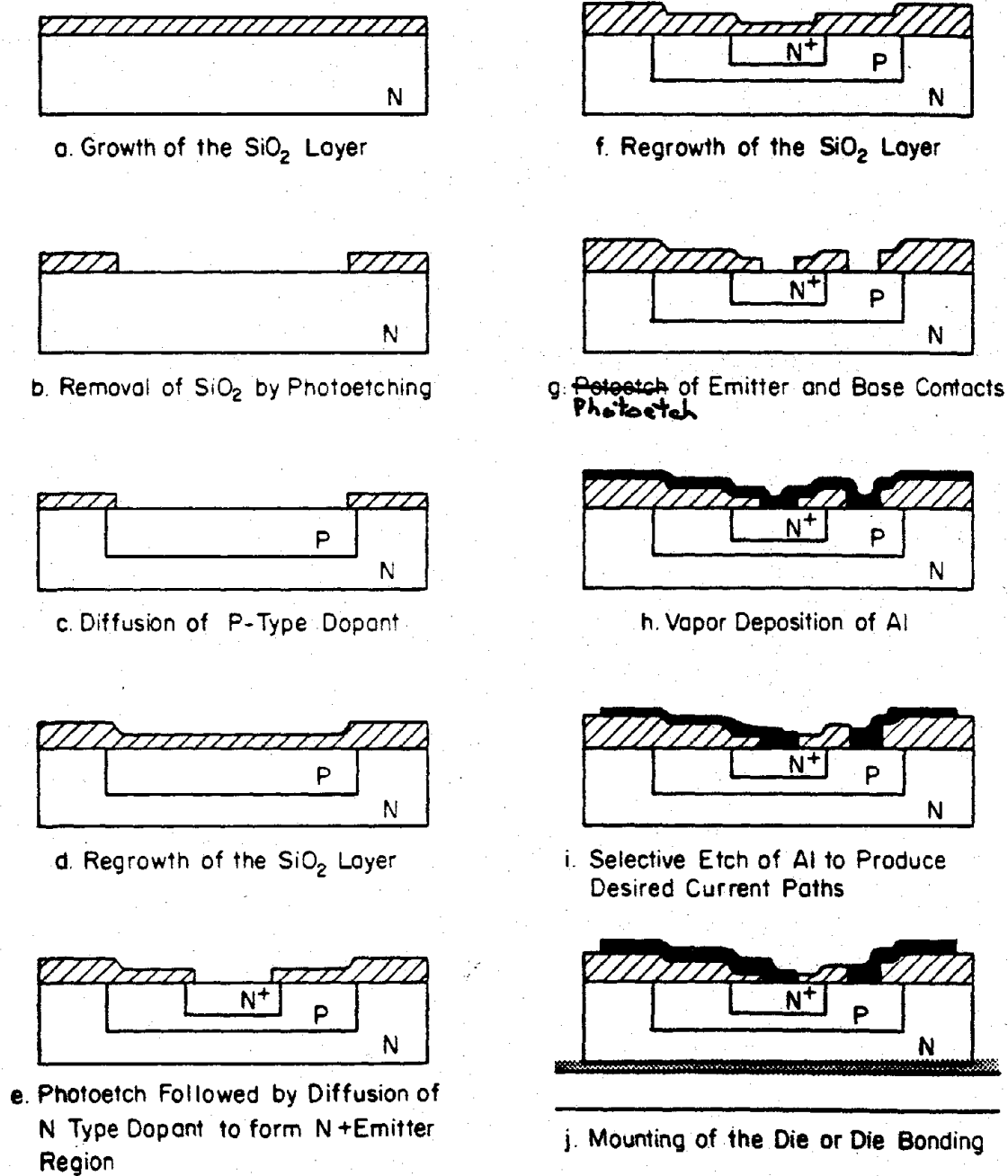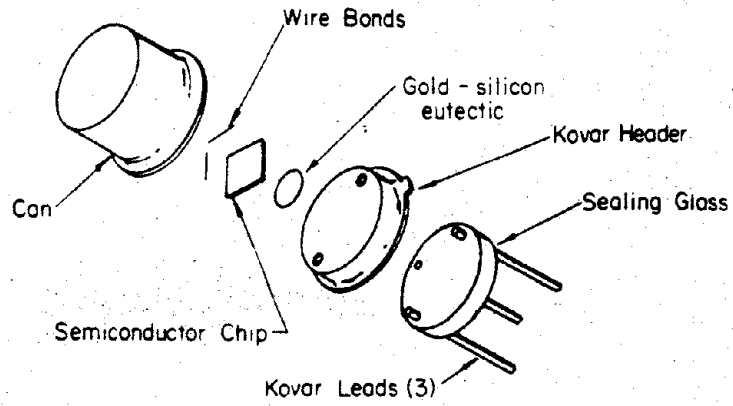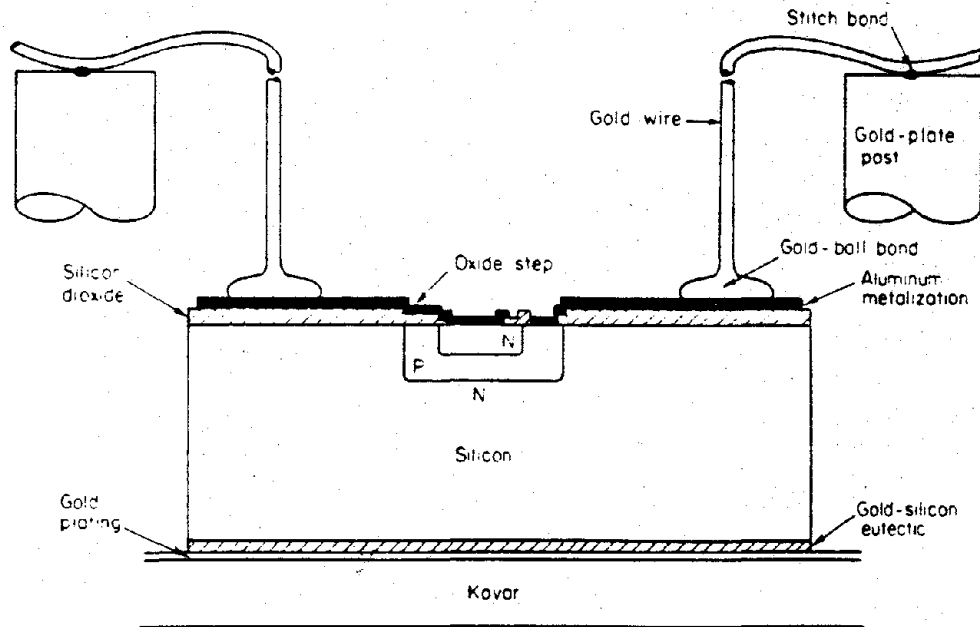
a. Growth of the SiO_2 Layer

b. Removal of SiO_2 by Photoetching

c. Diffusion of P-Type Dopant

d. Regrowth of the SiO_2 Layer

e. Photoetch Followed by Diffusion of N Type Dopant to form N +Emitter Region

f. Regrowth of the SiO_2 Layer

g. Potetch of Emitter and Base Contacts
Photoetch

h. Vapor Deposition of Al

i. Selective Etch of Al to Produce Desired Current Paths

j. Mounting of the Die or Die Bonding

Figure 9-57. ■ Steps in the Fabrication of an NPN Silicon Planar Transistor ■

Wire Bonds

Gold - silicon
eutectic

Kovar Header

Sealing Glass

Can

Semiconductor Chip

Kovar Leads (3)

a) Transistor Package

Stitch bond

Gold wire

Gold-plate
post

Silicon
dioxide

Oxide step

Gold - ball bond

Aluminum
metalization

N

P

N

Silicon

Gold
plating

Gold - silicon
eutectic

Kovar

b) Cross-Sectional View of NPN Silicon Planar
Transistor

Figure 9-58.   Transistor Cross Section and Package

The three Kovar leadout wires are electrically insulated from each other by glass feed-throughs in the Kovar header. Since Kovar oxidizes easily, the external leads, and often the internal leads, on the transistor usually are plated to facilitate subsequent soldering or welding.

The processed semiconductor chip is attached to the header by a fabrication step known as die bonding. Die bonding involves soldering, brazing, or glazing the die to the header. This attachment serves as a mechanical contact. a thermal path, and in some cases (such as the example being employed) an electrical contact. When the connection is to a metal portion of the header, the attachment usually is accomplished by brazing using a eutectic brazing alloy (generally containing gold). This is superior to a soft solder because the high melting point of the eutectic permits use of higher temperatures in sealing the top on the header and in preconditioning the devices if desired. Some disadvantages in the use of eutectic alloys for die bonding are that they generally are expensive, quite brittle. difficult to form into unusual shapes, and they cannot be vacuum evaporated to form thin films. A preform of the eutectic alloy is placed on the header on a platform directly connected to the collector leadout wire. In many applications, a simple gold plating on the Kovar platform suffices as the preform, since on heating in contact with the silicon chip, a gold-silicon eutectic will form. Heat is applied (390°-400°C), the transistor chip is placed on the preform, and the eutectic is chilled with a jet of nitrogen. This operation attaches the chip to header and forms the chip-to-header bond (Step j, Figure 9-57).

Wire bonding makes electrical contact to the emitter and base regions. In some devices this connection is made by attaching the bridging wires directly to suitably metallized etched-open areas on the silicon chip. In many devices, however, these areas are much too small to per-

mit forming quality connections, so the connections are made to extended tabs formed in the aluminum metallization on top of the silicon oxide. This latter configuration is illustrated in Figure 9-58b. The bridging wires, 1/2 to 3 mils in diameter, may be composed of any of a number of materials, but generally they are either gold or aluminum. Gold is used because it forms ohmic contact when alloyed with silicon, is available as extremely fine wire with reasonable strength, and may be bonded by thermocompression. Aluminum wire is used because it provides a one metal system when aluminum metallization is employed for extended tabs and avoids the formation of gold/aluminum alloys ("purple" and "white" plagues). it is available as fine wire, and it makes ohmic contact to both P-type and (N^+)-type silicon.

In thermocompression bonding, the two metals (such as the wire and the bonding pad) are made to seize without a third intermediate phase (such as solder) and without melting. This is accomplished with high pressures and temperatures. The high temperature keeps the metals in the annealing range as they flow into atomic intimacy under the bond. One form of thermocompression bonding (called ball bonding or nail-head bonding) employs gold wire that is heated at the tip with a hydrogen flame to form a ball, which is subsequently driven against the heated chip under pressure to form the bond and concurrently is flattened into a nailhead configuration. In stitch bonding (another form of thermocompression bonding), the wire is bent under pressure from the tool head and forced into the heated pad in such a way that the wire is wedged flat at the point of contact. Either gold or aluminum may be employed in stitch bonding. In ultrasonic bonding, ultrasonic energy is employed to force the two metals into atomic intimacy. The resultant bond resembles a stitch bond. These three bonding techniques are illustrated in Figures 9-59a, b, and c, respectively.
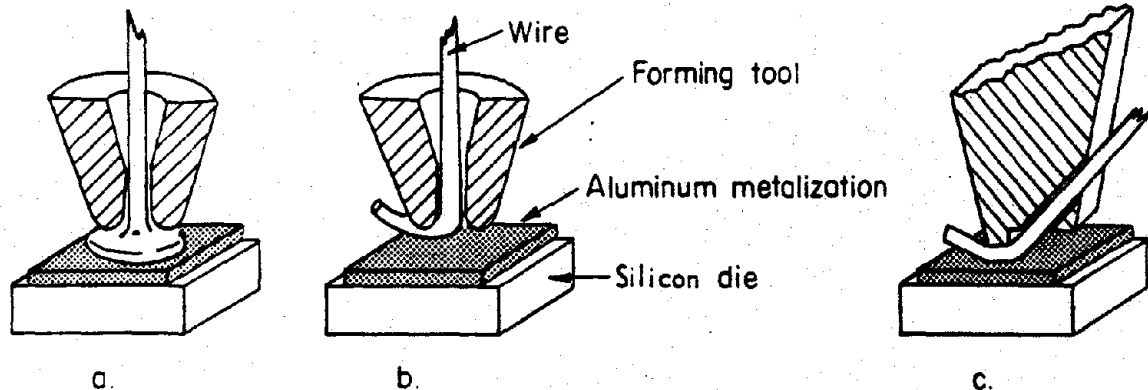
Figure 9-59. ███ Ball Stitch and Ultrasonic Bonding ███

DNA
(1)(3)

DNA
(1-)(3)

Several general modes of failure (see Figure 9-60) are apparent: (a) the wires may break: (b) the emitter or base bonds may separate from the chip: (c) the silicon chip might fracture: (d) the chip may separate from the header: (e) the aluminum metallization constituting the extended tabs might become discontinuous: and (f) the wire bonds at the post may separate.
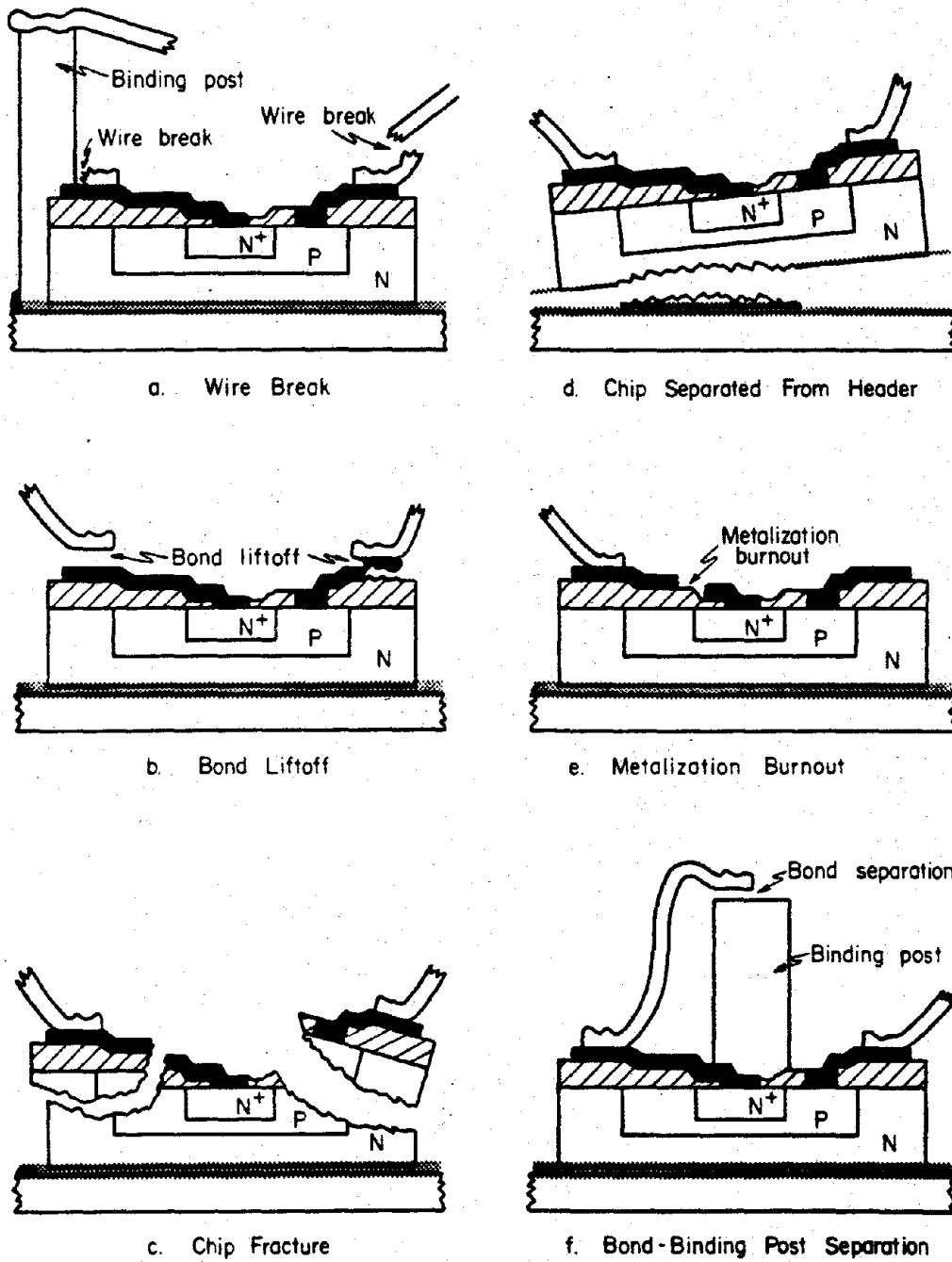
a. Wire Break

d. Chip Separated From Header

b. Bond Liftoff

e. Metalization Burnout

c. Chip Fracture

f. Bond-Binding Post Separation

Figure 9-60. Semiconductor Failure Modes

OTHER ELECTRONIC COMPONENT PARTS

9-47 Electron Tubes

The electron tubes discussed in this subsection are divided into three categories: vacuum tubes, gas-filled tubes, and phototubes. These categories include nearly all types of conventional electron tubes with the exception of microwave tubes. Because of the known differences in interaction of nuclear radiation with metals, gases, and photoemissive materials, as well as with glasses and other ceramics, the observable effects of these interactions might be expected to differ for each category of tube.

Permanent damage to vacuum tubes is associated with thermal and fast neutron exposure. No significant permanent damage has been observed in conventional vacuum tubes or Nuvistors exposed to test radiation pulses or to a thermal neutron fluence of less than 10^{13} n/cm^2 (fission). Moderate damage may occur in standard size glass or metal tubes at thermal neutron fluences from 10^{13} to 10^{16} n/cm^2 (fission), and severe damage may occur at fluences greater than 10^{16} n/cm^2 (fission). "Severe damage" is often the failure of the glass envelope, usually at a glass-to-metal seal; "moderate damage" is generally a permanent change in tube operating characteristics. Miniature, subminiature, and ceramic-type tubes are less subject to both moderate and permanent damage than standard size tubes, largely because of the smaller area and mass of the tube parts. However, thermal-neutron fluences sufficient to cause permanent damage to high-vacuum tubes are greater than neutron fluences expected to be encountered in the nuclear weapon environment. e.g., $>10^{16}$ n/cm^2 (fission).

The principal transient effect that results from exposure of vacuum tubes, including the Nuvistor, to nuclear radiation is produced by Compton scattering of electrons from structural members by gamma rays. Leakage currents caused by ionization of air between external electrodes, or reduction of resistance of insulating materials such as glass, ceramics, and mica, caused by electron excitation within the material, may have minor effects on tube performance. There is no appreciable radiation induced liberation of gas from tube parts, or ionization of residual gases within the tube.

Most of the Compton electrons produced in the structural parts of the tube and ejected into the evacuated region are too energetic to be influenced significantly by the electronic fields in the tube. However, the impact of

high energy electrons on the interior surfaces of the tube assembly produces low energy secondary electrons that can be influenced by the existing electric fields, and thus can alter the normal operating characteristics of the tube. The ejected electrons can be collected by one or more electrodes, depending upon the electrode potential and position. The magnitudes of the resulting transient voltages that appear at the respective electrodes depend on the magnitudes of the transient current and the circuit resistance. The grid circuit is particularly affected by this phenomenon, since it usually suffers a net loss of electrons and therefore may assume a positive charge. The resulting increase in plate current is determined largely by the grid resistance and the gain of the tube.

Gas filled tubes (thyratrons), under extensive neutron bombardment, most likely will fail by breaking of the glass envelope or glass-to-metal seals. Such damage occurs at thermal neutron fluences exceeding 10^{16} n/cm^2 (fission).

The principal transient effect in a thyratron subjected to a nuclear radiation pulse is spurious firing caused by ionization of the filling gas. The filling gas, in these cases xenon, becomes partially ionized, primarily by gamma rays. Additional ions are created by ion-neutral molecule collisions in the electric field between the plate and the grid. A positive ion sheath can form around the negatively-biased control grid, which will neutralize the grid charge and will permit electrons to be accelerated from the cathode space charge toward the plate. As ion density increases, a sustaining discharge ensues, which can be shut off only by removing the plate voltage.

Phototubes are designed to exhibit peak sensitivities to electromagnetic radiation in the visible and near-infrared regions by choosing photosensitive cathodes with low work functions. The presence of photosensitive material in a vacuum tube introduces effects other than those found in receiving type electron tubes in a radiation field.

Severe permanent damage to phototubes, as with other vacuum tubes, is attributable to large thermal neutron fluences. Severe damage starts in phototubes at about 10^{15} n/cm^2 (fission). However, moderate permanent damage may occur at thermal neutron fluences two orders of magnitude lower. Moderate damage in some cases is an increase in dark current, or a decrease in anode luminous sensitivity, but in most cases it is a darkening of the glass envelope. This darkening effectively reduces tube sensitivity. The glass discoloration has been observed at fast neutron fluences of 5.5 x 10^{12} ($E > 10$ keV, fission), and gamma ray doses of 6.3 x 10^6 rads (C). Thus, both gamma and neutron components of mixed radiation contribute to permanent damage.

The principal transient effect in photomultiplier exposed to pulsed X-ray radiation (and presumably to gamma radiation) is an increase in anode current. The increase can be as much as the space-charge-limiting value for a given tube. Furthermore, the duration of the current increase is much greater than that of the radiation pulse. At first, the current increases as a result of currents initiated by luminescence of those areas of the glass envelope that are optically coupled to the cathode of the photomultiplier. This current increase also has been demonstrated in steady-state gamma fields. Glass luminesces at wavelengths and intensities determined by the glass composition and by the dose rate. Since a great deal of the radiant energy is in the visible portion of the light spectrum, where common photomultipliers are sensitive, it would be expected that the degree of photomultiplier response to X-ray and gamma radiation would depend upon both the type of glass used for the envelope and the spectral sensitivity of the cathode material.

A second mechanism is required to explain the relatively slow decay of anode current after the radiation field is removed, since glass luminescence decays rapidly. It is believed that decay of anode current may be retarded by electric-field changes in the tube when electrical insulators become charged as a result of large initial current pulses.

DNA
(/)(1)

9-48 Capacitors

Nuclear radiation affects most of the electronic properties of capacitors to some extent. Changes in the capacitance value, dissipation factor, and leakage resistance have been observed during steady-state reactor experiments. These effects generally are not considered severe for fast neutron fluences less than 10^{15} n/cm^2 ($E > 10$ keV, fission), and for most capacitors this limit is about 10^{17} n/cm^2 ($E > 10$ keV, fission).

During a high-intensity pulse of nuclear radiation, the most pronounced effect in a capacitor is a transient change in the conductivity of the dielectric material with a corresponding increase in the leakage currents through the capacitor. The most recent concept of ionization effects in insulating and dielectric materials indicates that the ionizing particles create ionizing tracks in the irradiated material. This means that, microscopically, the material is not uniformly ionized (an exception to this occurs at very high dose rates, $\approx 10^{12}$ rads (Si)/sec, where there should be sufficient overlap of the ionized tracks for the material to be considered uniformly ionized).

The excess conductivity induced in a material irradiated with a short pulse of ionizing radiation is generally classified in two components: the prompt component, and the delayed component. The prompt component is primarily the result of excess carrier concentration from direct ionization by the radiation and the concurrent recombination and trapping of these carriers. The delayed component is that component of conductivity that remains after the termination of the ionizing pulse. This does not mean to imply that it does not make a small contribution during the radiation pulse. The delayed component is the result of thermal generation of excess carriers from shallow traps, in which they are caught during the prompt pulse, and their concurrent loss to recombination and retrapping. The rate at which these carriers are thermally regenerated depends on the energy level of the trap site, the concentration of filled traps, and the temperature. As there is usually more than one energy level trap in a material, more than one regeneration rate usually is observed in the delayed component.

The excess conductivity is proportional to the number of carriers available to drift under the influence of the applied electric field. However, the microscopic nonuniformity of the carrier concentration must be considered for the pulsed irradiation case. For irradiation with ionizing particles with a low specific ionization (the ratio of the number of ion pairs produced per unit path length to the number produced per unit path length by a minimum ionizing particle), the excess prompt conductivity will be the same as if these carriers were generated uniformly throughout the material. However, if the specific ionization is increased (by bombardment with more heavily ionizing particles), a point will be approached where the separation of ionization sites is less than the distance traveled by the electron before it has become thermalized and is able to drift under the influence of

the applied electric field. As this point is approached, the probability that the electron will be captured in the field of a neighboring ion increases, and the contribution to excess conductivity will be reduced. Thus, a plot of prompt conductivity as a function of specific ionization would show the prompt conductivity constant at low specific ionization and decreasing slowly after some threshold values of specific ionization is reached.

The rate at which carriers are lost concurrent with their generation by the ionizing radiation is proportional to the concentration of recombination centers and unfilled trapping centers. While an insignificant number of the total traps in the material might be filled at low doses, the concentration of filled traps within a track depends only on the specific ionization. Thus, the trapping rate is affected by the specific ionization. The result of this effect is to cause an increase in prompt conductivity with specific ionization, which would serve in part to compensate for the decreasing effect mentioned above. However, this effect on the carrier loss rate should be slight, since most of the carriers are lost to recombination rather than trapping.

When the radiation is delivered in a time short compared with the regeneration time of carriers from the traps, and the dose delivered in the pulse is large enough that significant numbers of tracks near the end of the pulse overlap tracks generated earlier, the concentration of filled traps in a track late in the pulse is different from that in a track created earlier in the pulse. When this occurs, the observed prompt conductivity becomes a function of the total dose delivered in the pulse, as well as of the specific ionization of the irradiating particle. It should be noted that a sufficient fraction of traps in a track must be filled to significantly affect the response. Hence, it is quite possible that trap densities in many insulators are high enough so that this condition is not realized in most pulse experiments.

The delayed conductivity component depends on the rates of carrier regeneration and retrapping from trap sites, which depend on the concentration of filled traps and the energy levels of the traps. The concentration of filled traps is a function of the specific ionization of the irradiating particle and, in the case of overlapping tracks, the total dose. As the initial concentration of filled traps within a track is usually a significant fraction of the total concentration of traps, the retrapping probability changes during the time the traps are emptying, thus altering the characteristic time for emptying the remainder of the filled traps. As a result, the decay of the delayed component does not usually follow a simple law. Only in certain cases, where the trapping probability is negligibly perturbed by the radiation, will simple exponential decays be observed.

Neutrons produce ionization by a number of collision processes that give rise to ionizing secondary particles. These processes include:

- Elastic scattering when the recoil atom receives sufficient energy to produce ionization.
- Inelastic scattering, producing a recoil atom that may or may not ionize but that emits a gamma photon that can produce a secondary ionization.
- Capture, resulting in the emission of a photon and/or an ionizing secondary particle (primarily thermal neutrons).
- Reactions resulting in an ionizing particle, e.g., (n,p), or (n,α) reactions (high-energy neutrons).

There are, therefore, many possible different specific ionizations associated with ionized tracks in neutron bombarded materials.

In hydrogenous materials, the principal ionization is caused by recoil protons, which have a high specific ionization. For this reason, neutron induced conductivity in hydrogenous dielectrics has been found to be approximately

one-fifth to one-half that of gamma ray induced conductivity for equal ionization energy deposition rates. For nonhydrogenous dielectrics, the most important contribution to neutron induced ionization is by the interactions of very high-energy neutrons ($E > 2$ MeV).

A "polarization effect" that is attributed to space charge buildup within the dielectric material due to nonuniform trapping has been observed with some capacitors, particularly with Mylar, mica, polycarbonate, tantalum oxide and Vitamin Q devices. This effect is manifested in several ways. One is an apparent decrease in the induced conductance with sequential radiation pulsing. Charge transfer across the dielectric during a radiation pulse builds up a space charge field opposing the applied electric field. If the applied electric field is then removed, subsequent radiation pulses result in a current in the external circuit opposite in direction to that observed with the field applied. This is caused by the discharge of the space charge field. Similarly, if the electric field is reversed rather than removed after the space charge has been built up, the space charge field enhances the applied field, and a larger current results than would be observed normally.

Saturation of the polarization effect, where no further decrease in the charge transfer is observed with subsequent radiation pulses, occurs after one or more pulses, depending on the capacitor and on the dose delivered in each pulse. Decreases of 50 to 70 percent for mica, 10 to 20 percent for tantalum oxide, and 30 percent for Mylar have been observed due to this space charge buildup during radiation pulsing.

9-49 Resistors

Radiation effects in resistors are generally small compared with effects in semiconductors and capacitors and are usually neglected. However, in circuits requiring high precision resistors transient effects may be significant at dose rates of as low as 10^7 rads (C)/sec and at neutron fluences of 10^{14} n/cm^2 ($E > 10$ keV, fission).

The transient effects are generally attributed to gamma rays that interact with materials to produce electrons, primarily by the Compton process; however, energetic neutrons can also produce significant ionization. Transient effects include (1) a change in the effective resistance due to radiation induced leakage in the insulating material and the surrounding medium, (2) induced current that is the result of the difference between the emission and absorption of secondary electrons by the resistor materials, and (3) change in the conductivity in the bulk material of the resistor. There is no substantial evidence, however, that the third effect is a first-order transient effect.

The permanent effects are generally caused by the displacement of atoms by neutrons, causing a change in the resistivity of the material.

9-50 Batteries and Cables

Batteries are affected much less by radiation than other component parts. The effects of radiation on nickel-cadmium batteries appear to be insignificant at dose rates up to 10^7 rads (air)/sec. No radiation damage was apparent in a number of batteries and standard cells that were subjected to 10^{13} n/cm^2 ($E > 10$ keV, fission). Transient radiation effects on an ammonia fuze indicated that pulsed gamma ray irradiation of 10^8 rads (air)/sec had no effect on the operation of the battery.

It has been recognized for some time that intense pulses of radiation produce significant perturbations in electrical cables and wiring, including coaxial and triaxial signal cables. Even with no voltage applied to a cable, a signal is seen when the cable is exposed to a pulsed radiation environment. The current associated with this signal is defined as a replacement current, since it is most likely a current in an external circuit that is necessary to replace electrons or other charged particles that are knocked out of their usual positions by the radiation. The replacement current definition also applies to the effect of charged carriers associated with the incident radiation embedded in a test sample.

The magnitude of the radiation induced signal varies with the voltage applied to the cable. This voltage-dependent portion of the signal, i.e., the total signal exclusive of the replacement current, is called conduction current, thus it is ascribed to the conductivity induced in the insulating dielectric by the radiation. However, it may also contain major contributions from polarization or depolarization processes in the dielectric. These can usually be identified by their gradual disappearance (saturation) after repetitive exposures and by their reappearance in additional "shots" in which the applied voltage is changed greatly, e.g., removed or reversed.

Ionizing radiation of any type produces free electrons that contribute to the conductivity of the material. Hence, insulators are expected to have a transient enhanced conductivity in an ionizing radiation environment. Conduction in the insulator is frequently characterized by two components: for very short radiation pulses, a prompt component whose magnitude is a function of only the instantaneous exposure rate, and frequently at the end of the short radiation exposure, a delayed component having approximately exponential decay.

Although the replacement, conduction, and polarization currents are fairly well understood in terms of the interactions between the ionizing radiation and the metal-dielectric target system, it is not yet possible to predict quantitatively the response for a given cable in a specified environment. In a mixed neutron-gamma environment, the induced replacement current usually contains positive and negative components, and may therefore assume either polarity. The conduction current sometimes exhibits a rather complicated time dependence consisting of prompt- and delayed-conductivity contributions. The polarization current appears to be greatly affected by the properties of the metal-dielectric interface.

Permanent damage effects in cables and wiring are manifested as changes in the physical and electrical properties of the insulating materials. When such damage becomes appreciable, e.g., when the insulation resistance is reduced severely, electrical characteristics may be affected. The extent of the damage to insulating materials is an increasing function of neutron fluence, exposure or dose, humidity, and irradiation temperature. Certain types of wire insulation are quite susceptible to permanent damage. For example, silicon rubber becomes severely cracked and powdered after approximately 2×10^{15} n/cm^2 ($E > 10$ keV, fission). The approximate damage thresholds for three common types of cable insulation are: polyethylene, 1×10^7 rads (C); Teflon TFE, 1×10^4 rads (C); and Teflon FEP, 2×10^6 rads (C). On the other hand, some irradiated polyolefins are capable of withstanding up to 5×10^9 rads (C). A considerable degree of annealing has been observed with respect to insulation resistance, which implies the possibility of adequate electrical serviceability after moderate physical damage.

It is not expected that radiation effects on wiring with thin insulation will exhibit the strange behavior observed in coaxial cables. In particular, the very limited measurements that have been performed indicate that the replace-

ment current is primarily a function of the gamma environment. To a good approximation, it can be assumed that the replacement current for a wire or most other objects placed in the radiation environment will amount to the emission of a number of electrons between 1 and 5 x 10^{-3} times the number of gamma photons traversing the object.

█████ The conduction current is a very sensitive function of the amount of insulation around the wire and its immediate environment. For a bare wire in air with a ground plane nearby, conduction is due predominantly to the ionization produced in the air. Placing insulation around the wire reduces this conduction, but at the price of increasing the area of the wire and hence the effective replacement current.

9-51 Quartz Crystals █████

█████ The radiation response of a quartz crystal oscillator is primarily a function of radiation dose. The type of material from which the oscillator is fabricated, e.g., natural quartz, Z-growth synthetic, Z-growth swept synthetic, etc., and to a lesser extent the type of cut, e.g., AT, BT, etc., and the frequency and mode of operation determine the sensitivity of the oscillator to the radiation. The primary effect of the radiation is a shift in the frequency of the oscillator. Both transient and steady-state shifts have been observed.

█████ The steady-state frequency offsets are a result of changes in the elastic stiffness constants of the crystal. For example, perturbations in the crystal bonds due to charge trapping at defects or to formation of new defect complexes will result in steady-state frequency offsets. Of materials tested to date, Z-growth swept-synthetic quartz has been the most radiation tolerant to steady-state frequency offsets. Swept natural quartz is slightly more sensitive and unswept natural quartz and unswept synthetic quartz, respectively, are even more sensitive. The

response of a particular crystal also varies with the manner in which the crystal is mounted, the material used for the electrodes, and to a lesser extent differs for each quartz bar grown, even among bars grown under similar conditions. Both swept synthetic and natural quartz crystals can recover 80 percent to 90 percent of their original frequency change after annealing at 500°C for times on the order of 100 to 160 hours.

█████ Transient shifts in the frequency of an oscillator and reduction or cessation of the output result from energy deposition and any subsequent temperature rise in the crystal. Temperature gradients in the crystal due to faster removal of heat near the support wires and due to the electrodes absorbing more energy than the crystal, can give rise to frequency shifts induced by the resulting strain.

█████ Irradiation of general purpose crystal units has shown that they do not suffer significant permanent effects, within the limits of their stability, at a neutron fluence of 10^{13} n/cm^2 ($E > 10$ keV, fission) and a gamma dose of 4.4 x 10^3 rads (air). Transient phase and amplitude changes resulting from this environment are not of sufficient magnitude to cause concern about their operation under such conditions.

█████ Moderate precision crystal units display negligible frequency and amplitude changes when subjected to a reactor pulse. Weapon tests as well as steady-state gamma source tests indicate that a gamma dose greater than 10^4 rads (air) is required to induce significant permanent frequency changes in these devices. Frequency changes up to almost one part in 10^5 were observed after exposure to 7.5 x 10^4 rads (air) and 10^{12} n/cm^2 at a weapon test. The possibility that causes other than radiation contributed to the changes observed at this test cannot be excluded.

█████ High precision natural quartz-crystal units either stop oscillating or exhibit appreci-

able decreases in the amplitude of the output signal during nuclear pulses of approximately 10^{12} n/cm^2 ($E > 3$ MeV, fission), and 3×10^3 rads (H$_2$O). If oscillation stops, its cessation persists for minutes. The cessation of oscillation is apparently independent of the voltage, current, or power at which the units are being driven. Resumption of oscillation occurs at a reduced drive current and lower frequency. The drive current is tens of microamperes below the specified rated drive when oscillation resumes. Frequency changes as high as 1 part in 10^7 have been observed when this type of crystal was exposed to 7.9×10^{11} n/cm^2 ($E > 3$ MeV, fission), and 2.9×10^3 rads (H$_2$O).

9-52 Solder Joints

9-53 Infrared Detectors

The infrared detectors that exhibit the greatest sensitivity to infrared radiation are also the most sensitive to nuclear radiation. For radiation pulses that are short compared to the

relaxation time, the response of a photoconductive type of infrared detector cell is an excess conductance that is proportional to the radiation exposure. For long pulses the excess conductance is proportional to the radiation intensity and the carrier recombination time. Neutron bombardment causes permanent degradation of output-signal level and signal-to-noise ratio.

Irradiation of a lead sulfide device to 1.3×10^{14} n/cm^2 ($E > 0.48$ eV, fission) at 134°F revealed a 67 percent reduction of output signal level and greater than 40 percent reduction in the signal-to-noise ratio. Damage was essentially catastrophic after 6.9×10^{15} n/cm^2 ($E > 0.48$ eV, fission).

Lead selenide devices appear to be somewhat more tolerant to neutron irradiation than lead sulfide detectors. After a neutron fluence of 1.2×10^{14} n/cm^2 ($E > 0.48$ eV, fission) at 135°F, the output signal level of a lead selenide cell was reduced by 36 percent, and the signal-to-noise ratio was down more than 46 percent. The output level was down by 96 percent after 1.8×10^{16} n/cm^2 ($E > 0.48$ eV, fission). Lead selenide cells that are designed to operate at low temperatures are more sensitive to radiation than those that are not designed for low temperatures.

Indium antimode photovoltaic cells that operate at liquid nitrogen temperature showed significant voltage signals at doses less than 0.88 rads (air). The cells exhibited radiation induced voltages roughly proportional to the logarithm of the dose when the radiation was delivered in short pulses. Recovery to within 2 percent of the maximum voltage occurred within 175 μsec after the highest intensity radiation pulses. A complete loss of output from these cells has been observed after a neutron fluence of 2×10^{16} n/cm^2 ($E > 0.48$ eV, fission).

Thermistor-bolometer infrared detectors are the most neutron tolerant of the devices that have been tested. After 9.6×10^{13} n/cm^2 ($E >$

0.48 eV, fission), the output signal level was down by 28 percent, and the signal-to-noise ratio was down about 11 percent. After 1.6 x 10^{16} n/cm^2 ($E > 0.48$ eV, fission), the output level was down 57 percent, and the signal-to-noise ratio was down 66 percent. The detector may be usable for some applications under these conditions.

Thermomechanical shock effects in infrared detectors will be similar to those discussed for semiconductor devices, and will occur at about the same levels.

ELECTRONIC CIRCUITS

9-54 Radiation Response of Discrete-Component-Part Circuits

Determination of the response of a circuit is complex because of the large variations in circuit configuration and in the component parts that can be used within a circuit configuration. Therefore, determining circuit response becomes a problem of detailed circuit analysis and/or testing. The radiation effects material necessary for this kind of analysis and testing are beyond the scope of this manual. Guidance may be obtained from the *TREE Handbook* and the *TREE Preferred Procedures* (see bibliography). General circuit effects and typical analysis techniques are discussed in this manual.

The transient effects that can cause a system to malfunction can result in circuit responses that, like component-part responses, can be both dose and dose rate dependent. If the radiation pulses are short with respect to component-part recovery times the circuit time constants, the circuits will integrate the effects and will be sensitive to the total dose rather than the dose rate. However, when the pulse widths are wide, the circuits are dose rate sensitive. This can be illustrated by reference to Figure 9-61. Assume that for the circuit response plotted, the malfunction threshold is 1.5 volts. Therefore, a

0.15 μs pulse at 1 x 10^9 rad (Si)/sec will cause a malfunction. It is obvious from the curve that the malfunction dose rate is much lower for wider pulses.

Discrete digital circuits and circuits that contain silicon controlled rectifiers (SCR's) have displayed failure at doses as low as 0.1 to 1.0 rad (Si) for short pulse widths. It is difficult to design a circuit specially that will not malfunction above a prompt dose of 100 rads (Si).

Another effect that can result from the ionizing radiation is the initiation of a catastrophic action or catastrophic failure. An example would be the firing of a pyrotechnic device or the premature initiation of a firing signal. A second type of catastrophic action occurs if a circuit destroys itself as a result of the effects caused by ionization (burnout). Figure 9-62 shows an output stage of a power supply inverter. In normal operation, Q1 and Q2 are turned on alternately. The output at the transformer secondary is a square wave. Ionizing radiation may cause Q1 and Q2 to turn on simultaneously. After the radiation pulse, the transistors will recover to normal operation, and one of the transistors will attempt to turn off. At this time a large voltage will be induced across the transistor that is attempting to turn off. If this voltage exceeds the breakdown voltage, the transistor may be damaged.

General statements applicable to both permanent and transient effects include:

- Circuits that use low frequency, thick base semiconductors usually are more susceptible to radiation effects than those circuits that contain high frequency, thin base devices
- Germanium devices generally will show larger photocurrents and leakage currents than comparable silicon devices
- High impedance circuitry generally will be more susceptible to radiation effects than low impedance circuitry
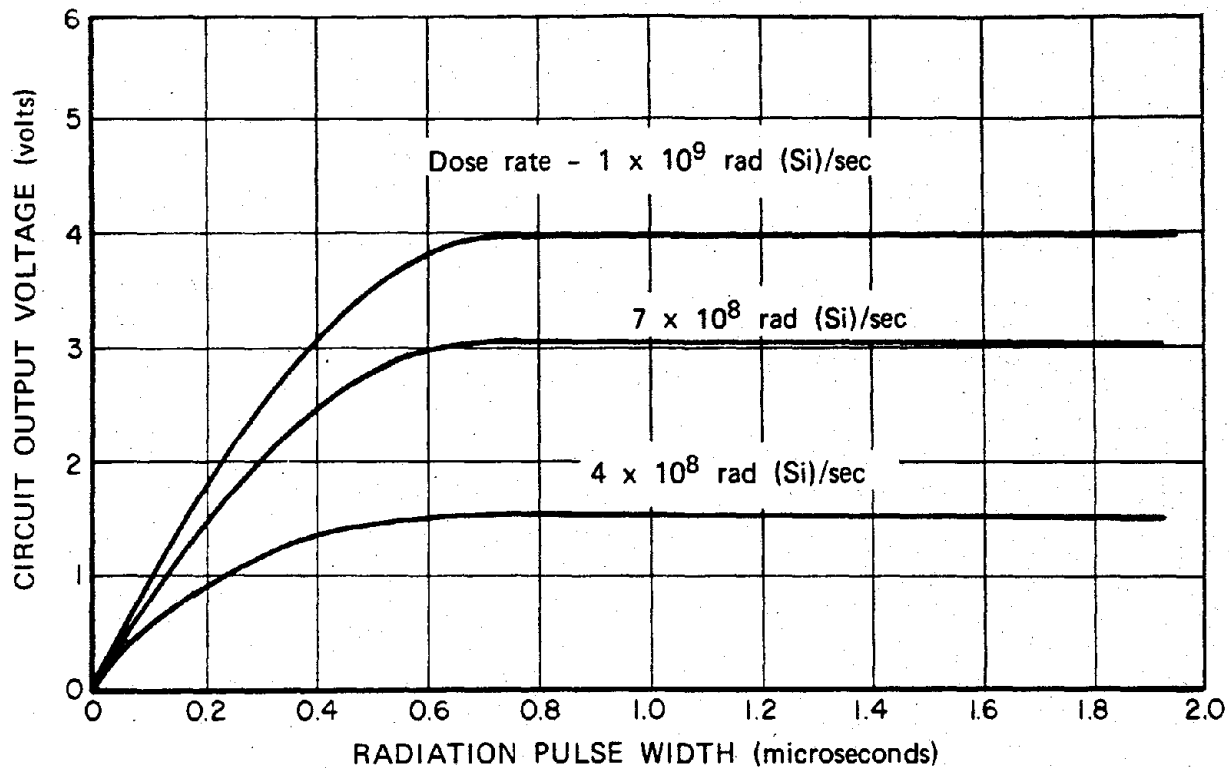
Figure 9-61. ▮ Circuit Response as a Function of Radiation-Pulse Width ▮

- Magnetic memory devices will not be sensitive to the neutron and gamma environments typically specified as the environment in which an electronic system must survive.

▮ The primary permanent effects on circuits will be the degradation of semiconductor devices. The solid-state power supplies and regulators with their low frequency transistors will fail to perform their required function when exposed to fluence between 10^{11} and 10^{13} n/cm^2 ($E > 10$ keV, fission) depending on the circuit configuration, component parts, and design margins in the system. Circuits that use MOSFET can fail at gamma doses between 10^3 and 10^5 rads (Si).

▮ The failure threshold for thermo-mechanical shock will be established by the threshold of the component parts.

▮ It is desirable to have a method of analysis that can be used to predict the response of components, circuits, and systems. The analysis methods that are used consist of established techniques to calculate circuit and system responses by replacing radiation effects by their corresponding electrical effects. Thus, the problem that is solved eventually is wholly electrical in character. A major advantage of analysis as a simulation tool is that it is not necessary for a circuit or system to exist in a physical state before it can be analyzed. In addition, the analyst has control over the "environment," and it is theoretically possible to simulate the total
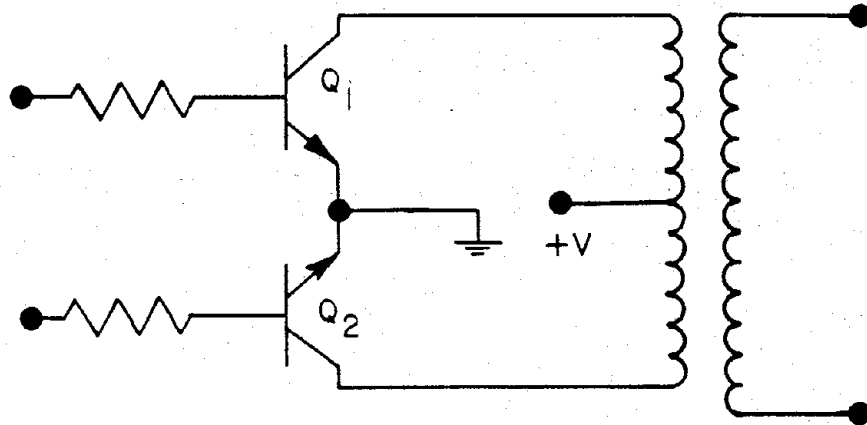
Figure 9-62. ██ Circuit in Which Burnout Could Occur ██

environment during a single (but complicated) analysis. Perhaps the major disadvantage of analysis (for TREE) is the relatively low confidence in the results. This low confidence level usually arises from the simplifying assumptions that are often made to expedite the analysis and which, themselves, are subject to verification. typically by environmental testing.

██ Certain requirements or inputs are needed for any circuit or system analysis. First, an accurate mathematical description of the electrical characteristics must be obtained. Such a description usually is checked by comparing the computed electrical response to the measured electrical response of a circuit or system. Second, the radiation effects on electronic materials and devices must be represented, or modeled, by electrical effects. For example, displacement effects may be modeled by making transistor current gain a function of time. This step generally requires environmental testing and/or sound analytical procedures to obtain the required radiation effects data. Third, an analysis method must be employed to make an accurate calculation of the steady-state and transient responses of the electronic network of

interest. This may be done by hand or with the aid of a computer.*

██ Hand analysis techniques are useful for a quick qualitative and, to a limited degree, quantitative appraisal of the sensitivity of linear circuits and logic circuits to radiation environments. Manual techniques are valuable in the prediction of permanent effects of transient radiation, particularly when the relevant electrical parameters assume constant, degraded values after irradiation. The hand analysis techniques are often quite adequate to establish the initial estimate of radiation induced voltage and current transients and of the steady-state performance degradation. This type of analysis is suitable for a rough estimate of the peak-amplitude radiation response. In practice, only small, simple circuits can be handled.

██ In doing analysis, there is an inevitable choice between time (man-hours) and accuracy. If great confidence in the results is not required (e.g., when the analysis results are to be used to

---

*██ A more detailed discussion of hand and computer analysis techniques is contained in the "TREE Handbook" (see bibliography).

plan further environmental tests), a large number of simplifying assumptions can be made, and the analysis can be carried out quickly by hand. ▮▮▮ If the results of an analysis are to be used directly in a survivability assessment, high accuracy is desirable. This implies that few simplifying assumptions may be made. If a circuit contains more than one or two active devices (e.g., transistors), the circuit model will be complex, and the speed and accuracy of a digital computer should be used. Both hand analysis and computer aided analysis require an equivalent-circuit model that represents electrical and radiation induced phenomena. A notable difference is that the computer can handle an equivalent circuit model in its entirety and can generate the desired response function without making engineering approximations.

▮▮▮ Both analog and digital computers have been used for response predictions, and each has advantages and disadvantages; however, recently developed mathematical techniques and programming capabilities make the digital computer preferable for most problems. Several digital programs are available for circuit analysis. These are described in some detail in the "TREE Handbook" (see bibliography). These codes do not do the analysis. They do perform the tedious, error-prone calculations. The individual who uses them must provide the accurate description of the equivalent circuit model and must interpret the results.

▮▮▮ Two factors control the accuracy of the results of any TREE analysis method. The first factor is the accuracy and completeness of the description of the response of individual components to a particular radiation environment. This information is basic to the success of any analysis technique and frequently has been the major stumbling block for analysis attempts.

▮▮▮ The second factor that affects the accuracy of the analysis results is the assumptions that are made to simplify the analysis problem.

Certain aspects of the radiation response of individual components generally are neglected by assuming that they will contribute only a small or negligible portion to the radiation response of the circuit. These assumptions are made on the basis of general experience with the radiation response of circuits and with knowledge of the limits over which they might be valid. Although these assumptions are generally correct, there are specific instances and specific circuit configurations for which they may not hold, and care must be taken in making such assumptions.

▮▮▮ In practice most of the analysis approaches result in a fairly reasonable correlation with experimental results. However, it is common knowledge that any experimental result can be explained by a theory, but the theory will not always predict the correct result in a new situation. Therefore, caution should be exercised when accepting a component representation or an analysis technique that predicts the results for a pulsed reactor environment reasonably accurately, if these results are to be applied to a nuclear weapon environment. It is also possible that techniques applicable to switching circuits or nonlinear circuits will not apply to all linear circuit analysis.

9-55 Radiation Response of Integrated Circuits ▮▮▮

▮▮▮ Integrated circuits include many circuit types differing in construction materials and methods. The four construction types are the monolithic semiconductor, thin film, multichip, and hybrid integrated circuits. The scope of this section will be limited to monolithic and thin film circuits since the radiation response of both multichip and hybrid circuits can be inferred from the discussion of monolithic and film circuits or discrete devices. The discussion includes junction isolated, dielectrically isolated, and air isolated integrated circuits.

In junction isolated circuits, the components are defined within a single crystalline substrate by regions of alternate doping that are electrically isolated by reverse biased PN-junction boundaries. The doped regions are formed by the geometrically controlled diffusion of appropriate impurities into the substrate. One or more uniformly doped, epitaxial layers may be grown upon the substrate prior to diffusion (planar epitaxial). The dielectric-isolated circuit is distinguished by the use of a dielectric (silicon dioxide or ceramic) instead of a PN-junction isolation between critical components. A single component or a small number of components are formed within individual single crystalline islands (called tubs) that are imbedded in a polycrystalline substrate. The active elements in both the junction and dielectric isolated circuits can be bipolar transistors, junction FET's, or insulated gate (MOS) FET's. The air isolated circuit usually employs aggregates of unipolar (i.e., field effect) transistors of metal-oxide-silicon construction.* Since this type of transistor may be used as a bias-dependent resistor, complete designs usually are constructed without the use of other circuit elements. Air isolated MOS integrated circuits are fabricated by growing silicon on sapphire (SOS). Portions of the silicon are etched away, leaving isolated islands of silicon upon which transistors are fabricated.

Thin-film integrated circuits employ geometrically controlled surface films of conductive and dielectric materials upon a glass or ceramic substrate to define passive circuit elements and interconnections. The active elements may be formed as an integral part of the process (thin film, insulated gate, field effect transistors) or welded to the circuit (conventional, discrete transistors). Circuits of the latter type are referred to as hybrid thin film circuits.

The categorization of circuit types given above is somewhat arbitrary. It is based on the present developments in the integrated circuit industry, rather than on strict lines of variance between the types. The categorization is used for convenience of discussion with respect to the effects of transient radiation, where distinctly different effects may occur. For example, the PN junction used for isolation is a source of photocurrents during an ionizing radiation pulse, and may result in large substrate (and hence, power-supply) currents in junction isolated monolithic circuits. This effect is absent in either the air or dielectric-isolated monolithic circuit or the thin film, hybrid circuit.

Transient radiation may cause both transient, permanent and thermomechanical shock effects. On a qualitative basis, the primary electrical effects introduced in integrated circuits by transient radiation are similar to the effects described for conventional solid-state circuitry. The magnitude, duration, and electrical consequences of these effects, however, do not follow directly from conventional circuit experience.

The effects of radiation on an integrated circuit are more closely related to its geometrical and physical characteristics than to its electrical function or circuit configuration. The proximity of circuit elements within the device, and in some cases its integral structure, make several modes of secondary interaction possible. This is especially important in the case of junction isolated integrated circuits.

The transient effects observed in integrated circuits result from the generation of excess charge carriers that cause photocurrents and voltage changes. As previously described for transistors, the motion of excess carriers is governed by the response of carriers to electric fields and concentration gradients. The charge carriers will cause currents to occur until they

---

* Air-isolated bipolar integrated circuits have also been constructed.

are swept out by external fields and electron-hole recombination. The peak photocurrents can be a function of either dose rate or dose depending on the duration of the radiation pulse. As a result, if the radiation pulse is long compared to the circuit radiation response time, the microcircuit response is dose rate dependent. However, for radiation pulses that are short compared to the circuit radiation response time, microcircuit response will be dose dependent. Thus, the width of the radiation pulse can be of considerable significance, since the peak photocurrent generated can be a function of the duration of the pulse as well as its amplitude.

In a transient-radiation environment, the semiconductor integrated circuit reacts to several mechanisms that have been discussed in connection with conventional circuitry. One point of departure that is made necessary by the monolithic nature of the circuit, is the significant and often predominant interelement effects that occur in addition to the intraelement effects. It is important to consider current paths between as well as within component parts of the microcircuit.

Quite generally, the transient effects in any integrated electronic device are a consequence of a sequence of events that may be described as follows:

- The radiation interacts with the circuit material and surrounding encapsulant to introduce charge carriers and to establish a nonequilibrium charge distribution.

- Acting under nonequilibrium electric fields and concentration gradients, mobile carriers flow in the direction that restores equilibrium and thereby produce primary electrical currents. These electrical currents may be semiconductor-junction photocurrents, replacement currents, dielectric-leakage currents, gas-ionization currents, etc.

- The nonequilibrium charge distribution and

the primary electrical currents may interact with the electrical circuit to produce secondary effects, e.g., secondary photocurrents. Under certain circumstances, the secondary effects may be sufficiently regenerative to be self-sustaining, and a new stable circuit state will result. In addition, localized electrical stresses may introduce permanent damage.

- The cumulative effects of the radiation induced currents and circuit action are voltage, current, and impedance changes of variable duration at the terminals of the integrated circuit.

In junction isolated circuits, the predominant effect is PN-junction photocurrents resulting from ionization in the semiconductor material. Important secondary effects include secondary photocurrents produced by transistor action in any three adjacent doped regions, potentially large substrate currents, and "latchup."

The predominant effect in dielectric isolated circuits is also PN-junction photocurrents. The major difference from other monolithic structures is the absence of the extra PN-junction between the components and the substrate and its associated photocurrent. Also, current paths are more restrictive.

In air isolated integrated circuits, the important primary transient effects are PN-junction photocurrents, replacement currents resulting from charge scattered from device lead wires and the case, and ionization currents through the surrounding encapsulant. The predominant secondary effect is a secondary photocurrent resulting from the radiation induced gate current and transistor action. In addition, photocurrent is generated in the Zener diode employed for protection in the gate lead of MOS circuits.

In MOS integrated circuits, the important primary transient effects are drain-substrate and source-substrate PN-junction photocurrents,

replacement currents resulting from charge scattered from device lead wires and the case, and ionization currents through the surrounding encapsulant. The predominant secondary effect is a secondary drain current resulting from the radiation induced gate current. In addition, photocurrent is generated in the Zener diode employed for protection in the gate load.

For the most part, thin film circuits may be treated as conventional circuits with extremely small geometries. Ionization currents within and between elements have specific importance, especially in the high-impedance circuitry associated with thin film circuits that employ field effect transistors. Nevertheless, in most cases of interest, the transistor is the predominant element that determines the transient radiation response of the circuit.

Semiconductor integrated circuits of the planar-diffused (or planar-epitaxial) type experience transient effects that may be attributed to the interaction of the circuit elements through the active substrate. Two predominant interelement effects that must be considered are the presence of large substrate currents and the occurrence of latchup.

In practice, the high packing density of elements on a substrate chip results in the presence of isolation diodes over most of the area of the chip. Thus, a chip 40 x 40-mils may have 1,500 mils^2 of effective isolation-diode area. The total substrate photocurrent may be 100 times that of a typical diode in the circuit. Since the substrate is connected to the power supply system, the substrate currents will be reflected in large currents appearing in the power supply leads. Radiation induced power supply currents of the order of 1 ampere, with durations of a few microseconds have been observed at prompt doses of approximately 10 rads (Si). The potential hazards to the power supply system, which must supply many such circuits, are evident.

Present evidence indicates that the very large power supply currents occur primarily in those circuits where transistor action through the substrate is possible. In circuits of this type, radiation thresholds above which the current increases suddenly have been observed. The thresholds have been attributed to the turning on of an equivalent four layer device. Other possibilities include second breakdown and sustaining voltage breakdown.

Transients induced in integrated circuits by pulsed ionizing radiation last from less than a microsecond in high speed digital circuits to several tens of microseconds in slower circuits. Occasionally, pulsed-radiation effects with considerably longer recovery times can be explained by circuit time constants. In the extreme case, the abnormal state persists until the dc power is interrupted. When this occurs, normal circuit operation is inhibited and latchup has occurred. In some cases, which are referred to as incipient latchup, the condition lasts only for periods that are long with respect to normal recovery times of the circuits. Latchup can be induced in three ways: by exposure to ionizing radiation; by particular sequences of applying voltage to circuits employing more than one power supply; and other electrical stimulations such as high voltage pulses. Only radiation induced latchup is considered here. Radiation induced latchup has been observed in only a small percentage of the device types that have been irradiated with pulsed ionizing radiation, and of these device types usually only a small percentage of the samples exhibit latchup. In a few cases, a majority of the samples of a certain part from a manufacturer of integrated circuit part types have exhibited latchup.

Integrated circuit latchup is always caused by one or more normally reverse biased PN junctions becoming conductive, either by the initiation of a breakdown mechanism or by becoming forward biased. In either case, a sustain-

ing mechanism must act to maintain the breakdown or forward bias condition, once it has been initiated. Three latchup mechanisms have been postulated and observed in junction isolated integrated circuits. These are: PNPN action, second breakdown, and transistor sustaining voltage breakdown. No other mechanisms for sustaining latchup are known, although several others have been postulated.

Latchup is normally associated with junction isolation since it usually involves some type of interaction with the silicon substrate through an isolating PN junction. Dielectric isolation is effective in isolating elements from one another and from the silicon substrate and, thus, is an important step in reducing the latchup vulnerability of integrated circuits. However, analyses of the structural characteristics of certain dielectric-isolated circuit types have indicated that the possibility of latchup cannot be ruled out in dielectric-isolated circuits. It is possible that some of the same mechanisms that are responsible for latchup in junction-isolated circuits also can exist in a dielectric-isolated circuit. These mechanisms include second breakdown, sustaining voltage breakdown of transistors and PNPN action if 4 layer structures are included within a dielectrically-isolated region.

No latchup mechanisms have been found that are peculiar to dielectric isolation. While photocurrents can be generated in dielectric isolation, there are no sustaining mechanisms for these currents unless the isolation is defective or is subjected to destructively high voltages.

Hybrid thin film circuits may be expected to be as tolerant of radiation as their conventional circuit counterparts. The radiation response is determined primarily by the active elements in the circuits.

Undoubtedly, dielectric isolated circuits are much less vulnerable to latchup than are their junction isolated counterparts. However, dielectric isolated circuits probably are more latchup-prone than discrete component circuits because: dielectric isolated process limitations occasionally permit four layer structures; diffused resistors are present in some dielectric isolated circuits; and protective surface coatings occasionally are used in special purpose potting compounds or encapsulants, which might compromise the isolation. Component isolation in a dielectric isolated circuit, while much superior to that in a junction-isolated circuit, is still somewhat less complete than that in a discrete component circuit because of photocurrents through the dielectric.

A large number of integrated circuits have been irradiated, but the testing has been concentrated on specific microcircuit types, and a broad base of experimental data on the response of microcircuits to radiation is not available. This lack of data is especially true for linear circuits. Representative radiation failure levels for some common digital junction-isolated types are shown in Table 9-23. The levels are listed either in terms of gamma dose or of dose rate, depending upon whether the circuit is normally dose or dose rate dependent. Design and production changes in integrated circuits are common in the industry. The broad ranges given reflect highly variable experimental results and indicate the necessity of considering each circuit as a separate problem.

The proximity and intercoupling of elements do not assume importance in the production of permanent effects by nuclear radiation. Integrated circuits may be treated as conventional circuits of small dimensions. The primary factor that determines the tolerance of the circuits to radiation induced permanent effects is the degradation of the active elements with accumulated radiation exposure.

Changes in the electrical parameters of diodes and transistors that result from radiation have been discussed. Experiments have shown that the circuits will experience failure when the

Table 9-23. ▉ Representative Radiation-Failure Levels ░ for Digital Junction-Isolated Semiconductor Integrated Circuits ▉

Type†	Radiation-Failure Level
Large area. slow speed	5 -20 rads (Si)
Large area, moderate speed	10^6-10^7 rads (Si)/sec 20 -60 rads (Si)
Small area, moderate or high speed	10^7-10^9 rads (Si)/sec

▉ Here, the "failure" level corresponds to exceeding the circuit's noise margin.

† ▉ Type designations defined as follows: Large area – chip area > 5,000 mil², Small area – chip area < 5,000 mil², Slow speed – propagation delay > 100 nsec, Moderate speed – propagation delay between 25 and 100 nsec, High speed – propagation delay < 25 nsec.

▉ gain of the transistors has dropped to the point that they will no longer support proper circuit action. The radiation resistance of the circuits is determined by the stability of the gain of the transistor elements with respect to radiation exposure and the tolerance of the circuit design with respect to gain degradation. Although no class of integrated circuits has been shown to be inherently superior to another, those circuits employing faster transistors usually can withstand a greater neutron fluence. Epitaxial transistors usually, but not exclusively, represent the faster transistor types. Radiation failure levels have been shown to vary from 10^{12} to 10^{15} n/cm² ($E > 10$ keV, fission), with the faster circuit types at the high end. The normally conservative design and digital function of most integrated circuits accounts for the circuit

longevity beyond what would be considered the minimum useful transistor gain point.

▉ The radiation induced circuit response of microcircuits is manifested by changes in both the dc and switching characteristics. The effect on the integrated circuit parameters of changes in components after irradiation will, of course, depend on the specific circuit configuration involved. Frequently, the radiation sensitivity of the circuit is determined by the tolerance of the circuit design with respect to gain degradation.

▉ The most radiation sensitive circuit parameter of digital gates and flip-flop circuits is the output low voltage. Circuit failures result when normally ON transistors leave saturation. The amount of current that an output transistor can sink is directly proportional to the current gain. The changes in the output transistor current gain are reflected directly in the current-drive capability (fan-out) of both digital gates and flip-flops.

▉ Changes resulting from radiation are observed for other digital-circuit parameters. The saturation voltage of transistors, V_{SAT}, increases with neutron fluence, even though sufficient base drive is supplied to maintain the transistor in saturation, as a result of an increase in the saturation resistance. These changes in saturation resistance usually are negligible at threshold fluences applicable for maximum fan-out. The input threshold voltage of gate circuits normally will increase with radiation exposure as a result of changes in the base-emitter voltage of the output transistor and increased diode forward voltage. Changes in this parameter, however, are not considered significant. Increases in leakage currents also have been observed with radiation exposure, but the changes in this parameter usually will not affect circuit performance.

▉ The switching characteristics of typical digital circuits also are affected by radiation.

The rise and fall times of the transistor elements of the microcircuit are increased and its storage time is decreased after neutron exposure. These effects combine. and usually a small net increase of switching time is observed.

A good estimate of the radiation tolerance (at different fan-out conditions) of digital circuits can be made by measuring the output current-voltage characteristics. The gain degradation can be calculated, and the degraded characteristics can be plotted with the measured characteristic. An example prediction with experimental results is shown in Figure 9-63 for the RD 308 flip-flop.*

Failure in MOS logic circuits results from changes in the threshold voltage of the transistors caused by ionizing radiation. Since a large. negative supply voltage permits greater degradation in threshold voltage before circuit failure occurs, the radiation failure threshold of MOS circuits depends on the maximum supply voltage rating. Experiments indicate that MOS digital microcircuits fail at radiation levels from 10^5 to 6×10^7 rads (Si) at manufacturer's rated supply voltages. Such an exposure can be associated with a neutron fluence of 1 to 2×10^{14} n/cm^2 ($E > 10$ keV, fission) for the mixed neutron-gamma flux of a typical fast-burst reactor. The characteristics of a particular MOS integrated circuit must be established with reasonable confidence before meaningful predictions can be made.

As with digital circuits, the primary cause of linear-microcircuit failure is transistor gain degradation. The degradation of performance of a linear circuit is characterized by radiation induced changes in the transfer characteristics. In linear circuits. the functional dependence of the overall circuit performance on individual transistor elements can be determined only by a detailed circuit analysis. This analysis usually is frustrated by circuit complexity and the inability to measure individual

microcircuit elements as a result of the lack of accessible terminals. Therefore, prediction of the performance of linear circuits under irradiation is difficult. The large variety of linear circuits precludes a discussion of each type; however, some general comments can be made concerning the performance of some devices.

The radiation responses of both differential and operational amplifiers have been studied. A typical transfer characteristic of a differential amplifier is shown in Figure 9-64. The gain of the circuit began to decrease at a fluence of 3×10^{13} n/cm^2 ($E > 10$ keV, fission) and was degraded to roughly 50 percent of its initial value after an order-of-magnitude-larger fluence. These amplifiers were found to maintain their balance during irradiation significantly better than amplifiers made from discrete devices.

The largest changes in operational amplifiers induced by radiation were observed in the open loop voltage gain and input bias current. The reduction in the open loop gain is a direct consequence of degradation of transistor gain. The use of lateral and substrate PNP transistors results in a relatively low radiation tolerance of these amplifiers compared to logic circuits. These PNP transistors are widebase units that are degraded at lower fluences than vertical NPN transistors. Changes in voltage gain begin to be observed (5 percent changes) at fluence levels near 10^3 n/cm^2 ($E > 0.1$ MeV, fission) for 709-type operational amplifiers. The neutron fluence where the voltage gain has decreased by 50 percent is about 8×10^{13} n/cm^2 ($E > 10$ keV, fission) for units with lateral and substrate transistors. Amplifiers that have eliminated lateral and substrate transistors show improved performance in the presence of radiation. The degradation in gain that is induced by radiation in operational amplifiers depends on the elec-

* More details are given in the "TREE Handbook" (see bibliography).

Legend

——— Load-terminal I-V characteristic, experimental
— — — Load-terminal I-V characteristic, predicted
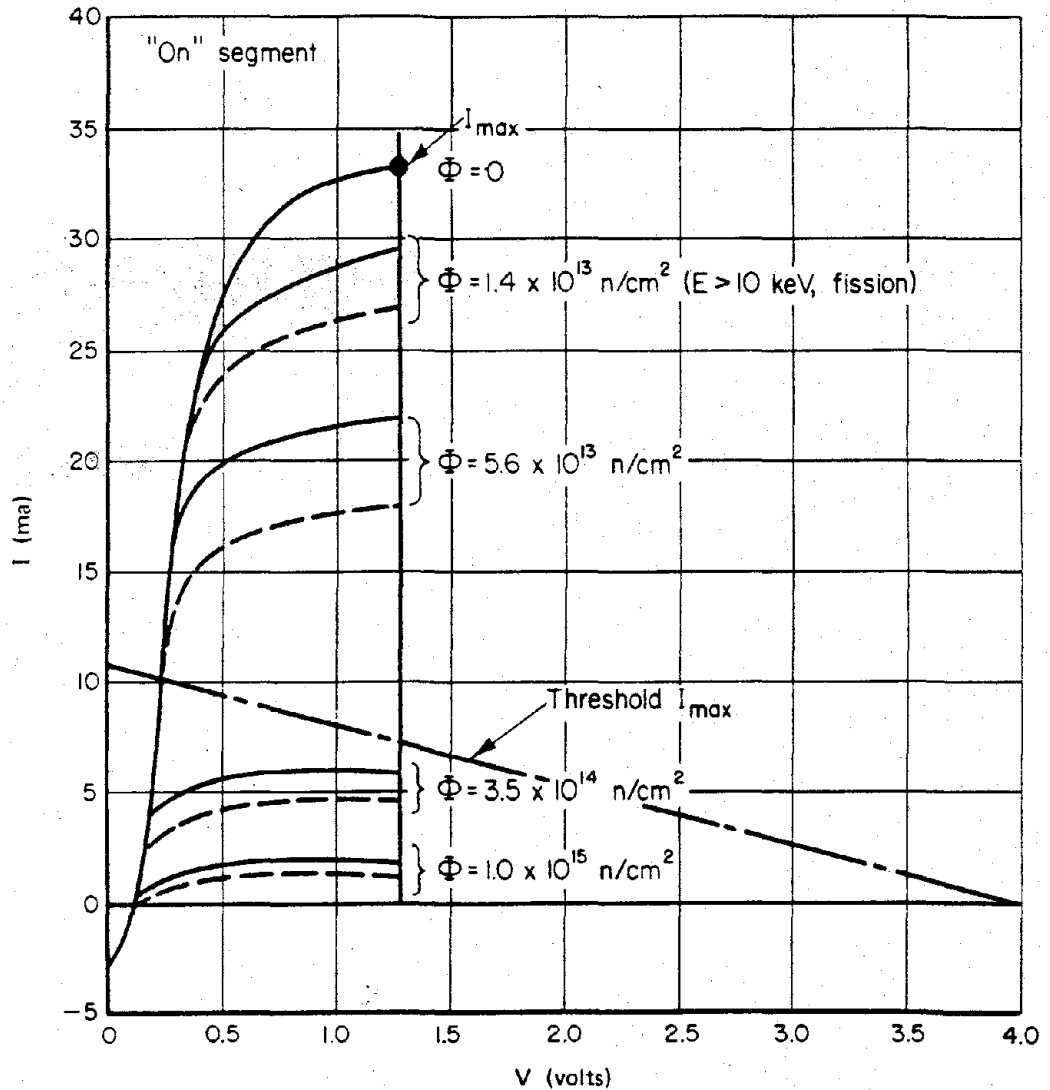———·— Load line at $R_L = 360\,\Omega$

Figure 9-63. ▮ Load-Terminal I-V Characteristic ("On" Segment) of RD 308 in Neutron Environment ▮
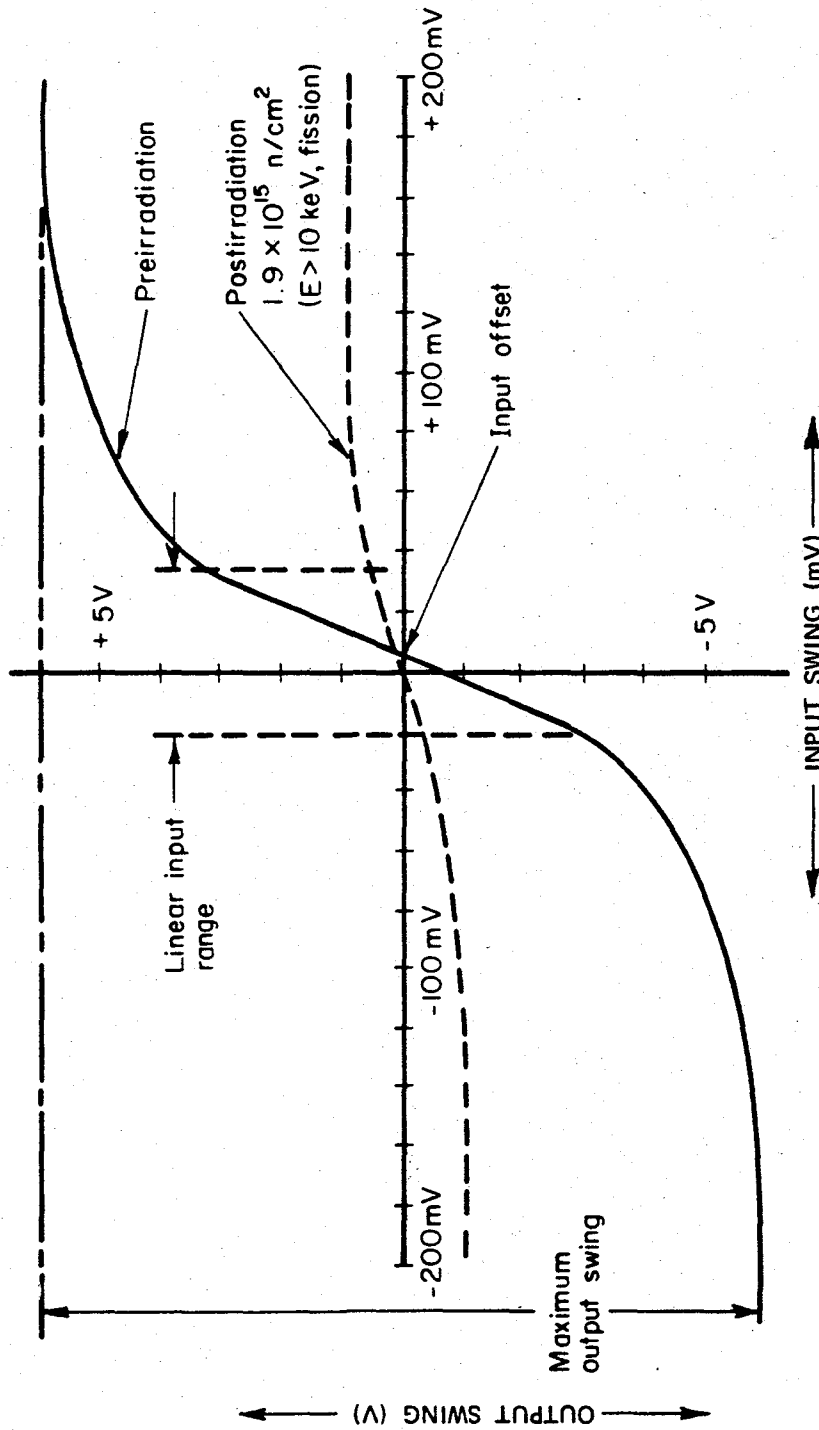
Figure 9-64. MC1525 Typical Transfer Characteristics

trical design. For example. it is important to determine whether the open-loop gain is determined by resistor ratios or by transistor gains. The changes in the input bias current can be correlated directly with changes in the common base current gain of the input transistors. It should be noted that the input transistors of operational amplifiers operate at very low currents (high input impedance), thus degradation of the base-transport factor is accompanied by degradation of the emitter efficiency as well. Factor-of-two increases in bias current have been observed for 709 amplifiers after 3×10^{13} n/cm² ($E > 10$ keV, fission). Offset voltage and offset current were found to increase after irradiation. These changes result from emitter-base-voltage and current-gain mismatches after irradiation. The changes in both current and voltage offsets were small at fluences where the gain and the bias current were degraded appreci-

ably, which indicates the uniformity of active elements on the same chip.

██████ Even though a large number of integrated microcircuits have been tested, data on the effects of neutron irradiation on microcircuits are still sparse. This is especially true for the linear types of integrated circuits. Radiation experiments indicate that the failure threshold of digital microcircuits is fairly independent of the construction technique. For buffered circuits the failure threshold, at unity fan-out, is near 10^{15} n/cm² ($E > 10$ keV, fission), while it is somewhat lower for the nonbuffered circuit types; however, the failure level at rated fan-out (~ 10) usually occurs over an order of magnitude lower in fluence than the failure level at unity fan-out. Representative radiation failure levels for some common digital microcircuits are shown in Table 9-24. The failure level is specified when the output voltage of the test circuit

Table 9-24. ██ Failure Thresholds for Typical Digital Microcircuits ██

Designation	Function	Construction	Failure Level, (n/cm²)	
MC 201	DTL Gate	Junction Isolation	1.5×10^{15}*	1.2×10^{14}†
DT μL 932	DTL Gate	Junction Isolation	3.0×10^{15}	1.5×10^{14}
RD 209	DTL Gate	Oxide Isolation	3.0×10^{15}	1.5×10^{14}
MC 507	TTL Gate	Junction Isolation	0.8×10^{15}	0.8×10^{14}
SN 54932	TTL Gate	Junction Isolation	1.5×10^{15}	1.2×10^{14}
DT μL 945	DTL Flip-Flop	Junction Isolation	1.5×10^{15}	1.2×10^{14}
SE 124	DTL Flip-Flop	Junction Isolation	0.85×10^{15}	0.8×10^{14}
RD 208	DTL Flip-Flop	Oxide Isolation	0.85×10^{15}	0.8×10^{14}

*██ Failure level at fan-out of 1; neutron fluence specified as ($E > 10$ keV, fission).
†██ Failure level at fan-out of 10; neutron fluence specified as ($E > 10$ keV, fission).

exceeds the noise margin of the following circuit. Typical radiation failure levels for some linear circuits are shown in Table 9-25. Table 9-26 contains irradiation test results for some representative MOS integrated circuits. The failure level is specified as the point when the circuit would not operate or when the threshold voltage exceeded the supply voltage.

█████ The test results presented are only intended to provide a broad range of failure levels for order-of-magnitude reference purposes and should be treated with appropriate caution. It should be borne in mind that design and production changes in integrated circuits are common in industry. For this reason, each circuit should be considered a separate problem.

█████ The thermomechanical shock effects for all integrated circuit types are the same as those effects on discrete semiconductor parts. The only difference to consider is the increased number of bonds used in each device package, which increases the change of bond failure.

Table 9-25. ██ Failure Thresholds for Typical Linear Microcircuits ██

Designation	Function	Construction	Failure Level* (n/cm^2)†
μA 709	Operational Amplifier	Junction Isolation	0.8×10^{14}
RA 909	Operational Amplifier	Oxide Isolation	0.8×10^{14}
Ph 709	Operational Amplifier	Oxide Isolation	3.0×10^{14}
MC 1709	Operational Amplifier	Oxide Isolation	3.0×10^{14}
MC 1525	Differential Amplifier	Junction Isolation	3.0×10^{14}
NM 1024	Differential Amplifier	Oxide Isolation	3.0×10^{14}
NM 1006	Differential Amplifier	Junction Isolation	4.0×10^{14}
RA 138	Amplifier	Oxide Isolation	1.5×10^{14}

* █ Failure level — gain degradation 50 percent.
† █ Neutron fluence specified as (E > 10 keV, fission).

Designation	Function	Failure Level	
		Gamma, (rads (Si))	Neutron.* (n/cm^2)
SC 1171	NAND gate	2×10^5†	—
MEM 529	Binary element	1.4×10^5‡	—
SC 1171	Binary element	$1. \quad 10^5$‡	—
MEM 501	Shift register	$1. \times 10^5$§	—
MEM 590	Chopper	Not measured**	3×10^{14}
SC 1149	Flip-Flop	Not measured**	8×10^{14}
MC 1155	AND/OR gate	2×10^5 (Cobalt-60)††	
3300	25-bit static shift register	$>5 \times 10^3$ (FXR)‡‡ $>8 \times 10^4$ (TRIGA)‡‡	
3003	100-bit shift register	$>2 \times 10^4$ (FXR)‡‡ $>5 \times 10^4$ (TRIGA)‡‡	
1406	100-bit shift register	$>10^5$ (FXR)‡‡ $<2.5 \times 10^4$ (TRIGA)	
1101	256-random access memory	4×10^4 (FXR) 2×10^4 (TRIGA)	3×10^{11}

* ▮ Neutron fluence specified as (E > 10 keV, fission).
† ▮ Supply voltage – 20 volts.
‡ ▮ Supply voltage – 15 volts.
§ ▮ Clock voltage – 10 volts.
** ▮ Supply voltage – 10 volts.
†† ▮ Type of facility in which test was performed.
‡‡ ▮ No failures at these levels.

ELECTROMAGNETIC PULSE (EMP) DAMAGE MECHANISMS

As described in Chapter 7, the nuclear electromagnetic pulse (EMP) is part of a complex environment produced by a nuclear environment. The EMP contains only a very small part of the total energy produced by a nuclear explosion; however, under the proper circumstances, EMP is capable of causing severe disruption and sometimes damage to electrical and electronic systems at distances where all other effects are absent.

As with the EMP generation described in Chapter 7, the complexity of the calculation of EMP damage mechanisms requires that heavy reliance be placed on computer code calculations for specific problems, and even these calculations must be supplemented by testing in most cases. Consequently, the information presented herein is largely qualitative and will only serve as an introduction to the subject. More complete treatments of EMP damage mechanisms may be found in the "DNA EMP (Electromagnetic Pulse) Handbook" (see bibliography).

Figure 7-18, Chapter 7, provides a matrix that provides some indication of whether EMP constitutes a threat in a given situation relative to the hardness of a system to blast overpressure. This section provides a brief description of EMP energy coupling, component damage, EMP hardening, and testing.

ENERGY COUPLING

9-56 Basic Coupling Modes

There are three basic modes of coupling the energy contained in an electromagnetic wave into the conductors that make up an electric or electronic system: electric induction, magnetic induction, and resistive coupling.

Electric induction arises as the charges in a conductor move under the influence of the tangential component of an impinging electric field. The overall result is that of a voltage source distribution along the conductor. One such point-voltage source is shown in Figure 9-65 for a simple conducting wire, where the current I is produced as a result of the tangential component $E_{i\ tan}$ of the incident electric field $\bar{E}_i$.
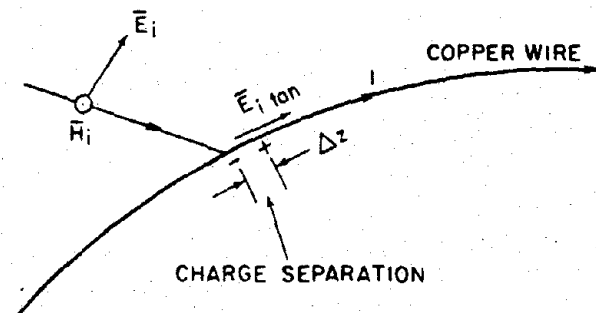

Figure 9-65. ▇ Electric Induction in a Copper Wire ▇

Magnetic induction occurs in conductors shaped to form a closed loop when the component of the impinging magnetic field perpendicular to the plane of the loop varies in time, causing charges to flow in the loop. This effect is illustrated in Figure 9-66 for a simple wire loop. Here the magnetic field is shown coming out of the plane of the loop. The loop need not be circular, and magnetic induction may occur with any set of conducting components assembled so as to form a loop.

Resistive coupling comes about indirectly as a conductor that is immersed in a conducting medium, such as ionized air or the ground, is influenced by the currents induced in the medium by the other coupling modes. In effect the conductor shares part of the current as an alternate conducting path. This effect is illustrated in Figure 9-67 for the simple case of a
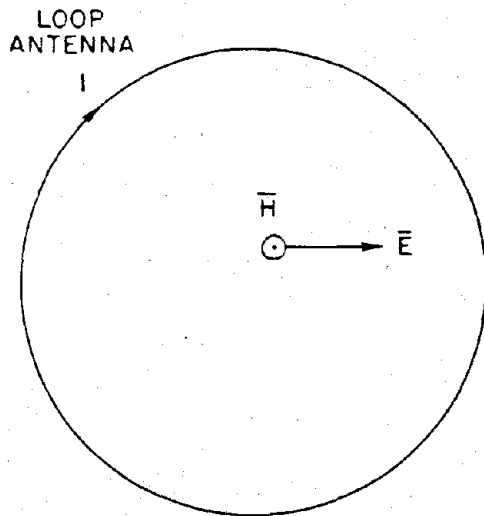
LOOP
ANTENNA

Figure 9-66. ▮ Magnetic Induction in a
Simple Loop ▮

conductor immersed in the ground. The tangen-
tial component of the incident electric field $\bar{E}_i$
induces a current density $\bar{J}$ in the ground. A
distributed voltage drop appears along the wire
as a result of the current flow in the ground, and
this incremental voltage causes current flow I in
the wire. Current also may be induced in the
wire directly by the tangential component of the
refracted electric field, shown as $\bar{E}_g$. The re-
flected EMP, $\bar{E}_r$, $\bar{H}_r$, is also shown in Figure
9-67. The potential importance of these re-
flected fields is discussed below.

9-57 Resonant Configurations ▮

▮ The coupling of energy to a conductor is
particularly efficient when the maximum dimen-
sion of the conductor configuration is about the
same size as the wavelength of the radiation. In
this event the voltages that are induced along the
conductor at various points are all approximate-
ly in phase, so the total voltage induced on the
conductor is a maximum. The conductor is said
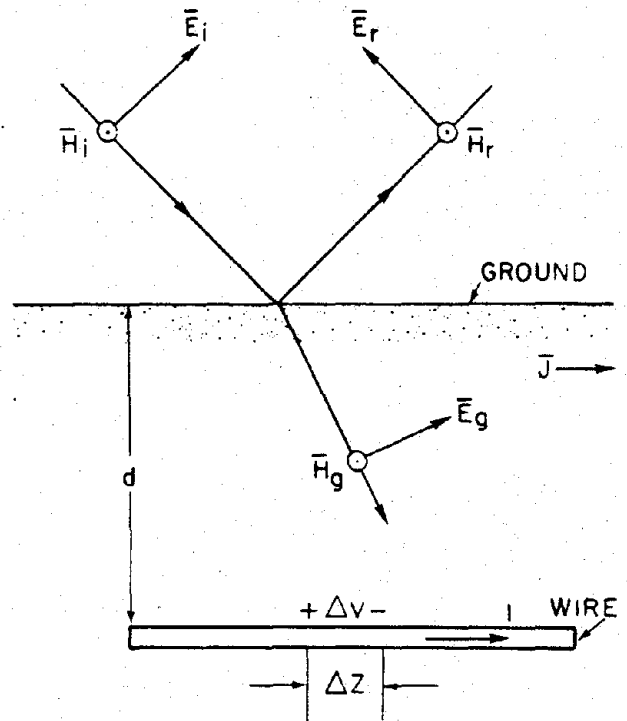to be resonant, or to behave as an antenna, for

Figure 9-67. ▮ Resistive Coupling as a Result
of Currents in the Ground ▮

frequencies corresponding to near this wave-
length. Since EMP has a broad spectrum of fre-
quencies (see Chapter 7), only a portion of this
spectrum will couple most efficiently into a
specific conductor configuration. Thus, a par-
ticular system of interest must be examined with
regard to its overall configuration as well as its
component configuration. Eash aspect will have
characteristic dimensions that determine what
part of the pulse (strength and frequencies) con-
stitutes the principal threat.

▮ Gross system features that are not nor-
mally considered antennas, such as structural
features, beams, girders, buried cable, overhead
conduit or ducting, wings, fuselage, missile skins,
and any wall apertures, must be considered to be
potential collectors and conductors of energy
into the system. In particular, radiation that

enters through an aperture is analogous to radiation that originates from a plate of the same size and shape as the aperture. Thus, it is resonant, and the aperture is resonant, and it admits a maximum of energy from the pulse for those frequencies near its resonance.

When the EMP strikes the ground, a portion of the pulse will be transmitted through the interface, inducing currents in the ground or any system components buried there, and a portion normally will be reflected as shown in Figure 9-68. Thus, a system that is above the ground will receive the reflected pulse as well as the direct pulse. These may cancel one another partially, but in the worst case they may reinforce and may constitute a greater threat level.

It can be seen that most practical systems in their operational environment present exceedingly complex coupling problems for an arbitrary explosion. The solution for any combination of system and environment is proba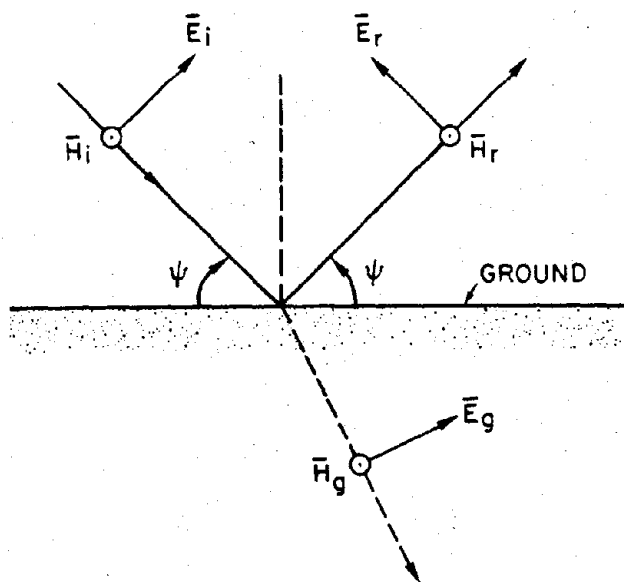bly unique and will be very sensitive to even minor changes in the parameters. Two approximate approaches have been tried: computer studies as mentioned in Chapter 7, and threat simulation, which will be discussed in succeeding paragraphs.

COMPONENT DAMAGE

9-58 Types of Damage

Degradation of system performance may occur as a result of functional damage or operational upset. A system will suffer damage if it is damaged permanently as a result of a large electrical transient. For example, a catastrophic failure of a device or component will render its operation unsatisfactory in any circuit. A parametric failure of a device occurs when degradation of some parameter has proceeded to a point where the circuit will continue to operate but at reduced efficiency. These latter failures are classed as functional damage. On the other hand, a system suffering operational upset is only impaired temporarily.

Electronic components that are sensitive to functional damage or burnout are listed below in the order of decreasing sensitivity to damage effects:

microwave semiconductor diodes,

field-effect transistors,

radio-frequency transistors,

audio transistors,

silicon-controlled rectifiers,

power rectifier semiconductor diodes,

vacuum tubes.

Thus, on the basis of components alone, vacuum tubes are less susceptible to EMP damage effects than transistors.

Electronic or electrical systems that are subject to malfunction include:

Most susceptible:

● Low power, high speed digital computer

Figure 9-68. ███ Reflected and Refracted Waves at the Air-Ground Interface ███

(upset) either transistorized or vacuum tube

- Systems employing transistors or semiconductor rectifiers (either silicon or selenium), such as

computers

computer power supplies

transistorized components terminating long cable runs, especially between sites

alarm systems

intercom systems

life-support system controls

some telephone equipment which is partially transistorized

transistorized receivers

transistorized transmitters

transistorized 60 to 400 cps converters

transistorized process control systems

power system controls; communication links

Less susceptible:

- Vacuum tube equipment (does not include high speed digital equipment and equipment with semiconductor or selenium rectifiers)

transmitters	intercoms
receivers	teletype-telephone
alarm systems	power supplies

- Equipment employing low current switches, relays, meters

alarms	panel indicators, status boards
life-support systems	process controls
power system control panels	

- Hazardous equipment containing

detonators	explosive mixtures
squibs	rocket fuels
pyrotechnical devices	

- Other

Long power cable runs employing dielectric insulation, equipment associated with high energy storage capacitors or inductors

Least susceptible:

- High-voltage 60 cps equipment

transformers, motors	rotary converters
lamps, filament	heavy duty relays, circuit breakers
heaters	air-insulated power cable runs

The less susceptible equipment or components would be made more susceptible if they are connected to long exposed cable runs, such as intersite wiring or overhead exposed power or telephone cables. The equipment can be made less vulnerable if it is protected.

9-59 Damage Levels

The nature of a circuit has a strong bearing on the transients that cause damage; however, in general pulse lengths of microsecond and submicrosecond duration are required to cause problems. Table 9-27 shows a list of common active devices and the approximate energy required to cause functional damage. The wide range of energies should be noted.

The minimum energy required to damage meters or to ignite fuel vapors is about the same as that required to damage semiconductors as shown in Table 9-28. Good composition resistors can withstand pulse powers more than 10,000 times their power rating for micro-

Table 9-27. ███ Minimum Observed Joule Energy to Cause Burnout ██

Type	Minimum Joule Energy	Material	Other Data
2N36	4.0×10^{-2}	Ge	PNP Audio Transistor
2N327A	1.6×10^{-2}	Si	PNP Audio Transistor
2N1041	2.0×10^{-2}	Ge	PNP Audio Transistor
2N1308	5.0×10^{-5}	Ge	NPN Switching Transistors
2N706	6.0×10^{-5}	Si	NPN Switching Transistors
2N594	6.0×10^{-3}	Ge	NPN Switching Transistors
2N398	8.0×10^{-4}	Ge	PNP Switching Transistors
2N240	1.0×10^{-2}	Ge	PNP Switching Transistors
MC715	8.0×10^{-5}	Si	Data Input Gate Integrated Circuit
2N4220	1.0×10^{-5}	Si	RF General Purpose FET
2N4224	3.0×10^{-5}	Si	VHF Amp and Mixer FET
1N3659	8.0×10^{-3}	Si	Automotive Rectifier Diode
1N277	2.0×10^{-5}	Ge	High Speed Switching Diode
1N3720	5.0×10^{-4}		Tunnel Diode
1N238	1.0×10^{-7}	Si	Microwave Diode
2N3528	3.0×10^{-3}	Si	Silicon Controlled Rectifier
67D-5010	1.0×10^{-4}		G.E. Varistar (30-joule Rating)
6AF4	1.0×10^{0}		UHF Oscillator Vacuum Tube
66N8	2.0×10^{0}		General Purpose Triode Vacuum Tube

Table 9-28. ██ Minimum Joule Energy to Cause Permanent Degradation Indicated ██

Designation	Minimum Joule Energy	Malfunction	Other Data
Relay	2×10^{-3}	Welded Contact	Potter-Brumfield (539) low-current relay
Relay	1×10^{-1}	Welded Contact	Sigma (IIF) one-ampere relay
Microammeter	3×10^{-3}	Slammed Meter	Simpson Microammeter (Model 1212C)
Explosive Bolt	6×10^{-4}	Ignition	EBW 8 amp for 10 μsec detonator, MK1
Squib	2×10^{-5}	Ignition	Electric Squib, N8 3.5 watts for 5 μsec detonator
Fuel Vapors	3×10^{-3}	Ignition	Propane-air mixture 1.75 mm ignition gap

second pulses. Capacitors are also fairly hard components. The approximate energies required for degradation of several common components are shown in Table 9-28.

██ The minimum energy necessary for operational upset is a factor of 10 to 100 less than that which is required to damage the most sensitive semiconductor component. Table 9-29 shows the levels required to cause operational upset to some common components to illustrate this factor.

██ A gross comparison of the energy required to damage several classes of electrical equipment is provided in Figure 9-69.

██ The large range of damage levels emphasizes the fact that it is important to consider EMP damage criteria early during the design stage of any piece of equipment that might be susceptible. It is also important to realize that energy collected in one part of a system may be transmitted to other parts of the system as a result of the currents that are induced. Thus, it is not necessary that the EMP couple directly to a sensitive component; energy coupled to various parts of a system may ultimately reach a particular component in sufficient quantity to cause malfunction. With the current state of the art in EMP vulnerability evaluation, the design and hardening of complicated systems requires the joint efforts of systems engineers and professional EMP effects personnel.

██ EMP HARDENING ██

9-60 System Analysis ██

██ A general approach to the examination

████████████

Table 9-29. ██ Minimum Joule Energy to Cause Circuit
Upset or Interference ██

Designation	Minimum Joule Energy	Malfunction	Other Data
Logic Card	3×10^{-9}	Circuit Upset	Typical logic transistor inverter gate
Logic Card	1×10^{-9}	Circuit Upset	Typical flip-flop transistor assembly
Integrated Circuit	4×10^{-10}	Circuit Upset	Sylvania J-K flip-flop monolithic integrated circuit (SF50)
Memory Core	2×10^{-9}	Core Erasure Via Wiring	Burroughs fast computer core memory (FC2001)
Memory Core	5×10^{-8}	Core Erasure Via Wiring	Burroughs medium speed computer core memory (FC8001)
Memory Core	3×10^{-9}	Core Erasure Via Wiring	RCA medium speed, core memory (269M1)
Memory Core	2×10^{-8}		Minimum observable energy in a typical high-gain subsystem
Amplifier	4×10^{-21}	Interference	Minimum observable energy in a typical high-gain amplifier

██

of a system with regard to its EMP vulnerability could include the following steps. First information concerning the system components and devices is collected. The information is categorized methodically into physical zones based on the susceptibility and worst case exposure for these items. Using objective criteria, problem areas are identified, analyzed, and tested. Suitable changes are made as necessary to correct deficiencies, and the modified system is examined and tested. The approach may be followed on proposed systems or those already in place, al-

though experience indicates that the cost of retrofitting EMP protection is usually overwhelming.

9-61 Recommended Practices ██

██ Within the scope of this manual it is only possible to mention a few of the practices that may be employed in hardening a system to EMP. The following discussion is intended to convey some impression of the extra effort involved in hardening a system to the EMP rather than to provide a comprehensive treat-

ENERGY, JOULES (watts - seconds)

Figure 9-69. ███ Energy Required to Damage Various
Classes of Equipment ███

ment of what is a highly technical and specialized field.

███ Some general methods for reduction of the EMP environment include geometric arrangement of the equipment, shielding, geographic relocation, and proper grounding.

███ Circuit layout recommendations include the use of common ground points, twisted cable pairs, system and intrasystem wiring in "tree" format (radial spikes) avoiding loop layouts and circuit routes coupling to other circuits, use of conduit or cope trays, and shielded isolated transformers. Avoiding ground return in cable shields is also recommended. Many specific practices carry over from communications and power engineering while many do not. Each must be examined carefully.

███ Good shielding practices include the use of independent zone shields, several thin shields to replace a thick one, continuous shield joints, and keeping sensitive equipment away from shield corners. Avoiding shield apertures, and avoiding the use of the shield as a ground or return conductor is also recommended. The shielding effectiveness of many enclosures frequently is defeated by energy carried by cables or pipes (including water pipes, sewage lines, etc.) into the enclosure.

███ Cabling recommendations include the use of deeply buried intersystem cables (more than 3 feet), shield layer continuity at splices, and good junction box contact. Ordinary braid shielding should be avoided. Cable design represents an extension of shielding and circuit practices from the viewpoint of EMP protection. It is an area where compromises frequently are made in the interests of economy, and thus is an area where professional EMP effects personnel can be

of considerable assistance.

Good grounding practices must be employed. In general, a "ground" is thought of as a part of a circuit that has a relatively low impedance to the local earth surface. A particular ground arrangement that satisfies such a definition may not be optimum, and may be worse than no ground from the EMP viewpoint. A ground can be identified as: the chassis of an electronic circuit, the "low" side of an antenna system, a common bus, or a metal rod driven into the earth. The last depends critically on local soil conditions, and it may result in resistive induced currents in the ground circuit. A good starting point is to provide a single point ground for a circuit cluster, usually at the lowest impedance element — the biggest piece of the system that is electrically immersed in the earth, e.g., the water supply system. It is beyond the scope of this manual even to list all of the grounding recommendations. Once again, this is an area where professional EMP effects personnel can be of considerable assistance.

Finally, various protective devices represent a means to counter other protective shortcomings indirectly. Filters, absorbers, limiters, decouplers, switching devices, arc arresters, fuses, etc., are part of this class of components. When other design practices cannot be used or are not adequate, such devices must be added. Typically they are found in an "EMP room" at the cable entrance to underground installations, in aircraft antenna feeds, in telephone lines, at power entry panels to shielded rooms, etc. On a smaller scale, diodes, nonlinear resistors, SCR clamps, and other such items are built into circuit boards or cabinet entry panels. Few of these devices by themselves are sufficient as a complete solution to a specific problem area, because each has some limitation in speed of response, voltage rating, power dissipation capacity or reset time. Thus, most protective devices are hybrids. A few prepackaged hybrids are available for the protection of audio and power lines from lightning strokes and power surges and, if modified, may be used for EMP protection. No such packages are readily available for high frequency lines, multiple wire cables, antennas, etc., and usually must be custom designed for each application.

TESTING

9-62 Importance of Testing

Even with present day sophistication in analytic techniques, it is clear from the complexities described above that sole reliance cannot be placed in analysis and prediction alone. Testing has a number of important functions.

Testing is essential to verify prior analysis of devices, components, and complete systems early in the design stage. Testing also is the only known method that can be used to identify surprises. Surprises can be unexpected coupling or interaction modes or weaknesses that were overlooked during the design. Nonlinear effects in interaction are a form of surprise that only can be found by testing. After the test, many of the original approximations made in analysis can be refined and improved for future analysis, and the data can improve the analytic capability for more complex problems.

Testing quickly locates weak or susceptible points in components or systems early enough for economic improvement. After the improvements, testing quickly verifies that the improvements bring the performance up to standards.

Testing provides assurance and confidence that the complete system is actually hardened to EMP to the specified threat level. Actual certification can only be obtained by providing the actual nuclear threat environment. Further, periodic testing insures that system hardness is not degraded as a result of environmental or human factors.

9-63 Simulation Facilities ▉

▉ As a result of the limited test ban treaty, heavy reliance must be placed on simulation to test the EMP hardness of systems. A brief description of generic simulation techniques is given below. A more thorough description of these techniques is contained in the "DNA EMP (Electromagnetic Pulse) Handbook, Volume 2, Analysis and Testing" (see bibliography).

▉ The classes of EMP tests are:

- Low level current mapping,
- High level current mapping,
- High level fields.

Low level current mapping is a good test for the beginning of any program. With the system power turned off and a low-level field, the magnitudes and signatures on internal cables are determined. This provides an insight on the work that must follow. After this test and the indicated improvements are made, a high-level current can be injected directly into the system with the system power on to explore for non-linearities, and to uncover initial indications of system effects. If subsystems malfunction, it may be desirable to conduct extensive subsystem tests in the laboratory. Finally, a high level field test is essential.

▉ The type of excitation must be defined in any type of test. The two principle choices are:

- Waveform simulations (time-domain data),
- Continuous wave signals (frequency-domain data).

If the intent is to match a system analysis in the frequency domain to measured system response, continuous wave (CW) signals may be more suitable. If the desire is to compare the test results to known electronic thresholds, it is frequently necessary to test in the time domain. For a complete analysis, it is advisable to consider both types of tests.

▉ Large-scale simulators are required for the final test of large systems. The two principal kinds of large simulators are:

- Metallic structures that guide an EM wave past a test object,
- Antennas that radiate an EM field to a test object.

Guided wave simulators use pulse generators that simulate EMP waveforms and operate in the time domain. Radiating antennas use either pulse generators (time domain) or continuous wave (CW) signal generators (frequency domain). Pulse generators themselves can be either high level single shot or low level repetitive.

(U) The essential elements of a guided wave or transmission line simulator include:

- Pulser
- Transition section
- Working volume
- Termination.

An electromagnetic wave of suitable amplitude and waveshape is generated by the pulser. This wave is guided by a tapered section of transmission line (the transition section) from the small cross sectional dimension of the pulser otuput to the working volume. The working volume, where the test object is located, should be large enough to provide a certain degree of field uniformity over the test object. A test object dimension one-fifth that of the working volume satisfies this condition. The termination region prevents the reflection of the guided wave back into the test volume, and consists of a transition section that guides the incident wave to a geometrically small resistive load whose impedance is equal to the characteristic impedance of the transmission line structure.

▉ The basic types of radiating simulators are:

- Long wire
- Biconic dipole or conical monopole.

The long wire is usually a long dipole oriented

parallel to the earth's surface. It is supported above the ground by nonconducting poles with high-voltage insulators. The two arms of the dipole are symmetric about the center and constructed from sections of light weight cylindrical conductor, such as irrigation pipe. Pipe sections decrease in diameter with increasing distance from the center, and resistors are placed between the pipe sections to shape the current wave and reduce resonances. The two arms of the dipole are oppositely charged, and when the voltage across the spark gap at the dipole center reaches the breakdown voltage, the gap begins conducting and a current wave front propagates away from the gap.

■■■■ Conical and biconical antennas use pulsers, such as Marx generators, or CW transmitters instead of relying on the discharge of static surface charges. The antennas are fabricated out of lightweight conducting surfaces or wire grids.

■■■ Differences between guided wave and radiating simulators are listed in Table 9-30.

■■■ Electromagnetic scale modeling is an important alternative to full scale testing under the following conditions:

- Test facilities or available equipment are at a premium,
- The system to be tested is very large,
- The system dedication cost for full scale testing is high.

In addition to the advantages of modeling under these conditions, benefits can be derived as follows:

- Perhaps sensors can be placed better during full scale testing as a result of model experiments,
- Design modifications or cable reroutes can be made prior to full scale testing,
- EM angles-of-arrival can be determined for worst- and best-case conditions,
- Effects of changes in the conductivity of

the surrounding media can be explored to an extent,

- Estimates can be made of some of the responses of a complex system prior to full scale testing,
- Design confirmation of costly systems can be made prior to system fabrication and costs can be reduced,
- Quantitative data can be obtained to validate analysis.

■■■ It should be pointed out that because of the difficulty in introducing minute openings or poor bonds into models, and since these often control interior fields, the usefulness of modeling ordinarily is limited to the measurement of external fields, voltages, and currents. Once the exterior fields, voltages, and currents are known for a complex structure, perhaps having cable runs, analysis can often provide internal field quantities of interest.

■■■ In actually setting up a scale model test, the following should be kept in mind:

- Broadband pulse response determination involves much more than a steady-state, single-frequency response test does.
- Special EM illumination sources that are coherent, have uniform time delay, and use antennas with constant effective height are required.
- Special modeling techniques are required to study exposed conductors that pass over or within a lossy dielectric, such as earth.

A pulse-type waveform theoretically can be replaced by a continuous wave (CW) source with a sensing system which references the sensed CW signal to a reference phase from the source. Complex Fourier transfer functions can be developed by processing the recorded data on a computer. However, long sweep times are required to ensure that all narrow band responses are explored adequately, and the actual physical implementation of such an approach in the

Table 9-30. ███ Comparison of Guided Wave and Radiating Simulators ███

	Guided Wave	Radiating
Energy use	Efficient — mostly directed toward test object	Energy radiated symmetrically about axis — only fraction directed toward test object
Test volume	Limited by size of simulator — difficult to construct large enough for sizable test objects	Limited by desired field intensity
Polarization	Fixed (or bipolar, e.g., ARES)	Variable*
Angle of incidence	Fixed†	Variable*
Earth reflection effects	No	Yes
Geometric attenuation of EM wave amplitude	No — relatively uniform within test volume	Yes (1/R)
Planar wave capability	Yes	Only at distance
Interference with nearby electronics	Limited	Yes

---

* ███ These are, however, limited by the height of the antenna unless it is airborne.

† ███ Polarization is fixed relative to earth coordinates; however, a range of polarizations and angles of incidence can be provided in some facilities by changing the position and orientation of the object that is being tested. For example, a missile can be rotated on several axes in ARES to change these to items relative to the missile.

microwave band poses additional difficulties. On the other hand, the use of scaled real time waveforms allows quick development of actual responses, from which complex Fourier transfer functions also can be developed with the aid of computers.

Several variations of each type of simulation technique described above are currently operational. Each has some advantages and disadvantages when compared to others. As mentioned previously, it is beyond the scope of this manual to describe individual facilities. The interested user should consult the "DNA EMP (Electromagnetic Pulse) Handbook, Volume 2, Analysis and Testing," (see bibliography), and the references listed therein.

BIBLIOGRAPHY

Abbott. L. S., H. C. Claiborne, and C. E. Clifford, Eds., *Weapons Radiation Shielding Handbook* ▮▮▮ DASA 1892-1, through 1892-6, Oak Ridge National Laboratory, Oak Ridge, Tennessee, December 1966 through March 1972 (Vols. I, II, III, V, ▮▮▮▮▮ Vol. VI, ▮▮▮▮▮▮▮▮▮▮ Vol. IV ▮▮▮▮

Barash, R. M., and J. A. Goertner, *Refraction of Underwater Explosion Shock Waves: Pressure Histories Measured at Caustics in a Flooded Quarry*, NOLTR-67-9, U.S. Naval Ordnance Laboratory, White Oak, Silver Spring, Maryland, 19 April 1967 ▮▮▮

Batter, J. F., *Transient Effects of a Time Varying Thermal Pulse*, Part II, AFSWP1058, TOI Report No. 58-7, Technical Operations Incorporated, Burlington, Massachusetts, March 1958 ▮▮▮

Bell, J. F., *Single Temperature-Dependent Stress-Strain Law for Dynamic Plastic Deformation of Annealed Face-Centered Cubic Metals*, Journal of Applied Physics, Vol. 34, No. 1, January 1963 ▮▮▮

Bergman, P., and N. Griff, *A Method for Evaluation of the Response of Coatings to Thermal Radiation from a Nuclear Weapon*, Naval Applied Science Laboratory Project 940-105, Progress Report 9, November 12, 1968 ▮▮▮

Bergman, P., et al., *Temperature Response Charts for Opaque Plates Exposed to the Thermal Radiation Pulse from a Nuclear Detonation*, Naval Applied Science Laboratory Project 940-105, Progress Report 10, July 10, 1969 ▮▮▮

Bethe, H. A., and W. L. Bade, *Theory of X-Ray Effects of High Altitude Nuclear Bursts and Proposed Vehicle Hardening Method* ▮▮▮ RAD-TR-9(7)-60-2, AVCO Corporation, Wilmington, Massachusetts, 8 April 1960 ▮▮▮

Bothell, L. E., *PUFF IV-EP Code Comparisons to Test Results* ▮▮▮ KN-664-67-2, Kaman Nuclear, Colorado Springs, Colorado, 16 January 1967 ▮▮▮

Bothell, L. E., and C. E. Archuleta, *PUFF V-EP Code* ▮▮▮ Parts I and II, KN-703-67-101(R), Kaman Nuclear, Colorado Springs, Colorado, December 1967 (Part I, ▮▮▮▮ Part II ▮▮▮▮

Bridges, J. E., *DNA EMP Awareness Course Notes*, DNA 2772T, Illinois Institute of Technology Research Institute, Chicago, Illinois, August 1971 ▮▮▮

Chandler, C. C., et al., *Prediction of Fire Spread Following Nuclear Explosions*, U.S. Forest Service Research Paper PSW-5, Pacific Southwest Forest and Range Experiment Station, Berkeley, California, 1963 ▮▮▮

Clarke, T. C., *Interaction Study, Vol. IV, Structural Degradation by Short Time Heating,* AFWL TR-70-157, Boeing Company, Seattle, Washington, December 1970

Cohen, M. L., *A Numerical Technique to Determine the Thermal Histories of Two-Dimensional Solids in the Nuclear Environments,* Naval Applied Science Laboratory Project 940-105, Progress Report 5, June 1958

Cole, R. H., *Underwater Explosions,* Dover Publications, Inc., New York, N.Y., 1965

Davis, G. T., et al., *Project TROIKA, Re-Entry Vehicle Vulnerability Assessment for Advanced Planning for Underground Tests* DASA 2230, AVCO Corporation, Wilmington, Massachusetts, January 1969

Derkesen, W. L., *Ship Vulnerability to Nuclear Attack-Thermal Radiation Effects,* Technical Briefing to the Chief of Naval Material, 2 March 1967.

DNA EMP (Electromagnetic Pulse) Handbook DNA 2114H1-2114H4, DASIAC, General Electric TEMPO, Santa Barbara, California, Volume 1, Design Principles, November 1971, Volume 2, Analysis and Testing, November 1971, Volume 3, Environment and Applications, to be distributed during early calendar year 1973, Volume 4, Resources, November 1971 (Volumes 1, 2, and 4, Volume 3,

Electromagnetic Pulse Sensor and Simulation Notes, Volumes 1-10, AFWL EMP 1-1 through EMP 1-10, Air Force Weapons Laboratory, Kirtland Air Force Laboratory, New Mexico, April 1967 through 1972

Goodwin, L. K., et al., *An Equation of State for Metals,* DASA 2286, Aeroneutronics Division of Philco-Ford, Newport Beach, California, April 1969

Hall, W. J., and N. M. Newmark, *Interpretation of Event Pile Driver Tunnel Liner Results* DASA 2374, University of Illinois, Urbana, Illinois, February 1970

Hall, W. J., and N. M. Newmark, *Supplemental Studies of Event Pile Driver Backpacked Tunnel Liner Results* DASA 2374-1, University of Illinois, Urbana, Illinois, October 1970

Harrison, G., *A Plan for the Development and Evaluation of an Advanced Re-Entry Vehicle* DASA 2208-I, General Electric Corporation, Philadelphia, Pennsylvania, June 1969

Hillendahl, R. W., *Theoretical Models for Nuclear Fireball* DASA 1589-1 through 1589-39, Lockheed Missiles and Space Company, Sunnyvale, California, 1965-68

Julian. A.. and C. E. Eves, *Thermal Effects on Strength of Aircraft Structural Sandwich-Type Panels*, WT 1341, Project 8.4, Operation REDWING, Cook Research Laboratories, Skokie, Illinois, 30 April 1958 ██████████████████████████

Julian, A. N.. *In-Flight Structural Response of FJ-4 Aircraft to Nuclear Detonations*, WT 1432, Project 5.3, Operation PLUMBBOB, Bureau of Aeronautics, Washington, D.C., 10 February 1960 ████████████

Kalinowski, J. J., *A Management Guide to Transient-Radiation Effects on Electronics (TREE)* ██ DNA 2051H. Battelle's Columbus Laboratories, Columbus, Ohio, February 1972 ████████████

Kaplan, K., and C. Wiehle, *Air Blast Loading in the High Shock Strength Region* ██ Part II. Prediction Methods and Examples, URS 633-3, DASA 1460-1, URS Corporation, Burlingame, California, February 1965 ██████████████

Kaufmann. R., and R. J. Heilferty, *Equations and Computer Program to Calculate the Temperature Distribution and History in a Cylinder Subject to Thermal Radiation from a Nuclear Weapon*, NASL Project 940-105, PR-8, U.S. Naval Applied Science Laboratory, Brooklyn, New York, 18 July 1968 ██████████████

Kaufmann, R., and R. J. Heilferty, *Equations and Computer Program to Calculate the Temperature Distribution and History in a Tee Beam Subject to Thermal Radiation from a Nuclear Weapon*, NASL Project 940-105, PR-6, U.S. Naval Applied Science Laboratory, Brooklyn, New York, 20 February 1968 ██████████████

Larin. F., *Radiation Effects in Semiconductor Devices*, John Wiley and Sons, Inc., New York, 1968 ██████████

Martin, S. B., and S. Holton, *Preliminary Computer Program for Estimating Primary Ignition Ranges for Nuclear Weapons*, USNRDL-TR-866, U.S. Naval Radiological Defense Laboratory, San Francisco, California, 3 June 1965 ██████████████

Melin, J. W., and S. Sutcliff. *Development of Procedures for Rapid Computation of Dynamic Structural Response*, University of Illinois Final Report on Contract AF33(600)-24994 for Physical Vulnerability Division of Intelligence, USAF ██████████████

Moon, D. P., and W. F. Simmons, *Methods for Conducting Short-Time Tensile, Creep, and Creep-Rupture Tests under Conditions of Rapid Heating*. Defense Metals Information Center Report 121, December 28, 1959 ██████████████

Moon, D. P., and W. F. Simmons, *Selected Short-Time Tensile and Creep Data Obtained under Conditions of Rapid Heating*. Defense Metals Information Report 130, June 17, 1960 ██████████████

Morris, P. J., *Proposed Addition to Chapter 7, DASA EM-1, Section 7.6, Thermal Radiation Degradation of Structural Resistance to Air Blast* ▮ URS 7029-6, URS Research Company, San Mateo, California, December 1971 ▮

Newmark, N. M., et al., *Analysis of Design of Flexible Underground Structures,* DA-22-079-eng-255, University of Illinois; Urbana, Illinois; 31 October 1962 ▮

Newmark, N. M., *An Engineering Approach to Blast Resistant Design,* Paper No. 2786, Transactions, ASCF, *121,* 45-64, 1956 ▮

Nuclear Weapons Blast Phenomena, DASA 1200-I, -II, -III, -IV, Defense Atomic Support Agency, Washington, D.C., Vol. I, March 1971, Vol. II, December 1970, Vol. III, March 1970, Vol. IV to be issued during calendar year 1972 (Vol. I, ▮ Vol. II ▮ Vol. III, ▮

Old, C. C., et al., *TROIKA Study Final Report* ▮ DASA 2191-I, -II, -III, and -IV, Lockheed Missiles and Space Company, Sunnyvale, California, August 1968 (Vols. I and II, ▮ Vols. III and IV, ▮

Reaugh, J., *Equation-of-State Evaluation Predix Topical Report* ▮ PITR-239-1, DASA 2596, Physics International Co., San Leandro, California, April 1972 ▮

Seaman, L., et al., *Dynamic Fracture Criteria of Homogeneous Materials,* AFWL-TR-71-156, Stanford Research Institute, Menlo Park, California, February 1972 ▮

Seaman, L., *Spall and Fracture Phenomena in the Response of Materials to Nuclear Effects* ▮ Third Annual Meeting of Nuclear Survivability Working Group on Propulsion and Ordnance, Stanford Research Institute, Menlo Park, California, 29-30 August 1971 ▮

Shelton, F., *Nuclear Weapons as X-Ray Sources, the Environments They Produce, and Some Effects on Aerospace Systems* ▮ Volume II, Some Effects on Aerospace Systems, DASA 2397-2, KN-770-69-30, Kaman Nuclear, Colorado Springs, Colorado, September 1969 ▮

Snay, H. G., *Underwater Explosion Phenomena: The Parameters of Migrating Bubbles,* NAVORD Report 4185, U.S. Naval Ordnance Laboratory, White Oak, Silver Spring, Maryland, 12 October 1962 ▮

Snay, H. G., *Hydrodynamic Concepts Selected Topics for Underwater Nuclear Explosions,* NOLTR 65-52, DASA 1240-1(2), U.S. Naval Ordnance Laboratory, White Oak, Silver Spring, Maryland, 15 September 1966 ▮

Staff of Kaman Avidyne, *Handbook for Analysis of Nuclear Weapon Effects on Aircraft* ████ KA-TR-50A, DASA-2048, Kaman Avidyne, Burlington, Massachusetts, April 1970

Staff of Kaman Avidyne, *Handbook of Computer Programs for Analysis of Nuclear Weapon Effects on Aircraft* ████ KA-TR-50S, DASA-2048S, Kaman Avidyne, Burlington, Massachusetts, April 1970 ████

Timoshenko, S., and S. Woinowsky-Krieger, *Theory of Plates and Shells*, McGraw-Hill Book Company, 1959 ████

TREE (Transient-Radiation Effects on Electronics) Handbook ████ DNA 1420H-1, Vol. 1, Edition 3, Battelle's Columbus Laboratories, Columbus, Ohio, December 1971 ████

TREE (Transient-Radiation Effects on Electronics) Handbook ████ DASA 1420-1, Edition 2, Revision 2, Battelle Memorial Institute, Columbus, Ohio, September 1970 ████ (to be replaced by DNA 1420H-2 during early calendar year 1973).

TREE Preferred Procedures (Selected Electronic Parts), DNA-2028H, Battelle's Columbus Laboratories, Columbus, Ohio, June 1972 ████

TREE Simulation Facilities, DASA 2432, Edition 1, Battelle Memorial Institute, Columbus, Ohio, September 1970 ████

Veigele, W. J., et al., *X-Ray Cross Section Compilation from 0.1 keV to 1 MeV*, DNA 2433F Vols. 1 and 2, Revision 1, KN-71-431(R), Kaman Nuclear, Colorado Springs, Colorado, 31 July 1971 ████.

Whitaker, W. A., and R. A. Deliberis, *Aircraft Thermal Vulnerability to Large High-Altitude Detonations* ████ AFWL-TR 67-85, Air Force Weapons Laboratory, Kirtland Air Force Base, New Mexico, August 1967 ████

Whitener, J. E., *Deflection of Ballistic Missiles by Nuclear Weapons* ████ RM-2345, RAND Corporation, Santa Monica, California, April 1959 ████

(This page intentionally left blank)